Universität Hamburg
DER FORSCHUNG | DER LEHRE | DER BILDUNG

A Two-Step Chemo-Enzymatic Oxidative Approach for Enhanced Bio-Based Recycling of Epoxy-Based Carbon Fiber-Reinforced Polymers (CFRPs)

Dissertation

with the aim of achieving the degree of

Doctor rerum naturalium (Dr. rer. nat.)

at the Department of Microbiology and Biotechnology
Subdivision at the Faculty of Mathematics, Informatics and Natural Science
of the University of Hamburg

Sasipa Wongwattanarat

Hamburg, 2025

1st evaluator: Prof. Dr. Wolfgang R. Streit

2nd evaluator: Prof. Dr. Andreas Liese

Date of oral defense: 02.12.2025

Eidesstattliche Versicherung:

Hiermit versichere ich an Eides statt, die vorliegende Dissertationsschrift selbst verfasst und keine anderen als die angegebenen Hilfsmittel und Quellen benutzt zu haben.
Sofern im Zuge der Erstellung der vorliegenden Dissertationsschrift generative Künstliche Intelligenz (gKI) basierte elektronische Hilfsmittel verwendet wurden, versichere ich, dass meine eigene Leistung im Vordergrund stand und dass eine vollständige Dokumentation aller verwendeten Hilfsmittel gemäß der Guten wissenschaftlichen Praxis vorliegt. Ich trage die Verantwortung für eventuell durch die gKI generierte fehlerhafte oder verzerrte Inhalte, fehlerhafte Referenzen, Verstöße gegen das Datenschutz- und Urheberrecht oder Plagiate.

Affidavit:

I hereby declare and affirm that this doctoral dissertation is my own work and that I have not used any aids and sources other than those indicated.
If electronic resources based on generative artificial intelligence (gAI) were used in the course of writing this dissertation, I confirm that my own work was the main and value-adding contribution and that complete documentation of all resources used is available in accordance with good scientific practice. I am responsible for any erroneous or distorted content, incorrect references, violations of data protection and copyright law or plagiarism that may have been generated by the gAI.

Hamburg, 17.07.25

ศศิภา วงศ์วัฒนารัตน์

.....

Sasipa Wongwattanarat

ABSTRACT

Carbon fiber-reinforced polymers (CFRPs), particularly epoxy-based CFRPs, have become essential materials in the aerospace, automotive, and wind energy industries due to their exceptional mechanical properties and lightweight characteristics. However, there is a lack of recycling technologies that are environmentally sustainable while also ensuring the recovery of carbon fibers in their original state. Although certain bacterial and fungal strains can colonize epoxy polymers, the identification of potential enzymes capable of efficiently degrading these materials remains elusive. Consequently, there is an urgent need for an effective, sustainable, and biologically inspired solution for eCFRP recycling.

In this study, a chemo-enzymatic treatment inspired by natural processes was developed, involving a two-step oxidation of eCFRPs.

Three novel bacterial laccases, derived from a metagenome of the European spruce bark beetle (*Ips typographus*), along with CueO from *E. coli* and the well-characterized horseradish peroxidase (HRP), were biochemically characterized in detail. These enzymes exhibited a preference for acidic pH conditions and moderate temperatures, with laccase ItL-03 demonstrating notable thermostability. Subsequently, their ability to oxidize three epoxy resin scaffolds containing tertiary amines and representing repeating units of the RTM6 epoxy used in aircraft applications was evaluated. Among them, ItL-03 showed the highest activity, converting over 80% of the substrates within 30 minutes. ItL-03 was therefore selected for application in a chemo-enzymatic treatment approach. For this, organic acids were screened for their effectiveness in recovering carbon fibers from epoxy composites, in comparison to the aggressive standard method using sulfuric acid. Propionic acid combined with hydrogen peroxide emerged as the most promising combination, capable of recovering clean carbon fibers with potential for reuse.

Integrating the organic pre-treatment with the enzymatic action on RTM6 (amine-cured epoxy powder) enabled the laccase to partially modify the epoxy and release defined products, which may potentially aid downstream processing. This sequential two-step oxidative treatment offers a more environmentally sustainable alternative, allowing the enzyme to participate in the degradation of recalcitrant polymers. This marks an initial step toward developing a bio-based recycling approach for epoxy-based CFRPs.

ZUSAMMENFASSUNG

Kohlenstofffaserverstärkte Polymere (CFRP), insbesondere CFRP auf Epoxidbasis, sind aufgrund ihrer außergewöhnlichen mechanischen Eigenschaften und ihres geringen Gewichts zu unverzichtbaren Werkstoffen in der Luft- und Raumfahrt, der Automobilindustrie und der Windenergieindustrie geworden. Es mangelt jedoch an Recyclingtechnologien, die umweltverträglich sind und gleichzeitig die Rückgewinnung der Kohlenstofffasern in ihrem ursprünglichen Zustand gewährleisten. Obwohl bestimmte Bakterien- und Pilzstämme Epoxidpolymere besiedeln können, ist die Identifizierung potenzieller Enzyme, die in der Lage sind, diese Materialien effizient abzubauen, noch nicht gelungen. Daher besteht ein dringender Bedarf an wirksamen, nachhaltigen und biologisch inspirierten Lösungen für das Recycling von eCFRP.

In dieser Studie wurde eine chemo-enzymatische Behandlung entwickelt, die von natürlichen Prozessen inspiriert ist und eine zweistufige Oxidation von eCFRP beinhaltet.

Drei neue bakterielle Laccasen, die aus einem Metagenom des Europäischen Fichtenborkenkäfers (*Ips typographus*) stammen, wurden zusammen mit CueO aus *E. coli* und der gut charakterisierten Meerrettichperoxidase (HRP) biochemisch detailliert charakterisiert. Diese Enzyme zeigten eine Präferenz für saure pH-Bedingungen und moderate Temperaturen, wobei die Laccase ItL-03 eine bemerkenswerte Thermostabilität aufwies. Anschließend wurden diese auf ihre Fähigkeit untersucht, drei Epoxidharzgerüste zu oxidieren, die tertiäre Amine enthalten und wiederholende Einheiten von RTM6 Epoxidharz darstellen, das in der Luftfahrt verwendet wird. Unter ihnen zeigte ItL-03 die höchste Aktivität, indem es über 80% der Substrate innerhalb von 30 Minuten umwandelte. ItL-03 wurde daher für die Anwendung in einem chemo-enzymatischen Behandlungsansatz ausgewählt. Zu diesem Zweck wurden organische Säuren auf ihre Wirksamkeit bei der Rückgewinnung von Kohlenstofffasern aus Epoxid-Verbundwerkstoffen untersucht, im Vergleich zum aggressiven Standardeinsatz von Schwefelsäure. Propionsäure in Kombination mit Wasserstoffperoxid erwies sich als die vielversprechendste Kombination, die in der Lage ist, saubere Kohlenstofffasern mit Potenzial für die Wiederverwendung zu gewinnen.

Die Integration der organischen Vorbehandlung mit der enzymatischen Wirkung auf RTM6 (amingehärtetes Epoxidpulver) ermöglichte es der Laccase, das Epoxid teilweise zu modifizieren

und definierte Produkte freizusetzen, die möglicherweise die nachfolgende Verarbeitung unterstützen können. Diese sequentielle zweistufige oxidative Behandlung bietet eine umweltfreundlichere Alternative, die es dem Enzym ermöglicht, am Abbau von persistenten Polymeren teilzunehmen. Dies ist ein erster Schritt zur Entwicklung eines biobasierten Recyclingansatzes für CFRPs auf Epoxidbasis.

Table of contents

ABSTRACT ..... **I**
ZUSAMMENFASSUNG ..... **II**
Table of contents ..... **IV**
List of abbreviations ..... **VII**
List of figures ..... **IX**
List of tables ..... **XII**
List of publications ..... **XIII**
1 INTRODUCTION **1**
1.1 Epoxy resins: from monomeric units to rigid cross-linked network 1
1.2 Epoxy-based CFRPs – an essential material in aerospace applications 4
1.3 Current recycling technologies for epoxy composites 5
1.3.1 Mechanical recycling 5
1.3.2 Thermal recycling 6
1.3.3 Chemical recycling 6
1.4 Advances in biodegradation of epoxy resins 8
1.4.1 Microorganisms involved in epoxy degradation 8
1.4.2 Enzymes involved in epoxy degradation 12
1.5 Oxidoreductases as potential enzymes for epoxy biodegradation 13
1.5.1 Heme peroxidases 13
1.5.2 Multicopper oxidases (MCOs), including laccases 15
1.6 Aim of the study 19
2 MATERIALS AND METHODS **20**
2.1 Bacterial strains, constructs, and cultivation conditions 20
2.1.1 Bacterial strains, vectors, and constructs 20
2.1.2 Cultivation of *E. coli* strains 21
2.2 DNA techniques 22
2.2.1 Restriction enzyme cloning 22
2.2.2 Agarose gel electrophoresis 25

2.3 Protein production techniques....25
2.3.1 Protein expression....25
2.3.2 Protein purification....26
2.3.3 SDS-Polyacrylamide gel electrophoresis (SDS-PAGE)....27
2.4 Characterization of oxidoreductases....29
2.4.1 ABTS assay....29
2.4.2 Enzyme kinetics using ABTS as substrate....30
2.4.3 Enzymatic activity on epoxy surrogates....31
2.4.4 Liquid chromatography-mass spectrometry (LC-MS)....32
2.4.5 Mediator-specific enzyme activity....32
2.5 Chemical pre-treatment....34
2.5.1 Pre-treatment process: eCFRPs....34
2.5.2 Weight loss....35
2.5.3 Fourier transform infrared (FTIR) spectroscopy....35
2.5.4 Scanning electron microscopy (SEM) analysis....36
2.6 Chemical-enzymatic treatment....36
2.6.1 Pre-treatment process: RTM6....36
2.6.2 Enzymatic treatment on epoxy extract....37
2.6.3 Enzymatic treatment on remaining epoxy powder....37
2.6.4 Direct electrospray ionization-mass spectrometry (ESI-MS)....37
2.6.5 Gas chromatography-mass spectrometry (GC-MS)....38
2.7 Bioinformatics....38
2.7.1 Sequence alignment and phylogenetic analysis....38
2.7.2 Protein structure analysis....38
3 RESULTS....40
3.1 Novel bacterial laccases from bark beetle metagenomes....40
3.1.1 Phylogenetic comparative analysis....40
3.1.2 Three-dimensional protein structure alignment....41
3.2 Recombinant laccase production and initial activity screening....48
3.3 Biochemical characterization of laccases and HRP....49
3.3.1 pH stability and buffer preference....49

3.3.2 Temperature stability and thermostability 49
3.3.3 Effect of H_2O_2 and Cu^{2+} 51
3.3.4 Kinetic constants of ABTS as a substrate 52
3.4 Screening potential oxidoreductases for epoxy degradation 52
3.4.1 Enzymatic activity on epoxy surrogates 53
3.4.2 Laccase ItL-03-mediators activity 56
3.5 Screening promising acidic-peroxide pre-treatments for eCFRPs 59
3.5.1 Effectiveness of organic acid-H_2O_2 treatments 60
3.5.2 Visualization of pre-treated composites 62
3.5.3 Functional group modification of pre-treated composites 64
3.6 Chemical-enzymatic treatment of RTM6 66
3.6.1 Epoxy extract 66
3.6.2 Remaining epoxy powder 72
4 DISCUSSION 79
4.1 Bacterial laccase ItL-03 is an acidophile promiscuous enzyme from insect gut with potential biotechnological applications 79
4.2 Oxidoreductases are effective in oxidizing epoxy model substrates seamlessly 85
4.3 Bacterial laccase ItL-03 induces partial surface modification of epoxy resins post pre-treatment targeting amine linkages 88
4.4 Pre-treatment as a key to enhancing bio-based recycling efficiency of eCFRPs 91
5 CONCLUSION AND FUTURE PERSPECTIVES 97
6 REFERENCES 100
7 ACKNOWLEDGEMENTS 123
8 APPENDIX 124

List of abbreviations

ABTS	2,2′-azinobis (3-ethylbenzothiazoline-6-sulfonic acid)
BBCM	Bis(4-dimethylamino-cyclohexyl) methane
BMAP	1,3-bis(methyl(phenyl)amino) propan-2-ol
BPA	Bisphenol A
BPF	Bisphenol F
BSA	Bovine Serum Albumin
CAGR	Compound Annual Growth Rate
CBS	Copper Binding Site
CF	Carbon Fiber
CFRP	Carbon Fiber-Reinforced Polymer
eCFRP	Epoxy-based CFRP
CYP	Cytochrome P450
DCM	Dichloromethane
DGEBA	Diglycidyl Ether of Bisphenol A
DMF	Dimethylformamide
DMSO	Dimethyl Sulfoxide
DNA	Deoxyribonucleic Acid
EC	Enzyme Commission
ECH	Epichlorohydrin
ESI-MS	Electrospray Ionization-Mass Spectrometry
ET	Electron Transfer
FPLC	Fast Protein Liquid Chromatography
FTIR	Fourier-Transform Infrared Spectroscopy
GC-MS	Gas Chromatography-Mass Spectrometry
HAT	Hydrogen Atom Transfer
HBT	1-hydroxybenzotriazole
HRP	Horseradish Peroxidase
H_2O_2	Hydrogen peroxide
IC	Ionic or Covalent mechanism
IMG	Integrated Microbial Genomes
K_{cat}	Turnover number
K_{cat}/K_m	Catalytic efficiency
K_m	Michaelis-Menten constant
LCM	Liquid Composite Molding
LC-MS	Liquid Chromatography-Mass Spectrometry
LiP	Lignin Peroxidase
LMS	Laccase Mediator System
MCO	Multicopper Oxidase
MDEA	4,4′-methylenebis(2,6-diethylaniline)
MNC	Mononuclear copper Center
M-MIPA	4,4′-methylenebis(2-isopropyl-6-methylaniline)
MnP	Manganese Peroxidase
Mpa	Megapascal
Mt	Million metric tons
m/z	mass-to-charge ratio
NCBI	National Center for Biotechnology Information
NNBT	N,N-bis(2-hydroxypropyl)-p-toluidine
PA	Polyamide

PE	Polyethylene
PET	Polyethylene Terephthalate
PMSF	Phenylmethylsulfonyl Fluoride
PP	Polypropylene
PS	Polystyrene
PUR	Polyurethane
PVC	Polyvinyl Chloride
RTM	Resin Transfer Molding
SEM	Scanning Electron Microscopy
SLAC	Small Laccase
SRB	Sulfate-reducing bacteria
TEMPO	(2,2,6,6-tetramethylpiperidin-1-yl)oxidanyl
T_g	Glass transition temperature
TGMDA	Tetraglycidyl Methylene Dianiline
TNC	Trinuclear copper Center
T_{opt}	Optimal temperature
TvL	*Trametes versicolor* Laccase
UHPLC	Ultra High-Performance Liquid Chromatography
UPO	Unspecific Peroxygenase
V_{max}	Maximum reaction rate
VP	Versatile Peroxidase

List of figures

Figure 1. Bisphenol A diglycidyl ether (DGEBA)-based amine-cured epoxy 2
Figure 2. Current epoxy composite recycling techniques for the recovery of high-quality carbon fibers (CFs) 5
Figure 3. Heme peroxidase structure and its catalytic mechanism 14
Figure 4. Structures of multicopper oxidases (MCOs) 16
Figure 5. Catalytic mechanism of MCOs.....17
Figure 6. The development of a chemo-enzymatic oxidative treatment method for eCFRPs.....19
Figure 7. A phylogenetic tree of putative and characterized MCOs.....41
Figure 8. Structural comparisons of the putative and characterized laccases with CueO 42
Figure 9. Potential two-domain multicopper oxidases (2dMCOs) 43
Figure 10. Evolutionary conservation profile of CueO compared to ItL-01-03 44
Figure 11. Expression of CueO and ItL-01-03 and initial activity screening with ABTS 48
Figure 12. Biochemical characteristics of oxidoreductases, determined using ABTS 50
Figure 13. Epoxy scaffolds—BBCM, BMAP, and NNBT—derived from RTM6 epoxy resin 53
Figure 14. Enzymatic activity of epoxy scaffolds—BBCM, BMAP, and NNBT— by HRP and bacterial laccases 54
Figure 15. Enzymatic activity of ItL-03 on epoxy scaffolds —BBCM, BMAP, and NNBT 55
Figure 16. LC-MS chromatogram of the reaction involving laccase ItL-03 and BMAP .56
Figure 17. Determination of pH and buffer preference for each mediator of laccase ItL-03.....57
Figure 18. Specific activity of ItL-03 towards different mediators and optimal copper concentration for its activity 58
Figure 19. Enzymatic activity of ItL-03 on NNBT with different mediators.....59

Figure 20. Weight loss of the resin mass in eCFRPs treated with a 5 M acidic-peroxide solution (A-H_2O_2) 60
Figure 21. Weight loss of the resin mass in eCFRPs treated with a 9 M acidic-peroxide solution (A-H_2O_2) 61
Figure 22. Morphological changes in eCFRPs after 24 and 48 hours of 5 M acidic-peroxide pre-treatment 63
Figure 23. SEM images of eCFRPs after 48-hour treatment with 5 M acidic-peroxide solution (A-H_2O_2). 64
Figure 24. FTIR analysis of the 8-hour acidic-peroxide pre-treatment of eCFRPs 65
Figure 25. ESI-MS analysis of epoxy extract following chemo-enzymatic treatment using PA-H_2O_2 and laccase ItL-03 on RTM6 67
Figure 26. The relative abundance of *m/z* values of interest from the ESI-MS analysis in Figure 25 68
Figure 27. Proposed compounds potentially oxidized by the enzyme following PA-H_2O_2 treatment 68
Figure 28. GC-MS analysis of epoxy extract following chemo-enzymatic treatment using PA-H_2O_2 and laccase ItL-03 on RTM6 69
Figure 29. The relative abundance of peaks A, B, and F from the GC-MS analysis in Figure 28 70
Figure 30. Proposed species for the peaks (a) A (12.4 min) and (b) C (13.5 min) 71
Figure 31. Proposed species for the peaks (a) B (13.2 min) and (b) D (10.1 min) 71
Figure 32. Proposed species for the peak E (14 min) 72
Figure 33. FTIR analysis of RTM6 epoxy powder 73
Figure 34. FTIR analysis of the enzymatic activity of ItL-03 after 5 days on non-treated epoxy resins (RTM6) 75
Figure 35. FTIR analysis of the enzymatic activity of ItL-03 after 5 days on pre-treated epoxy powder (PT-RTM6) 76
Figure 36. FTIR analysis comparison of ItL-03 activity with different mediators 77
Figure 37. Sequence alignment and phylogenetic analysis of the methionine loops from CueO and ItL-01 to ItL-03 83

Figure 38. Proposed possible reaction scheme for the oxidation of BMAP by bacterial laccase, involving indirect N-dealkylation through radical oxidation 86
Figure 39. Reaction pathway for the breakdown of amine cross-linked epoxy resin initiated by acyloxy radicals generated from peracids....92
Figure S1. Evolutionary conservation profile of putative and characterized laccases....124
Figure S2. Evolutionary conservation profile of potential two-domain multicopper oxidases (2dMCOs) 125
Figure S3. Kinetic constants of oxidoreductases for ABTS oxidation 126
Figure S4. LC-MS analysis identifying epoxy model compounds 126
Figure S5. Standard calibration for concentration determination and temperature control 127
Figure S6. LC-MS chromatogram of the reaction involving laccase ItL-03 and BBCM 127
Figure S7. LC-MS chromatogram of the reaction involving laccase ItL-03 and NNBT....128
Figure S8. SEM images of eCFRPs after 24-hour treatment with 5 M acidic-peroxide solution (A-H_2O_2). 128
Figure S9. Blank sample compared to negative controls for ESI-MS analysis 129
Figure S10. Significant differences between sample pairs for each *m/z* peak 129
Figure S11. Blank sample compared to negative controls for GC-MS analysis 130
Figure S12. Significant differences between sample pairs for peaks A, B, and F 130
Figure S13. FTIR analysis of enzyme controls....131

List of tables

Table 1. Reported microorganisms and enzymes involved in epoxy degradation.....10
Table 2. Base strains used in this study.....20
Table 3. Vector used in this study. 21
Table 4. Constructs used in this study.....21
Table 5. LB broth 21
Table 6. Primers used in this study 22
Table 7. Master mix composition for PCR 22
Table 8. Cloning procedure.....23
Table 9. Master mix composition for colony PCR.....24
Table 10. Colony PCR program.....24
Table 11. 50X TAE Buffer.....25
Table 12. Autoinduction media.....26
Table 13. Buffers used for purification 27
Table 14. Solutions and buffers used for SDS-PAGE 28
Table 15. Size of purified protein (kDa) containing His-tag.....29
Table 16. Preparation of 0.1 M citrate-phosphate buffers at the specified pH values 30
Table 17. Preparation of 0.1 M buffers at the specified pH values.....33
Table 18. Putative multicopper oxidase enzymes from *I. typographus* and other bacterial laccases known for their association with lignin and synthetic polymer modification 46
Table 19. Kinetic constants of purified oxidoreductases for ABTS substrate 52

List of publications

- Towards Sustainable Recycling of Epoxy-Based Polymers: Approaches and Challenges of Epoxy Biodegradation

Klose, L., Meyer-Heydecke, N., **Wongwattanarat, S.**, Chow, J., Pérez García, P., Carré, C., Streit, W., Antranikian, G., Romero, A. M., & Liese, A. (2023). Towards Sustainable Recycling of Epoxy-Based Polymers: Approaches and Challenges of Epoxy Biodegradation. *Polymers*, 15(12). https://doi.org/10.3390/polym15122653

- Microbial Plastic Degradation: Enzymes, Pathways, Challenges and Perspectives

Pérez-García, P., Sass, K., **Wongwattanarat, S.**, Amann, J., Feuerriegel, G., Neumann, T., Bäse, N., Schmitz, LS., Dierkes, RF., Gurschke, MF., Wypych, A., Bounabi, H., Divitiis, M., Vollstedt, C. and Streit, WR. (2025). Microbial plastic degradation: enzymes, pathways, challenges, and perspectives. *Microbiol Mol Biol Rev* 0:e00087-24. https://doi.org/10.1128/mmbr.00087-24

- A Combined Chemo-Enzymatic Treatment for the Oxidation of Epoxy-Based Carbon Fiber-Reinforced Polymers (CFRPs)

Wongwattanarat, S., Schorn, A., Klose, L., Carré, C., Malvis Romero, A., Liese, A., Pérez-García, P. and Streit, W. R. (2025). A combined chemo-enzymatic treatment for the oxidation of epoxy-based carbon fiber-reinforced polymers (CFRPs). *Front. Bioeng. Biotechnol.* 13:1670548. https://doi.org/10.3389/fbioe.2025.1670548

1 INTRODUCTION

For over a century, synthetic polymers have become an integral part of modern life, making their presence unavoidable in our daily lives. Annual plastic production surpassed 400 million metric tons (Mt) since 2022 (Plasticseurope, 2024), and consumption is projected to reach approximately 900 Mt annually by 2050 (Dokl et al., 2024). The majority of virgin plastics production, accounting for 75% of total output, consists of synthetic polymers polyethylene (PE), polypropylene (PP), polyvinyl chloride (PVC), polyethylene terephthalate (PET), polyurethane (PUR), and polystyrene (PS). Other thermosetting polymers, including epoxy resins, consist of less than 9% of total production (Plasticseurope, 2024). Despite their relatively small share, the demand for epoxy resin is steadily increasing, with a compound annual growth rate (CAGR) of 5.5% by 2028 (Marketsandmarkets, 2023). Epoxy resins have also emerged as key materials in sustainable technologies, such as wind turbines and electric vehicles, driven by the global shift toward sustainability (Mohanty et al., 2023; Subadra & Griskevicius, 2021). Their lightweight nature contributes to energy efficiency, while their durability and recalcitrant nature pose significant environmental challenges at end-of-life. Consequently, increasing concerns over the accumulation of epoxy waste, alongside economic incentives to lower costs through material reuse and recycling, have emphasized the urgent need for recent research into efficient and sustainable waste management strategies for these polymers.

1.1 Epoxy resins: from monomeric units to rigid cross-linked network

Epoxy resins are a class of reactive prepolymers that contain epoxide or oxirane functional groups, typically comprising an oxygen atom bonded to two carbon atoms (May, 2018). Most epoxy monomers are produced by introducing an epoxide group into compounds containing acidic hydroxyl groups, typically through a reaction with epichlorohydrin (ECH) (Figure 1a). Common compounds with hydroxyl groups include aliphatic diols, polyether polyols, and phenolic compounds, with Bisphenol A (BPA) and Novolac being among the most well-known. These epoxy monomers, formed by reacting with ECH, are referred to as glycidyl-based epoxy resins (Pham & Marks, 2005). An alternative route for producing epoxy monomers involves the

epoxidation of aliphatic or cycloaliphatic alkenes using peracids, which utilizes aliphatic double bonds instead of acidic hydrogen atoms. The resulting epoxy monomers from this process are classified as non-glycidyl-based epoxy resins (Gall & Greenspan, 1955). Thus, there is a wide variety of epoxy monomers available.

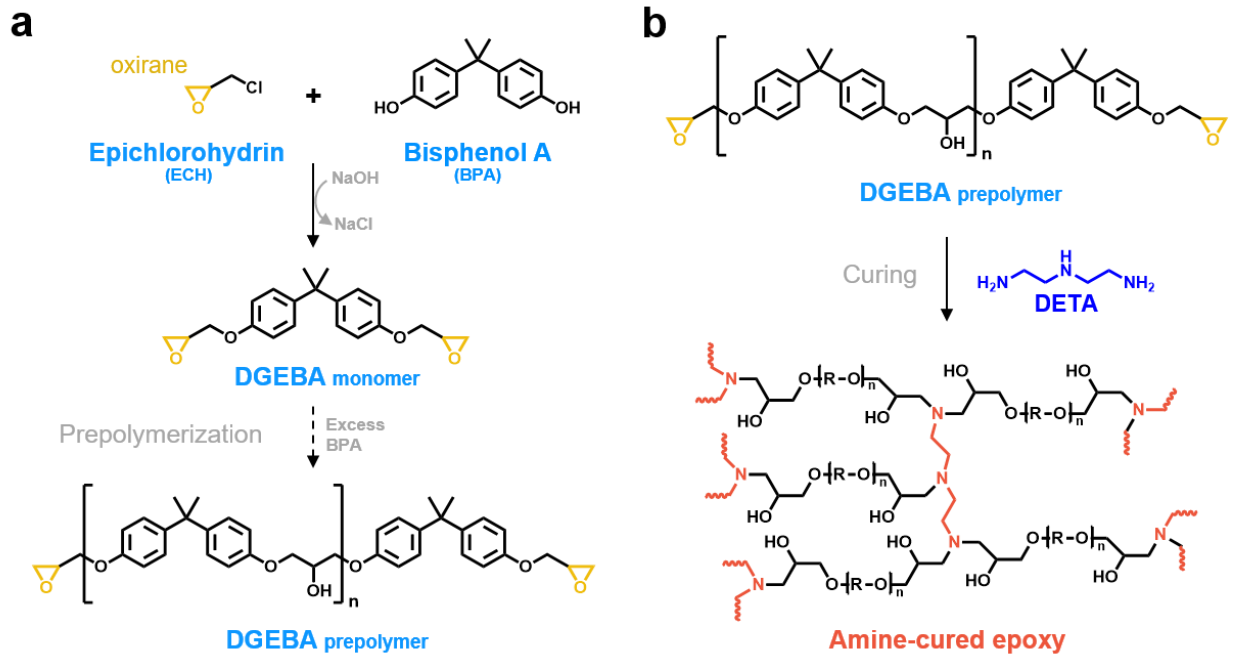

Figure 1. Bisphenol A diglycidyl ether (DGEBA)-based amine-cured epoxy. (a) Synthesis of epoxy monomer DGEBA from bisphenol A (BPA) and epichlorohydrin (ECH). The oxirane or epoxy ring is highlighted in yellow. (b) Formation of a crosslinked epoxy network by curing with an amine hardener diethylenetriamine (DETA). Figure modified from (Capricho et al., 2020).

One of the most commercially utilized epoxy monomers is diglycidyl ether of bisphenol A (DGEBA), which is produced by reacting BPA with ECH (Figure 1a). Initially, a product with only a few repeat units appears as a viscous, clear liquid. As DGEBA continues to react with excess BPA at room temperature, more repeating units can form, potentially transforming the epoxy into a solid state (Jin et al., 2015). This process, where monomeric building blocks are pre-polymerized prior to curing, is referred to as pre-polymerization. However, epoxy prepolymers are only partially polymerized and not fully cross-linked, which means their molecular chains remain reactive (Zhang et al., 2024). These uncured epoxies (in liquid, solid, or semi-solid form) are typically linear or lightly branched molecules, making them less robust with weaker mechanical and chemical properties, and more prone to degradation.

Curing is a crucial chemical process that transforms epoxy from a liquid or soft state into a rigid solid structure, by forming a robust three-dimensional network of covalently bonded chains (Shundo et al., 2022; Sukanto et al., 2021). This transformation occurs through the reaction of epoxy monomers with curing agents or hardeners, such as aliphatic and aromatic amines, anhydrides, thiols, and acids, leading to the formation of various chemical linkages, including secondary amine (R-NH-CH_2-R'), tertiary amine (R-N(CH_2-CH_3)-CH_2-R'), carboxyl ester (R-(C=O)-O-R'), ether (R-O-R'), and thiol (R-S-R') (Figure 1b). By adjusting the type and ratio of curing agents and controlling the curing temperature and time, epoxy systems can be tailored for various applications, resulting in highly versatile materials (Pradhan et al., 2015). Catalysts, such as Lewis's acids and bases, can also initiate and accelerate homo-polymerization, although these catalysts will not remain in the polymer after curing. The resulting epoxy products typically form ether bridges that exhibit high thermal and chemical resistance; however, they tend to be brittle (Aziz et al., 2024). Therefore, these properties may limit their applicability compared to cured epoxies with hardeners, making them suitable primarily for niche applications.

Epoxy resins, renowned for their versatility, chemical resistance, and excellent mechanical properties, are widely utilized across a diverse array of industries. Their applications span protective coatings, structural adhesives, electronic encapsulants, construction, and advanced composites (Saba et al., 2016). For example, BPA or Bisphenol F (BPF)-based epoxies are commonly used in the coatings and adhesives industry due to their strong adhesion and long-term durability (Tator, 2015). Cycloaliphatic epoxy resins are preferred in the electronics and electrical sectors because of their excellent dielectric properties and resistance to thermal cycling (W. Liu et al., 2012). In the construction industry, epoxy resins serve as structural adhesives, sealants, flooring systems, and concrete repair materials, offering superior adhesion to damp surfaces along with outstanding mechanical performance (Song & Gupta, 2012). In the automotive and aerospace industries, epoxy resins are a critical component in the manufacture of carbon fiber-reinforced polymers (CFRPs), where achieving an optimal balance of strength, durability, and lightweight properties is essential for high-performance structural applications (Hegde et al., 2019; Othman et al., 2019).

1.2 Epoxy-based CFRPs – an essential material in aerospace applications

CFRPs, especially those used in aerospace applications, are exceptionally strong and lightweight materials composed of carbon fibers (CFs) embedded in epoxy resin matrices. One of the most common manufacturing techniques is the use of prepreg materials, in which CFs are pre-impregnated with partially cured epoxy resin and then laid up in molds before being fully cured (Kim et al., 2022; Somarathna et al., 2024). This method ensures precise resin content and consistent fiber distribution. In aircraft, prepreg-based CFRPs, such as HexPly® M21E (Hexcel, USA), are commonly used for primary structural components, including fuselage sections, wing skins, stabilizers, and control surfaces (Sasal et al., 2015; Shetty et al., 2020). Another widely used composite manufacturing method is resin transfer molding (RTM), which falls under the broader category of liquid composite molding (LCM). In RTM, dry CFs are placed into a closed mold, and a low-viscosity epoxy resin is injected to impregnate the fiber (Sozer et al., 2012). The mold is then heated to cure the resin, producing parts with high fiber volume fractions, and the ability to form complex geometries, such as those made with HexFlow® RTM6 (Hexcel, USA) (Parsons et al., 2022). RTM is particularly advantageous for medium- to large-scale production of complex aerospace components, including engine nacelles, access panels, brackets, and aerodynamic fairings (Yonglin Chen et al., 2023). Notably, CFRPs constitute up to 53% (w/w) of the structures in current commercial aircraft e.g., Airbus A350, Boeing 787 (Gondaliya et al., 2016). The primary epoxy resins used in composites are glycidyl-based resins with diglycidyl ether of BPA (DGEBA), and tetraglycidyl methylene dianiline (TGMDA) being the most prevalent commercially (Budelmann et al., 2022; Flippen-Anderson, 1981).

The global demand for CFRPs has been steadily increasing by about 10% over the past decade (Schüppel, 2023; J. Zhang et al., 2023). Consequently, global CFRP waste is projected to reach 20 kt by 2025 (Jin Zhang et al., 2020), with an estimated 7,000 aircraft expected to be retired by 2036 (Bombardier, 2017; Scheelhaase et al., 2022). Furthermore, Airbus, a leading aircraft manufacturer, plans to increase its fleet to nearly 50,000 aircrafts by 2040 (Airbus, 2025), indicating a significant number of aircraft will be retired and potentially enter the waste stream in the coming decades. Hence, there is a pressing concern about how to manage CFRPs disposal effectively, despite advances in current recycling approaches.

1.3 Current recycling technologies for epoxy composites

Recycling is an essential process for reducing waste, minimizing environmental impact, and conserving resources. Despite increasing awareness and advancements in recycling technologies, only 9% of plastic waste is recycled globally (d'Ambrières, 2019). This is especially important for epoxy-based CFRPs (eCFRPs), as CFs are costly to produce due to energy-intensive manufacturing processes, and they retain much of their mechanical strength and stiffness even after use (Nunna et al., 2019). However, the thermoset nature of the epoxy matrix presents significant challenges, as it cannot be remelted or reshaped. Consequently, industry efforts primarily focus on recovering CFs from epoxy matrices while minimizing damage to preserve fiber quality. Nevertheless, it is also beneficial when the degradation products of epoxy can be reused. Current recycling methods include mechanical, thermal, and chemical treatments, each offering distinct advantages and limitations (Figure 2).

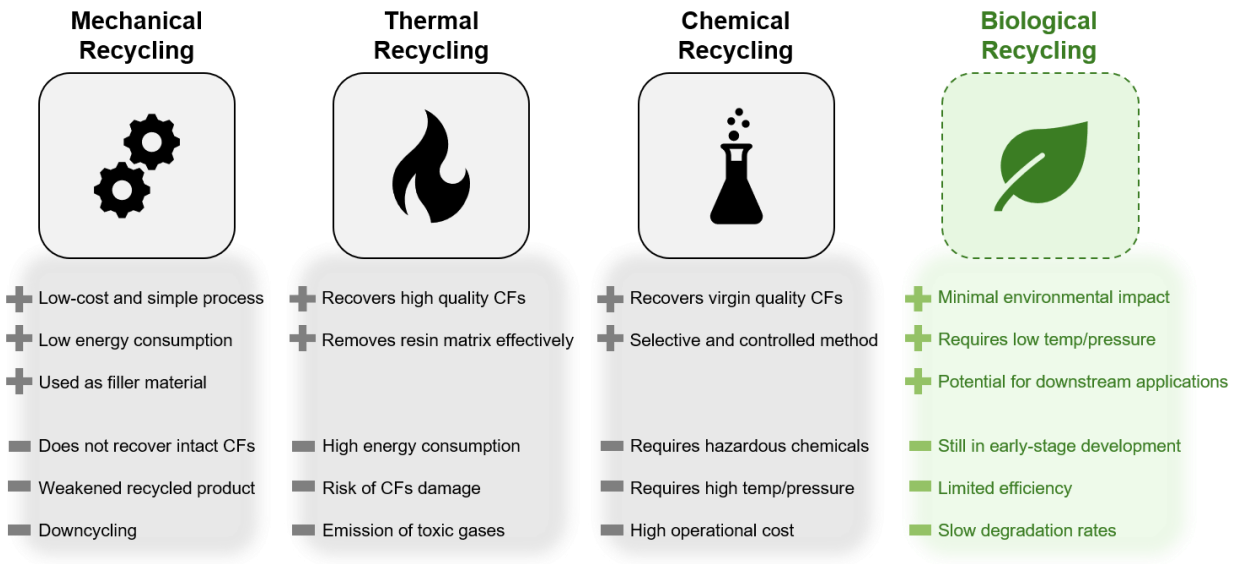

Figure 2. Current epoxy composite recycling techniques for the recovery of high-quality carbon fibers (CFs), highlighting their benefits and limitations, with biological recycling emerging as a promising, eco-friendly alternative.

1.3.1 Mechanical recycling

Mechanical recycling involves cutting and grinding composite materials into small pieces or powder, which can then be reused as filler materials in low-performance applications (Thamizh Selvan et al., 2021; Yang et al., 2012). Although this method is cost-effective and straightforward,

it often results in a significant reduction of fiber properties, making it generally unsuitable for structural reuse. The recovered CFs are typically shorter and may contain residual epoxy, and separating the fibers from the epoxy after grinding proves to be challenging (Martínez-Franco et al., 2024). Mechanically recycled CFRPs are often incorporated into new materials at low ratios, primarily to contribute to overall mass reduction, although this approach may compromise the mechanical performance of the final product (Asokan et al., 2009).

1.3.2 Thermal recycling

Thermal recycling employs high temperatures, typically between 400 and 600 °C, to thermally decompose the resin, leaving behind recovered CFs. However, the intense heat can damage the fiber surface and diminish their mechanical performance (Manis et al., 2015). Pyrolysis, a related technique, decomposes the resin in an inert atmosphere (often nitrogen) at temperatures ranging from 400 to 700 °C. This method better preserves fiber integrity, maintaining approximately 90% of the fibers' tensile strength (Kim et al., 2017). Despite this advantage, pyrolysis often leaves char residues on the fibers, necessitating additional cleaning steps (Soni et al., 2021). In the absence of oxygen, the epoxy resin does not burn but instead breaks down into smaller molecules such as gases, oils, and char, making separation of byproducts challenging. While thermal recycling can retrieve high-quality CFs, it is generally considered unfavorable due to its high energy consumption and the potential release of hazardous waste and pollutants during the process (Batista et al., 2024).

1.3.3 Chemical recycling

Among all recycling methods, chemical recycling, often referred to as solvolysis, holds the most promise for recovering CFs while yielding useful byproducts from the resin (Liu et al., 2022). This approach involves using solvents such as water, alcohols, acids, or supercritical fluids, to penetrate the cross-linked epoxy matrix and cleave covalent bonds, thereby breaking down the epoxy at moderate to high temperatures and pressures.

Chemical recycling of epoxy can be conducted at temperatures below 120 °C; however, it typically requires the use of hazardous solvents such as strong acids (nitric acid, sulfuric acid), as well as solvents like acetone and dimethylformamide (DMF), often combined with oxidizing agents such

as hydrogen peroxide (H_2O_2) to enhance the reaction through free radical generation (Das et al., 2018; Feraboli et al., 2012; Li et al., 2012; Ma et al., 2009). CFRPs are usually thick and multilayered, which impedes solvent penetration below their glass transition temperature (T_g), making the process longer and less efficient. To address this, a common pre-treatment involves swelling the composites at temperatures above T_g for a short duration, such as treating with acetic acid at around 180 °C for 6 hours, to weaken interlayer adhesion and increase surface access (Wang et al., 2015). This pre-treatment facilitates more efficient subsequent solvent penetration, reducing overall treatment time. Chemical recycling at low temperatures and atmospheric pressure offers advantages, such as reduced energy consumption; however, it often takes a prolonged duration, risking damage to the carbon fibers (Dang et al., 2002). Additionally, the use of harsh chemicals is costly, generates hazardous waste, and presents safety concerns for personnel.

In recent developments, modern approaches employ supercritical fluids, such as supercritical water, alcohols, or acetone, operating at high temperatures (>230 °C) and pressures (> 5 Mpa) to accelerate polymer decomposition efficiently and in shorter periods (Gong et al., 2015). Supercritical water, with its dielectric constant comparable to that of organic solvents, can penetrate the epoxy resin effectively, enabling breakdown of the matrix (Patrick et al., 2001). Nonetheless, this method requires high-pressure equipment and costly reactors, and the cleavage of epoxy bonds can occur randomly. Alcohols like methanol, propanol, butanol, and ethanol are used to selectively cleave ester bonds in anhydride-cured epoxy systems, whereas their effectiveness in amine-cured epoxy varies, often resulting in non-specific cleavage (Okajima et al., 2014; Yan et al., 2013). These solvents typically operate at lower pressures than supercritical water but are prone to self-reaction and decomposition, which complicates recycling and reuse efforts (Huang et al., 2017). Catalysts such as potassium hydroxide (KOH) are sometimes employed to enable milder reaction conditions (Y. Liu et al., 2012). Furthermore, combining water with alcohol, acetone, or carbon dioxide under supercritical conditions holds potential to improve the efficiency of epoxy decomposition (Oliveux et al., 2015).

Overall, chemical recycling typically requires high temperatures and pressures, and significant challenges remain in identifying environmentally friendly solvents that can operate effectively under milder conditions (Cheng et al., 2017; Keith et al., 2019). Despite the progress made, there

is still a lack of a truly sustainable, and biologically inspired approach for the degradation of eCFRPs (Klose et al., 2023).

1.4 Advances in biodegradation of epoxy resins

Biological recycling has advantages over conventional methods, as it operates under mild conditions, reducing energy use and environmental impact by utilizing microorganisms or enzymes to break down polymers into smaller components (Figure 2). The resulting enzymatic byproducts can also be used in downstream processing or upcycling, supporting a sustainable, circular economy (Zhu et al., 2022). Enzymatic solution have already been identified for polyester-based polymers such as PET and PUR, which can be readily degraded by discovered enzymes (see PAZy database: https://www.pazy.eu/) (Buchholz et al., 2022). However, no such solutions currently exist for polymers with saturated hydrocarbon backbones like PE, PP, and PVC. Similarly, biodegradation of epoxy polymers remains highly challenging due to their synthetic nature, characterized by extensive cross-linking, stable chemical motifs (such as ethers and tertiary amines), and the absence of easily hydrolysable linkages. These features make epoxy polymers highly resistant to biodegradation. Consequently, this resistance remains a major challenge, as no microorganisms or enzymes have yet been conclusively shown to effectively degrade epoxy materials (Klose et al., 2023).

1.4.1 Microorganisms involved in epoxy degradation

In most studies, BPA- or DGEBA-based epoxy has been used primarily to identify potential microorganisms capable of degrading the polymer (Table 1). For example, co-cultivation of *Rhodococcus rhodochrous* and *Ochrobactrum anthropi*, isolated from soil near an epoxy-producing facility, enabled these bacteria to utilize low-viscosity Araldite® LY 5052 resin as the sole carbon source for growth (Eliaz et al., 2018). Given that this resin was in an uncured form, it appears more susceptible to microbial degradation. Similarly, studies utilizing BPA, a pre-epoxy derivative monomer, have demonstrated that certain microorganism (e.g., *Bacillus* sp., *Sphingomonas* sp.) and enzymes (e.g., laccases) can effectively convert or oxidize this precursor (Nicolucci et al., 2011; Oh & Choi, 2019; Xiong et al., 2017; Yang et al., 2014).

Microbial activity on fully cured epoxy coatings has also been explored. Marine bacteria such as *Pseudomonas putida* (Wang et al., 2016), *Bacillus flexus* (Deng et al., 2019), and *Pseudomonas aeruginosa* (S. Zhang et al., 2023) have demonstrated the ability to decrease the corrosion resistance of epoxy-coated steel. After one month of immersion in seawater, biofilm formation by these bacteria was observed, often with tiny holes in the coating. Fourier-transform infrared spectroscopy (FTIR) analyses revealed that *P. putida* facilitated oxidation of hydroxyl (C-OH) groups, while *B. flexus* was capable of modifying aromatic rings and epoxy groups. *P. aeruginosa* caused a more pronounced reduction in C-O-C and C-O groups in the amine-cured epoxy. Sulfate-reducing bacteria (SRB), e.g. *Desulfovibrio desulfuricans*, have also been shown to deteriorate the epoxy coating on steels (Tambe et al., 2016). SRB reduces sulfate to sulfide, which reacts with iron in steel to form ferrous sulfide, a black precipitate that signals coating decomposition. While evidence suggests that marine bacteria and SRB could contribute to epoxy corrosion, it remains unclear whether this modification is due to direct microbial breakdown or mediated through environmental factors. The saline and chemically harsh marine environment may accelerate epoxy corrosion, impairing its protective function. Biofilm formation can further hasten deterioration, likely through the secretion of organic acids and corrosive metabolites by microorganisms (Pal & Lavanya, 2022).

Epoxy coatings used for protection often contain additives, pigments, and fillers that enhance adhesion, durability, and chemical resistance. These components can provide nutrients or create environments conducive to microbial growth, especially if they include esters or other vulnerable functional groups. For example, a study on epoxy coatings applied to marble in Milan Cathedral (Duomo di Milano) identified diverse microorganisms, including bacteria such as *Bacillus*, *Pseudomonas*, and *Micrococcus*, as well as fungi like *Alternaria* and *Cladosporium*, on DGEBA-based epoxy surfaces (Cappitelli et al., 2007). While epoxy presence was confirmed, microbial degradation was likely driven more by other protective agents, such as poly(isobutylmethacrylate), which are more susceptible to microbial attack due to ester bonds. Biodegradation assays showed that fungi could degrade poly(laurylmethacrylate) and poly(isobutylmethacrylate) but not epoxy resin, indicating that deterioration was primarily due to these ester-linked agents rather than the epoxy itself.

Table 1. Reported microorganisms and enzymes involved in epoxy degradation. Table adapted from (Klose et al., 2023).

	Epoxy type	Tested resin	Biocatalyst(s)	Experimental settings	Analytics	References
Microorganisms	Precursor	Bisphenol A	*Sphingomonadaceae* sp. (*Sphingobium*, *Novosphingobium*, and *Sphingopyxis*)	25 °C aerobically for 70 days	HPLC	(Oh & Choi, 2019)
	Precursor	Bisphenol A	*Bacillus, Thiobacillus, Phenylobacterium, and Cloacibacterium*	25 °C aerobically for 7 weeks	GC-MS	(Xiong et al., 2017)
	Precursor	Bisphenol A	Gammaproteobacteria and Alphaproteobacteria	25 °C aerobically for 4 days	HPLC	(Yang et al., 2014)
	Uncured epoxy	Araldite® LY 5052 (Huntsman Corp., USA) (DGEBA-based epoxy)	*Rhodococcus rhodochrous Ochrobactrum anthropi*	30 °C aerobically for 1 week	Turbidity measurement SEM, LC-MS	(Eliaz et al., 2018)
	Cured epoxy coating	Epoxy vanish (DGEBA-based epoxy)	*Pseudomonas putida*	26 °C aerobically for 1 month in seawater	Coating permeability analysis EIS, Contact angle test, SEM, FTIR,	(Wang et al., 2016)
	Cured epoxy coating	Epoxy vanish (DGEBA-based epoxy)	*Bacillus flexus*	26 °C aerobically for 1 month in seawater	EIS, SEM, FTIR	(Deng et al., 2019)
	Cured epoxy coating	BADGE hardened with Jeffamine D230 hardener (DGEBA-based epoxy, amine hardener)	*Pseudomonas aeruginosa* (1A00099)	30 °C aerobically for 2 weeks in marine media	SEM, FTIR, EIS, Contact angle test	(S. Zhang et al., 2023)
	Cured epoxy coating	Epoxy-Polyamide/Steatite (not specified epoxy, amine hardener)	*Desulfovibrio desulfuricans* (NCIM 2047)	37 °C anaerobically for 3 days	Zone-inhibition, SEM, EIS, Adhesion test	(Tambe et al., 2016)

	Epoxy type	Tested resin	Biocatalyst(s)	Experimental settings	Analytics	References
Microorganisms	Cured epoxy coating	DGEBA-based epoxy coated on marble	Bacteria: genera *Bacillus, Brevibacillus, Micrococcus, Staphylococcus, Kocuria, Pseudomonas, Agrobacterium and Ochrobacter.* Fungi: *Alternaria* sp. *Cladosporium* spp.	Polluted area samples since 1972	X-ray Diffraction, SEM, FTIR, Fluorescence microscope, FISH, Biodegradation assay (ASTM method)	(Cappitelli et al., 2007)
	Epoxy composites	Epoxy Hercules 3501-6 (amine-cured epoxy resin)	*Aspergillus versicolor* *Cladosporium cladosporioides*	30 days	EIS, SEM, Mechanical testing	(Gu et al., 1997)
	Cured epoxy	Epoxy and epoxy-silicone blends (DGEBA-based epoxy, amine hardener)	*Bacterium Te68R* *Microbacterium sp. (strain MK3)* *Pseudomonas putida*	37 °C aerobically for 15 days	FTIR, TG-DTG-DTA	(Negi et al., 2009)
	Cured epoxy	Epoxy resin L + hardener GL2 (Suter Kunststoffe, Switzerland) (DGEBA-based epoxy, amine hardener)	*Ganoderma adspersum* Trichoderma harzianum ITEM908 Aspergillus calidoustus Kw18-1 Variovorax sp. Methyloversatilis discipulorum FAM1	Microcosms: 1-9 months Microbial water: 3 months, >3 years	Weight loss, Contact angle test, Mechanical testing, FTIR, ESEM	(Pardi-Comensoli et al., 2022)
Enzymes	Precursor	Bisphenol A, Bisphenol B Bisphenol F, Tetrachlorobisphenol A	Laccase (*rametes versicolor*) Tyrosinase (mushroom)	25 °C aerobically for 90 minutes in citrate buffer pH 5	HPLC	(Nicolucci et al., 2011)
	Tertiary amine epoxy model substrate	N,N-bis(2-hydroxypropyl)-p-toluidine (NNBT) derived from Hexflow® RTM6	Unspecific peroxigenases (UPOs): PaDa-I (*Agrocybe aegerita*) GroGu (*Psathyrella aberdarensis*) rMroUPO (*Marasmius rotula*) PabUPO-II (*Psathyrella aberdarensis*)	30 °C aerobically for 2 hours in potassium phosphate buffer pH 6	GC-MS	(Dolz et al., 2022)

One of the first investigations into the biodegradation of eCFRPs, primarily used in aerospace and advanced composite applications, was conducted by Gu et al. (1997). Hercules 3501-6 epoxy (Magna, USA) was susceptible to colonization by a fungal consortium, comprising *Aspergillus versicolor*, *Cladosporium cladosporioides*, and *Chaetomium* sp. after 30 days. Fungal activity caused pore formation and weakened fiber-resin bonds, potentially utilizing both the epoxy matrix and chemical additives as substrates.

DGEBA-based amine-cured epoxy has also been examined. Negi et al. (2009) demonstrated that bacterial consortia, comprising Bacterium Te68R PN12, *Microbacterium* sp. MK3, and *P. putida* MK4, can utilize the aforementioned epoxy as the primary carbon source, with notable weight loss observed after 15 days. The presence of filler in the material was also noted. FTIR analysis showed significant reductions in functional groups, such as C–N, C–OH, and C–O, in treated samples. Thermal stability tests at 325 °C showed a 34% weight loss for epoxy treated with the consortium, compared to 19% in the control epoxy. A study by Pardi-Comensoli et al. (2022) highlighted fungi' potential in depolymerizing DGEBA-based amine-cured epoxy. *Ganoderma adspersum* reduced the polymer's hydrophobicity over 9 months, indicating surface modification. A consortium of fungi (*Trichoderma harzianum*, *Aspergillus calidoustus*) and bacteria (*Variovorax* sp., *Methyloversatilis discipulorum*) colonized epoxy samples immersed for over three years in freshwater, with scanning electron microscopy (SEM) revealing surface cracks and holes.

Although studies have shown that microorganisms can colonize cured epoxy and possibly alter its surface through metabolic activity, they have not demonstrated clear evidence of epoxy polymer degradation at meaningful (micro- or millimolar) levels. Unlike the breakthrough discovery of *Ideonella sakaiensis* for PET degradation (Yoshida et al., 2016), no comparable microorganisms have yet been identified for efficient epoxy breakdown.

1.4.2 Enzymes involved in epoxy degradation

Dolz et al. (2022) presents the first novel insights into enzymes involved in epoxy degradation (Table 1). To understand enzyme mechanisms, they used an epoxy model substrate, N,N-bis(2-hydroxypropyl)-*p*-toluidine (NNBT), derived from Hexflow® RTM6, instead of cured epoxy resins. NNBT contains key motifs such as a tertiary amine, and is soluble in organic solvents, reducing hydrophobicity and enhancing enzymatic accessibility. GC-MS confirmed that UPOs

(EC 1.11.2.1) catalyze N-dealkylation of NNBT. When 5 mM NNBT was incubated for 2 hours, the conversion rates to the secondary amine were 12%, 9%, 8%, and 4% for PaDa-I (an evolved long-UPO mutant of *Agrocybe aegerita*), GroGu (an evolved long-UPO mutant of *Psathyrella aberdarensis*), rMroUPO (short-UPO from *Marasmius rotula*), and PabUPO-II (long-UPO), respectively. Though no enzyme capable of degrading epoxy polymers has been definitively identified thus far, some already discovered enzymes might have shown potential in modifying or breaking down related chemical structures. In particular, those involved in oxidative or reductive transformations could be harnessed to target the chemically resistant nature of epoxy resins.

1.5 Oxidoreductases as potential enzymes for epoxy biodegradation

Epoxy polymers are characterized by a cross-linked network of aromatic rings and ether bonds, similar to lignin, a complex biopolymer found in plant cell walls (Ralph et al., 2019). Due to these structural similarities, ligninolytic enzymes, such as peroxidases and laccases, are of interest for their potential to catalyze the breakdown of epoxy-based materials (Kumar & Chandra, 2020). These enzymes belong to the oxidoreductases (EC 1) family, which catalyzes oxidation-reduction reactions involving electron transfer (May & Padgette, 1983). Their catalytic versatility and substrate promiscuity make oxidoreductases attractive candidates for modifying non-hydrolysable polymers (e.g., PE, PP and PS) by randomly oxidizing their long chains into small molecules (Han et al., 2024).

1.5.1 Heme peroxidases

Heme peroxidases are heme-containing enzymes that use H_2O_2 as an oxidizing agent to catalyze the oxidation of a wide range of substrates with high redox potentials, including phenolic and non-phenolic lignin-like compounds (Vlasits et al., 2010). The peroxidase-catalase superfamily, formerly known as the superfamily of bacterial, fungal, and plant heme peroxidases, is classified into three classes (Zámocký et al., 2014). Class I includes intracellular peroxidases such as cytochrome c peroxidase (Ccp; EC 1.11.1.5). Class II extracellular fungal peroxidases, such as lignin peroxidase (LiP; EC 1.11.1.14), manganese peroxidase (MnP; EC 1.11.1.13), and versatile peroxidase (VP; EC 1.11.1.16), play a crucial role in lignin decomposition. These enzymes are primarily found in white rot fungi (e.g., *Phanerochaete chrysosporium* and *Pleurotus ostreatus*),

and they have also been reported to break down plastics (Jha, 2019; Temporiti et al., 2022). Class III comprises secretory plant peroxidases, exemplified by the well-studied horseradish peroxidase (HRP; 1.11.1.7). Extracellular heme peroxidases, including those in class II and class III, share highly conserved structural features. These enzymes are monomeric glycoproteins with a predominantly alpha-helical structure surrounding a heme pocket. This pocket contains a protoporphyrin IX ring with a central Fe^{3+} ion, stabilized by four conserved disulfide bridges and two Ca^{2+}-binding sites (Figure 3a) (Battistuzzi et al., 2010).

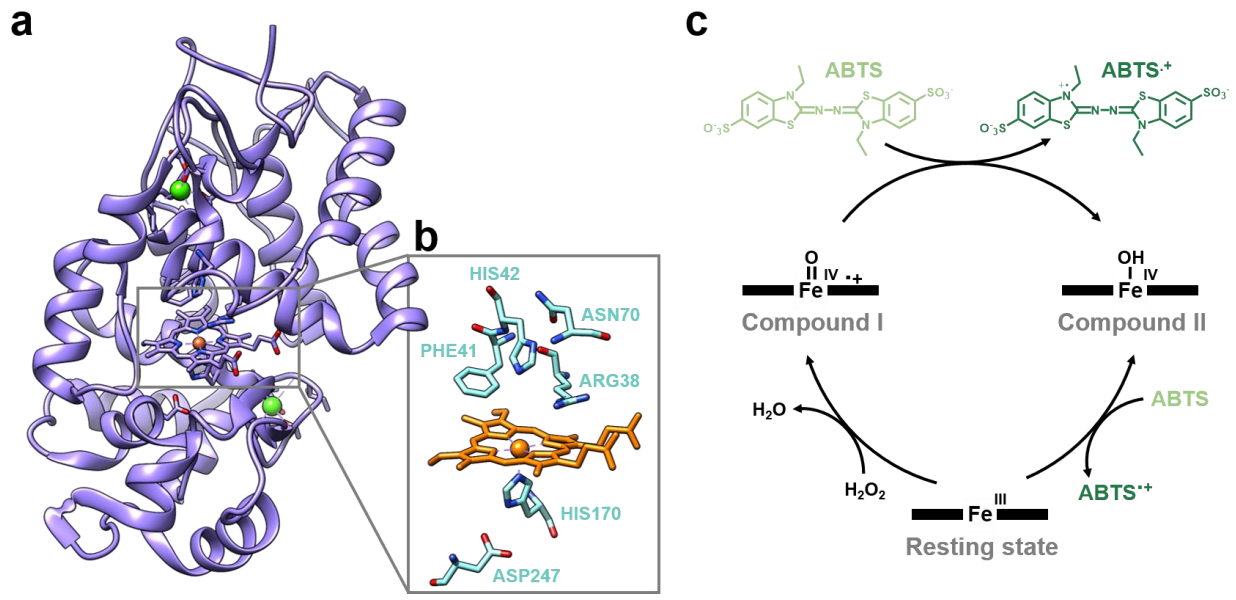

Figure 3. Heme peroxidase structure and its catalytic mechanism. (a) 3D crystal structure of horseradish peroxidase isoenzyme C (PDB: 1H5A; (Berglund et al., 2002)) depicts the heme group in the center, surrounded by α-helical structures of the enzyme. Two calcium atoms are shown in green. (b) The protoporphyrin IX ring with Fe^{3+} ion (orange) is coordinated with key amino acid residues, specifically HIS42 and ARG38, which are the distal residues essential in H_2O_2 activation. (c) The catalytic mechanism of HRP involves the heme group with ABTS (2,2'-azino-bis(3-ethylbenzothiazoline-6-sulfonic acid)) as a reducing substrate. Figure modified from (Veitch, 2004).

The catalytic cycle of these enzymes follows two one-electron redox reactions (Figure 3c) (Veitch, 2004). First, the heme protein of the enzyme reacts with H_2O_2, which is reduced to water, while the enzyme itself is oxidized to compound I [Fe(IV)=O $Por^{\cdot+}$]. Compound I then proceeds through a one-electron reduction to form compound II [Fe(IV)-OH Por], while oxidizing a substrate, such as 2,2′-azinobis (3-ethylbenzothiazoline-6-sulfonic acid) (ABTS). In the final step, compound II completes another one-electron reduction, returning to its resting state [Fe(III) Por],

simultaneously oxidizing another substrate. The distal histidine and arginine residues near the heme group play essential roles in facilitating H_2O_2 activation, leading to the formation and stabilization of compounds I and II (Figure 3b) (Ozaki et al., 2001).

LiP is effective at oxidizing high redox potential non-phenolic aromatic compounds, while MnP requires Mn^{2+} ions to oxidize phenolic substrates. VP, which combines catalytic features of both LiP and MnP, can act on a broader range of substrates, including phenolic and non-phenolic compounds (Falade et al., 2017; Morales et al., 2012). Given that lignin is the primary substrate for these enzymes, their substrate binding pockets are large and broad, enabling them to accommodate bulky molecules (Mester et al., 2001). Plant peroxidases, including HRP, are mainly involved in removing H_2O_2 from chloroplasts and cytosol and in oxidizing toxic compounds (Pandey et al., 2017). Typical substrates for HRP are small phenolic and aromatic compounds, and its substrate-binding pocket is relatively compact, making it well-suited for smaller molecules (Henriksen et al., 1998; Navapour et al., 2014).

1.5.2 Multicopper oxidases (MCOs), including laccases

MCOs are a diverse group of enzymes that catalyze the oxidation of various substrates, including phenolic compounds, amines, and aromatic molecules. They achieve this by utilizing copper ions to facilitate the reduction of molecular oxygen to water (Reiss et al., 2013). These enzymes are found across a broad range of organisms, including fungi, bacteria, plants, and animals, and they play vital roles in processes such as lignin degradation, metal homeostasis, bioremediation, and defense mechanisms. Examples of MCOs include laccases (EC 1.10.3.2), ascorbate oxidases (EC 1.10.3.3), ceruloplasmin (EC 1.16.3.1), and laccase-like MCOs, such as cuprous oxidase (EC 1.16.3.4), including CueO from *E. coli*, which functions in copper homeostasis (Sakurai & Kataoka, 2007).

To perform catalytic function, MCOs depend on copper ions distributed across two active sites: at least one type I (T1) copper and one type II (T2) copper, along with two type III (T3) copper ions. The T1 copper site, located in the mononuclear copper center (MNC), is where substrate oxidation occurs. The T2/T3 copper center, known as the trinuclear copper center (TNC), is responsible for dioxygen reduction (Mot & Silaghi-Dumitrescu, 2012). These copper ions are generally coordinated by histidine residues; in the case of the T1 site, cysteine is also involved in bridging

the copper ions. According to structure predictions, cupredoxin-like domains are arranged in three different ways: two-domain (2dMCO), three-domain (3dMCO), and six-domain (6dMCO) structures (Figure 4) (Komori & Higuchi, 2010).

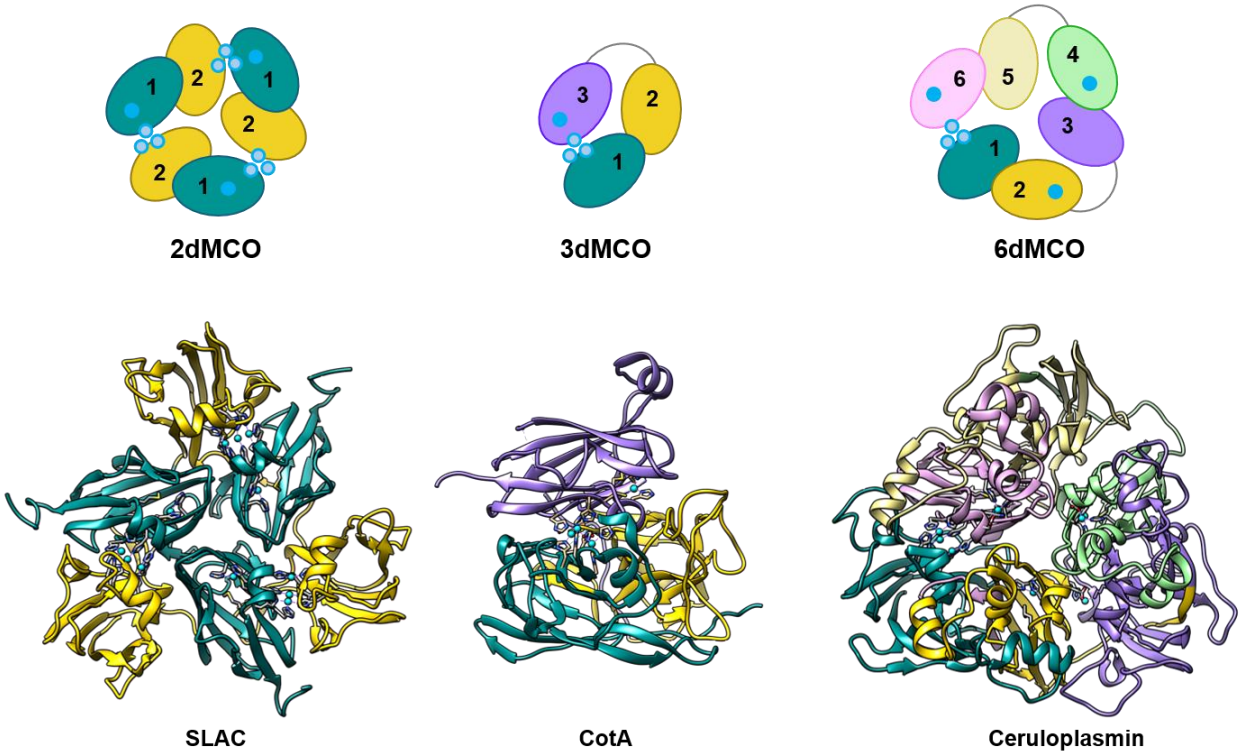

Figure 4. Structures of multicopper oxidases (MCOs). Structures of 2dMCO, 3dMCO, and 6dMCO. 2dMCO has two domains arranged in a trimeric structure, while 3dMCO and 6dMCO form single-chain proteins. Type I copper ion (T1) is depicted as a single blue circle and is located within one domain. Type II and type III copper ions (T2/3) are grouped together at the interface between two domains. 3D crystal structure of SLAC (small laccase; PDB: 3CG8; (Skálová et al., 2009)), CotA (4Q89; (Liu et al., 2016)), and ceruloplasmin (5N0K; (Samygina et al., 2017)) illustrate the MCO architecture, each representing distinct structural classes. The copper ions are depicted in blue, highlighting their positions within the active sites of the multi-copper domains. Figure modified from (Komori & Higuchi, 2015).

The most common and extensively studied form, 3dMCOs—such as bacterial laccase CotA from *Bacillus subtilis* and fungal laccase TvL from *Trametes versicolor*—feature three domains, with the MNC located in one domain and the TNC at the interface between two domains (Piontek et al., 2002). 2dMCOs are often found in small laccases (SLAC) or laccase-like enzymes from certain *Streptomyces* species. These typically form homo-trimers arranged in a hexagonal configuration, with each monomer containing two domains: the MNC in one domain and the TNC at the interface between the two domains (Komori et al., 2009). 6dMCOs, such as ceruloplasmin, contain multiple

MNC domains, with the TNC located at the interfaces between domains (Harris, 2019). Unlike 3dMCOs, which primarily facilitate single-site oxygen reduction and substrate oxidation, 6dMCOs can support multiple substrate oxidation events and may enable cooperative or sequential electron transfer processes.

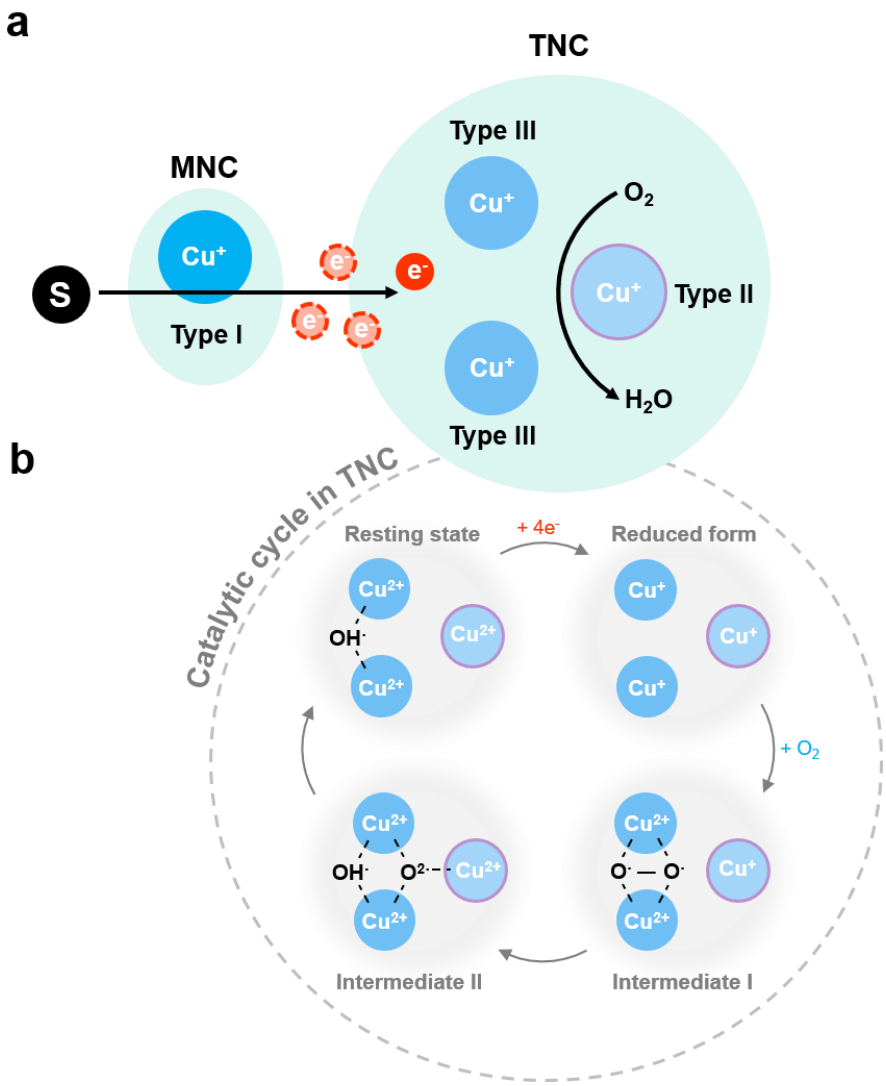

Figure 5. Catalytic mechanism of MCOs. (a) The catalytic mechanism of MCOs involves two copper active sites: mononuclear center (MNC) and trinuclear center (TNC). The enzyme catalyzes the oxidation of substrates (S), coupled with four-electron (e^-) reduction of O_2 to H_2O. (b) The O_2 reduction mechanism at the TNC site. Figure modified from (Komori & Higuchi, 2015).

A crucial step in the MCO redox cycle involves the four-electron reduction of O_2 (Komori & Higuchi, 2015) (Figure 5a). The enzyme first oxidizes a substrate, transferring an electron to T1

copper site. This process repeats four times per O_2, providing the four electrons for complete oxygen reduction. The T1 copper subsequently transfers these electrons to the TNC. The reduced TNC enables stable binding of O_2, forming a di-copper peroxide intermediate (Intermediate I) after a two-electron reduction (Figure 5b). Another two-electron reduction leads to Intermediate II, with the T2 copper assisting in O–O bond cleavage. Finally, O_2 is fully reduced to two water molecules through four sequential electrons, occurring in two two-electron steps.

Enzymes involved in the partial oxidation of PE have been reported to be laccases (Buchholz et al., 2022). They have potential for oxidizing high redox potential substrates, such as synthetic dyes, lignin, and environmental pollutants, as they have evolved naturally and can be further engineered to extend their oxidative activity through the laccase-mediator system (LMS), which uses mediators as electron shuttles to enhance oxidation (Jin et al., 2016; Könst et al., 2013). Although bacterial laccases typically have lower redox potentials than fungal ones, they can benefit from the LMS, which enables them to effectively target high redox potential substrates despite their inherent limitations (Loi et al., 2021). Mediators are oxidized by an enzyme into stable radicals, which then diffuse and oxidize target substrates while being regenerated. This mechanism allows laccases to indirectly oxidize larger substrates outside their active site (Obleser et al., 2022). Mediators are classified into three groups based on their action mechanism. Class I (electron transfer, ET) mediators are oxidized by laccase into stable radicals or cations that directly oxidize substrates, e.g., ABTS, guaiacol. Class II (hydrogen atom transfer, HAT) mediators are oxidized to radicals that abstract hydrogen atoms from substrates, e.g., 1-hydroxybenzotriazole (HBT) (Barreca et al., 2004). Class III (ionic or covalent mechanism, IC) mediators form reactive intermediates that undergo chemical reactions such as nucleophilic attack or covalent bonding, e.g., (2,2,6,6-tetramethylpiperidin-1-yl)oxidanyl (TEMPO) (Bailey et al., 2007). Mediators are also classified by structure (aromatic amines, phenolics, nitroxyl radicals), origin (synthetic or natural mediators), and redox potential (Christopher et al., 2014; Fang et al., 2020).

1.6 Aim of the study

As there is a lack of bio-based solutions for recycling eCFRPs, this work aimed to develop an enzymatic treatment to break down this recalcitrant polymer, with an additional chemical step incorporated to enhance and accelerate the overall process (Figure 6). The primary goal was to recover carbon fibers while obtaining defined products from epoxy decomposition to facilitate downstream processing. To achieve this, potential bacterial laccases derived from the beetle metagenome were biochemically characterized, and their activities were screened against three epoxy model substrates containing tertiary amine motifs, representing the repeating units of RTM6, an amine-cured epoxy commonly used in aerospace applications. HRP was also employed as a model heme peroxidase for comparison with laccases, due to its commercial availability and well-characterized structure. Another part of this work was to assess alternative mild pre-treatments to replace the harsh standard methods typically involving sulfuric acid and H_2O_2, and to determine whether these alternatives can retrieve clean carbon fibers. Ultimately, the combination of pre-treatment with enzymes was assessed to determine if it enhances the enzyme's ability to decompose epoxy more effectively.

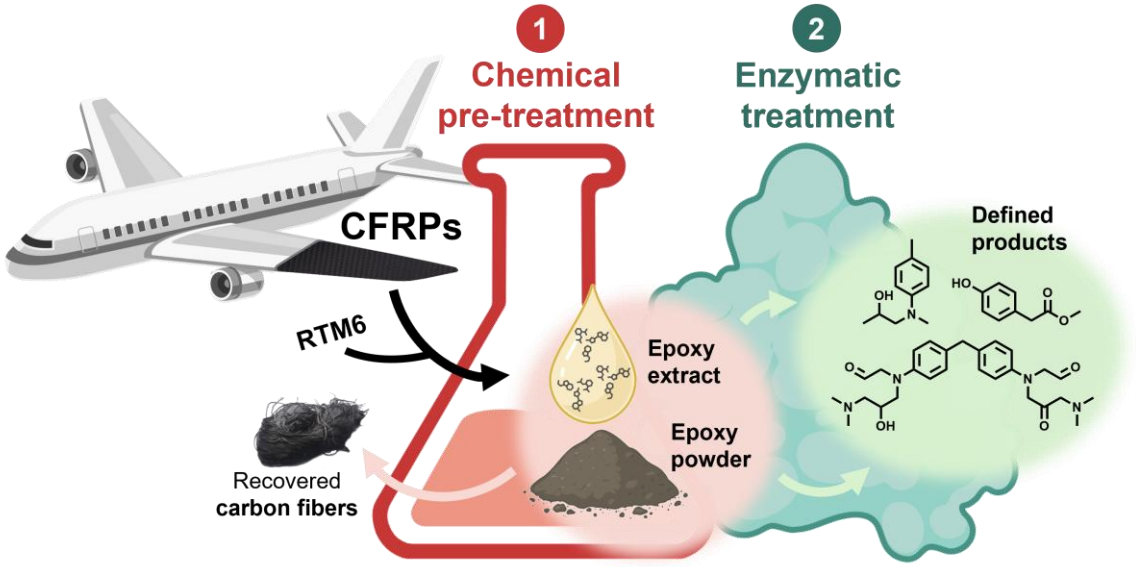

Figure 6. The development of a chemo-enzymatic oxidative treatment method for eCFRPs is a goal of this study. Promising candidates for pre-treatment and enzymes were initially screened using eCFRPs and epoxy model substrates. The most effective pre-treatment was able to recover clean carbon fibers for potential reuse. RTM6 epoxy resin, commonly used in aircraft applications, was tested in the chemo-enzymatic oxidation process. The epoxy extract and residual powder from the pre-treatment were then treated with the selected enzyme, which can further oxidize and modify the defined low-molecular-weight epoxies.

2 MATERIALS AND METHODS

2.1 Bacterial stains, constructs, and cultivation conditions

2.1.1 Bacterial strains, vectors, and constructs

The *E. coli* strains were selected to clone and express genes coding for multi-copper oxidases (MCOs) or laccases (Table 2). The vector pET21a(+) was employed, featuring a T7 promoter for the expression of laccase-associated genes, an ampicillin resistance gene to ensure selection pressure, and a His-6 tag that facilitates purification through Ni-NTA affinity chromatography (Table 3). The constructs used were obtained from the culture collection at the Department of Microbiology and Biotechnology at the University of Hamburg, Hamburg, Germany (Table 4). The laccase genes were extracted and sequenced from metagenomic data from the bark beetle *Ips typographus*, with gene IDs: *ips2204* (Ga0063521_10002204), *ips14138* (Ga0063521_100014138), and *ips24328* (Ga0063521_100024328), which are stored in the Integrated Microbial Genomes (IMG) database (Markowitz et al., 2012). For further details, see the dissertation by Schorn (2020). In this work, these laccases were renamed from Ips2204, Ips14138, and Ips24328, to ItL-01, ItL-02, and ItL-03, respectively.

Table 2. Base strains used in this study.

Strain	Genotype	Reference
E. coli DH5α	**Cloning and subcloning strain:** F⁻ Φ80 *lac* ZΔM15 Δ *(lac* ZYA- *arg* F*)* U169 *rec* A1 *end* A1 *hsd* R17 (r_k^-, m_k^+) *pho* A *sup* E44 *thi* -1 *gyr* A96 *rel* A1 λ⁻	Invitrogen, Germany
E. coli BL21(DE3)	**Transformation and expression strain:** *fhuA2 [lon] ompT gal (λ DE3) [dcm] ΔhsdS λ DE3 = λ sBamHIo ΔEcoRI-B int::(lacI::PlacUV5::T7 gene1) i21 Δnin5*	NEB, Germany
E. coli T7 Shuffle	**Expression strain for protein purification:** *fhuA2 lacZ::T7 gene1 [lon] ompT ahpC gal λatt::*pNEB3-r1-*cDsbC* (Spec^R*, lacI^q) ΔtrxB sulA11 R(mcr-73::miniTn10--*Tet^S)2 [dcm] *R(zgb-210::Tn10 --*Tet^S) *endA1 Δgor Δ(mcrC-mrr)114::IS10*	NEB, Germany

Table 3. Vector used in this study.

Vector	Properties	Reference/Source
pET21a(+)	**Expression vector:** lacI, AmpR, T7-lacpromoter, C-terminal His6-tag coding sequence	Novagen/Merck, Germany

Table 4. Constructs used in this study.

Strain	Construct	Characteristics	Source
E. coli BL21 (DE3)	pET22b-SDM::*ips2204*::StrepII	StrepII-tag containing MCO	AG Streit
	pET22b::*ips14138*::StrepII	StrepII-tag containing MCO	AG Streit
	pET22b-SDM::*ips24328*::StrepII	StrepII-tag containing MCO	AG Streit
	pET21a::*ItL-01*	His-6-tag containing MCO	This work
	pET21a::*ItL-02*	His-6-tag containing MCO	This work
	pET21a::*ItL-03*	His-6-tag containing MCO	This work
E. coli T7 SHuffle	pET22b::*cueo*::StrepII	StrepII-tag containing MCO	AG Streit
	pET21a::*CueO*	His-6-tag containing MCO	This work

2.1.2 Cultivation of *E. coli* strains

Unless otherwise indicated, *E. coli* stains were cultured in lysogeny broth (LB) medium (Bertani, 1951) (Table 5) supplemented with a final concentration of 100 µg/mL ampicillin (Carl Roth, Germany) and were incubated at 37 °C overnight. For the preparation of LB agar plates, 15 g of agar was added to 1 L of LB broth before autoclaving.

Table 5. LB broth

Components	Quantity
Yeast extract	5 g/L
Tryptone	10 g/L
NaCl	10 g/L
(agar	15 g/L)

Glycerol stocks for long-term storage of cultures were prepared by mixing 1 mL of the overnight inoculum with 500 µL of 86% glycerol. The bacterial stocks were stored at -70 ºC.

2.2 DNA techniques

2.2.1 Restriction enzyme cloning

The nucleotide sequences of the laccases were synthesized following codon usage optimization for *E. coli* (MWG Eurofins, Germany) and was subsequently inserted into pET22b(+) expression vectors containing a StrepII-tag for purification (Schorn, 2020). While this tag allows for purification via fast protein liquid chromatography (FPLC) with very high purity, the procedure is time-consuming and relatively costly. Therefore, the laccases were cloned to remove the StrepII-tag and instead incorporate a His-tag, enabling quicker and more cost-effective purification.

Table 6. Primers used in this study.

Primer	Sequence (5' → 3')	Length [bp]	GC content [%]	Source
T7_prom	TAATACGACTCACTATAGGG	20	40	Eurofins, Germany
T7_term	CTAGTTATTGCTCAGCGGT	19	47	Eurofins, Germany
pET_for	ATATAGGCGCCAGCAACC	18	56	Eurofins, Germany
MCO_HindIII_rev	CGTCAGAAGCTTGCTCCATGCAGAGAGCTC	30	57	This work

Table 7. Master mix composition for PCR.

Component	50 µL Reaction
Phusion DNA Polymerase	0.5 µL
5X Phusion HF Buffer	10 µL
10 mM dNTPs	1 µL
Forward Primer (pET_for)	2.5 µL
Reverse primer (MCO_HindIII_rev)	2.5 µL
Template DNA	1 ng
Nuclease-free water	to 50 µL

Table 8. Cloning procedure.

	Step	Volume	Temp.	Time	
PCR	Initial denaturation		98 °C	30 sec	
	Denaturation		98 °C	10 sec	32 cycles
	Annealing		60 °C	30 sec	
	Elongation		72 °C	30 sec	
	Final elongation		72 °C	5 min	
	PCR cleanup				
Restriction Digestion	DNA	0.5 µg	37 °C	60 min	
	10X rCutSmart buffer	2.5 µL			
	XbaI	1 µL			
	HindIII-HF	1 µL			
	Nuclease-free water	to 25 µL			
	Heat inactivation		80 °C	20 min	
Vector DNA Dephosphorylation	Digested vector mix	25 µL	37 °C	20 min	
	FastAP buffer	3.6 µL			
	FastAP	3 µL			
	Heat inactivation		65 °C	15 min	
Ligation	Insert	3 µL	16 °C	overnight	
	Dephosphorylated vector	1 µL			
	T4 DNA ligase buffer	2 µL			
	T4 DNA ligase	1 µL			
	10 mM ATP	1 µL			
	Nuclease-free water	to 20 µL			
	Heat inactivation		80 °C	10 min	
Transformation	Ligation mix	5 µL	on ice	30 min	
	Heat shock		42 °C	1.5 min	
			on ice	5 min	
	LB medium	400 µL	37 °C	60 min	

The primers used in this study are listed in Table 6. The PCR reactions were prepared according to the reaction setup detailed in Table 7, and the cloning procedure is outlined in Table 8. After PCR amplification, the PCR products or inserts were purified using a PCR clean-up kit (Macherey Nagel, Germany). Both the inserts and the pET21a(+) vectors were digested with XbaI and HindIII-HF to generate compatible ends for ligation. Prior to ligation, the vector DNA was dephosphorylated and subsequently ligated with the inserts to form circular DNA constructs. The plasmids were then transformed into *E. coli* DH5α.

Table 9. Master mix composition for colony PCR.

Component	25 µL Reaction
DCS *Taq* DNA polymerase	0.25 µL
10X Buffer B	2.5 µL
10 mM dNTPs	0.5 µL
Forward Primer (T7_prom)	1 µL
Reverse primer (T7_term)	1 µL
Template DNA	variable
Nuclease-free water	to 25 µL

Table 10. Colony PCR program.

	Step	Volume	Temp.	Time	
PCR	Initial denaturation		95 °C	10 min	
	Denaturation		95 °C	30 sec	32 cycles
	Annealing		49 °C	45 sec	
	Elongation		68 °C	2 min	
	Final elongation		68 °C	5 min	

The constructs were verified through colony PCR screening (Tables 9, 10) and sequenced at Microsynth Seqlab, Germany. The newly constructed plasmids were transformed into *E. coli* BL21(DE3) for ItL-01-03 and into *E. coli* T7 SHuffle for CueO to facilitate further expression and enzymatic activity analysis.

2.2.2 Agarose gel electrophoresis

The sizes of the DNA fragments were assessed using 0.8% agarose gel electrophoresis, which was prepared in 1X TAE buffer (Table 11). A DNA ladder (GeneRuler™ 1 kb, Thermo Fisher Scientific, Germany) along with DNA loading dye (0.25% bromophenol blue, 0.48% SDS, 0.03% xylene cyanole, 0.12% orange G, 60% glycerol, 60 mM EDTA, 20 mM Tris-HCl pH 8.0) were used. The electrophoresis was performed with a power supply (EPS 301, Cytiva, UK) at a voltage of 100 V for a duration of about 40 minutes. Following this, the gels were stained in an ethidium bromide solution (~10 µg/mL) for 15 minutes and then de-stained in water to eliminate any excess stain. For visualization, the ChemiDoc™ MP imaging system (Bio-Rad Laboratories, Germany), was employed.

Table 11. 50X TAE Buffer

Components	Quantity
Tris	2 M
EDTA (pH 8.0)	100 mM
H_2O_{bidest}	*ad* 1 L
Acetic acid	to pH 8.1

2.3 Protein production techniques

2.3.1 Protein expression

1% of the overnight inoculum was cultivated aerobically in autoinduction medium (ZYM-5052; (Studier, 2005) with a modification that excluded the addition of 200 µL of the 1000X trace elements (Table 12). The culture was supplemented with 100 µg/mL ampicillin and incubated at 37 °C until an OD_{600} of 0.6 was reached. Then, 250 µM of $CuSO_4$ was added to the culture to ensure proper protein folding during the expression process. The copper concentration utilized during expression was limited to the low amount reported (Y. Zhang et al., 2023). This is crucial, as copper can bind to the His-tag and potentially interfere with protein purification using nickel (Ni) chromatography (2.3.2). Additionally, copper supplementation during the enzyme assay was subsequently implemented, as it has been shown to enhance enzyme activity (Zampolli et al., 2023). Afterward, the culture was shifted to 28 °C for expression for 16 to 20 hours. Upon reaching

optimal protein production, the cells were collected by centrifugation at 10,000 rpm for 15 minutes at 4 °C, and the resulting pellets were stored either at -20 °C for short-term preservation or at -70 °C for long-term storage.

Table 12. Autoinduction media

Media	Components	Quantity
Autoinduction medium	Tryptone-yeast extract	958 mL
	50X Saline solution	20 mL
	50X Sugar solution	20 mL
	500X $MgSO_4$	2 mL
Tryptone-yeast extract	Tryptone/Peptone	10 g
	Yeast extract	5 g
	H_2O_{bidest}	*ad* 1 L
50X Saline solution	$Na_2HPO_4 \cdot 2H_2O$	222.48 g
	KH_2PO_4	170.10 g
	NH_4Cl	133.72 g
	Na_2SO_4	35.52 g
	H_2O_{bidest}	*ad* 1 L
50X Sugar solution	Glycerol	250 mL
	D-Glucose	25 g
	α-Lactose	100 g
	H_2O_{bidest}	*ad* 1 L
500X $MgSO_4$ solution	$MgSO_4 \cdot 7H_2O$	24.65 g
	H_2O_{bidest}	*ad* 100 mL

2.3.2 Protein purification

The pellet was resuspended in a lysis buffer containing 10 mM imidazole at a ratio of 1:4 g/mL (Table 13). The suspension was treated with 1 mM phenylmethylsulfonyl fluoride (PMSF) to inhibit the activity of any pre-existing proteases and was subsequently lysed three times using a French Press at 1,250 psi (American Instrument, USA). After lysis, the supernatant was collected following centrifugation at 15,000 rpm for 20 minutes at 4 °C to eliminate cellular debris. The target proteins were then purified using Ni-NTA agarose (Qiagen, Germany) according to the manufacturer's instructions (for buffer preparations, refer to Table 13). Following purification, the proteins were subjected to dialysis in a 50 mM Tris-HCl buffer, pH 7, using a 30 kDa Amicon tube (GE Health Care, Germany). Protein concentration was determined using a NanoPhotometer® (Implen, Germany), employing the following extinction coefficients: CueO, ε = 56,045 $M^{-1}cm^{-1}$;

ItL-01, ε = 78,045 $M^{-1}cm^{-1}$; ItL-02, ε = 67,170 $M^{-1}cm^{-1}$; and ItL-03, ε = 74,160 $M^{-1}cm^{-1}$. The purified laccases were stored at 4 °C.

Table 13. Buffers used for purification.

Media	Components	Quantity
Lysis buffer	50 mM $NaH_2PO_4 \cdot 2H_2O$	7.8 g
	300 mM NaCl	17.54 g
	10 mM Imidazole	0.68 g
	H_2O_{bidest}	*ad* 1 L
	Adjust to pH 8	
Wash buffer	50 mM $NaH_2PO_4 \cdot 2H_2O$	7.8 g
	300 mM NaCl	17.54 g
	20 mM Imidazole	1.36 g
	H_2O_{bidest}	*ad* 1 L
	Adjust to pH 8	
Elution buffer	50 mM $NaH_2PO_4 \cdot 2H_2O$	7.8 g
	300 mM NaCl	17.54 g
	250 mM Imidazole	17 g
	H_2O_{bidest}	*ad* 1 L
	Adjust to pH 8	
Dialysis buffer	50 mM Tris	6.06 g
	H_2O_{bidest}	*ad* 1 L
	Adjust to pH 7 with HCl	

2.3.3 SDS-Polyacrylamide gel electrophoresis (SDS-PAGE)

To confirm successful protein expression based on their expected sizes, purified samples were mixed with a 5X loading dye in a 4:1 ratio and heated at 95 °C for 5 minutes. Acrylamide gels of 12% and 7% were prepared and placed in an electrophoresis chamber (Bio-Rad Laboratories, Germany), which was then filled with 1X running buffer. A protein marker (PageRuler™ Unstained Protein Ladder, Thermo Fisher Scientific, Germany) was included for size comparison.

Table 14. Solutions and buffers used for SDS-PAGE.

Media	Components	Quantity
5X Loading dye	50% Glycerol	
	100 mM Dithiothreitol (DTT)	
	0.4% SDS	
	0.02% Bromophenol blue	
	150 mM Tris-HCl (pH 6.8)	
	1 mM EDTA	
	30 mM NaCl	
	H_2O_{bidest}	*ad* 10 mL
10X Running buffer	250 mM Tris	
	1.92 M Glycine	
	1% SDS	
	H_2O_{bidest}	*ad* 10 mL
Ammonium persulfate	10% in H_2O_{bidest}	
Separating gel solution	1.5 M Tris	
	0.4% SDS	
	H_2O_{bidest}	*ad* 250 mL
	Adjust pH to 8.8	
Stacking gel solution	0.5 M Tris	
	0.4% SDS	
	H_2O_{bidest}	*ad* 100 mL
	Adjust pH to 6.8	
12% Separating gel	Acrylamide (37.5:1)	3 mL
	Separating gel solution	2.5 mL
	TEMED	9 µL
	10% APS	45 µL
	H_2O_{bidest}	4.5 mL
7% Stacking gel	Acrylamide (37.5:1)	0.7 mL
	Stacking gel solution	0.96 mL
	TEMED	4 µL
	10% APS	20 µL
	H_2O_{bidest}	2.34 mL
Staining solution	Brilliant blue R 250	1 g
	Ethanol	400 mL
	Acetic acid	100 mL
	H_2O_{bidest}	*ad* 500 mL
Destaining solution	Ethanol	400 mL
	Acetic acid	100 mL
	H_2O_{bidest}	*ad* 500 mL

Electrophoresis was performed at 80 V for 20 minutes, or until the dye front reached the stacking gel, after which the voltage was increased to 120 V. Once the protein reached the desired position, the SDS gel was stained for one hour or overnight and then de-stained for three hours or until the bands were clearly visible. The solutions and buffers for SDS-PAGE are listed in Table 14. The expected sizes of purified proteins are presented in Table 15.

Table 15. Size of purified protein (kDa) containing His-tag.

Enzyme	Protein (kDa)	Characteristics
ItL-01	59.2	His-6-tag containing laccase
ItL-02	57.3	His-6-tag containing laccase
ItL-03	58.8	His-6-tag containing laccase
CueO	53.8	His-6-tag containing laccase

2.4 Characterization of oxidoreductases

2.4.1 ABTS assay

Recombinant laccases were produced in-house as previously described (2.3), while horseradish peroxidase (HRP) was purchased from Sigma Aldrich, Germany (Type VI; product-no.: P8375). To determine the activity of the oxidoreductases and to characterize them, a series of spectrophotometric assays were conducted using 2,2′-azino-di-(3-ethylbenzthiazoline sulfonic acid) (ABTS; Merck, Germany). The enzymatic transformation of ABTS into its radical form yields a measurable color change, with an absorption maximum observed at 420 nm (ε = 36,000 M^{-1} cm^{-1}), which was monitored using a Synergy HT microplate reader from BioTek, Germany.

Initially, these enzymes were tested to confirm their successful expression and functionality. In each assay, 10 µL or an appropriate dilution of purified enzymes was mixed with 1 mM ABTS in a total volume of 200 µL within a 96-well plate, along with the addition of 1 mM $CuSO_4$ for laccases or 1 mM hydrogen peroxide (H_2O_2) for HRP. For characterization, approximately 2 µM laccase or 2 nM HRP was used under the same experimental conditions. The optimal pH was determined using 0.1 M citrate-phosphate buffers covering a range from pH 3 to 7 (refer to Table 16 for buffer preparation). This was followed by temperature optimization within a range of

20 to 80 °C. Additionally, the effect of buffer preference was examined using citrate-phosphate and acetate buffers, each tested at their respective optimal pH values.

Table 16. Preparation of 0.1 M citrate-phosphate buffers at the specified pH values.

Desired pH	0.1 M Citric acid [mL]	0.2 M Na_2HPO_4 [mL]	H_2O [mL]
3.0	39.8	10.2	50
3.4	35.9	14.1	50
3.8	32.3	17.7	50
4.2	29.4	20.6	50
4.6	26.7	23.3	50
5.0	24.3	25.7	50
5.4	22.2	27.8	50
5.8	19.7	30.3	50
6.2	16.9	33.1	50
6.6	13.6	36.4	50
7.0	6.5	43.6	50

Thermostability assays were conducted at 30 °C, 40 °C, 50 °C, and 60 °C, measuring enzyme activity at various intervals over seven days. Furthermore, the effect of Cu^{2+} and H_2O_2 on the activity of laccases and HRP was investigated across a concentration range from 0 µM to 1 mM, using 0.1 M acetate buffer at pH 4 and at their respective optimal temperatures (T_{opt}). Laccase ItL-03 was further evaluated to determine the optimal concentration of copper ions that would enhance its activity, using a range of 0 to 100 mM $CuSO_4$.

2.4.2 Enzyme kinetics using ABTS as substrate

Kinetic constants for the enzymes were evaluated by using ABTS in a total volume of 200 µL, with 0.1 M acetate buffer at pH 4 and a temperature of 25 °C for a duration of 30 minutes. Initial reaction rates were recorded within the linear range by monitoring substrate conversion over time at various concentrations of ABTS (ranging from 0 to 20 mM for laccases and 0 to 4 mM for HRP), with absorbance measured at 420 nm. The Michaelis-Menten constant (K_m) and maximum reaction rate (V_{max}) were determined by fitting the initial rates to the Michaelis-Menten equation using Solver (Microsoft Excel add-in, Frontline Systems, Inc., USA) (Chris & Nithesh Chandrasekharan, 2020; Kemmer & Keller, 2010) as outlined in equation (1):

$$V = \frac{V_{max}[S]}{K_m + [S]} \quad (1)$$

where V is the theoretical rate, and [S] is the substrate concentration (mM). The sum of squared residuals (SSR) was calculated to refine the estimates of V_{max} (µM/min) and K_m (mM) and to assess the model fit. From these measurements, the turnover number (K_{cat}, min^{-1}) was calculated using the equation (2):

$$K_{cat} = \frac{V_{max}}{[E]} \quad (2)$$

where [E] represents the enzyme concentration (µM). Additionally, catalytic efficiency (K_{cat}/K_m, $mM^{-1}\ min^{-1}$) was subsequently determined.

2.4.3 Enzymatic activity on epoxy surrogates

The oxidative activities of laccases and HRP were evaluated with bis(4-dimethylamino-cyclohexyl) methane (BBCM), provided by the Institute of Technical Biocatalysis at Hamburg University of Technology, Germany; 1,3-bis(methyl(phenyl)amino) propan-2-ol (BMAP), contributed by the Manchester Institute of Biotechnology, University of Manchester, UK; and N,N-bis(2-hydroxypropyl)-p-toluidine (NNBT), purchased from Toronto Research Chemicals, Canada. A stock solution of 100 mM was prepared by dissolving these substrates in dimethyl sulfoxide (DMSO).

Each reaction involved the incubation of 0.02 U/mg of purified enzyme with 3 mM of the substrate. Supplementation with 1 mM $CuSO_4$ was performed for laccases, while 1 mM H_2O_2 was added for HRP, alongside either 1 mM ABTS or without it, all conducted in 0.1 M acetate buffer at pH 4 and at T_{opt}. Controls without enzyme were included to assess the effect of temperature on the substrates. The mixtures were continuously shaken at 450 rpm for a duration of 2 hours. For the endpoint analysis, samples were diluted at a ratio of 1:3 with buffer, subjected to centrifugation at 13,000 rpm for 6 minutes, and the supernatant was extracted using dichloromethane (DCM) in a 1:1 ratio. A second centrifugation at the same speed for another 6 minutes was conducted, after which the DCM layer was diluted 100-fold in LC-MS-grade water for LC-MS analysis (2.4.4).

The activity of laccase ItL-03 was further evaluated against BBCM, BMAP, and NNBT at time points of 0, 30, 60, and 120 minutes, conducted without the addition of a mediator under identical experimental conditions. Additionally, the activity of ItL-03 on NNBT was examined in the presence and absence of various mediators such as, ABTS, syringol (Merck, Germany), and guaiacol (Merck, Germany), at their optimal pH values, measured at 0, 30, and 120 minutes. The experimental conditions remained consistent, except for the inclusion of 1 mM mediators in the reactions. Samples were prepared for LC-MS analysis (2.4.4) as previously described.

2.4.4 Liquid chromatography-mass spectrometry (LC-MS)

LC analysis was conducted using a Dionex Ultimate 3000 UHPLC system equipped with an Agilent Zorbax Extend-C18 Rapid Resolution HT column (2.1 × 50 mm, 1.8 µm). The mobile phase comprised acetonitrile and water with 0.1% (v/v) formic acid, employing a gradient elution that transitioned from 5% to 95% acetonitrile over a 28-minute period at a flow rate of 0.3 mL/min. Elution was monitored at an absorbance of 254 nm. Mass detection was performed using a Bruker maXis ESI-QTOF mass spectrometer featuring an electrospray ionization (ESI) source in positive mode. The capillary voltage was set to 4 kV, and the mass range was calibrated from *m/z* 50 to 2,300. Data analysis was carried out using MestReNova x64 software (Mestrelab Research S.L.U, Spain). For assessing the activity of ItL-03 on NNBT in the presence and absence of mediators (ABTS, syringol, and guaiacol), the LC system was replaced with an Agilent 1260 HPLC, and the runtime was increased to 30 minutes, while all other parameters remained unchanged. The concentrations of the analytes were determined based on calibration curves obtained under identical conditions. The initial observation (t_0) defined the starting concentration of the epoxy (µM), set to 100%, and the conversion was calculated by subtracting the percentage of remaining epoxy from 100%.

2.4.5 Mediator-specific enzyme activity

For further characterization of laccase ItL-03, substrates such as ABTS, syringol, and guaiacol were utilized. The optimal pH of the enzyme towards these substrates was evaluated using various 0.1 M buffers: citrate-phosphate buffer (pH 3-6), phosphate buffer (pH 6-8), Tris buffer (pH 8-9), and carbonate-bicarbonate buffer (pH 9-10) (see Table 17 for buffer preparation).

Table 17. Preparation of 0.1 M buffers at the specified pH values.

0.1 M Citrate-phosphate buffer			
Desired pH	0.1 M Citric acid [mL]	0.2 M Na_2HPO_4 [mL]	H_2O [mL]
3	39.8	10.2	50
4	30.7	19.3	50
5	24.3	25.7	50
6	17.9	32.1	50
8	1.4	48.6	50
0.1 M Citrate buffer			
Desired pH	Citric acid [g]	Sodium citrate dihydrate [mg]	H_2O [mL]
4	1.3	992.9	*ad* 100
0.1 M Acetate buffer			
Desired pH	Sodium acetate [mg]	Acetic acid [µL]	H_2O [mL]
4	186.1	446.4	*ad* 100
0.1 M Potassium-phosphate buffer			
Desired pH	0.2 M KH_2PO_4 [mL]	0.2 M K_2HPO_4 [mL]	H_2O [mL]
6	86.8	13.2	-
7	39.0	61.0	-
8	5.3	94.7	-
0.1 M Tris buffer			
Desired pH	0.1 M Tris [g]	Concentrated HCl	H_2O [mL]
8	1.21	adjust to desired pH	*ad* 100
9	1.21	adjust to desired pH	*ad* 100
0.1 M Carbonate-bicarbonate buffer			
Desired pH	$NaHCO_3$ [mg]	Na_2CO_3 [mg]	H_2O [mL]
9	764.5	95.4	*ad* 100
10	387.6	570.9	*ad* 100

The substrate concentration was set at 3 mM and was supplemented with 5 mM $CuSO_4$. Following this, the impact of buffer preference at their respective optimal pH values was examined. The activity of laccase ItL-03 with different substrates (or mediators) was evaluated using a substrate concentration of 1 mM, supplemented with 1 mM $CuSO_4$ at their optimal pH, in a total volume of 200 µL in a 96-well plate. Absorbance changes were monitored over a 3-minute period at ε420 = 36,000 M^{-1} cm^{-1} for ABTS, ε468 = 14,800 M^{-1} cm^{-1} for syringol, and ε465 = 12,000 M^{-1} cm^{-1} for guaiacol. Specific activity is defined as the mol of substrate converted per milligram of enzyme per minute, expressed in U/mg under the assay conditions (Baltierra-Trejo et al., 2015). Enzyme activity (U/mL) was initially calculated using the following equation (3):

$$U/mL = \frac{\Delta A}{t(\varepsilon)(d)} \quad (3)$$

where ΔA is the difference between the final absorbance and the initial absorbance, t is the reaction time (min), ε is the molar extinction coefficient (M^{-1} cm^{-1}), and d is the optical path length (0.56 cm in this case). Once the enzyme activity was determined, specific activity (U/mg) was calculated according to the following equation (4):

$$U/mg = \frac{(U/mL)\, V_t}{[E]\, V_s} \quad (4)$$

Where V_t is the total volume of the reaction (µL), V_s is the sample volume (µL), and $[E]$ is the enzyme concentration (mg/mL).

The unit of enzyme activity, assessed using ABTS, was expressed in U/mg for further evaluation of oxidative activity on epoxy substrates.

2.5 Chemical pre-treatment

2.5.1 Pre-treatment process: CFRPs

Carbon fiber-epoxy resin composites (eCFRPs) were purchased from Goodfellow, Ltd., Germany (product no.: C-42-SH-000150). This material consists of Toray T300 carbon fiber (or an equivalent) combined with Elantas EC157 epoxy resin (or an equivalent), with a 50% volume fraction of fibers. The composite, based on diglycidyl ether of bisphenol A (DGEBA), had a thickness of 0.5 mm and dimensions of 150 × 150 mm, and was subsequently laser-cut into smaller pieces measuring 6 × 12 mm. The samples underwent incubation in various acidic solutions, each comprising 9 M acid and 9 M H_2O_2 mixed in a 95:5 ratio. The acids used included formic acid (FA), acetic acid (AA), propionic acid (PA), lactic acid (LA), malic acid (MA), tartaric acid (TA), citric acid (CA), nitric acid (NA), and sulfuric acid (SA). Additionally, they were treated with acid-peroxide mixtures containing a reduced concentration of 5 M while maintaining the same ratio. A volume of 60 mL/g of acid solution was applied to each sample. This treatment lasted for periods

of 8, 24, and 48 hours at 65 °C, with continuous shaking at 200 rpm. For the control group, the composites were exposed solely to acid, H_2O_2, and water. After the treatment, the samples were thoroughly washed with warm water and then dried at 60 °C overnight.

2.5.2 Weight loss

The mass fraction of resin was assessed using a method involving sulfuric acid (SA) and H_2O_2, as outlined in DIN EN 2564:2018 (e.V., 2019), which also served as one of the control conditions. The process for recovering carbon fibers from the epoxy matrix was followed, allowing for the calculation of fiber content by mass (W_f) using the following equation (5):

$$W_f = \frac{100 \times m_2}{m_1} \tag{5}$$

where m_1 represents the initial mass of the composite and m_2 denotes the residual mass of fiber after SA-H_2O_2 treatment. Subsequently, the resin content by mass (W_r) was calculated using equation (6):

$$W_r = 100 - W_f \tag{6}$$

To evaluate the efficiency of the acid solutions in dissolving the epoxy matrix, specifically the resin weight loss rate (D_r, %), the calculation followed the formula (Das et al., 2018) (7):

$$D_r = \frac{m_1 - m_2}{m_1 \times W_r} \times 100 \tag{7}$$

where m_1 is the mass of the untreated composite, and m_2 is the mass of the treated sample after washing and drying.

2.5.3 Fourier transform infrared (FTIR) spectroscopy

FTIR spectra of the pre-treated CFRPs were acquired using a Vertex 70v spectrometer (Bruker, Germany) operating in attenuated total reflection (ATR) mode. The analysis was conducted over

a spectral range from 4,000 to 650 cm^{-1}, maintaining a resolution of 2 cm^{-1}. Each spectrum was composed of 50 scans to improve the signal-to-noise ratio, while the background signal was recorded at a channel temperature of 27 °C. The measurements of the RTM6 powder used in chemo-enzymatic treatment were conducted similarly, but over a range of 4,000 to 600 cm^{-1} with 32 scans. Data processing on the obtained spectra was executed using OPUS software (Bruker, USA). The results were then visualized after normalization to a scale of [0, 1] and subjected to Savitzky-Golay smoothing over 20 points using OriginPro 2024 (OriginLab Inc., USA).

2.5.4 Scanning electron microscopy (SEM) analysis

The pre-treated composites from AA-H_2O_2, PA-H_2O_2, SA-H_2O_2, and the control samples were analyzed using SEM. Imaging was conducted using a LEO 1525 Field Emission Scanning Electron Microscope (LEO Electron Microscopy Inc., USA), set to operate at an electron high tension (EHT) ranging from 5 to 10 kV, with a working distance (WD) between 8.1 and 9.6 mm. The resulting data were processed utilizing SmartSEM V06.00 software (Carl Zeiss Microscopy GmbH, Germany).

2.6 Chemical-enzymatic treatment

2.6.1 Pre-treatment process: RTM6

RTM6-based epoxy powder (particle size ~0.6 mm) was kindly provided by the Institute of Technical Biocatalysis at Hamburg University of Technology, Germany. This powder, synthesized from tetraglycidyl methylene dianiline (TGMDA) and two di-amine hardeners, namely 4,4′-methylenebis(2,6-diethylaniline) (MDEA) and 4,4′-methylenebis(2-isopropyl-6-methylaniline) (M-MIPA), underwent immersion in a solution of propionic acid and H_2O_2, prepared at a concentration of 5 M in a 95:5 ratio, using a volume of 60 mL/g of powder. The mixture was incubated at 65 °C for 48 hours while continuously agitated at 230 rpm. After incubation, the mixture was neutralized with 5 M NaOH and subsequently extracted with DCM in a 1:1 ratio. Following the evaporation of the DCM phase, the remaining precipitate was resuspended in DMSO, resulting in a final DCM to DMSO ratio of 10:1 relative to the initial volume of DCM used. This mixture is referred to as the epoxy extract solution. The leftover powder that was not

decomposed during the treatment was filtered through Whatman grade 1 filter paper (Merck, Germany), thoroughly washed with water, and then dried overnight at a temperature of 60 °C.

2.6.2 Enzymatic treatment on epoxy extract

A volume of 10 µL of the epoxy extract was combined with 0.1 U/mg of ItL-03. The reactions were supplemented with 5 mM $CuSO_4$, along with the addition of 5 mM ABTS, or were conducted without it, all in a 0.1 M acetate buffer adjusted to pH 4. The mixtures were shaken at a speed of 900 rpm and maintained at 50 °C, and samples were taken after 2 and 24 hours. Bovine serum albumin (BSA) served as a control in these experiments. After the reactions, samples were extracted with DCM in a 1:1 ratio relative to the reaction solution, followed by centrifugation at 13,000 rpm for 5 minutes. The organic phase was then collected for analysis via mass spectrometry (2.6.4, 2.6.5).

2.6.3 Enzymatic treatment on remaining epoxy powder

A total of 15 mg of both non-treated and pre-treated epoxy powder (2.6.1) was incubated with 0.05 U/mg of ItL-03 under the previously described conditions (2.6.2), but for a duration of 5 days. Other mediators such as syringol and (2,2,6,6-tetramethylpiperidin-1-yl)oxidanyl (TEMPO; Thermo Fisher Scientific, Germany) were also employed, utilizing the appropriate 0.1 M buffer adjusted to the optimal pH for each mediator. Given that TEMPO is a non-chromogenic substance, assays were conducted at pH 4, in accordance with previously reported literatures (Azimi et al., 2016; Wong et al., 2013). After the enzymatic treatment, the powder was thoroughly rinsed with water and dried overnight at 60 °C in preparation for analysis via FTIR (2.5.3).

2.6.4 Direct electrospray ionization-mass spectrometry (ESI-MS)

ESI-MS analysis was conducted through direct injection utilizing an Agilent 6224 ESI-TOF mass spectrometer, which was connected to an Agilent 1200 Series HPLC system. Ionization in positive mode was accomplished with a spray voltage set at 4 kV, covering a mass scan range from *m/z* 110 to 3,200. The direct injection configuration facilitated a flow rate of 0.3 mL/min, while the autosampler was maintained at a temperature of 15 °C. The flow of the drying gas was adjusted to 10 L/min, with a nebulizer pressure of 15 psi and a gas temperature kept constant at 325 °C. Data analysis was performed using MestReNova x64 software (Mestrelab Research S.L.U, Spain). The

relative abundance is presented as the mean ± standard deviation (n = 3). Significant differences were determined using one-way ANOVA followed by Tukey's post-hoc test for multiple comparisons, with statistical significance defined as *$p < 0.05$.

2.6.5 Gas chromatography-mass spectrometry (GC-MS)

GC-MS analysis was carried out using an Agilent GC 7890A gas chromatograph connected to an Agilent 5975C VL-MSD mass spectrometer. The analysis employed a Thermo Fisher Scientific TG-5MS column (30 m × 0.25 mm, with a film thickness of 0.25 µm). Initially, the column temperature was set to 80 °C for 1 minute, followed by a temperature increase of 10 °C/min until reaching a final temperature of 300 °C, which was maintained for 10 minutes. The inlet temperature was held at 250 °C. Helium (5.0) served as the carrier gas, with a flow rate of 1 mL/min and a split ratio of 1:10. Data acquisition was performed in full scan mode over a mass range of *m/z* 35 to 500, with the ion source temperature set to 230 °C. The mass spectra were analyzed using MestReNova x64 software (Mestrelab Research S.L.U, Spain). Data processing and statistical analysis were performed as described in 2.6.4.

2.7 Bioinformatics

2.7.1 Sequence alignment and phylogenetic analysis

Local alignments were performed using non-redundant protein sequences from the NCBI database with BLASTp (Boratyn et al., 2012). Amino acid sequence alignments were performed using the t-coffee server (www.tcoffee.crg.cat) in structural alignment mode (Expresso), and methionine loop sequences in combine popular aligners mode (M-Coffee) (Armougom et al., 2006; Moretti et al., 2007). The phylogenetic tree was generated using MEGA11, employing the maximum-likelihood approach with the JTT matrix-based model and 1,000 bootstrap replicates (Tamura et al., 2021).

2.7.2 Protein structure analysis

The presence of signal peptides was predicted using SignalP 6.0 (https://services.healthtech.dtu.dk/services/SignalP-6.0/) (Nielsen et al., 2024) and subsequently

removed from the protein sequences of 19 laccases. The 3D structural models were predicted using AlphaFold 3 (Abramson et al., 2024). The potential 3D structures of the enzymes, classified as two-domain (2dMCO), were predicted using the SWISS-MODEL workspace (Waterhouse et al., 2018). The high-resolution crystal structure of the CueO from *E. coli* (PDB 4NER) served as a reference for identifying copper binding sites (CBSs) in the putative enzymes and the already-characterized laccases (Komori et al., 2014). Evolutional conservation profiles of the proteins were analyzed using the Consuf server (https://consurf.tau.ac.il/consurf_index.php) with default settings (Yariv et al., 2023). The resulting models were visualized, aligned, and analyzed using UCFS Chimera v.1.16. (Huang et al., 2014).

3 RESULTS

3.1 Novel bacterial laccases from bark beetle metagenomes

European spruce bark beetles colonize and feed on the inner bark of trees, exhibiting xylophagous behavior associated with laccase-like activity in their digestive (Christiansen & Bakke, 1988; Geib et al., 2008). This suggests they are a promising source of enzymes with potential ligninolytic activity. A metagenomic dataset targeting potential multicopper oxidases (MCOs) or laccases was obtained from the gastrointestinal tracts of the bark beetles. From this dataset, six candidate MCOs were identified (Ips2204, Ips14138, Ips24328, Ips1282, Ips21622, Ips28714), of which three were successfully expressed and produced (Schorn, 2020). In this study, they were designated ItL-01 to ItL-06 respectively, with ItL-01, ItL-02, and ItL-03 being the successfully expressed variants.

3.1.1 Phylogenetic comparative analysis

A phylogenetic tree was constructed using the protein sequences of six newly identified laccases to analyze their evolutionary relationships in comparison with well-established CueO from *E. coli* (Blattner et al., 1997; Grass & Rensing, 2001), eight recognized laccases associated with lignin-rich habitats or plant pathogenesis (Avison et al., 2000; Hornung et al., 2013; Trinick, 1980), and three laccases reported to partially modify polyethylene (PE) (Zampolli et al., 2023; Y. Zhang et al., 2023). The analysis revealed that most of these laccases are affiliated with the phylum Pseudomonadota, with fewer representatives from Actinomycetota and Bacillota (Figure 7). This finding is consistent with the classification of bacterial laccases in the LccED database (Gräff et al., 2020) and aligns with recent studies identifying these three phyla as key sources of lignin-degrading bacteria that produce laccases (Bugg et al., 2011).

The phylogenetic analysis identified two distinct clades (Figure 7). The first one includes CueO and the six laccases ItL-01 to ItL-06, all classified within the class Gammaproteobacteria. This group also contains LfLAC3, a laccase from a Bacilli known for its ability to oxidize PE (Y. Zhang et al., 2023). The second clade comprises LMCO2 and LMCO3, two laccases derived from Actinomycetes that also exhibit PE-oxidizing activity (Zampolli et al., 2023). In addition, this

clade includes several recognized laccases from the Alphaproteobacteria, Betaproteobacteria, and Gammaproteobacteria.

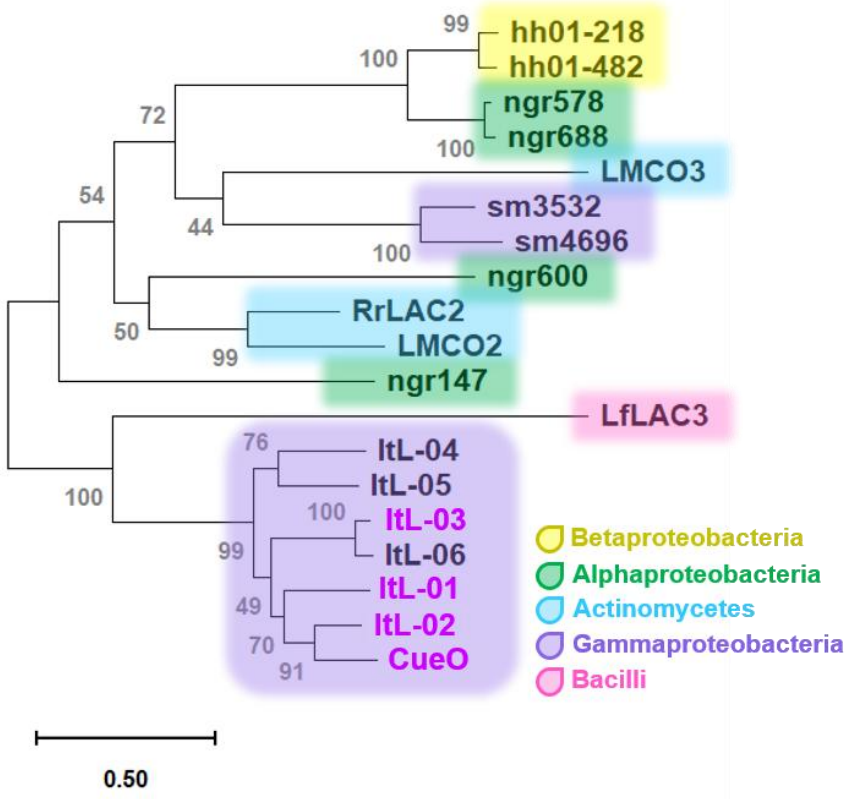

Figure 7. A phylogenetic tree of putative and characterized multicopper oxidases (MCOs), or laccases, was constructed based on amino acid sequences derived from the gut metagenome of the bark beetle *Ips typographus* (ItL-01-06) and bacteria associated with lignin and synthetic polymer modification. The accession numbers, including UniProt or IMG entries for the 19 sequences used, are listed in Table 18. Structural alignment was performed using T-Coffee Expresso (Armougom et al., 2006), and the phylogenetic tree was generated with MEGA11 (Tamura et al., 2021) employing the maximum-likelihood method with 1,000 bootstrap replicates. Phylogenetic groups were classified into distinct bacterial classes, color-coded as shown in the legend. ItL01-03 and CueO (highlighted in purple) were further characterized in this study.

3.1.2 Three-dimensional protein structure alignment

The three-dimensional structures of the putative and characterized laccases were modeled and compared to CueO to evaluate evolutionary structural variations. The analysis showed that these laccases share common features with CueO, such as prominent helical and beta-sheet structures, and exhibit structural characteristics that classify them as typical three-domain multicopper oxidases (3dMCOs), with high confidence supported by predicted template modeling (pTM) scores of ≥ 0.89 (Figure 8).

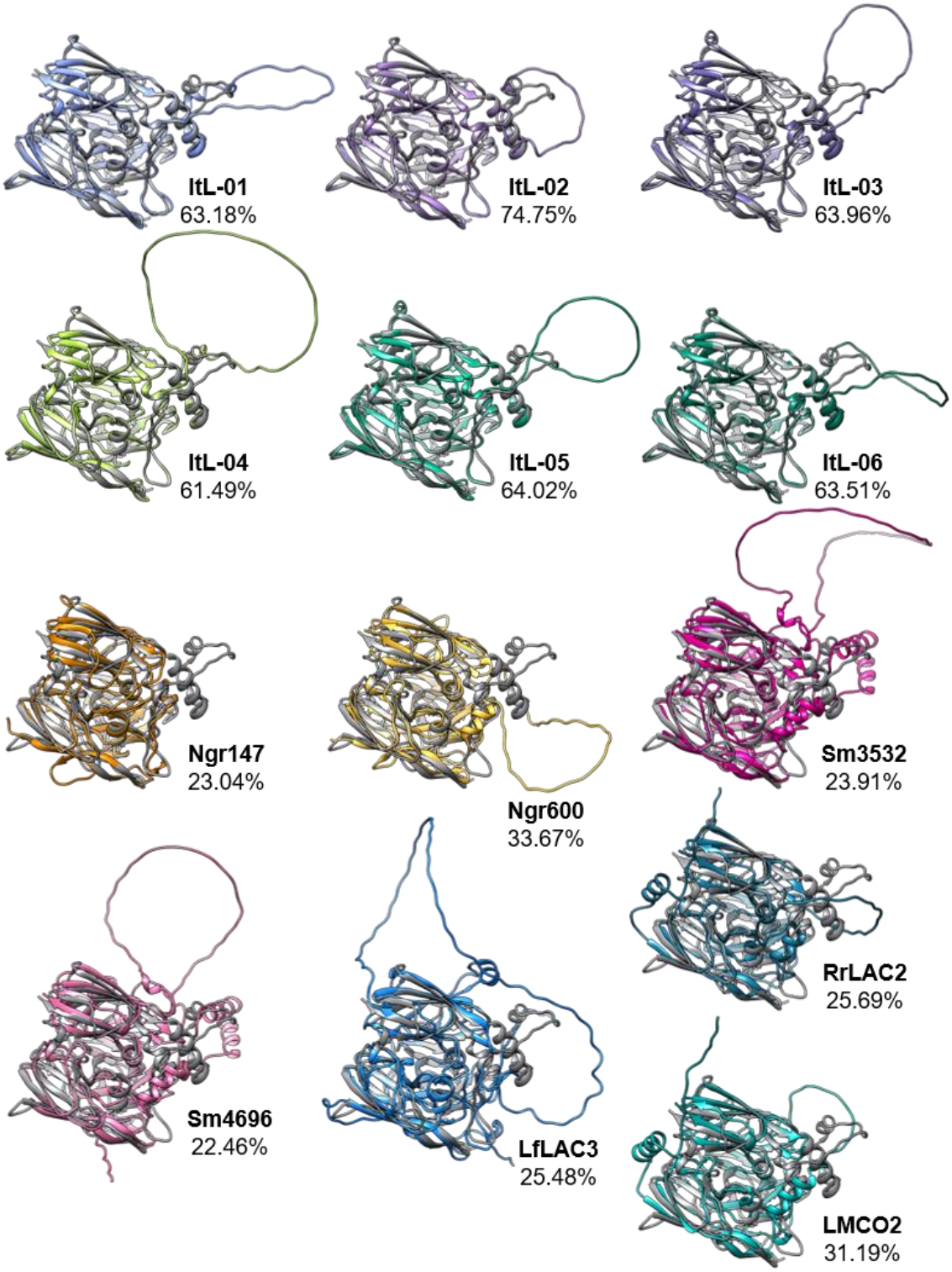

Figure 8. Structural comparisons of the putative and characterized laccases with CueO. Laccases derived from the beetle and bacteria associated with lignin and synthetic polymer modification were aligned with CueO from *E. coli* (shown in grey), and sequence identity (%) were calculated using BLASTp (Boratyn et al., 2012). Further supporting information is provided in Table 18.

BLASTp analysis revealed that ItL-01 to ItL-06 have over 60% sequence identity with CueO, whereas the other laccases fall below 40%. Among the homologs, ItL-02 exhibits the highest identity at 74.75%, followed by ItL-05 at 64.02%, and ItL-03 at 63.96%. These findings suggest that the bark beetle laccases are not only highly homologous among themselves but also evolutionarily related to CueO. Hh01-218, Hh01-482, and LMCO3 have been reported to belong to two-domain MCOs (2dMCOs) (Schorn, 2020; Zampolli et al., 2023), which form a homotrimer as their catalytically active configuration by combining three protein chains in a hexagram-like arrangement (Nakamura et al., 2003) (Figure 9). The potential structures of Ngr578 and Ngr688 were predicted using the SWISS-MODEL workspace, showing a highest sequence identity of 34% to the homotrimeric protein (PDB 3G5W; (Lawton et al., 2009)) with moderate model quality (GMQE ≈ 0.4), which suggest that they may also be classified as 2dMCOs.

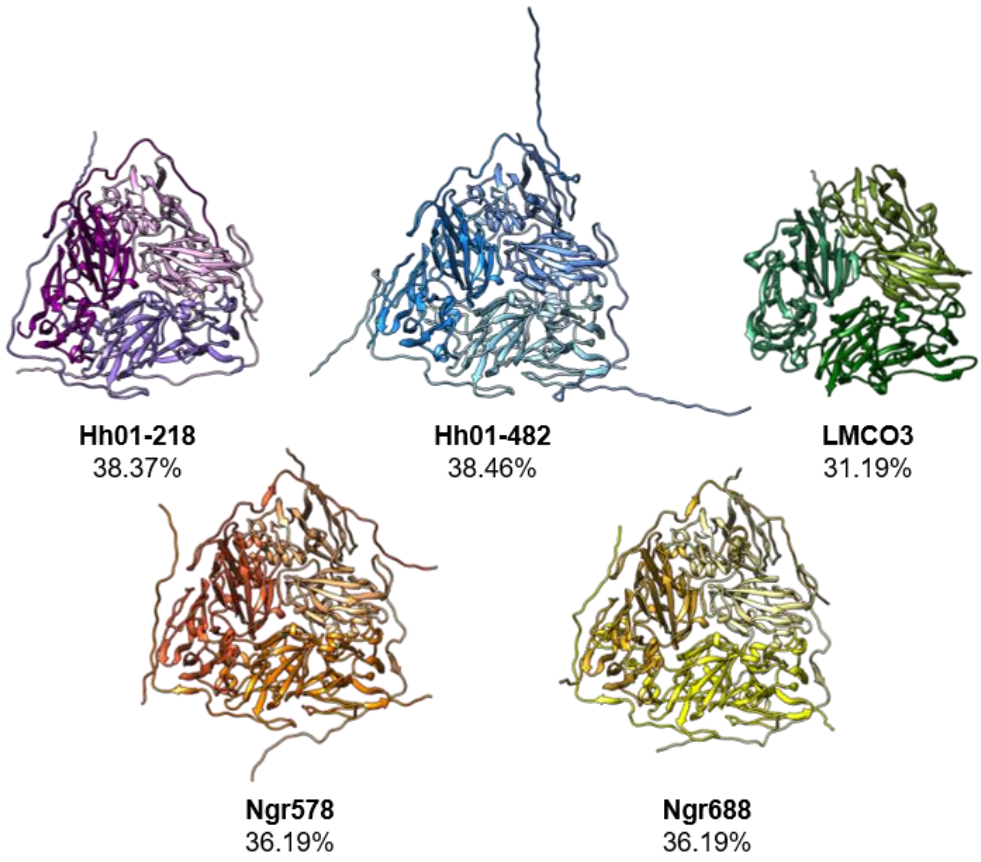

Figure 9. Potential two-domain multicopper oxidases (2dMCOs) were predicted by submitting the sequences to the SWISS-MODEL server (Waterhouse et al., 2018). The models present three distinct domains that form a homotrimeric quaternary protein structure. Sequence identity (%) were calculated using BLASTp (Boratyn et al., 2012), comparing a single chain to CueO. Further supporting information is provided in Table 18.

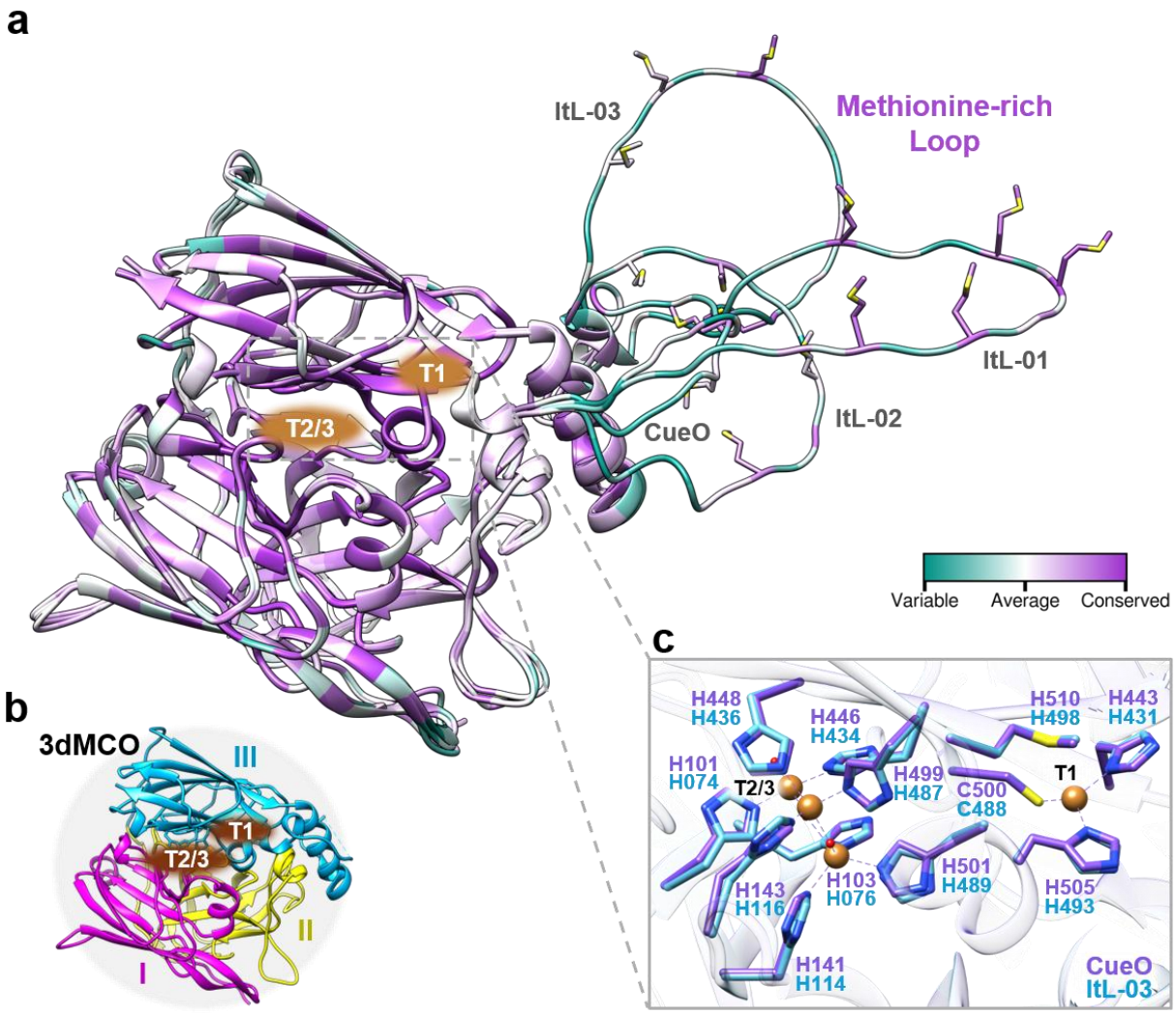

Figure 10. Evolutionary conservation profile of CueO compared to ItL-01-03. (a) The alignment of the 3D structures of CueO and ItL-01-03 illustrates the conservation of amino acid positions, with B-factors predicted by Consurf (Yariv et al., 2023) indicating variable and conserved regions as depicted by the color scheme in the legend. Structural details highlight the copper binding sites (CBSs) T1 and T2/3, and the methionine-rich loop, with methionine residues indicated. Conservation profiles for additional enzymes can be found in Figures S1-S2. (b) These MCOs, represented by CueO (PDB: 4NER; (Komori et al., 2014)), consist of three cupredoxin-like domains (3dMCO), labelled I, II, and III, which accommodate the T1 and T2/3 sites. (c) The amino acids at the CBSs of CueO (purple) and ItL-03 (blue) are predominantly conserved with histidine (H) residues. The corresponding amino acids for CBSs in other laccases are presented in Table 18.

The evolutionary conservation inferred from amino acid sequences indicates that most regions of these enzymes are highly conserved, particularly those near the T1 and T2/3 copper centers (Figures 10a, S1, S2). CueO, along with ItL-01, ItL-02, and ItL-03, feature copper ions located at two main active sites: the T1 copper in the third domain, which catalyzes substrate oxidation, and

the T2/3 copper cluster at the interface between the first and third domains, where dioxygen reduction takes place (Figure 10b) (Gräff et al., 2020; Reiss et al., 2013). Both the second and third domains of 3dMCOs have been reported to play roles in substrate binding (Larrondo et al., 2003). In contrast, the methionine-rich loops adjacent to the T1 site, notably in ItL-01, ItL-02, and ItL-03, show significant variability in composition, length, and structure (Figure 10a). Modeling these loops has been challenging, and they have not been crystallized for CueO (PDB 2FQE, 4NER, 5B7M) (Akter et al., 2016; Komori et al., 2014; Li et al., 2007), suggesting a high degree of flexibility. While methionine residues are relatively conserved, variability occurs mainly in the non-methionine positions. The conserved methionines are hypothesized to play a key role in copper recruitment and transport (Contaldo et al., 2024).

Crystals of CueO, resolved to 1.60 Å and containing copper (II) ions (PDB 4NER; (Komori et al., 2014)), were compared regarding their copper-binding sites (CBSs) with those of ItL-03, revealing a high degree of similarity (Figure 10c). The copper ions are located at two distinct active sites: the T1 center (His443, Cys500, and His505 in CueO; and His431, Cys488, and His493 in ItL-03) and the T2/T3 centers (His101, His103, His141, His143, His446, His448, His499, and His501 for CueO; and His74, His76, His114, His116, His434, His436, His487, and His489 for ItL-03). These binding motifs are identical in ItL-01 and ItL-02 and are highly conserved among other laccases. Given the conserved nature of the CBSs within laccases, it is suggested that the methionine-rich loops near the T1 copper site may influence enzyme specificity and reactivity. Table 18 provides a summary of the bioinformatics analysis of the putative and characterized laccases in relation to CueO, including their accession numbers, taxonomic affiliations, and CBSs.

Table 18. Putative multicopper oxidase enzymes from *I. typographus* and other bacterial laccases known for their association with lignin and synthetic polymer modification.

Name	Accession number	Cluster	Phylogenetic affiliation	aa identity with CueO [%]	Copper binding motifs				Reference
					i	*ii*	*iii*	*iiii*	
CueO	P36649*	γ-Proteobacteria/C1	*Escherichia coli*	100.00	**H**W**H**	**H**P**H**	**H**PF**H**I**H**	**HCH**LLE**H**EDTG**M**	(Grass & Rensing, 2001)
ItL-01	Ga0063521_10002204**	γ-Proteobacteria/C1	*Erwinia* sp.	63.18	**H**W**H**	**H**P**H**	**H**PF**H**I**H**	**HCH**LLE**H**EDTG**M**	(Schorn, 2020)
ItL-02	Ga0063521_100014138**	γ-Proteobacteria/C1	*Dryocola clanedunensis*	74.75	**H**W**H**	**H**P**H**	**H**PF**H**I**H**	**HCH**LLE**H**EDTG**M**	(Schorn, 2020)
ItL-03	Ga0063521_100024328**	γ-Proteobacteria/C1	*Rahnella* sp.	63.96	**H**W**H**	**H**P**H**	**H**PF**H**I**H**	**HCH**LLE**H**EDTG**M**	(Schorn, 2020)
ItL-04	Ga0063521_1000001282**	γ-Proteobacteria/C1	*Providencia* sp.	61.49	**H**W**H**	**H**P**H**	**H**PF**H**V**H**	**HCH**LLE**H**EDTG**M**	(Schorn, 2020)
ItL-05	Ga0063521_100021622**	γ-Proteobacteria/C1	*Morganella morganii*	64.02	**H**W**H**	**H**P**H**	**H**PF**H**I**H**	**HCH**LLE**H**EDTG**M**	(Schorn, 2020)
ItL-06	Ga0063521_100028714**	γ-Proteobacteria/C1	*Rahnella* sp.	63.51	**H**W**H**	**H**P**H**	**H**PF**H**I**H**	**HCH**LLE**H**EDTG**M**	(Schorn, 2020)
Hh01-218	2523500218**	β-Proteobacteria/C2	*Janthinobacterium* sp.	38.37	**H**W**H**	**H**P**H**	**H**P**H**L**H**	**HCH**KSH**H**TMNA**M**	(Hornung et al., 2013)
Hh01-482	2523500482**	β-Proteobacteria/C2	*Janthinobacterium* sp.	38.46	**H**W**H**	**H**P**H**	**H**P**H**I**H**	**HCH**KSH**H**TMNA**M**	(Hornung et al., 2013)
Sm3532	642693532**	γ-Proteobacteria/C2	*Stenotrophomonas maltophilia*	23.91	**H**W**H**	**HSH**	**H**P**H**L**H**	**HCH**LLY**H**MEAG**M**	(Avison et al., 2000)
Sm4696	642694696**	γ-Proteobacteria/C2	*Stenotrophomonas maltophilia*	22.46	**H**W**H**	**HSH**	**H**P**H**L**H**	**HCH**LLY**H**MEAG**M**	(Avison et al., 2000)
Ngr147	643825147**	α-Proteobacteria/C2	*Sinorhizobium fredii*	23.04	**H**W**H**	**H**P**H**	**H**P**H**L**H**	**HCH**IIE**H**QKTG**M**	(Trinick, 1980)
Ngr578	643822578**	α-Proteobacteria/C2	*Sinorhizobium fredii*	36.19	**H**W**H**	**H**P**H**	**H**P**H**M**H**	**HCH**KSH**H**TMNA**M**	(Trinick, 1980)

Name	Accession number	Cluster	Phylogenetic affiliation	aa identity with CueO [%]	Copper binding motifs				Reference
					i	*ii*	*iii*	*iiii*	
Ngr600	643822600**	α-Proteobacteria/C2	*Sinorhizobium fredii*	33.67	**H**W**H**	**HSH**	**H**PM**H**L**H**	**HCH**HLY**H**MNGG**M**	(Trinick, 1980)
Ngr688	643822688**	α-Proteobacteria/C2	*Sinorhizobium fredii*	36.19	**H**W**H**	**H**P**H**	**H**PI**H**M**H**	**HCH**KSH**H**TMNA**M**	(Trinick, 1980)
LMCO2	AII11185.1	Actinomycetes/C2	*Rhodococcus opacus*	26.38	**H**W**H**	**H**P**H**	**H**PM**H**L**H**	**HCH**NLY**H**GEAG**M**	(Zampolli et al., 2023)
LMCO3	AII11221.1	Actinomycetes/C2	*Rhodococcus opacus*	31.19	**H**L**H**	**H**A**H**	**H**TM**H**F**H**	**HCH**VGPLAE**H**	(Zampolli et al., 2023)
LfLAC3	WP_193831439.1	Bacilli/C1	*Lysinibacillus fusiformis*	25.48	**H**L**H**	**H**D**H**	**H**PI**H**L**H**	**HCH**FLE**H**EDHD**M**	(Y. Zhang et al., 2023)
RrLAC2	WP_318283942.1	Actinomycetes/C2	*Rhodococcus ruber*	25.69	**H**F**H**	**HSH**	**H**PM**H**V**H**	**HCH**NAY**H**QEAG**R**	(Y. Zhang et al., 2023)

*UniProt, **IMG, *i-iiii* indicate amino acids involved in copper binding motifs, two-domain MCOs (2dMCOs) are highlighted in blue, with their predicted structures illustrated in Figure 9.

3.2 Recombinant laccase production and initial activity screening

Initially, laccases ItL-01 to ItL-03 (ItL-01-03) and CueO were constructed with a StrepII-tag purification via fast protein liquid chromatography (FPLC), ensuring high purity (Schorn, 2020). To improve practicality and reduce purification time, the constructs were later modified to replace the StrepII-tag with a His-tag. The proteins were expressed and purified using affinity chromatography, and SDS-PAGE confirmed successful expression, with molecular weights predicted between 50 and 60 kDa (Figure 11a). While the recombinant laccases were produced in-house, horseradish peroxidase (HRP) was obtained commercially.

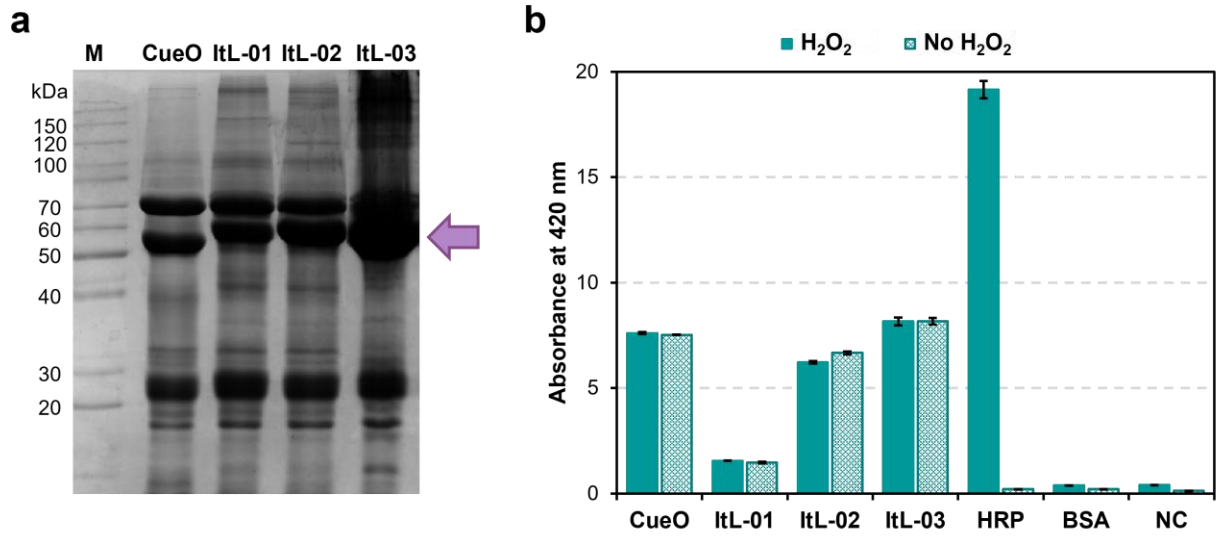

Figure 11. Expression of CueO and ItL-01-03 and initial activity screening with ABTS. (a) SDS-PAGE analysis demonstrates the successful expression and purification of the recombinant laccases using Ni-NTA chromatography. M indicates an unstained protein ladder (ThermoScientific, Germany), with the arrow pointing to the expected bands, which are around 55-65 kDa. Additional non-specific bands observed at 25 kDa and 70 kDa reflect the complexity of the protein sample, as these bands were expressed concurrently by the *E. coli* host. (b) Activity screening was conducted using the ABTS assay, measuring absorbance at 420 nm. The reactions were quickly assessed within 5 min at room temperature using appropriate dilutions of purified enzymes. BSA and a negative control without enzyme (NC) were included as controls. The addition of H_2O_2 was also tested, as it is required for catalysis in HRP. Error bars denote standard deviation (n = 3).

ABTS was chosen as the initial screening substrate, as it is a common substrate for oxidoreductases (Bach et al., 2013; Kadnikova & Kostić, 2002), widely used mediator in laccase/mediator systems, and can enable activity towards larger substrates such as polymers (Guan et al., 2018; Hilgers et al., 2018). The enzymatic activity was rapidly screened using a small amount of purified enzyme in an ABTS assay at room temperature, measuring radical formation at 420 nm. To assess

hydrogen peroxide (H_2O_2) dependence which is required by HRP, assays were conducted in the absence and presence of H_2O_2. The results showed that CueO and the recombinant laccases ItL-01-03 oxidized ABTS regardless of H_2O_2 presence (Figure 11b), while HRP only oxidized ABTS with H_2O_2. These findings confirm the expression and activity of the recombinant laccases, contrasted with negative controls, bovine serum albumin (BSA), and reactions without enzyme (NC).

3.3 Biochemical characterization of laccases and HRP

The oxidoreductases CueO, ItL-01-03, and HRP were biochemically analyzed for their optimal temperature, pH, thermostability, effect of H_2O_2 and Cu^{2+}, and kinetic properties, through a comprehensive investigation utilizing the ABTS assay.

3.3.1 pH stability and buffer preference

All laccases exhibited a preference for the acidic pH range, maintaining more than 50% activity between pH 3.0 and 4.6 (Figure 12a). In contrast, HRP demonstrated lower tolerance to acidity, losing all activity below pH 3.4 but retaining 50% activity up to pH 5.4. ItL-01 shared a pH optimum of 4.2 with HRP, while CueO, ItL-02, and ItL-03 reached their maximum activity at pH 3.8. Notably, ItL-03 displayed exceptional stability within the acidic range, retaining over 90% activity between pH 3.0 and 3.8, indicating a significant acidophilic characteristic. Given that these oxidoreductases demonstrated a similar optimal pH range of 3.8 to 4.2 and preferred acetate buffer over citrate-phosphate buffer, acetate buffer at pH 4.0 was chosen for further characterization (Figure 12b).

3.3.2 Temperature stability and thermostability

The temperature profile and thermostability of the enzymes were further assessed, with the latter involving incubation of the enzymes at 30-60 °C over a period of 7 days (Figure 12c,d). HRP exhibited its optimal activity (T_{opt}) at 30 °C, while maintaining nearly optimal relative activity in the temperature range of 20 to 40 °C. However, it showed a 40% decrease in activity after just 2 hours at its T_{opt}. Unlike HRP, laccases typically displayed higher T_{opt} values and demonstrated a greater ability to sustain their activity for extended periods.

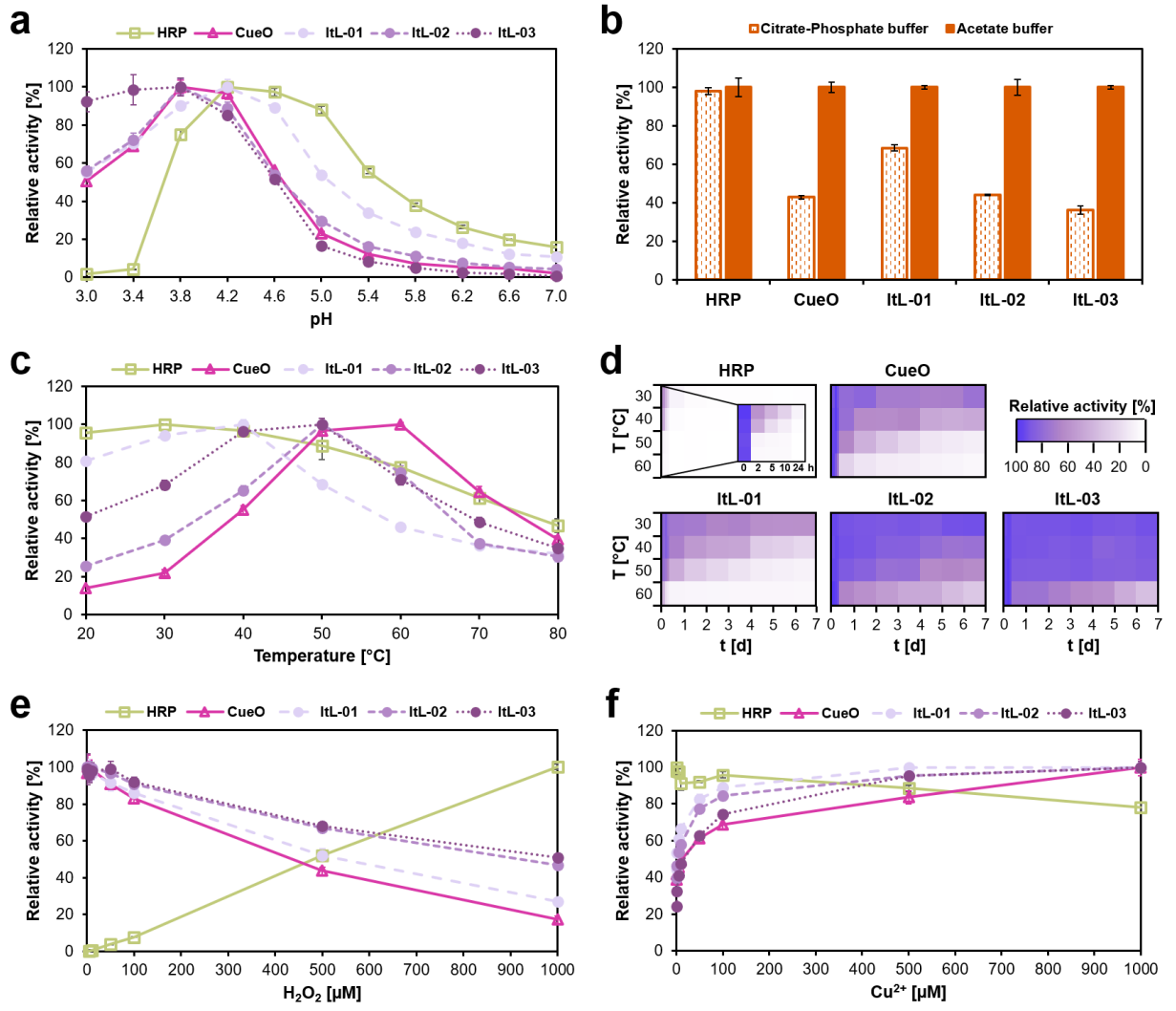

Figure 12. Biochemical characteristics of oxidoreductases, determined using ABTS, reveal their stability and limitations in synergistic enzyme activity. (a) pH profile: the enzymes prefer low pH, exhibiting maximum activity at pH 4.0. (b) Buffer Preference: laccases show a 30-50% increase in activity in acetate buffer, while HRP maintains similar activity in both buffers. (c) Temperature profile: each enzyme demonstrates a distinct temperature stability within the mesophilic range of 30-60 °C. (d) Thermostability: most enzymes retain activity for only a few hours, losing nearly 80% within a day at elevated temperatures, while ItL-02-03 maintains over 60% activity at 50 °C for a week. The standard deviation was below 6%. (e) Effect of H_2O_2: the activity of HRP increases with H_2O_2 concentration, while other laccases decline, dropping below 50% at 1 mM H_2O_2. (f) Effect of Copper Ions (Cu^{2+}): laccase activity significantly increases with higher Cu^{2+} concentrations, while HRP activity decreases by about 20% at 1 mM Cu^{2+}. Error bars indicate the standard deviation (n = 3).

ItL-01, which had a pH profile similar to HRP, presented a T_{opt} of 40 °C, retaining over 80% of its activity between 20 and 40 °C. Additionally, ItL-01 maintained more than 60% activity at its T_{opt} for approximately one day. CueO, on the other hand, achieved the highest T_{opt} among all laccases

at 60 °C and was capable of functioning at nearly maximal activity at 50 °C. Despite its elevated T_{opt}, however, CueO experienced a 30% reduction in activity after 10 hours and nearly lost its activity entirely after three days. ItL-02 and ItL-03 exhibited the same T_{opt} of 50 °C, with ItL-03 also demonstrating comparable activity at 40 °C. While ItL-02 retained 80% of its activity at the optimal temperature after two days, ItL-03 sustained this level of activity even after a week. These findings position ItL-03 as the most thermophilic and thermostable enzyme within this study.

3.3.3 Effect of H_2O_2 and Cu^{2+}

Ligninolytic enzymes like laccases and peroxidases are key to lignin breakdown, a complex biopolymer with a cross-linked network (Pollegioni et al., 2015). Its aromatic and branched structure resembles cured epoxy, making both materials resistant to degradation. Therefore, degrading epoxy likely requires a combination of different enzymes. Peroxidases facilitate oxidation reactions of substrates using H_2O_2 (Pandey et al., 2017), whereas laccases depend on oxygen and copper ions (Cu^{2+}) as essential cofactors for substrate oxidation (Janusz et al., 2020). Even small amounts of elevated H_2O_2 and Cu^{2+} can adversely affect enzymes that do not require these cofactors. Thus, the impact of H_2O_2 and Cu^{2+} on the enzymes was assessed within a 1 mM range.

The activity of HRP increases to 100% with the addition of 1 mM H_2O_2, while it decreased to 50% with a concentration of 0.5 mM H_2O_2, highlighting the critical role of H_2O_2 in enhancing HRP activity (Figure 12e). Conversely, laccases were found to tolerate H_2O_2 well at levels below 0.1 mM; however, their activity declined by 50% when exposed to 0.5 mM H_2O_2. Both ItL-02 and ItL-03 exhibited superior tolerance to H_2O_2 compared to the other laccases. On the other hand, up to a concentration of 1 mM copper ions had a negligible effect on HRP's activity (Figure 12f). During enzyme production, laccases were supplemented with 250 µM $CuSO_4$ to promote proper protein folding. Introducing Cu^{2+} in the enzymatic reactions led to a progressive increase in the activity of purified laccases, reaching a peak at a concentration of 1 mM. Given the laccases' sensitivity to H_2O_2, the combined use of these two enzyme classes in the same reaction may not be ideal.

3.3.4 Kinetic constants of ABTS as a substrate

The steady-state kinetics of these oxidoreductases were assessed using ABTS as the substrate by fitting the initial rates to the Michaelis-Menten equation (Figure S3). HRP demonstrated an exceptionally high catalytic turnover for ABTS, reaching a K_{cat} value of 128.47 min^{-1}, which is nearly 500 times higher than that of laccases, and it presented a relatively low K_m value of 0.70 mM (Table 19). Conversely, laccases showed significantly slower catalytic turnover, along with higher K_m values. Among the laccase enzymes, ItL-03 exhibited the highest catalytic turnover for ABTS, with a K_{cat} of 3.04 min^{-1}, but displayed relatively high substrate affinity, as evidenced by a K_m value of 7.76 mM. When evaluating catalytic efficiency by considering both the turnover rate and affinity (K_{cat}/K_m), ItL-03 outperformed the other laccases, yielding a value of 0.39 min^{-1} mM^{-1}. Following these initial characterizations, further investigation of these enzymes was conducted to assess their catalytic properties toward epoxy model building blocks.

Table 19. Kinetic constants of purified oxidoreductases for ABTS substrate.

Enzymes	K_m [mM]	K_{cat} [min^{-1}]	K_{cat}/K_m [min^{-1} mM^{-1}]
Peroxidase			
HRP	0.70 ± 0.23	128.47 ± 2.11	182.47 ± 0.91
Laccases			
CueO	2.39 ± 0.23	0.27 ± 0.03	0.11 ± 0.01
ItL-01	4.50 ± 1.42	0.10 ± 0.01	0.02 ± 0.01
ItL-02	3.64 ± 0.26	0.80 ± 0.01	0.22 ± 0.01
ItL-03	7.76 ± 0.88	3.04 ± 0.24	0.39 ± 0.02

3.4 Screening potential oxidoreductases for epoxy degradation

The oxidoreductases were evaluated for their capacity to break down bis(4-dimethylamino-cyclohexyl) methane (BBCM), 1,3-bis(methyl(phenyl)amino) propan-2-ol (BMAP), and N, N-bis(2-hydroxypropyl)-p-toluidine (NNBT) (Figure 13). These substrates, which are simpler and more defined, contain essential motifs of the resin, such as a tertiary amine present in RTM6, a commercial amine epoxy resin extensively utilized in the aerospace industry (Zotti et al., 2020). These models are representative of the repeated units found in the epoxy backbone, rendering them

suitable for investigating the mechanisms of the enzyme on key functional groups characteristic of the original polymer.

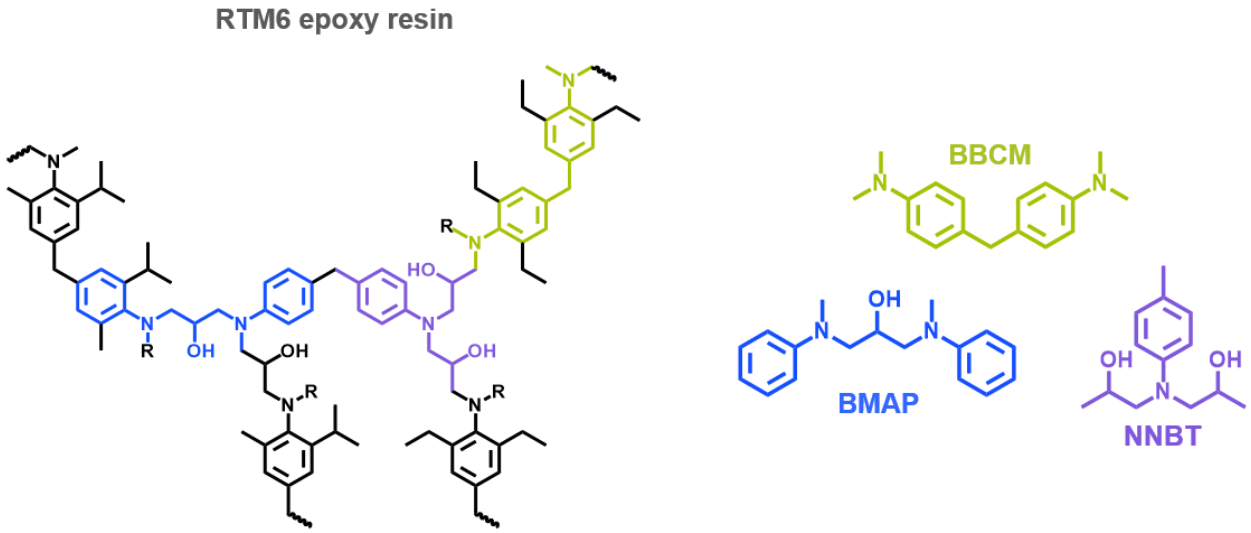

Figure 13. Epoxy scaffolds—BBCM, BMAP, and NNBT—derived from RTM6 epoxy resin.

3.4.1 Enzymatic activity on epoxy surrogates

Liquid chromatography-mass spectrometry (LC-MS) was used to assess the conversion of these epoxy scaffolds. BBCM (A), BMAP (B), and NNBT (C, D) were detected and eluted at retention times of 4, 7, and 5 minutes, respectively (Figure S4). Each peak displayed the respective compounds, which were confirmed by their exact mass. The concentrations of the substrates were quantified using extracted-ion chromatograms and a calibration curve (Figure S5), where the initial measurement (t_0) established the starting concentration of the epoxy at 100% (µM). The conversion was then calculated by subtracting the percentage of remaining epoxy from 100%. In the control sample without the enzyme, BMAP exhibited significant sensitivity to heat compared to the other epoxy substrates, showing a 60% decomposition rate at 60 °C after 2 hours, while the other substrates only reached a 20% decomposition rate (Figure S5).

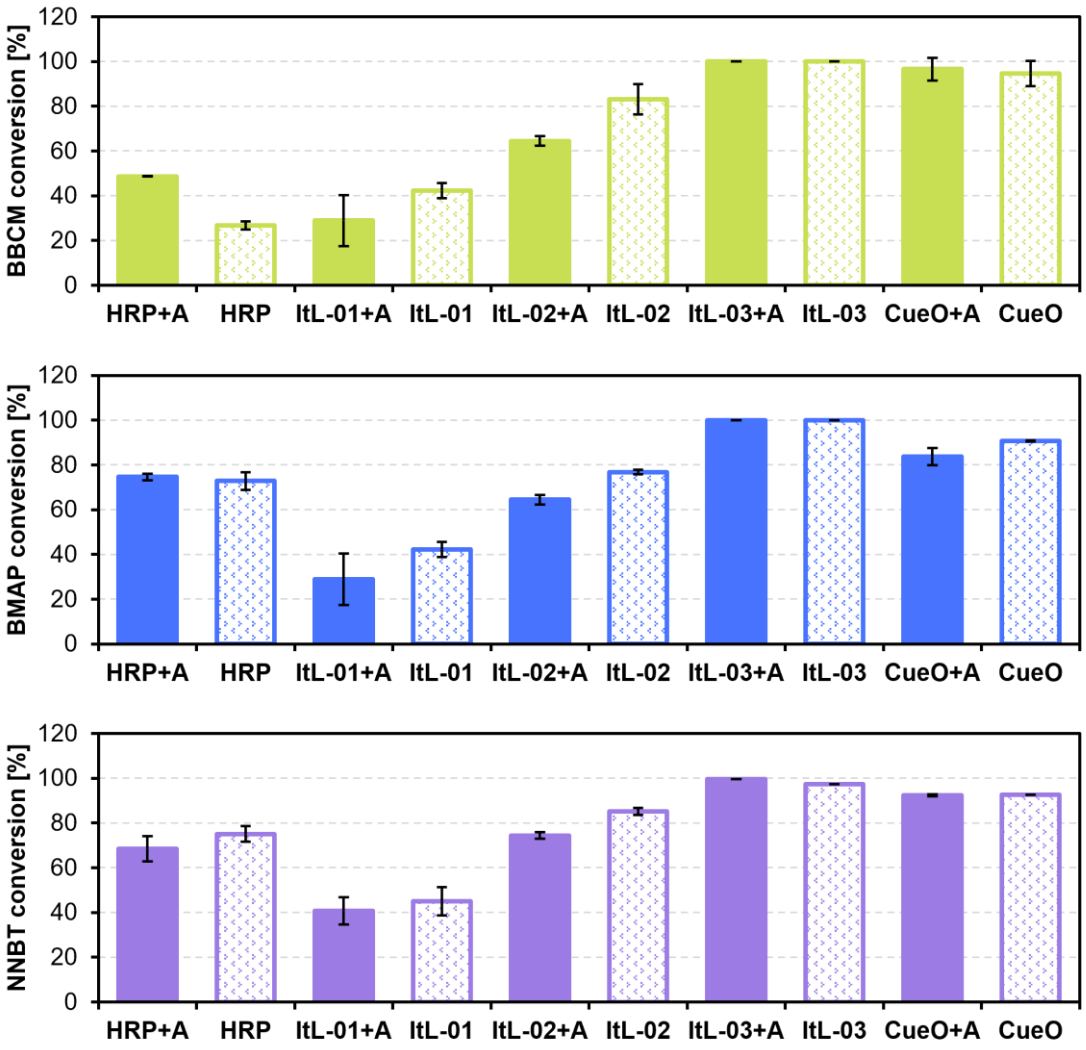

Figure 14. Enzymatic activity of epoxy scaffolds—BBCM, BMAP, and NNBT—by HRP and bacterial laccases. The tests were performed in the presence and absence of 1 mM ABTS (A) under their respective optimal pH and temperature conditions. The remaining concentration of the epoxy substrate after 2 hours was measured using LC-MS. The initial observation (t_0) represents the starting amount of epoxy, set at 100%. The conversion is calculated by subtracting the percentage of remaining epoxy from 100%. Error bars indicate the standard deviation (n = 3). The calibration curve for concentration determination and controls is presented in Figure S5.

In the presence of enzyme, ItL-03 proved to be the most active enzyme, converting all three substrates (BBCM, BMAP, and NNBT) within the 2-hour period (Figure 14). Additional analysis revealed that ItL-03 was capable of breaking down these substrates by 80% in just 30 minutes (Figure 15). CueO followed as the second most efficient enzyme, achieving nearly 90% conversion of the substrates after 2 hours (Figure 14). HRP and ItL-02 exhibited similar conversion efficacy

for the epoxy functional groups, converting more than 70% of BMAP and NNBT. In contrast, ItL-01 showed a conversion rate similar to that of HRP for BBCM conversion, but with a lower effectiveness of less than 40%. Overall, ItL-01 was identified as the least effective enzyme, with nearly 60% of the substrates still present after treatment. LC-MS analysis indicated possible N-dealkylation via radical cleavage of BMAP (Figure 16), while for BBCM and NNBT, the resulting products remained ambiguous, precluding definitive insights into their enzymatic reaction mechanisms (Figures S6, S7).

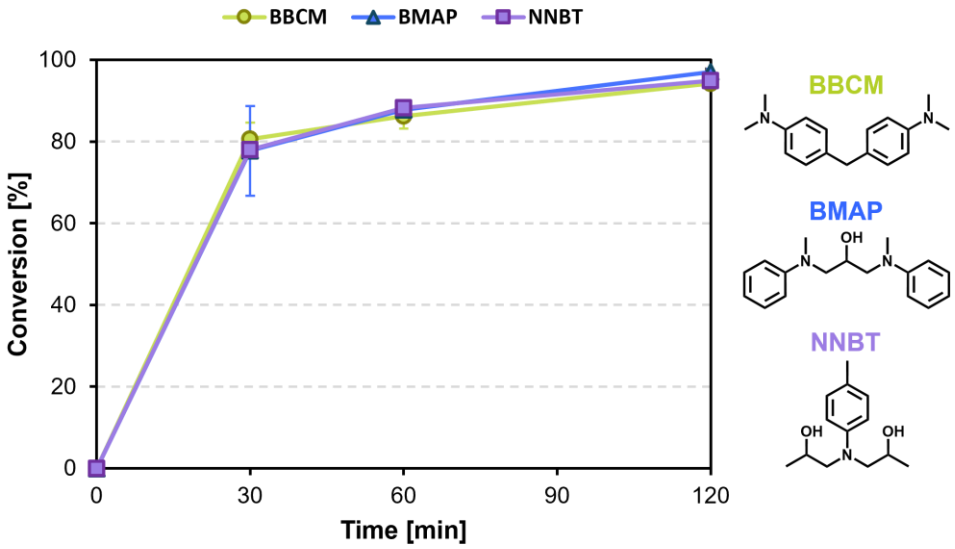

Figure 15. Enzymatic activity of ItL-03 on epoxy scaffolds—BBCM, BMAP, and NNBT—was measured at intervals of 0, 30, 60, and 120 minutes of incubation at 50 °C in 0.1 M acetate buffer pH 4.0. The initial observation (t_0) defines the starting amount of epoxy, set at 100%. The conversion is calculated by subtracting the percentage of remaining epoxy from 100%. ItL-03 achieves approximately 80% conversion of these substrates within 30 minutes and nearly complete conversion after 2 hours. Error bars indicate the standard deviation ($n = 3$).

Considering that laccases can improve their activity in the presence of mediators, an investigation was conducted to determine if this effect extends to the breakdown of epoxy models when ABTS (A) was included in the reactions. The findings showed that adding the mediator had slightly effect (<20%) on the activity of these enzymes with small substrates, which showed reduced efficiency specifically toward BBCM and BMAP (Figure 14, +A). The relatively small size of the model substrates might allow them to reach the enzyme's active site directly, making the mediator

potentially competing for enzymatic activity. Among the various bacterial laccase candidates, ItL-03 emerged as the most effective in breaking down the epoxy scaffolds and was subsequently chosen for further evaluation of its effectiveness in decomposing cured epoxy.

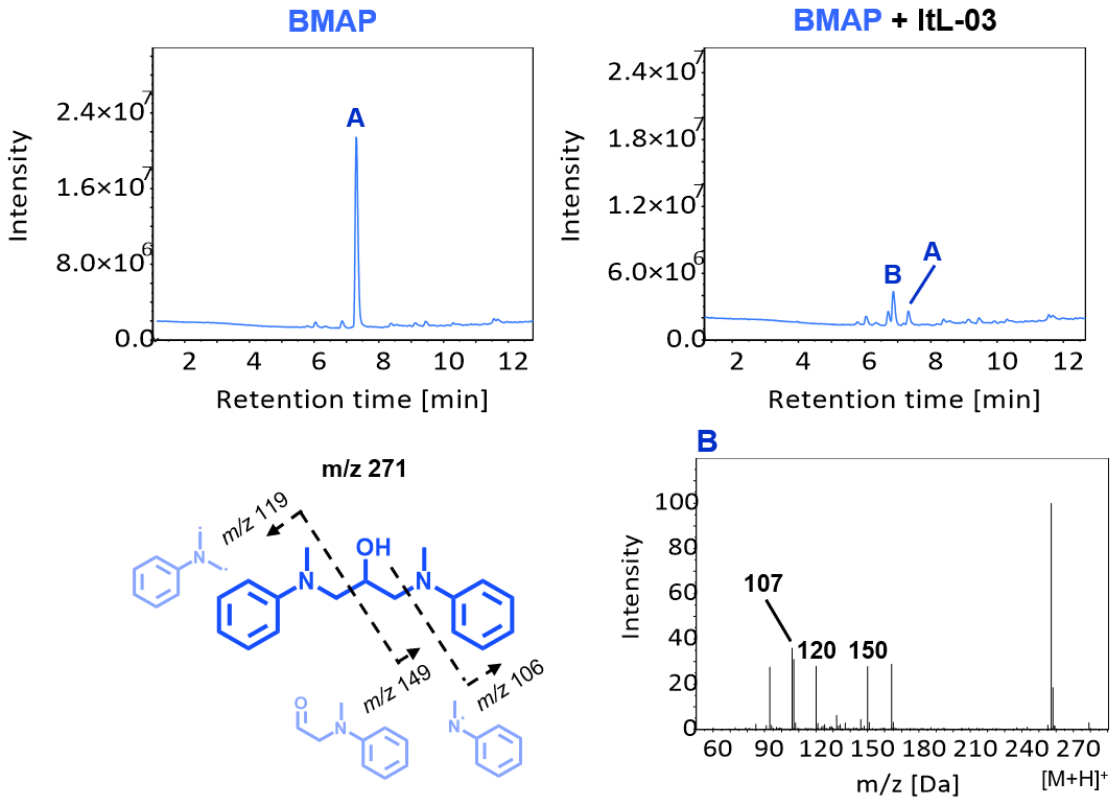

Figure 16. LC-MS chromatogram of the reaction involving laccase ItL-03 and BMAP. (A) The mass of BMAP is observed at 7.3 minutes. (B) The mass spectrum of the N-dealkylation product reveals a peak that appears at 6.7 minutes.

3.4.2 Laccase ItL-03-mediators activity

The performance of laccase ItL-03 was further investigated using alternative mediators to evaluate their potential for enhancing enzymatic efficacy. Syringol and guaiacol were selected mainly because they are chromophores that can be easily quantified with a spectrophotometer. Prior to analyzing the specific activities of ItL-03 with ABTS, syringol, and guaiacol, the optimal pH and buffer conditions for each mediator were established. ItL-03 displayed optimal activity with ABTS in acetate buffer at pH 4, while the best performance for syringol and guaiacol was observed in Tris buffer at pH 8 (Figure 17). Among the mediators tested, ItL-03/syringol achieved the highest activity, nearly four times greater than ItL-03/ABTS. In contrast, ItL-03/guaiacol exhibited

comparatively low activity (Figure 18a). Additionally, it was determined that the optimal concentration of copper ions for enhancing the activity of ItL-03 was 5 mM (Figure 18b).

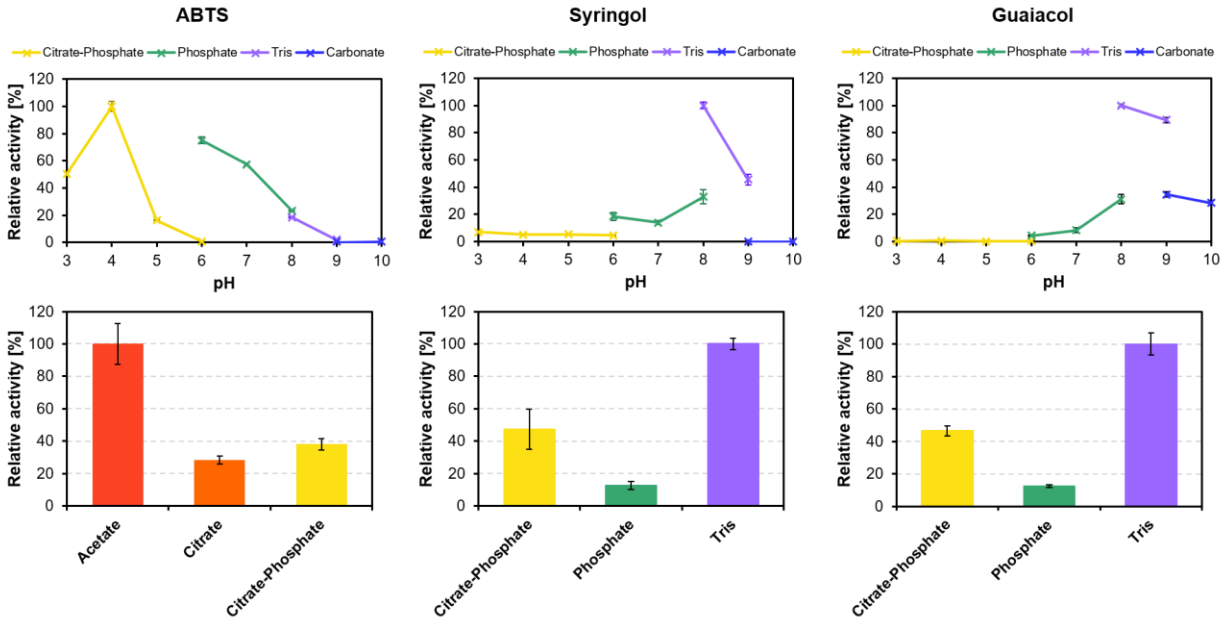

Figure 17. Determination of pH and buffer preference for each mediator of laccase ItL-03. (top) pH profile with mediators: ABTS, syringol, and guaiacol. The enzyme exhibits maximum activity at pH 4 for ABTS, while displaying a preference for pH 8 for both syringol and guaiacol. (bottom) Buffer preference with each mediator. For ABTS, ItL-03 shows the highest activity in acetate buffer, whereas optimal activity for syringol and guaiacol is observed in Tris buffer. Error bars represent the standard deviation (n = 3).

Building upon previous experiments, an investigation was conducted to determine how each mediator—ABTS, syringol, and guaiacol—affects the activity of ItL-03 on NNBT under their respective optimal conditions. In the absence of a mediator, ItL-03 exhibited better performance at an acidic pH of 4 compared to a basic pH of 8 (Figure 19). The presence of mediators significantly enhanced enzyme activity, with ItL-03 converting NNBT more rapidly when combined with guaiacol than with ABTS. Specifically, ItL-03 achieved a conversion rate of 90% after just 30 minutes in the presence of guaiacol, although both conditions ultimately reached similar conversion levels after two hours. In contrast, ItL-03/syringol catalyzed the substrate at a lower rate, approximately 40% after 30 minutes, but still managed to exceed 80% conversion after two hours. These results indicate that the presence of a mediator at acidic pH has only a slight effect on enzymatic activity, confirming previous findings (Figure 14), whereas mediators at basic pH significantly enhance ItL-03 activity (Figure 19).

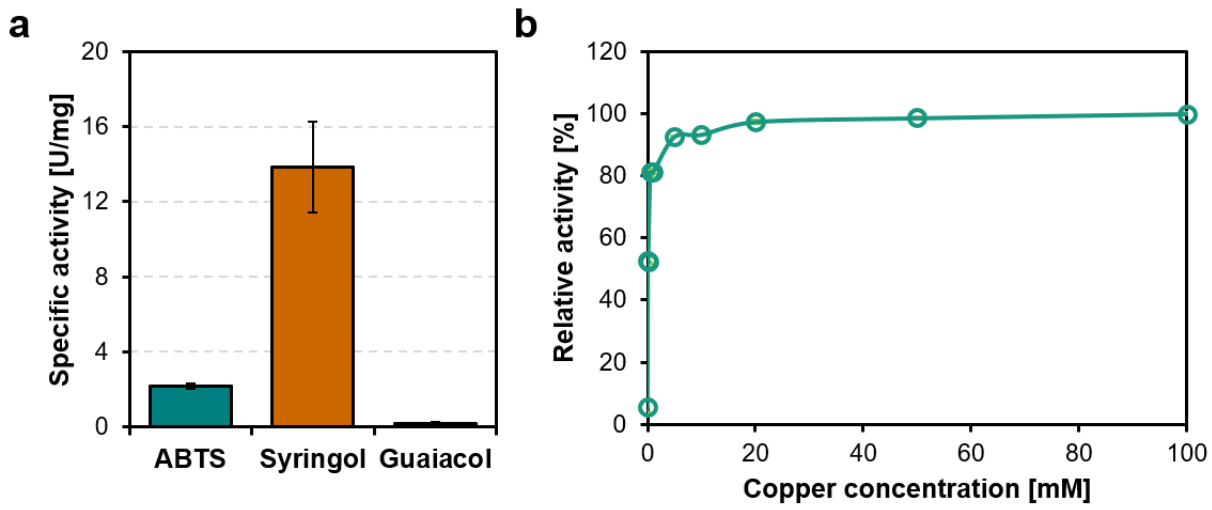

Figure 18. Specific activity of ItL-03 towards different mediators and optimal copper concentration for its activity. (a) Specific activity of laccase ItL-03 toward ABTS, syringol, and guaiacol was assessed in their respective optimal buffer and pH environment (Figure 17). The results indicated that syringol exhibited the highest activity, about four times greater than that of ABTS, while guaiacol displayed relatively low activity. (b) Optimal concentration of copper ions for ItL-03 activity was determined. Enzyme activity significantly increases with higher Cu^{2+} concentrations, saturating at around 5 mM. Error bars represent the standard deviation (n = 3).

However, the observed discrepancy in the enzyme's specificity with syringol (Figure 18a) and its role as a mediator in NNBT conversion (Figure 19) may be attributed to substrate competition, with syringol potentially fitting more effectively into the active site of ItL-03, thereby enabling slower conversion of NNBT. On the other hand, guaiacol exhibits very low specific activity with the enzyme, likely because it does not bind or react efficiently with the enzyme. This allows the enzyme to convert NNBT more effectively, resulting in greater overall conversion. Since guaiacol is a phenolic mediator like syringol but has a lower specific activity with ItL-03, it was excluded from further investigation in the chemo-enzymatic treatment of cured epoxy. Nevertheless, despite the possibility that guaiacol competes with epoxy models for substrate binding, this mediator-laccase system should still be considered in future studies to determine whether it can enhance enzyme activity on cured epoxy.

Preliminary tests on the eCFRPs, however, showed no significant degradation. Therefore, organic chemical pre-treatment was explored to assess its potential in helping enzymes overcome steric hindrance and improve their accessibility to the resulting oligomers or degradation byproducts.

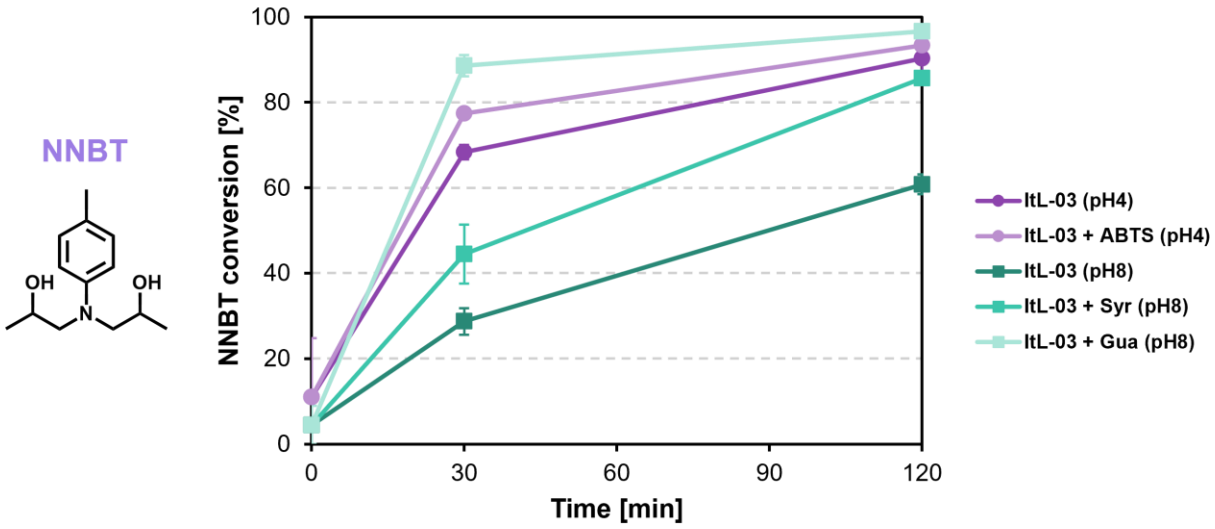

Figure 19. Enzymatic activity of ItL-03 on NNBT with different mediators—ABTS, syringol (Syr), and guaiacol (Gua)—was measured using LC-MS after 0, 30, and 120 minutes of incubation. The initial observation (t_0) represents the starting amount of epoxy, set at 100%. The conversion is calculated by subtracting the percentage of remaining epoxy from 100%. ItL-03/guaiacol exhibits higher activity than ItL-03/ABTS at the 30-minute mark; however, both conditions achieve similar levels of activity, exceeding 90%, after 2 hours. Error bars indicate the standard deviation (n = 3).

3.5 Screening promising acidic-peroxide pretreatments for eCFRPs

The European standard (DIN EN 2564:2018; e.V. (2019)) employs sulfuric acid and 30% H_2O_2 at temperatures ranging from 160 to 260 °C to determine fiber, resin, and void contents of eCFRPs. This method, however, poses significant risk due to its corrosive nature and extreme toxicity (Agarwal & Pandey, 2023). To address these concerns, alternative mixtures using organic acids such as formic acid (FA), acetic acid (AA), propionic acid (PA), lactic acid (LA), malic acid (MA), tartaric acid (TA), and citric acid (CA) combined with H_2O_2 were selected for the pre-treatment of CFRPs. These organic acids are preferred because they are less toxic, have a reduced impact on the environment, originate from renewable resources, and can break down into harmless byproducts (Liu et al., 2023; Ström et al., 2001). For comparison, inorganic acids such as nitric acid (NA) and sulfuric acid (SA) were utilized as controls.

3.5.1 Effectiveness of organic acid-H_2O_2 treatments

eCFRPs based on the diglycidyl ether of bisphenol A (DGEBA) were subjected to treatment at 60 °C for 24- and 48-hours using reaction mixtures that contained 60 mL/g of a solution with 95% acid and 5% H_2O_2 at a concentration of 5 M. The 95:5 ratio was chosen deliberately, as the small proportion of H_2O_2 helps to mitigate potential damage to the carbon fibers (Das et al., 2018). After the pre-treatment process, the composites were rinsed thoroughly with water and then dried overnight at 60 °C. The remaining weights, which were indicative of only the mass of the resin, were measured to evaluate the effectiveness of the different acids used for pre-treatment, i.e., weight loss. Treatments that included H_2O_2, with the exception of NA, showed a greater level of resin decomposition compared to those lacking H_2O_2 (Figure 20). This highlights the importance of H_2O_2 in the reaction process, likely due to the *in-situ* formation of peracids.

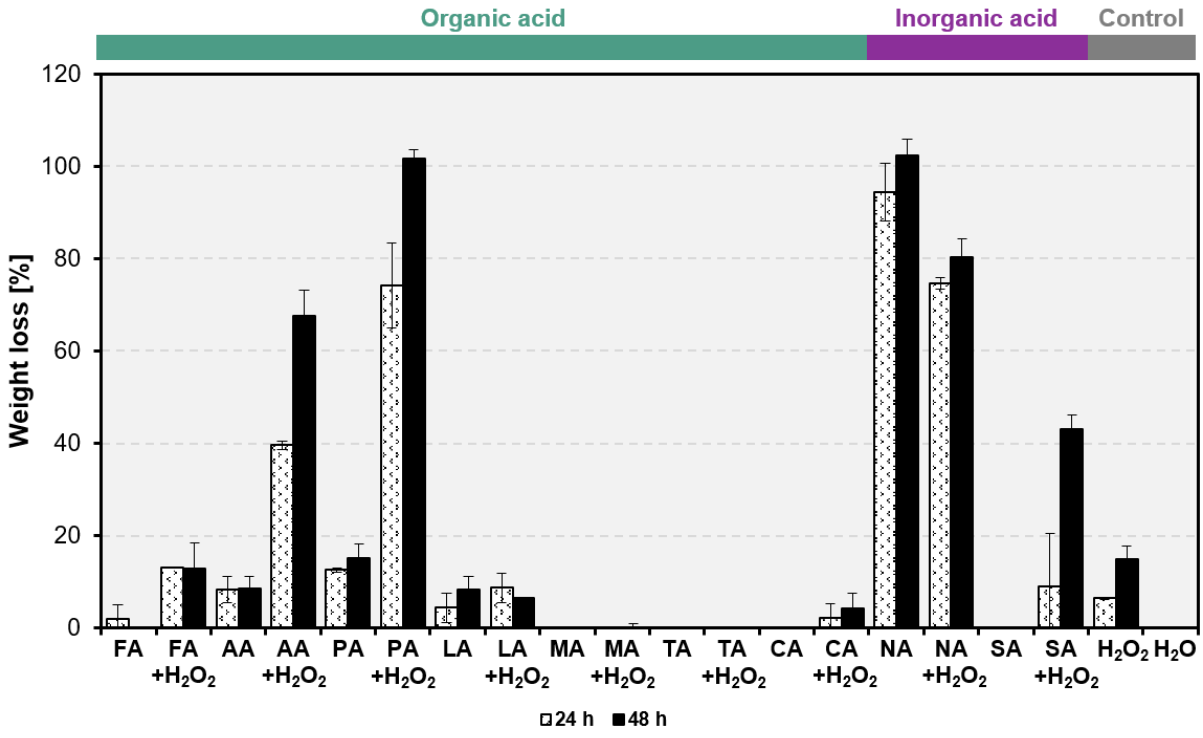

Figure 20. Weight loss of the resin mass in eCFRPs treated with a 5 M acidic-peroxide solution (A-H_2O_2). The composites were treated with organic acids, both with and without H_2O_2, in a 95:5 acid-to-peroxide ratio at 5 M in a 60 mL/g solution, at 65 °C and 200 rpm for 24 and 48 hours. The treatments were compared against inorganic acids and controls (H_2O and H_2O_2). The acids tested included formic acid (FA), acetic acid (AA), propionic acid (PA), lactic acid (LA), malic acid (MA), tartaric acid (TA), citric acid (CA), nitric acid (NA), and sulfuric acid (SA). Error bars represent the standard deviation (n = 3).

AA and PA in combination with H_2O_2 were particularly effective, achieving epoxy resin decomposition of 40% and 80%, respectively, after 24 hours, with propionic acid achieving complete decomposition by the 48-hour mark. Conversely, FA and high molecular weight organic acids (LA, MA, TA, CA) and SA demonstrated limited oxidative activity towards the composites when paired with H_2O_2. When utilizing 9 M solutions of AA-H_2O_2 and PA-H_2O_2, complete decomposition of the epoxy was achieved within 8 hours, which was comparable to the outcomes with NA-H_2O_2 and SA-H_2O_2 (Figure 21).

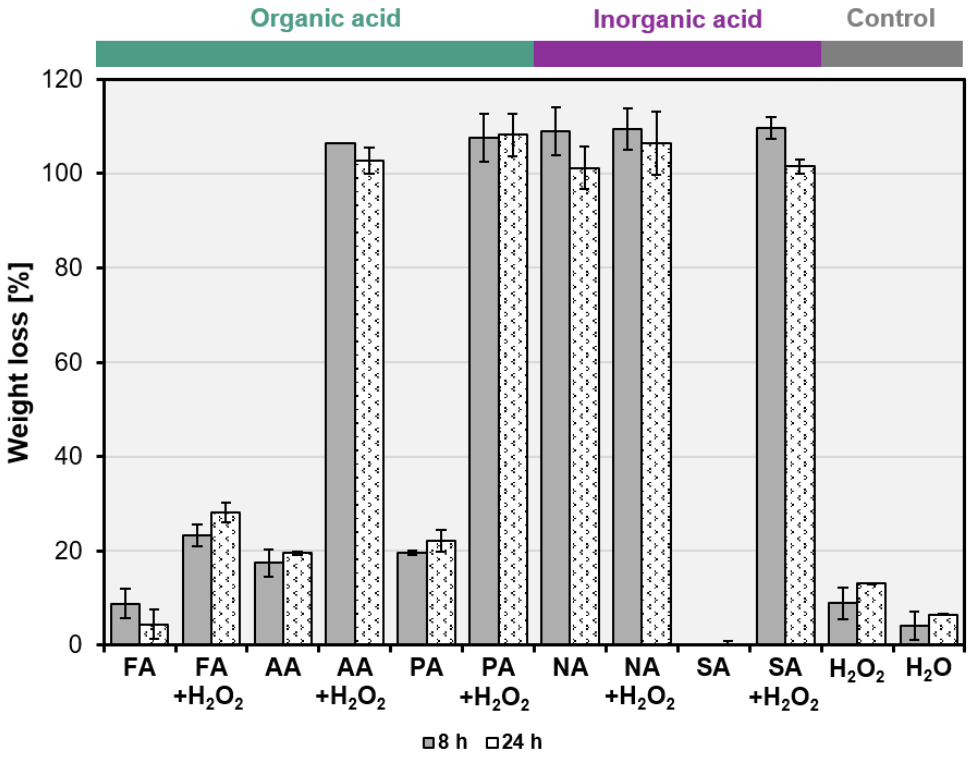

Figure 21. Weight loss of the resin mass in eCFRPs treated with a 9 M acidic-peroxide solution (A-H_2O_2). The acids tested included formic acid (FA), acetic acid (AA), propionic acid (PA), nitric acid (NA), and sulfuric acid (SA). The reaction conditions were consistent with those described in Figure 20, but with shorter treatment durations of 8 and 24 hours. Error bars indicate the standard deviation (n = 3). The effectiveness of these acid-peroxide treatments resulted in complete fiber recovery, which likely caused some loss of carbon fibers during washing and may explain the weight loss values exceeding 100%.

3.5.2 Visualization of pre-treated composites

The physical appearance of the composites pre-treated with 5 M A-H_2O_2 was consistent with the weight loss data obtained. After 48 hours, the carbon fibers (CFs) became noticeable in the composites treated with PA-H_2O_2, indicating the breakdown of the epoxy matrix (Figure 22). Composites treated with AA-H_2O_2 also exhibited some fragments of CFs, whereas those subjected to other acid mixtures maintained their integrity, resembling the control sample treated with H_2O. The composites treated with NA and NA-H_2O_2 showed significant removal of the epoxy matrix; however, they left the CFs largely intact, maintaining their original structure. Additionally, small white particles were observed in these samples, with the exception of those treated with NA, SA, and H_2O. These particles could be metal-organic salts, which are poorly soluble in water. It is possible that cured epoxy composites still contain trace amounts of metal catalysts, pigments, or additives (e.g., Zn, Fe) (Hamerton et al., 2002), which can react with organic acids to form stable chelates (do Nascimento et al., 2006). On the other hand, inorganic acids typically do not form chelating complexes but instead produce soluble ionic salts (Voisin et al., 2017).

Based on the results, only the composites pre-treated with 5 M AA-H_2O_2, PA-H_2O_2, SA-H_2O_2, as well as the controls (untreated composites, UT; H_2O; and those treated according to the European protocol, SH_{EU}), were analyzed using scanning electron microscopy (SEM). After 24 hours, some areas of the eCFRPs treated with these acidic-peroxide solutions still exhibited polymer residues (Figure S8). However, after 48 hours of treatment with PA-H_2O_2, clean, undamaged, and elongated CFs were recovered, resembling those obtained through the European protocol treatment (Figure 23). Meanwhile, remnants of epoxy were still present in the composites treated with AA-H_2O_2 and SA-H_2O_2. Both the untreated samples and the water control, however, showed no visible CFs, as the epoxy matrix remained intact.

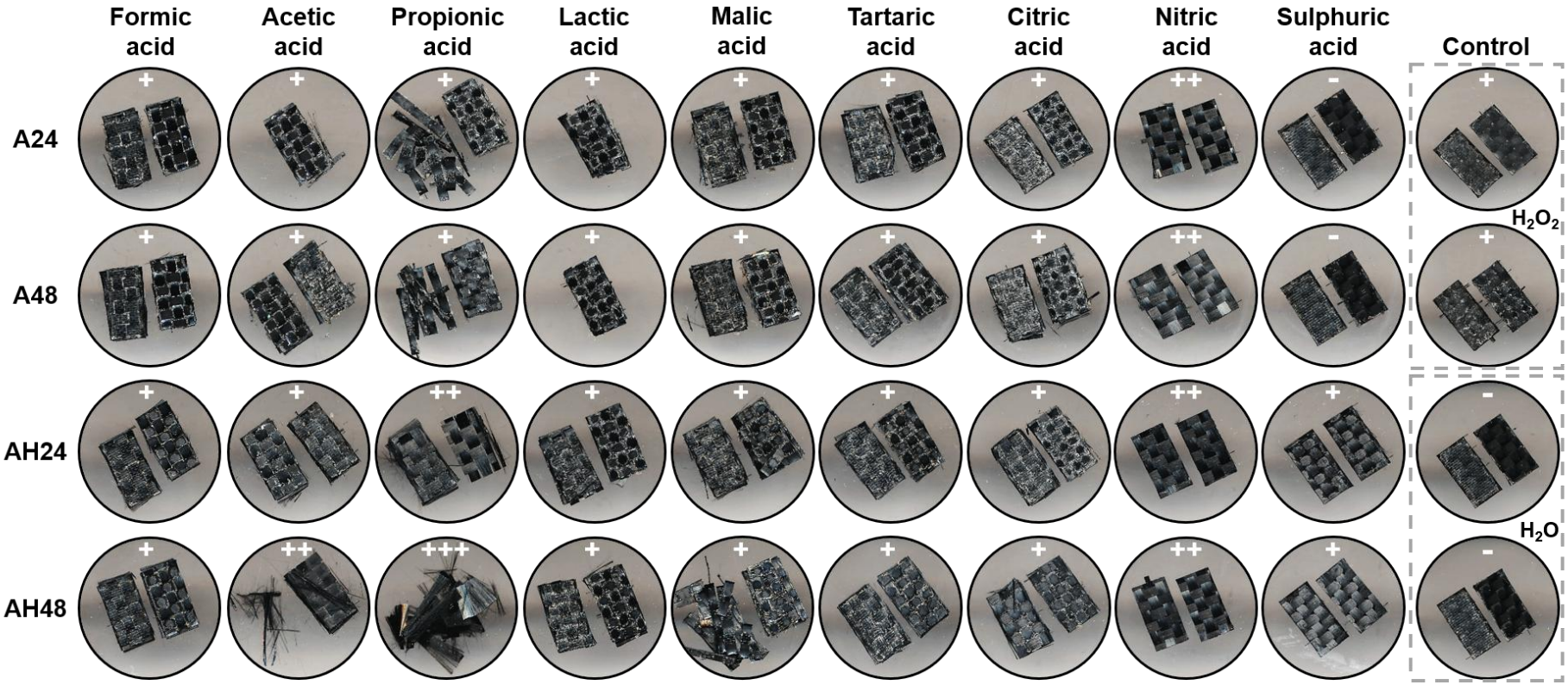

Figure 22. Morphological changes in eCFRPs after 24 and 48 hours of 5 M acidic-peroxide pre-treatment, with only acid (A) and with both acid and H_2O_2 (AH), were assessed and compared to controls (H_2O and H_2O_2). The composites were incubated with a 95:5 acid-to-peroxide ratio at a 5 M, 65 °C and 200 rpm. The symbols +, ++, and +++ represent the degree of carbon fiber exposure, ranging from low to high, while – indicates no change observed.

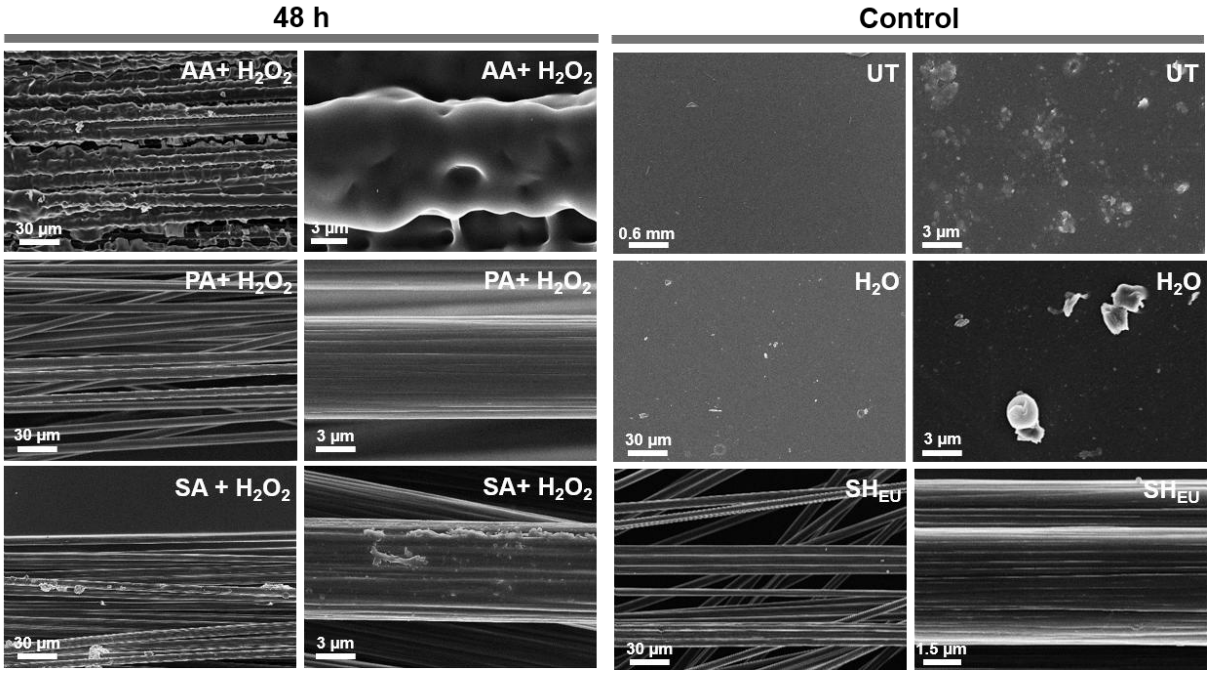

Figure 23. SEM images of eCFRPs after 48-hour treatment with 5 M acidic-peroxide solution (A-H_2O_2). The acids tested included acetic acid (AA), propionic acid (PA), and sulfuric acid (SA). These results are compared to those obtained from European protocol (SH_{EU}) and controls, which include an untreated sample (UT) and H_2O. Scale bars indicate size in micrometers (µm) and millimeters (mm). PA-H_2O_2 treatment recovered clean carbon fibers after 48 hours, whereas some epoxy residues were still present with AA-H_2O_2 and SA-H_2O_2 treatments. 24- hour treatment can be found in Figure S8.

3.5.3 Functional group modification of pre-treated composites

Fourier Transform Infrared Spectroscopy (FTIR) was employed to investigate the formation or modification of specific functional groups in the composites following pre-treatment. The FTIR spectra revealed a similar pattern of peaks, although with varying intensities, for both the water control and the acid-peroxide-treated samples, with a few notable exceptions (Figure 24). For example, a peak corresponding to the C=C aromatic band (around 1,600 cm^{-1}), which indicates the presence of a benzene ring structure, was identified in all epoxy composite samples. However, the C=O stretching band (around 1,750 cm^{-1}) was detected exclusively in composites that underwent acid-peroxide pre-treatment, suggesting possible oxidation. Treatments with AA- and PA-H_2O_2 exhibited higher peak intensities in the C=C aromatic band range compared to SA-H_2O_2, possibly due to the formation of additional carbonyls groups and potentially primary or secondary amines. Other absorption bands associated with the epoxy functional groups, such as C–N stretching in aromatic amines around 1,240 cm^{-1}, and CH_2 and CH_3 stretching in aliphatic around

2,960-2,860 cm^{-1}, showed a significant reduction in intensity in the spectra of the pre-treated composites, indicating alterations to the epoxy matrix's surface. Additionally, the observed shift of the OH peaks from 3,400 to 3,250 cm^{-1} provided further evidence of epoxy oxidation following treatment. The stretching peaks associated with OH and C=O bonds in composites treated with organic acid-H_2O_2 were more pronounced than those in SA-H_2O_2-treated samples, suggesting that SA-H_2O_2 was particularly effective in converting C–N bonds in aromatic amines to C–N bonds in primary amines. This observation indicates that organic and inorganic acids target different functional groups within epoxy materials.

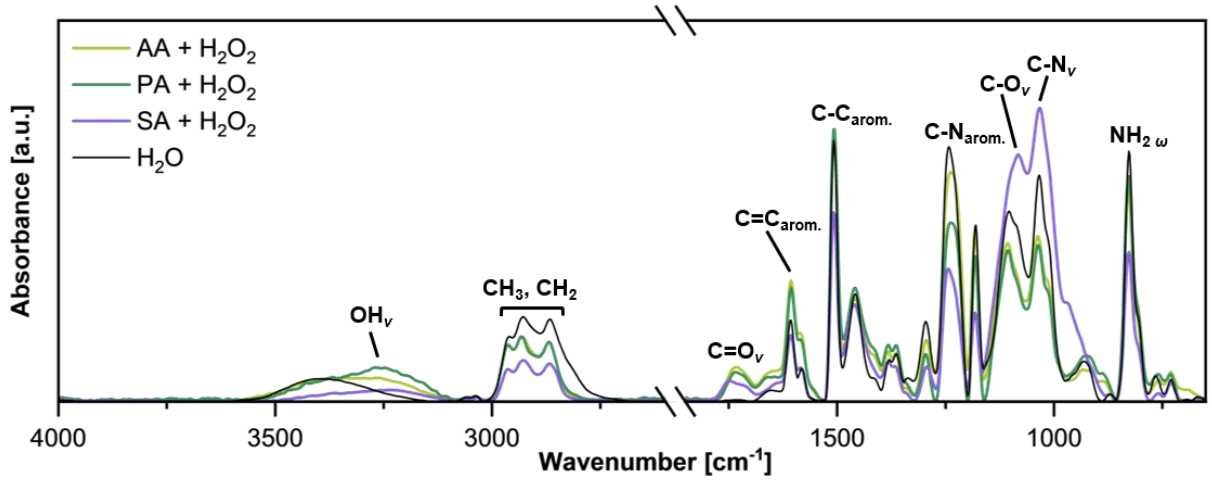

Figure 24. FTIR analysis of the 8-hour acidic-peroxide pre-treatment of eCFRPs. The acids used were acetic acid (AA), propionic acid (PA), and sulfuric acid (SA). The corresponding functional groups are indicated. *v* denotes stretching, while *ω* denotes wagging. Both organic and inorganic acid treatments were found to target different functional groups within the material. PA-H_2O_2 demonstrated superior efficacy compared to AA-H_2O_2 in decomposing epoxy.

These findings confirm the effectiveness of acid-peroxide pre-treatments in promoting the decomposition of epoxy resins. Notably, PA-H_2O_2 stands out as a promising alternative for pre-treatment, exhibiting effectiveness comparable to that of inorganic acids while posing lower environmental risks. The use of pre-treatment techniques to depolymerize eCFRPs enables the recovery of clean CFs, which could potentially be reused in future applications.

3.6 Chemical-enzymatic treatment of RTM6

The pre-treatment using PA-H_2O_2 effectively depolymerized the epoxy matrix of the composite primarily based on DGEBA, resulting in the recovery of CFs. Although the pre-treatment alone can yield clean CFs, it is essential to investigate whether enzymes can further decompose the residual polymer matrix to produce a more defined product that would facilitate downstream processing. Laccase ItL-03 exhibited significant activity towards epoxy model substrates featuring tertiary amine structures that are characteristic of RTM6 epoxy. Hence, the combination of these two oxidative approaches was assessed for their potential to improve the bio-based recycling of RTM6 resin, which is derived from TGMDA amine epoxy precursors and two di-amine hardeners, namely 4,4′-methylenebis(2,6-diethylaniline) (MDEA) and 4,4′-methylenebis(2-isopropyl-6-methylaniline) (M-MIPA). The choice of RTM6 epoxy over the composite was made because the carbon fiber content was no longer a focus, allowing for an investigation into the effects of PA-H_2O_2 pre-treatment on this high-performance amine epoxy (Addou et al., 2016).

3.6.1 Epoxy extract

Following the application of PA-H_2O_2 pre-treatment to the RTM6 resin powder, the resulting solution was neutralized and extracted, referred to as "epoxy extract". This epoxy extract was then treated with ItL-03, either with the addition of ABTS or without it. Bovine serum albumin (BSA) was included for comparison. After the completion of the chemical-enzymatic treatment, the samples were subjected to analysis using electrospray ionization-mass spectrometry (ESI-MS) via direct injection to identify polar compounds and larger biomolecules. Meanwhile, gas chromatography-mass spectrometry (GC-MS) was employed to characterize volatile and semi-volatile compounds (Konermann et al., 2013; Tsizin et al., 2017; Vázquez-Loureiro et al., 2021).

The ESI mass spectra, recorded in positive mode, indicated that the PA-H_2O_2 treatment effectively decomposes epoxy resins into various small compounds within the mass-to-charge ratio (*m/z*) ranges of 150-200 and 300-500, showing high intensity across all samples (Figure 25). However, the detected ions at *m/z* 483.3 were significantly lower in the treatment with ItL-03, particularly when ABTS was included as a mediator, compared to the negative control that contained BSA and the buffer controls (t_0, t_2, and t_{24}).

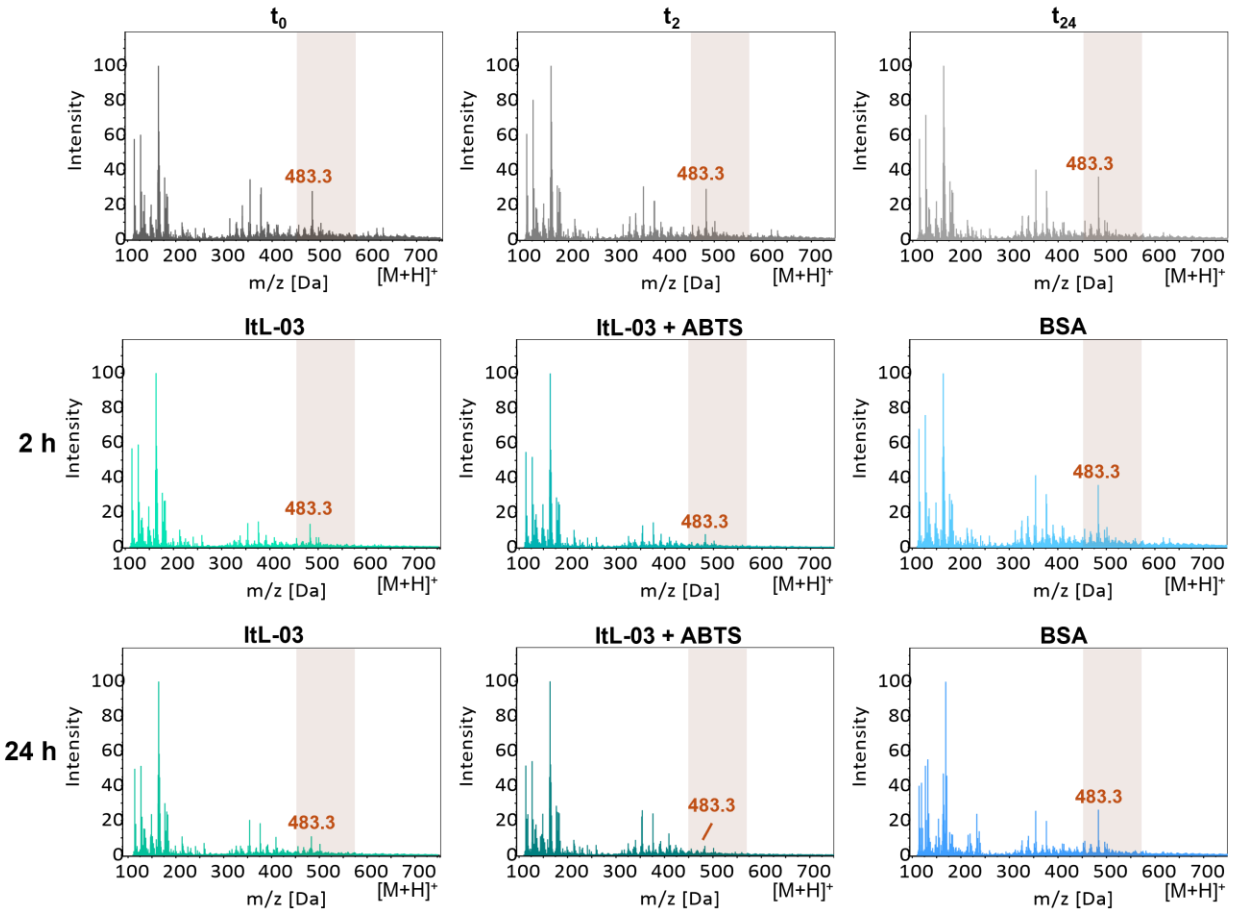

Figure 25. ESI-MS analysis of epoxy extract following chemo-enzymatic treatment using PA-H_2O_2 and laccase ItL-03 on RTM6. The ESI-MS spectrum was obtained via direct injection in positive mode, illustrating the activity of ItL-03 with and without ABTS, compared to BSA. Samples were collected after 0, 2, and 24 hours, with t_0, t_2, and t_{24} representing controls without the enzyme at the beginning, between, and end of the incubation period, respectively. The ion at *m/z* 483.3 was mostly absent in the laccase samples but remained present in the controls. Negative controls compared to the blank sample are shown in Figure S9.

Furthermore, ions at *m/z* 354.2, and 501.3 were observed at lower intensities in the laccase samples, regardless of the presence of ABTS, compared to the other samples (Figure 26). The marked decrease in the intensities of ions with *m/z* 354.2 and 483.3 in the presence of laccase ItL-03 suggests that the enzyme may oxidize or modify these compounds. Possible structures for the resulting products observed following ItL-03 treatment were proposed, considering the formation of adducts (Figure 27).

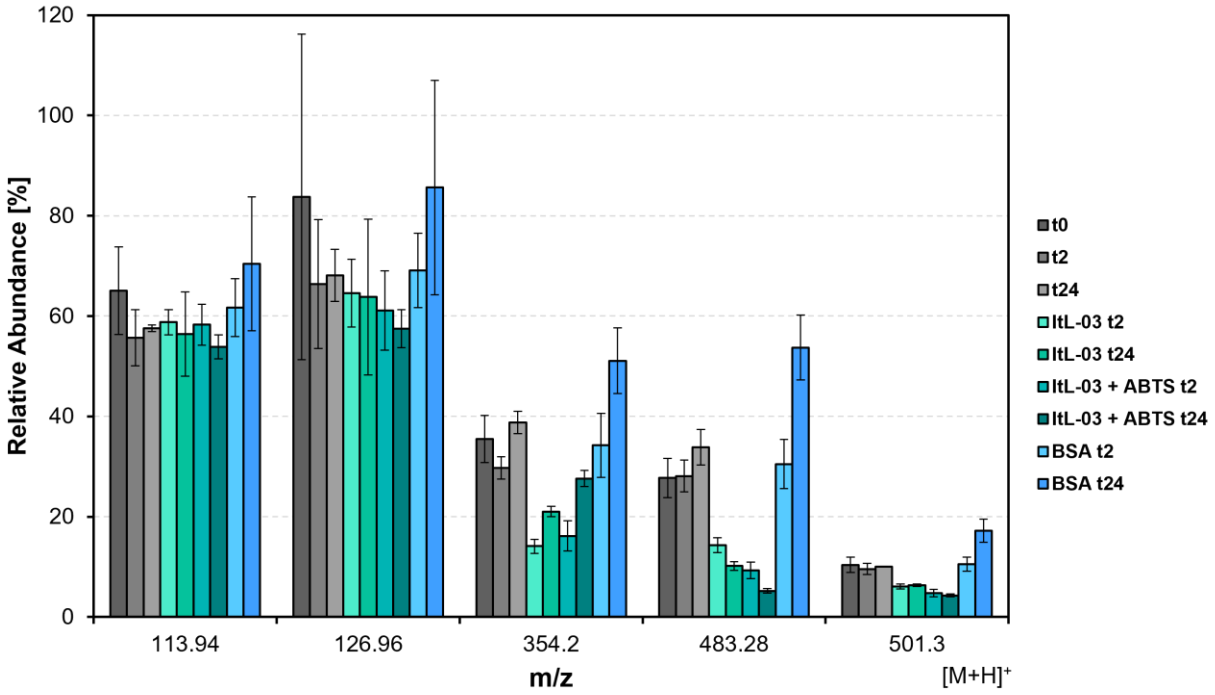

Figure 26. The relative abundance of *m/z* values of interest from the ESI-MS analysis in Figure 25. The spectra were normalized using the *m/z* value at 163.9 as a reference peak. t_0, t_2, and t_{24} represent controls without enzyme at the beginning, between, and end of the incubation period. The abundance of the five ions is lower in the samples treated with the ItL-03 compared to the controls, particularly at *m/z* 354.2 and 483.3. Error bars represent the standard deviation (n = 3). Significant differences between sample pairs are shown in Figure S10.

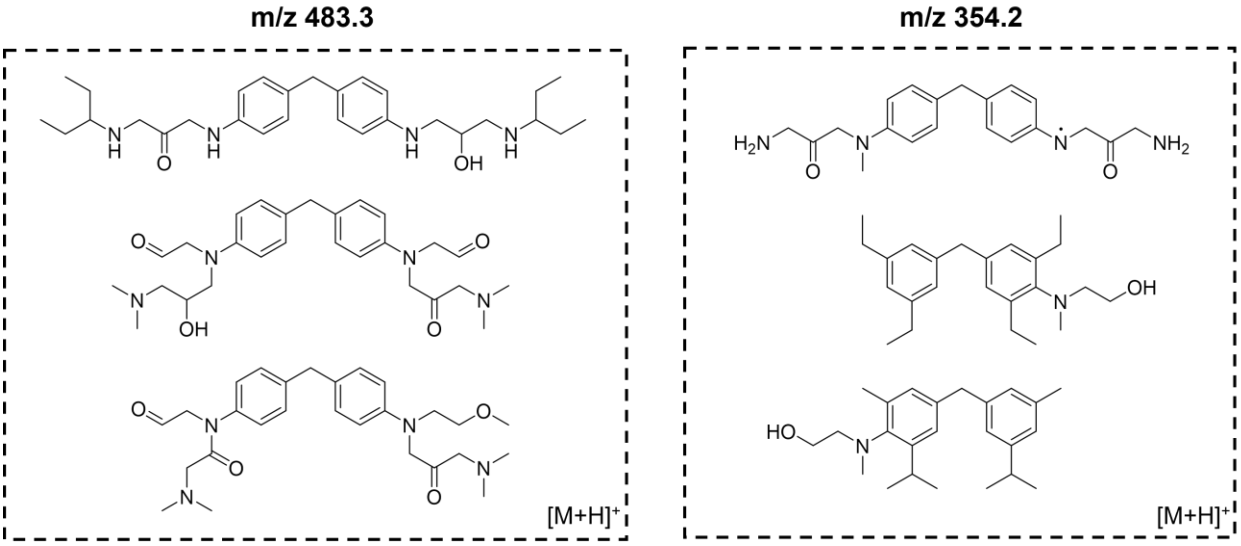

Figure 27. Proposed compounds potentially oxidized by the enzyme following PA-H_2O_2 treatment. These are with *m/z* values of 483.3 and 354.2, considering possible adduct formation. The structures of these compounds are predicted based on the RTM6 formulation.

The GC-MS chromatograms, which displayed a lower range of *m/z* compounds, exhibited peaks with retention times between 7-9 minutes and 12-14 minutes (Figure 28). Specifically, within the latter interval, distinct peaks A and B were identified at 12.4 and 13.2 minutes, respectively, in the BSA and control samples (t_0, t_2, and t_{24}), which are regarded as byproducts of the pre-treatment.

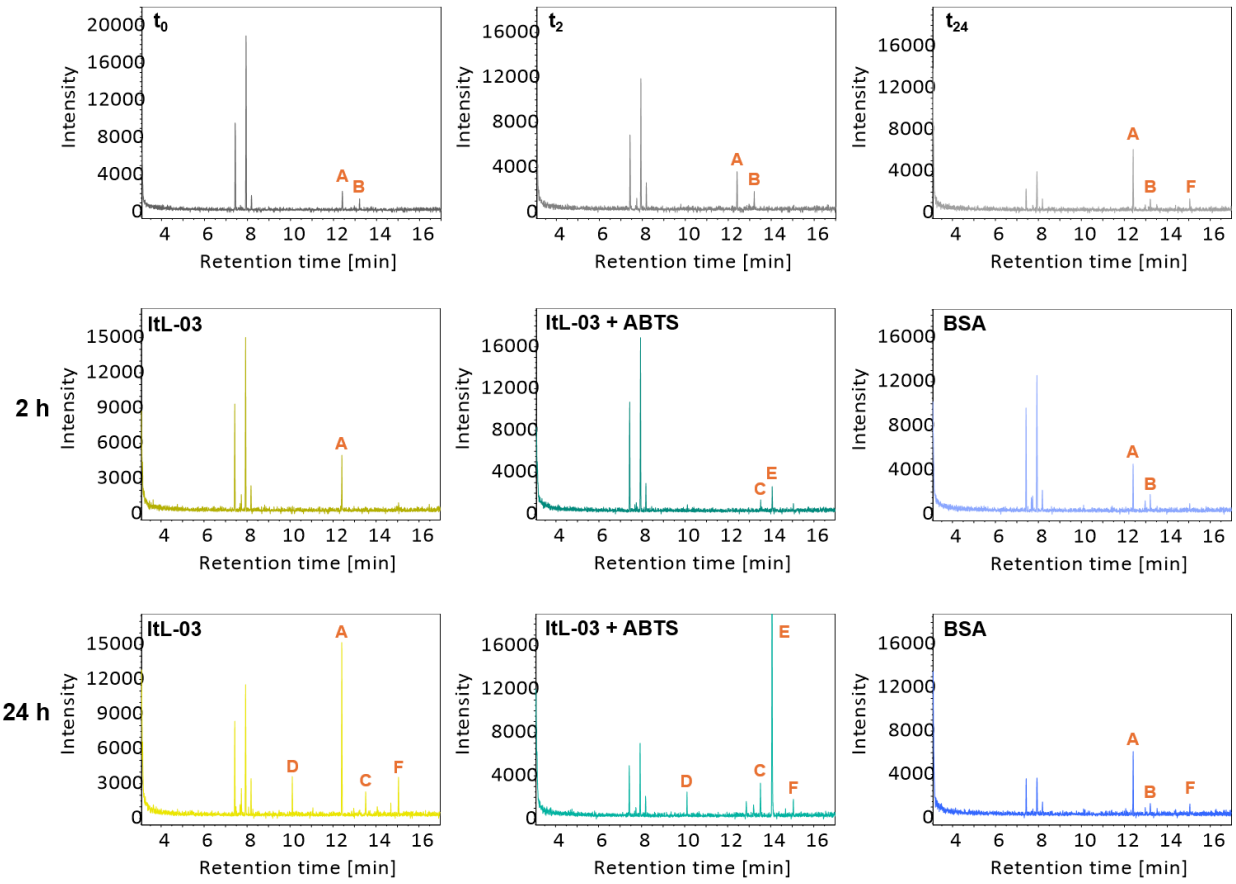

Figure 28. GC-MS analysis of epoxy extract following chemo-enzymatic treatment using PA-H_2O_2 and laccase ItL-03 on RTM6. Measurements were collected after 0, 2, and 24 hours. t_0, t_2, and t_{24} represent controls without enzyme at the beginning, between, and end of the incubation period. The peaks of interest are labelled A-F. Peaks A and B were observed in BSA and control samples but were absent in the ItL-03/ABTS samples. Peaks C and D were detected in ItL-03 samples after 24 hours, while peak E was only present in samples containing ABTS. Peak F was detected in all samples after 24 hours. Negative controls compared to the blank sample are shown in Figure S11.

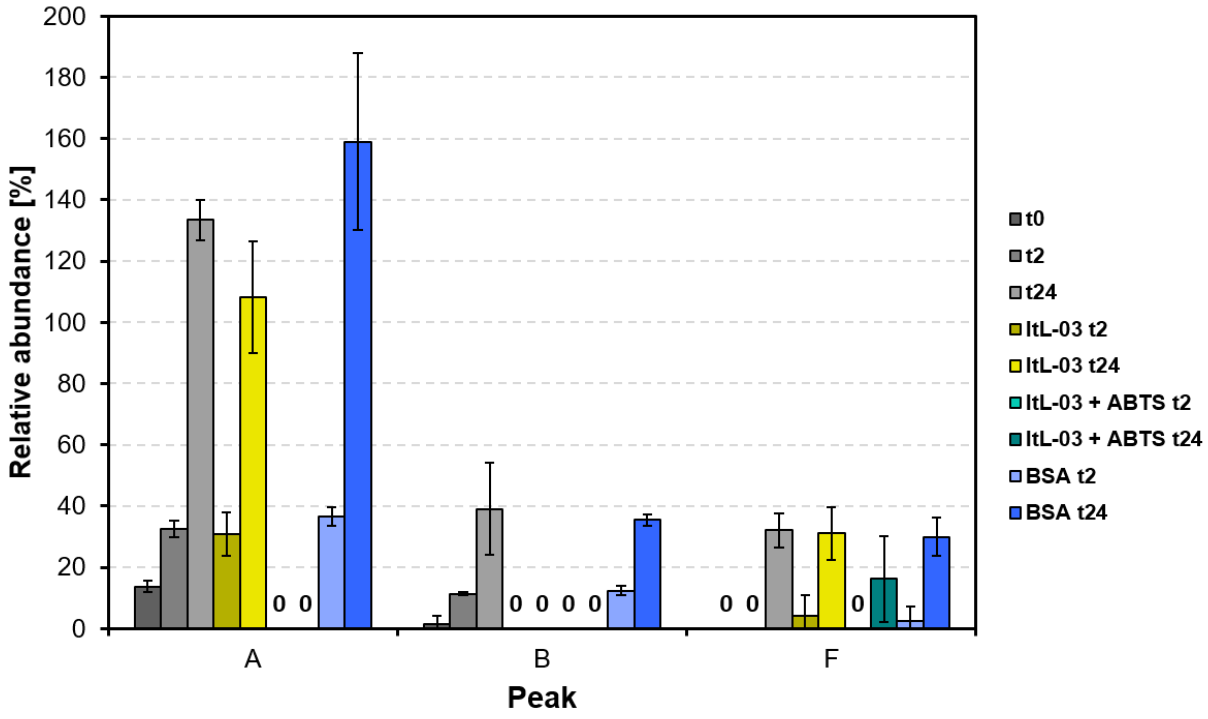

Figure 29. The relative abundance of peaks A, B, and F from the GC-MS analysis in Figure 28. The spectra were normalized using the peak at 7.9 min as a reference. t_0, t_2, and t_{24} represent controls without enzyme at the beginning, between, and end of the incubation period. Peaks A and B were observed in the BSA and control samples; however, peak A was absent in the ItL-03/ABTS samples, and peak B was additionally absent in all ItL-03 samples. Peak F was detected in most samples after 24 hours. Error bars represent the standard deviation (n = 3). Significant differences between sample pairs are shown in Figure S12.

Notably, peak A was absent in the ItL-03/ABTS samples, while peak B was not detected in the samples containing ItL-03 (Figure 29). In the samples treated with ItL-03/ABTS, peak C was observed, and after 24 hours, an additional peak D was identified. Peak E appeared in samples containing ABTS, while peak F was only detected in samples incubated for 24 hours. The species associated with peaks A and B, corresponding to *m/z* 178 and 166 respectively, may have been oxidized by laccase and could originate from NNBT or fractions of RTM6. Additionally, it is possible that the ions at *m/z* 178 underwent deprotonation to form the ions at *m/z* 177, related to Peak C, as they exhibited similar ionization patterns (Figure 30). Alternatively, these ions might represent distinct molecules that have nearly identical masses, such as the proposed *m/z* pairs of 166-165 for peaks B and D (Figure 31). To validate the hypothesis regarding these byproducts, the compounds should be isolated and analyzed using NMR spectroscopy.

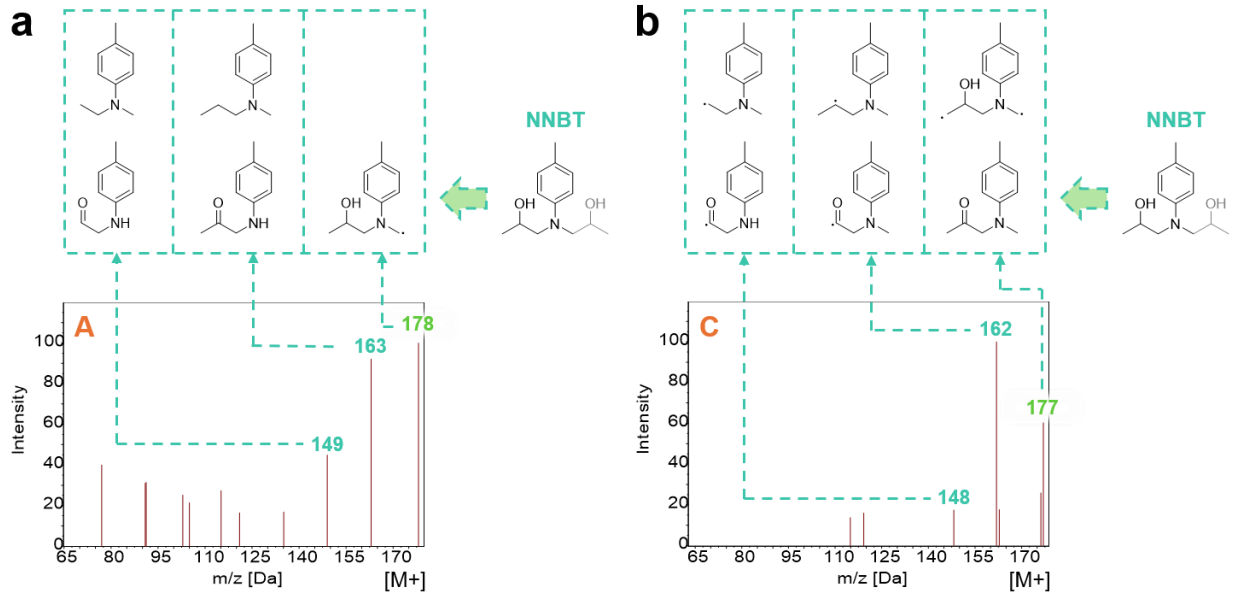

Figure 30. Proposed species for the peaks (a) A (12.4 min) and (b) C (13.5 min) that may be oxidized by ItL-03 are identified based on the GC-MS chromatogram shown in Figure 28. Specifically, these ions may originate from NNBT, with the *m/z* pairs of 177 and 178 likely resulting from the protonation and deprotonation of the same species, as they exhibit similar ionization patterns.

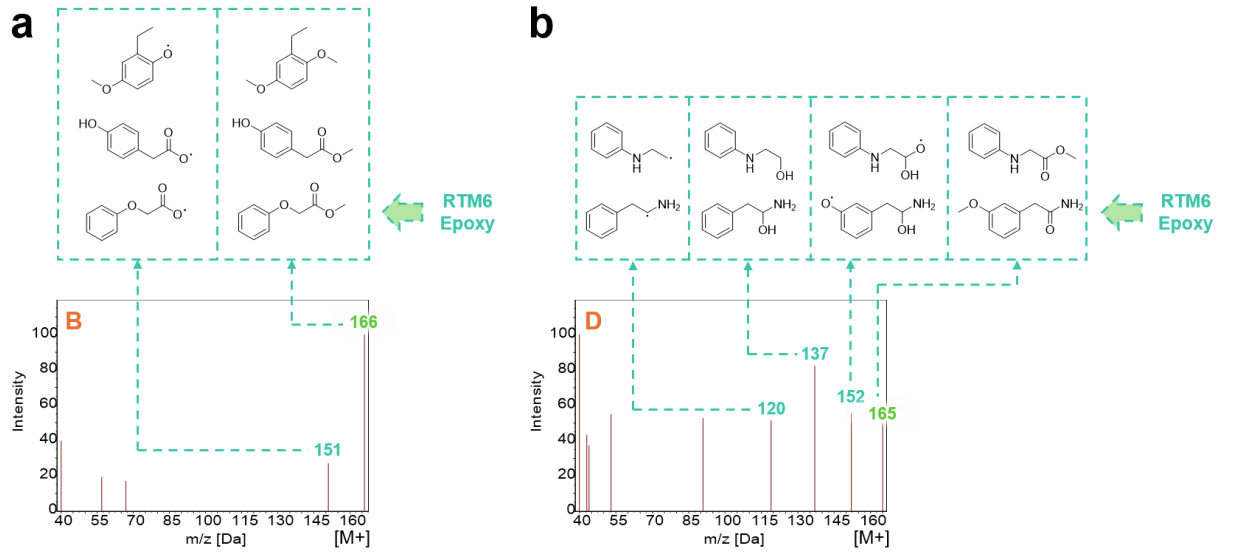

Figure 31. Proposed species for the peaks (a) B (13.2 min) and (b) D (10.1 min) that may be oxidized by ItL-03 are identified based on the GC-MS chromatogram shown in Figure 28. These ions may originate from the amine epoxy resins that are decomposed by either pre-treatment or the enzyme. As the *m/z* pairs of 165-166 exhibit different ionization patterns, they could represent completely different species.

The prominent peak E produced from ItL-03/ABTS treatment corresponds to *m/z* 144. This peak is likely a fragment of ABTS, as its ionization patterns align with its mass fraction (Figure 32). Another possibility is that this peak originated from the breakdown of components within RTM6, potentially due to the enzyme's activity.

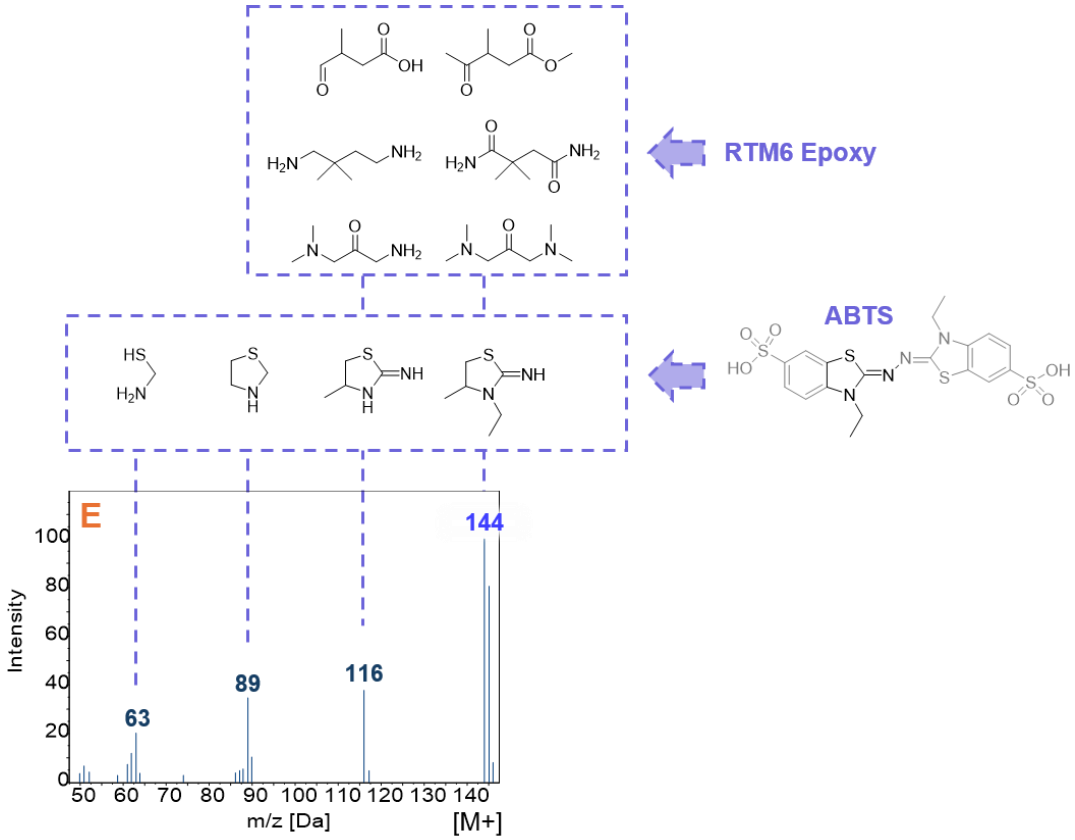

Figure 32. Proposed species for the peak E (14 min) that may be oxidized by ItL-03 are identified based on the GC-MS chromatogram shown in Figure 28. This compound is most likely derived from the fraction of ABTS, as it exhibits ionization patterns consistent with the ABTS mass fraction. Another possibility is that it results from the decomposition of epoxy resins.

3.6.2 Remaining epoxy powder

The PA-H_2O_2 treatment was unable to completely decompose the RTM6 epoxy powder following a two-day incubation, resulting in some residual epoxy powder. This excess was filtered, thoroughly washed with water, and dried overnight at 60 °C. The FTIR spectra displayed distinct band patterns between the non-treated (RTM6) epoxy, which refers to the epoxy that was not pre-treated with PA-H_2O_2, and the pre-treated (PT-RTM6) epoxy powders, both measured prior to

enzyme treatment (Figure 33). This finding suggests that the PA-H_2O_2 treatment led to modifications in the functional groups of the epoxy resins. Notably, the C=O stretching band (approximately 1,750 cm^{-1}) was present only in PT-RTM6 and not in RTM6, further confirming the oxidative effects of the prior pre-treatment on the DGEBA-based epoxy resin (Figure 24). RTM6 and PT-RTM6 were subsequently introduced to ItL-03, with or without the addition of mediators (ABTS, syringol, and TEMPO). TEMPO was selected for its relatively high redox potential. The FTIR spectra for the controls (laccase ItL-03, BSA, and the tris buffer used for the enzyme stock solution) are presented in Figure S13. They predominantly display bands corresponding to OH groups, C=O functionalities, and NH groups.

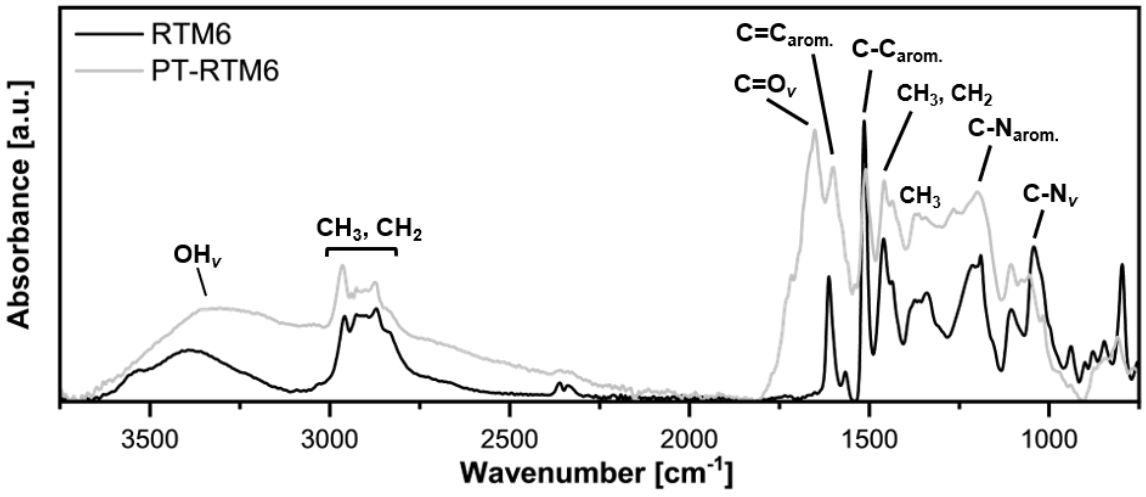

Figure 33. FTIR analysis of RTM6 epoxy powder. Non-treated epoxy powder (RTM6), which did not undergo any treatment, compared to pre-treated epoxy (PT-RTM6), which was treated with 5 M PA-H_2O_2 for 2 days. These epoxy samples were not subjected to enzymatic treatment. The corresponding functional groups are indicated. ν — stretching; δ — deformation.

After the enzymatic treatment with ItL-03 on the non-treated RTM6 powder with mediators, a significant change in the peak intensity of the C–N stretching associated with aromatic amines (1,210-1,180 cm^{-1}) was observed. However, this effect resembled that of the control, which was BSA, indicating that the band shifts could be attributed to water incubation rather than enzymatic activity (Figure 34). Epoxy resin tends to absorb water and swell, which may weaken its structural integrity (Walter et al., 2013). This was not the case for the ItL-03/syringol treatment, which exhibited slight changes that differed from the control. In addition to this functional group, the OH

(3,500-3,250 cm^{-1}) and C=O stretching bands (approximately 1,750 cm^{-1}) exhibited higher intensity in the enzyme samples without a mediator (ItL-03) and ItL-03/syringol compared to the BSA controls. Thus, it is possible that ItL-03 and ItL-03/syringol can slightly oxidize RTM6 without prior treatment.

For PT-RTM6 samples treated with ItL-03, the epoxy functional groups, such as C–N stretching in both aromatic (around 1,200 cm^{-1}) and primary (1,085-1,050 cm^{-1}) amines, along with CH_3 and CH_2 stretching (2,970-2,870 cm^{-1} and 1,460 cm^{-1}), exhibited lower intensities compared to those without the enzyme (Figure 35). This effect was even more pronounced in the presence of mediators, particularly syringol and TEMPO. The pre-treatment of the epoxy may facilitate the enzyme's access to the embedded epoxy functional groups, leading to further modification and a partial reduction of amine functionalities. Unlike RTM6, the OH and C=O bands in the PT-RTM6 samples showed similar intensities between the enzyme and control samples, except in those that contained syringol. This implies that, without pre-treatment, the enzyme is likely to modify the more accessible and reactive OH and C=O groups on the surface of the material, while it can affect the less reactive amine functional groups of the epoxy when the material is treated.

Overall, ItL-03/syringol has proven to be the most effective enzyme candidate for modifying the amine-based epoxy, as indicated by its ability to reduce the intensities of epoxy functional groups (e.g., $C–N_{arom.}$, $C–N_{\nu}$, CH_3, CH_2) (Figure 36). Additionally, three distinct peaks in the FTIR spectra, appearing at 1,558 cm^{-1}, 1,270 cm^{-1}, and 1,116 cm^{-1}, were associated with epoxy functional groups and correspond to NH stretching in secondary amides, C–O stretching in epoxides, and C–O–C antisymmetric stretching in aliphatic ethers, respectively. These peaks were even more pronounced than those observed in PT-RTM6. This observation suggests that these peaks may result from specific interactions between syringol and epoxy that could remain on the surface. Therefore, it may be necessary to investigate the reaction of syringol with epoxy alone to determine whether these peaks would reappear and correlate with the abovementioned findings.

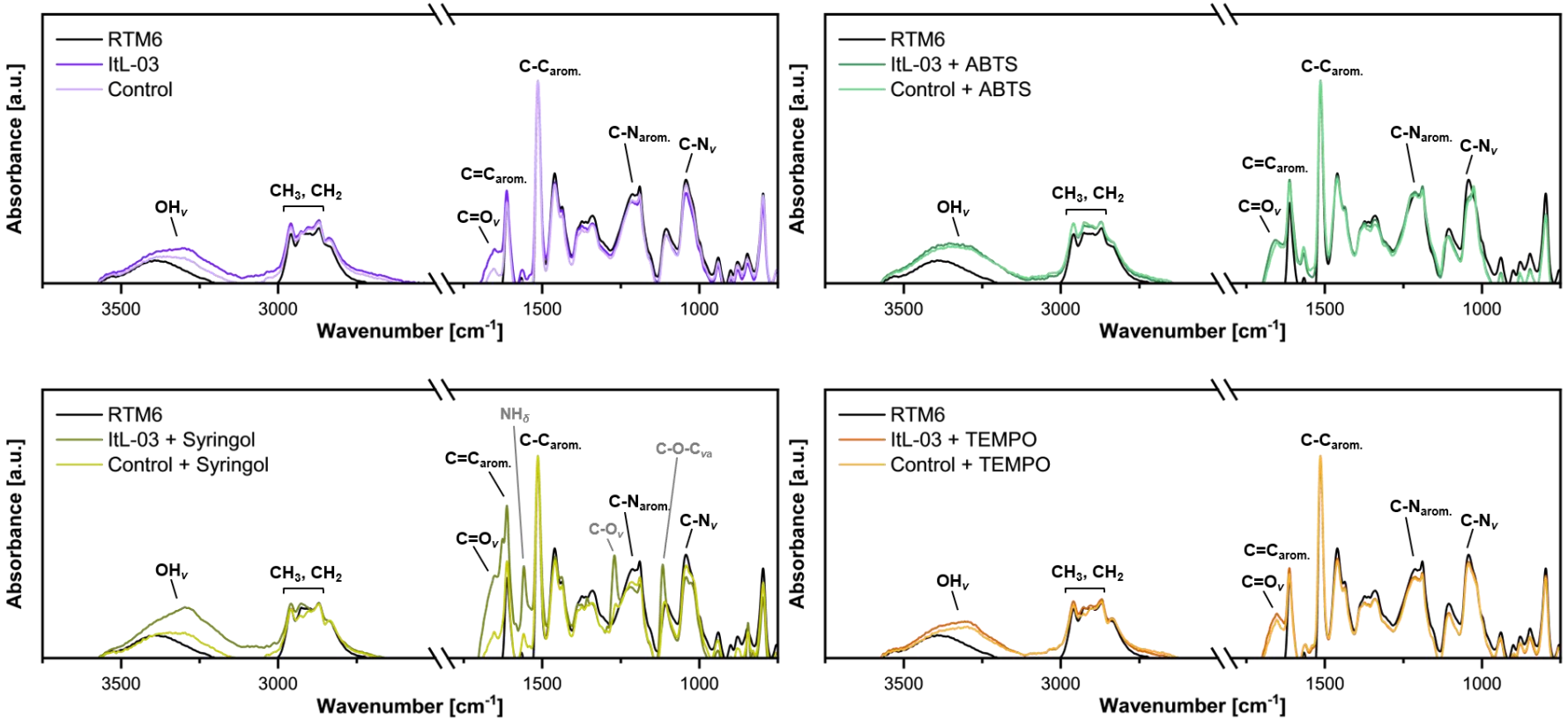

Figure 34. FTIR analysis of the enzymatic activity of ItL-03 after 5 days on non-treated epoxy resins (RTM6) with and without mediators: ABTS, syringol, and TEMPO. A sample labeled RTM6 was not subjected to chemical-enzymatic treatment. BSA was used as a control. The corresponding functional groups are indicated. *v* — stretching; *v*a — asymmetric stretching; *δ* — deformation. Most ItL-03 exhibits activity similar to that of the control, suggesting that the laccase barely oxidizes the epoxy, even in the presence of mediators. The exception is that ItL-03/syringol shows slightly more activity than the control, particularly in relation to the functional groups C-$N_{arom.}$ and C-N_v.

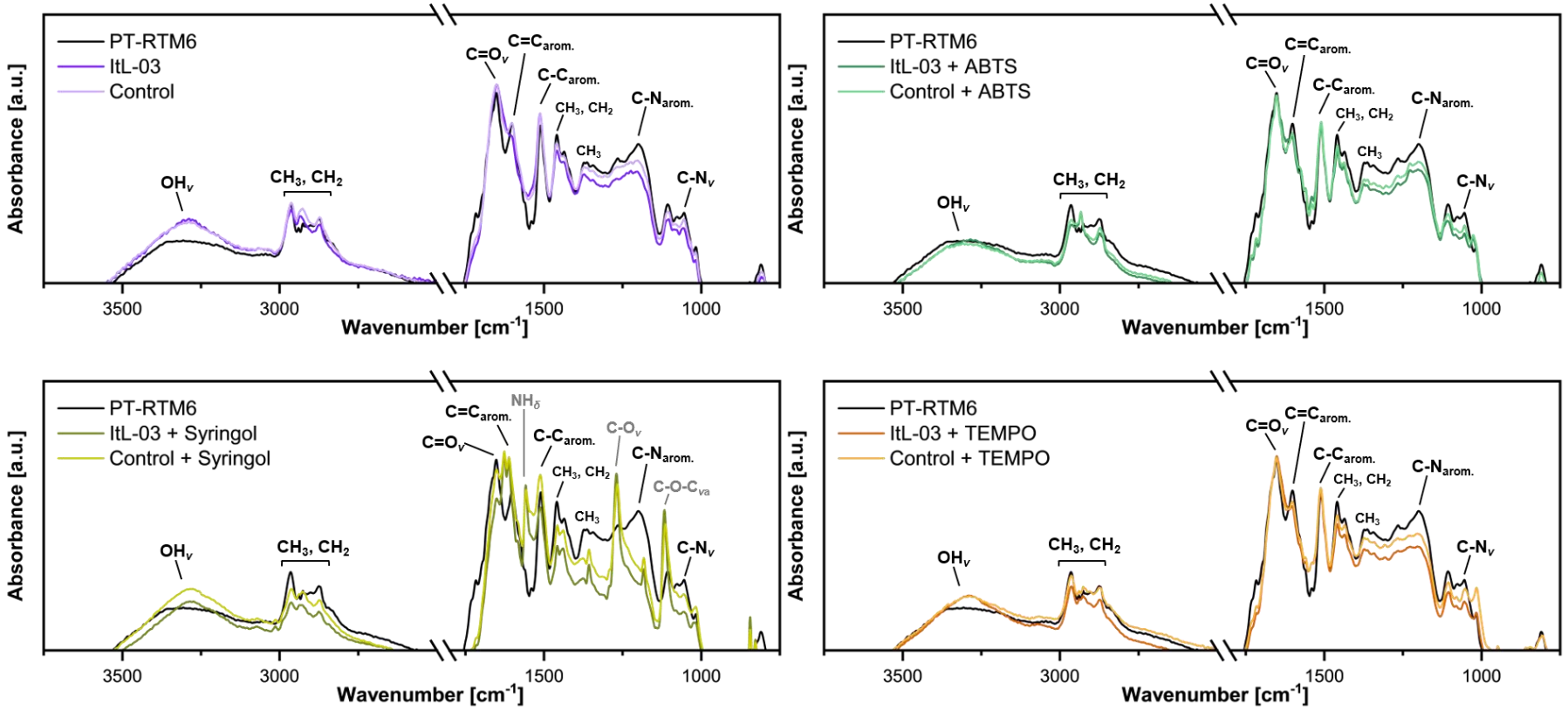

Figure 35. FTIR analysis of the enzymatic activity of ItL-03 after 5 days on pre-treated epoxy powder (PT-RTM6) with and without mediators: ABTS, syringol, and TEMPO. A sample labeled PT-RTM6 was treated previously with an acidic-peroxide solution but was not subjected to enzymatic treatment. BSA was used as a control. The corresponding functional groups are indicated. *v* — stretching; *v*a — asymmetric stretching; *δ* — deformation. ItL-03, with or without the mediators, can slightly modify the pre-treated epoxy, which shows changes compared to the control, particularly concerning the functional groups C-$N_{arom.}$ and C-N_{v}.

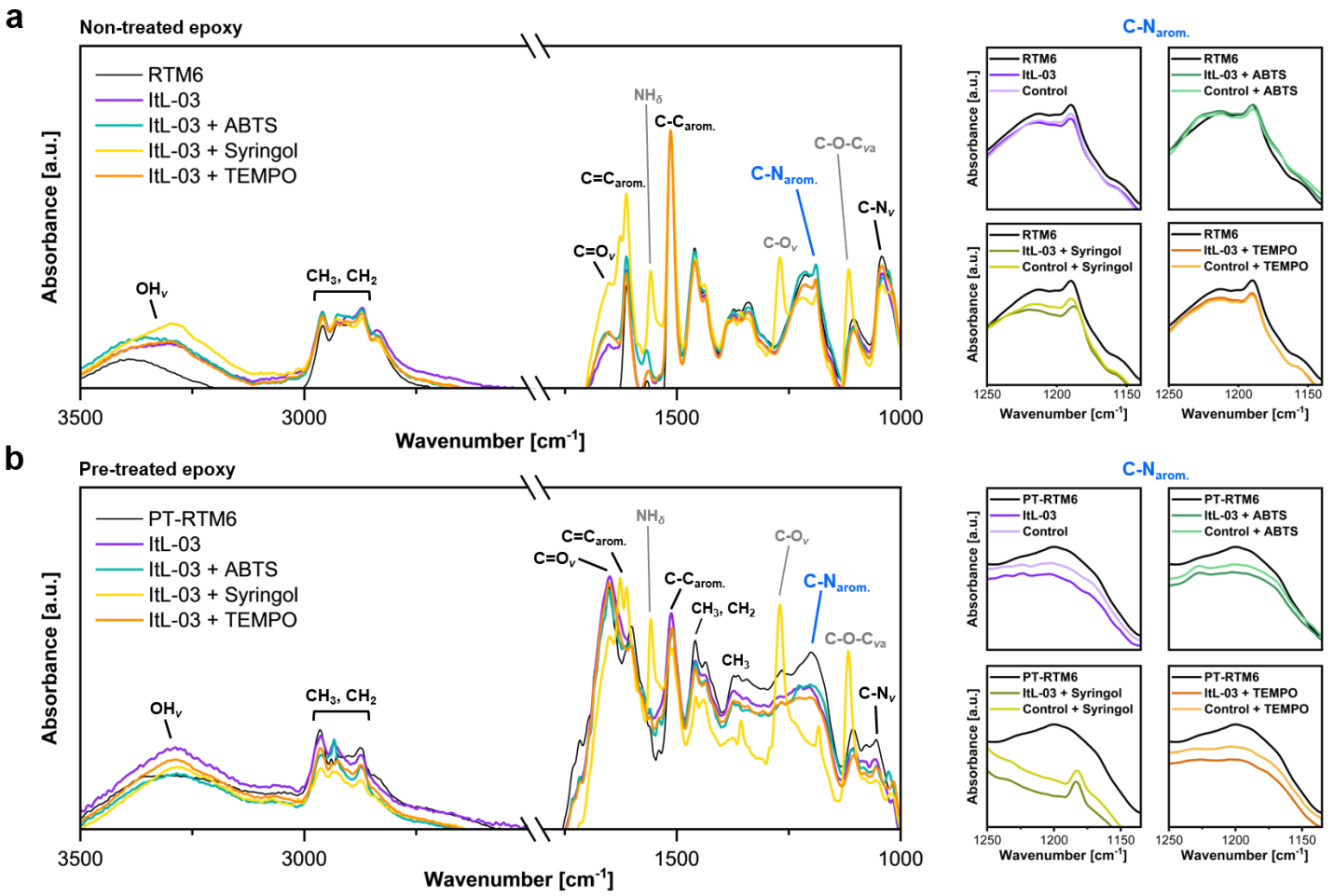

Figure 36. FTIR analysis comparison of ItL-03 activity with different mediators on (a) RTM6 epoxy powder, focusing on C-$N_{arom.}$ (highlighted in blue), compared to (b) pre-treated residual epoxy powder (PT-RTM6) using PA-H_2O_2, with a focus on C-$N_{arom.}$, after 5 days of treatment with laccase ItL-03 and different mediators: ABTS, syringol, and TEMPO. BSA was used as a control. The corresponding functional groups are indicated. *v* — stretching; *va* — asymmetric stretching; *δ* — deformation. The enzyme activity under specific conditions compared to BSA is illustrated in Figures 34 and 35.

These findings demonstrate that the laccase ItL-03 was able to partially modify the amine functionalities, particularly when the material was pre-treated with PA-H_2O_2. The presence of a redox mediator further enhanced the enzyme's catalytic activity, indicating that the laccase-mediator system plays a crucial role in facilitating enzyme-substrate interactions, especially with high-redox-potential substrates such as cured epoxy resins. Additionally, ItL-03 was also capable of modifying specific byproducts generated during the pre-treatment process. This suggests that the enzyme exhibits a degree of substrate selectivity, which holds potential for downstream applications, including enzyme-assisted upcycling and sustainable byproduct recovery.

4 DISCUSSION

In recent years, the pursuit of sustainable waste management solutions has increasingly targeted the complex challenge of biodegrading recalcitrant synthetic polymers such as PE, PP, and epoxy resins—materials that are especially critical in the aerospace and construction industries. While certain enzymes have demonstrated the capacity to degrade polymers like PET, PUR ester, and PA oligomers, no microorganism or enzyme has yet been clearly shown to efficiently degrade cured epoxy polymers (PAZy database; (Buchholz et al., 2022)). Although some studies have reported microbial colonization and growth on epoxy surfaces, they do not provide conclusive evidence of enzymatic breakdown. This study developed a two-step oxidative process comprising an organic acid pre-treatment followed by application of a bacterial laccase, resulting in the recovery of clean carbon fibers from epoxy composites, the further breakdown of certain defined products, and the partial modification of RTM6 epoxy resins. While the bacterial laccase alone faced challenges in achieving complete degradation of epoxy resins, the combined treatment provides key insights into the mechanistic barriers of epoxy breakdown. These findings highlight the challenges and emerging opportunities in circular bioconversion of eCFRPs, paving the way toward more sustainable solutions in the future.

4.1 Bacterial laccase ItL-03 is an acidophile promiscuous enzyme from insect gut with potential biotechnological applications

Laccases represent the largest subfamily of MCOs and are widely distributed across insects, plants, fungi, and bacteria. In this work, laccases Itl-01, ItL-02, and Itl-03 were isolated from the gut of the bark beetles *Ips Typographus*, and were classified as bacterial laccases within Gammaproteobacteria. In insects such as the red flour beetles, *Tribolium castaneum*, laccase-2 mainly functions in cuticle tanning and pigmentation, usually expressed in epidermal tissues, while laccase-1 is involved in the oxidation of toxic compounds in the salivary glands and midgut (Arakane et al., 2005; Janusz et al., 2020). Bark beetles, major pests of spruce trees, colonize and feed on the lignocellulosic inner bark. Bacterial laccases in their guts are involved in the degradation of plant-derived lignin and the oxidation of toxic plant defense phenolic compounds

(e.g., terpenes, tannins) (Boone et al., 2013; Scully et al., 2013). Additionally, the wood-feeders have fungal symbionts that produce laccases, which efficiently break down complex lignin. These fungi are typically dispersed in beetle galleries and directly on decaying wood (Birkemoe et al., 2018). Interestingly, beetles are not typically associated with true wood-decaying fungi, such as white rot fungi from the phylum Basidiomycota (Six, 2013). Species like *Trametes versicolor*, *Pleurotus ostreatus*, and *Phlebia radiate* are among the most prolific producers of lignin-degrading enzymes, which often exhibit high redox potentials around 800 mV, making them highly effective in breaking down lignin (Brijwani et al., 2010; Kunamneni et al., 2007). Instead, beetles form symbiotic relationships with ophiostomatalean fungi, belonging to Ascomycetes, which help reduce wood decay by competing with wood-degrading fungi, thereby protecting their habitats and reducing competition for nutrients (Skelton et al., 2019). Bacterial laccases are often not true lignin degraders, but act on smaller phenolic compounds and diverse xenobiotics, which may explain their low redox potential, typically below 460 mV (Gunne et al., 2014; Sharma et al., 2007). The initial breakdown of lignin occurs externally and, in the mouth, where a combination of mechanical forces and chemo-enzymatic degradation, mediated by saliva and its enzymes, initiates the process. The pre-processed lignin is then further degraded by bacterial laccases in the beetle's gut, representing a natural example of combined mechanical and chemo-enzymatic degradation. By increasing the surface area of lignin through chewing, beetles facilitate faster enzymatic depolymerization. Such mechanical pre-treatment is mandatory in industrial PET recycling to achieve high yields (Arnal et al., 2023). A recent study similarly showed that wax worm saliva contains enzymes that are key to polyethylene degradation (Sanluis-Verdes et al., 2022), highlighting the broader potential of saliva-driven chemo-enzymatic mechanisms. More studies nowadays have shown that bacterial laccases can aid in lignin depolymerization, such as *Streptomyces* small laccases (SLACs) and LacZ1 from *Bacillus* sp. (Majumdar et al., 2014; Zhang et al., 2021). Although high redox potential laccases are more common in fungi, bacterial laccases are gaining increasing interest due to their simpler genetic manipulation, faster enzyme production, and cost-effectiveness for industrial applications (Yadav & Kudanga, 2023).

Bacterial laccase ItL-03 showed a preference for acidic pH over alkaline pH for converting NNBT and demonstrated great stability at 50 °C (Figure 19). These characteristics are similar to fungal laccases, which are typically most active within an acidic pH range of 2.6–6.9 and have an average

T_{opt} of 55 °C, ranging from 25 to 80 °C (More et al., 2011; Strong & and Claus, 2011; Zheng et al., 2017). In contrast, most bacterial laccases tend to be more active at alkaline pH and exhibit greater stability at higher temperatures. Several SLACs and CotA (from *Bacillus subtilis*) exhibited optimal activity at pH 7–9 with substrates such as guaiacol, syringol and syringaldazine (Gunne & Urlacher, 2012; Koschorreck et al., 2008; Machczynski et al., 2004). SilA showed the highest activity on phenolic compounds at pH 8 (Molina-Guijarro et al., 2009). However, an enzyme's pH preference could be influenced by substrates. For example, CotA exhibited maximal activity on syringaldazine at pH 7.0 but remained active at pH below 3 when using ABTS (Martins et al., 2002). Similarly, laccase ItL-03 showed the highest activity at pH 8 for substrates such as syringol and guaiacol, but its optimal activity shifted to pH 4 when using ABTS (Figure 17). The optimal pH for a laccase with a specific substrate depends on the pH at which the substrate's redox potential is minimized, or it is easier to oxidize (Xu et al., 2000). ABTS, a non-phenolic compound, is readily oxidized at acidic pH due to its high solubility. Syringol, a phenolic compound, is better oxidized at alkaline pH when its hydroxyl deprotonates to form a phenolate ion with a lower redox potential (Xu, 1997). Since pH affects substrate redox properties, it explains the variation in enzyme pH preferences for different substrates. As enzymes exhibit different optimal pH values and activity levels depending on the substrate, future kinetic studies should incorporate a broader range of non-phenolic substrates (beyond ABTS, Table 19), along with phenolic substrates, to allow for a more comparative and comprehensive evaluation of their catalytic potential.

Laccases ItL-01, ItL-02, ItL-03 (ItL-01-03) and CueO are most active on ABTS at similar pH levels, but their optimal temperatures range from 40 to 60 °C. Despite sharing over 60% sequence homology (Table 18) and having highly conserved structures around the copper-binding sites (Figure 10), differences in lengths and amino acid sequences within the Met-loop may account for variations in flexibility and enzymatic activity at different temperatures. CueO, with a smaller loop compared to ItL-01-03, exhibits higher optimal temperatures. This is because loops are inherently more flexible than structured regions like α-helices and β-sheets, which can easily lead to destabilization at higher temperatures (Karshikoff et al., 2015; Rahban et al., 2022). Additional features that contribute to an enzyme's tolerance to high temperatures include an increased number of disulfide bridges, fewer thermolabile amino acids, a higher abundance of hydrophobic residues, enhanced hydrophobic contacts, aromatic and inter-subunit interactions, a tightly packed surface

structure, metal or substrate binding, and a higher aliphatic index, all of which are more commonly observed in thermophilic enzymes (Ikai, 1980; Ladenstein & Ren, 2006; Nguyen et al., 2019; Pérez-García, 2020). For example, the extracellular laccase SN4 from *Bacillus tequilensis* had an optimum temperature of 80–90 °C (Sondhi et al., 2015), and a hyperthermophilic McoP from archaeon *Pyrobaculum aerophilum* exhibited optimal activity at 85 °C (Fernandes et al., 2010). The highest temperature optimum has been reported for a hyperthermophilic laccase from *Thermus thermophilus* HB27 at 92 °C, with a half-life maintained at 80 °C for more than 14 h (Miyazaki, 2005). In comparison, the bacterial laccases in this work function optimally at moderate temperatures and are much less thermophilic than these enzymes.

Analysis of amino acid sequences indicates that CueO and ItL-01-03 share a high degree of evolutionary conservation across most regions, particularly those surrounding the copper centers (Figure 10). Thus, the methionine-rich loops may also contribute to enzymatic activity. These Met-loops have been reported to influence enzyme specificity and reactivity by modulating substrate access and stabilizing substrate interactions (Borges et al., 2020). However, this influence may not fully explain the catalytic activity observed toward epoxy model substrates in the studied laccases. ItL-03 and CueO showed similarly high activity against BBCM, BMAP, and NNBT, with over 90% conversion, followed by ItL-02 at approximately 80%, and ItL-01 showing the lowest activity at around 40% conversion (Figure 14). Interestingly, sequence alignment of the Met-loops revealed that ItL-03 is more closely related to ItL-01 than to CueO or ItL-02, with both sharing a longer loop length compared to the latter two (Figure 37). However, since this phylogenetic analysis was based on a small sample size and very short sequences (<40 amino acids), the resulting tree is prone to error and may not provide biologically meaningful insights. Furthermore, structural modeling of these loops was not possible due to their high flexibility and the absence of suitable structural templates (Figure 10). Therefore, although Met-loops may influence certain enzyme properties, such as thermal stability as suggested by shorter loop in CueO, these regions may not be the primary determinants of catalytic activity. The fact that ItL-03 and CueO exhibit the highest activity toward epoxy models further supports that M-loop length may not directly correlate with enzymatic activity. Instead, non-conserved regions distant from the copper centers may play a more significant role and should be subjected to further investigation, particularly regarding their influence on enzymatic activity in the oxidation of epoxy model substrates.

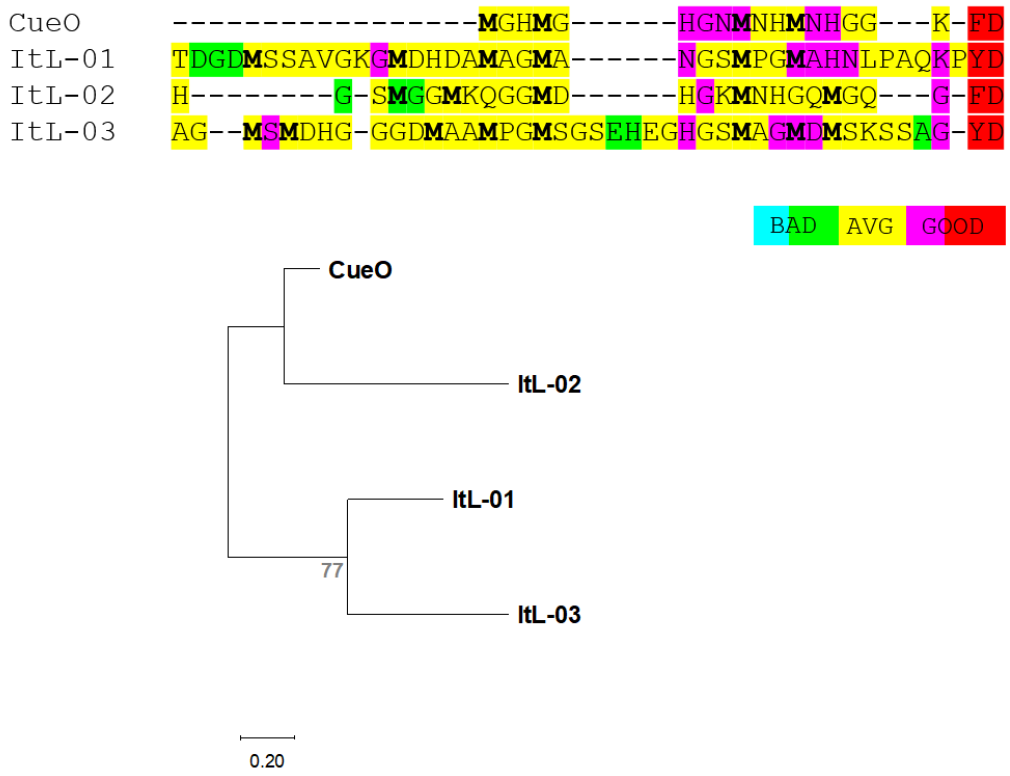

Figure 37. Sequence alignment and phylogenetic analysis of the methionine loops from CueO and ItL-01 to ItL-03 were performed to assess evolutionary relationships. Multiple sequence alignment was conducted using T-Coffee in M-Coffee mode (Moretti et al., 2007), with color-coding indicating alignment confidence. A phylogenetic tree was generated using MEGA11 (Tamura et al., 2021) based on the maximum likelihood method with 1,000 bootstrap replicates. Bootstrap values are shown for nodes exceeding a predefined confidence threshold.

Laccases and peroxidases (e.g., lignin peroxidase; LiP, manganese peroxidase; MnP) are classified as ligninolytic enzymes that function cooperatively in lignin degradation (Kumar & Chandra, 2020). Peroxidases require H_2O_2 as a co-substrate to catalyze the oxidation of lignin, whereas laccases function independently of it. In this study, laccase activity declined by 50% at just 0.5 mM H_2O_2, while HRP exhibited increased activity in the presence of 1 mM H_2O_2 (Figure 12e). This highlights the low tolerance of laccases to H_2O_2 and the importance of carefully regulating H_2O_2 concentrations when designing enzymatic systems involving both enzyme types. In nature, lignin depolymerization can involve the coordinated action of laccase and peroxidases through controlled coexistence mechanisms, such as temporal or spatial separation of their activity and regulation of H_2O_2 levels via H_2O_2-scavenging enzymes (e.g., catalase) (Fujii et al., 2013; Milgrom, 2016). These enzymes are not directly synergistic but act on different lignin structures

and bonds, contributing to more comprehensive lignin breakdown (Higuchi, 2004). However, this study did not investigate the regulated coexistence of laccase and peroxidase in epoxy modification, an aspect that should be addressed in future research. A recent study demonstrated that the combined action of laccase, LiP, and MnP achieved the highest lignin degradation from corn stover, approximately 26% greater than when each enzyme was used individually, though the method of H_2O_2 application during the reaction was not specified (S. Zhang et al., 2022). Furthermore, enzymes that utilize H_2O_2 as co-substrates can be inactivated when concentrations exceed their limits, as they can act as inhibitors (Nicell & Wright, 1997). The inhibitory effects of such cofactors should also be thoroughly investigated to better understand their impact on, and limits to, enzyme activity.

Laccases have been commonly used in industries such as paper and pulp, textiles, food processing and pharmaceuticals (Khatami et al., 2022). Moreover, due to accelerated industrial development and heavy use of xenobiotics (e.g., drugs, pesticides, pollutants, carcinogens), laccases are excellent biocatalysts also for bioremediation, especially for phenolic and aromatic compounds (Strong & and Claus, 2011). Some industries produce toxic effluents or engage in certain bioremediation processes prefer laccases to be active and stable at acidic pH (Christov & Driessel, 2003; Dutta et al., 2021; Ruggaber Timothy & Talley Jeffrey, 2006). In this context, the acidophilic nature of the bacterial laccases derived from beetles in this study—particularly ItL-03, which exhibits excellent thermostability at 50 °C and maintains 80% activity after one week—can help fill this gap for industrial applications that typically rely on fungal laccases. The potential of laccases extends further with the increasing environmental concern over plastics, prompting extensive studies on using laccases for the biodegradation of recalcitrant polymers such as PE, PP, and PVC (Sabellico et al., 2025; Sumathi et al., 2016; Zampolli et al., 2023). A study by Y. Zhang et al. (2023) showed that LfLAC3 treatment of LDPE films over 8 weeks resulted in a 3% weight loss and partial surface modification, evidenced by increased signals of carbonyl and carboxyl groups on the PE surface. Similar modifications of functional groups were observed with the laccase rPsLAC from *Psychrobacter* sp. NJ228, which acted on PE films within 7 days and led to a decrease in crystallinity (A. Zhang et al., 2022). Additionally, the laccases LMCO2 and LMCO3 from *Rhodococcus opacus* R7 oxidized LDPE powder, as demonstrated by GC-MS analysis, with the released products primarily consisting of carboxylic acids (e.g., octanoic acid, nonanoic acid,

and hexadecanoic acid) after 24 hours (Zampolli et al., 2023). Although bacterial laccases primarily act on the surface of polymers with limited capacity for complete degradation, they remain promising candidates for oxidizing recalcitrant materials, including epoxy resins. Their application in epoxy is still relatively unexplored, a gap this study addressed by demonstrating the potential of laccases to expand enzymatic polymer modification to include epoxy-based materials. To what extent the laccases characterized in this work could also be applied to the oxidation of other synthetic polymers, such as PE and PP, remains to be elucidated.

4.2 Oxidoreductases are effective in oxidizing epoxy model substrates seamlessly

RTM6 epoxy resins are the target polymers for biodegradation in this study. In the context of enzyme screening, particularly when understanding of enzymatic interactions with the actual polymer is limited, model compounds are employed to facilitate initial investigations. Such models enable high-throughput screening, conserve time, and assist in determining whether enzymes can act upon specific functional groups or linkages. Accordingly, three epoxy model compounds—BBCM, BMAP, and NNBT—were selected. These models contain tertiary amine groups within their structures and are representative of the repeating units present in RTM6 (Figure 13).

The study by Dolz et al. (2022) remains among the first investigations to utilize epoxy model for examining the enzymatic degradation of amine-cured epoxy resins. They demonstrated that NNBT can be degraded by unspecific peroxygenases (UPOs) via N-dealkylation. This study showed that three metagenomic laccases, CueO, and HRP can also catalyze the transformation of NNBT, as well as BBCM and BMAP. LC-MS analysis indicated that laccase ItL-03 may react with BMAP through laccase-mediated oxidative N-dealkylation, potentially involving radical cation intermediates and resulting in degradation (Figure 16). While the mechanisms underlying laccase-mediated conversion of BBCM and NNBT remain unclear due to ambiguous predicted products (Figures S6, S7), it is hypothesized that similar radical oxidative cleavage processes may be involved. Concerning the catalytic mechanism of ItL-03 with BMAP, it is proposed that the initial step involves the formation of an alkoxy radical through the removal of one electron and one hydrogen atom from the hydroxyl group (Figure 38a). This alkoxy radical may then induce the breakdown of C-alkyl bonds, whereby N-dealkylation is mediated indirectly via laccase oxidation.

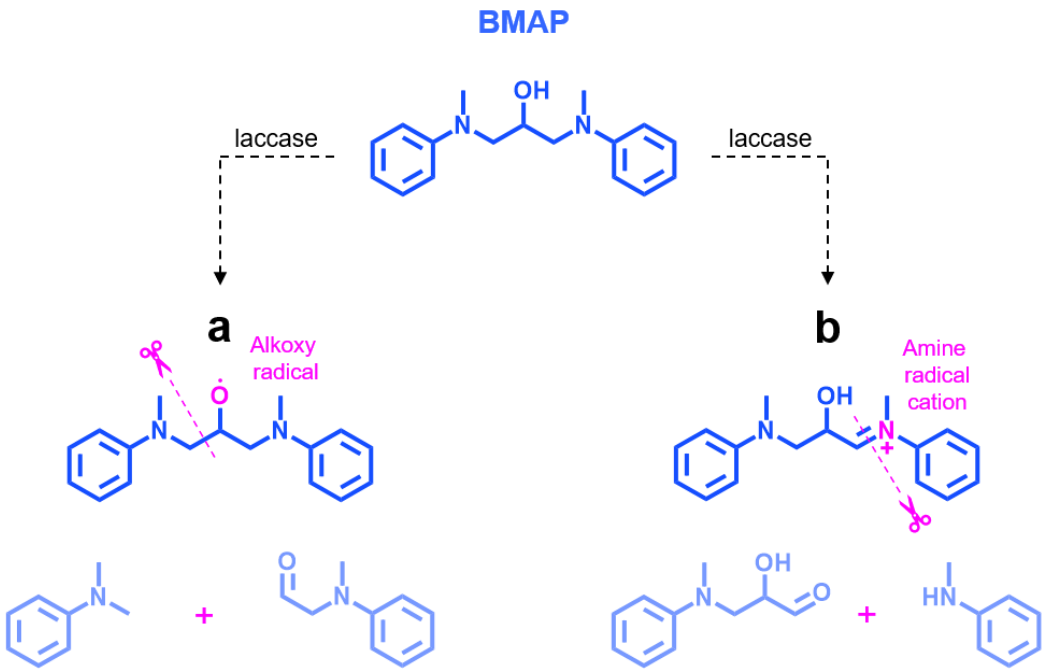

Figure 38. Proposed possible reaction scheme for the oxidation of BMAP by bacterial laccase, involving indirect N-dealkylation through radical oxidation. (a) Formation of an alkoxy radical-mediated induces the cleavage of C-alkyl bonds. (b) Formation of an amine radical cation results in the cleavage of the C-N bond.

Similar oxidative catalysis has been observed in *Trametes versicolor* laccase (TvL), which catalyzed the one-electron oxidation of N',N'-dimethyl-N-(4-hydroxyphenyl)urea. After 96 h at pH 3, this reaction achieved 40% conversion, primarily producing *p*-benzoquinone. The authors indicated that the laccase first oxidized the hydroxyl group, which led to the subsequent cleavage of the C-aryl and C-alkyl bonds (Jolivalt et al., 1999). Another possible route for laccase-mediated N-dealkylation of BMAP involves indirect oxidation via radical coupling. In this process, the tertiary amine is oxidized to form an amine radical cation (Figure 38b). Subsequently, a hydrogen atom is abstracted from the alkyl group or the hydroxyl group, generating a radical. This radical then undergoes fragmentation, resulting in the cleavage of the C-N bond and the formation of a secondary amine. While laccases can oxidize substrates through an initial single electron transfer step (Mehra & Kepp, 2019), there is limited literature supporting their ability to convert tertiary amines into secondary amines via radical-mediated oxidation. However, the oxidation of aromatic amines attached to primary or secondary amines, as well as benzylamines, where a benzyl group is attached to an NH_2 group, has been reported with TvL (Bassanini et al., 2023; Galletti et al., 2015).

Most well-documented N-dealkylation reactions of tertiary amines are facilitated by cytochrome P450 (CYP) monooxygenases (Najmi et al., 2022). The CYP enzyme from the bacterium *Streptomyces griseus* efficiently catalyzes N-demethylation. Isolated CYP enzymes from animal liver and intestines, as well as a mutant from *Bacillus megaterium*, have demonstrated the formation of N-dealkylated metabolites of drugs such as diphenhydramine and amitriptyline. Hence, UPOs, enzymes which exhibit characteristics of both peroxidases and cytochrome P450s, can catalyze N-dealkylation (Hofrichter et al., 2015), as also demonstrated in the study mentioned previously (Dolz et al., 2022). Other enzymes that may contribute to N-dealkylation include peroxidases (e.g., horseradish peroxidase, HRP) and FAD-dependent enzymes (e.g., trimethylamine dehydrogenase) (Shaffer et al., 2001; Zhu et al., 2016). The latter indirectly catalyzes N-demethylation through N-oxidation (Taniguchi-Takizawa et al., 2015). Recently, a morphinan N-demethylase from *Methylobacterium*, which typically catalyzes C–C bond formation, has been recently discovered to catalyze the removal of the N-methyl group (Gandomkar et al., 2015). Additionally, a catalytic cascade involving two enzymes, a monoamine oxidase and an ω-transaminase, was reported for the dealkylation of secondary amines (O'Reilly & Turner, 2014). While there are enzymes that cleave directly at the C–N linkage, their activity depends on the specific chemical nature of the substrate. For example, deaminases primarily remove primary amines from molecules; a well-known reaction is in DNA, where cytosine is converted into uracil, releasing ammonia (Aučynaitė et al., 2018). Amidases cleave C–N bonds in amides, which have the general formula R−C(=O)−N−R' (Wu et al., 2020). Lyases, on the other hand, break C–N bonds without hydrolysis or oxidation, through elimination reactions that result in the formation of a double bond or a new ring (Duan et al., 2022; J. Zhang et al., 2020). Since tertiary amines lack a hydrogen atom on the nitrogen suitable for elimination, most lyases that cleave C–N bonds typically target primary and secondary amines. Therefore, enzymes that facilitate the catalysis of tertiary amines through N-dealkylation, such as cytochrome P450 monooxygenases and UPOs, are the enzymes with the highest potential to catalyze these C–N linkages, which are commonly found in amine-cured epoxy resins.

In addition to the common tertiary amine linkage (R–N(CH_2–CH_3)–CH_2–R') formed during the curing of epoxy resins and curative agents, other types of bonds can also be present, including secondary amines (R–NH–CH_2–R'), carboxyl esters (R–(C=O)–O–R'), ethers (R–O–R'), and thiol

(R–S–R') linkages (González et al., 2012; Meure et al., 2010; Thomas et al., 2014). While this study primarily focused on tertiary amines, developing epoxy model substrates that incorporate these diverse linkages will aid in screening for enzymes capable of oxidizing a broader range of epoxy structures and improve our understanding of their mechanistic pathways. However, using epoxy model substrates may not accurately represent the complexity of actual polymers and could produce false positives, where enzymes appear active on model substrates but may not effectively interact with the full polymer. Therefore, employing larger and more complex substrates can help better assess both the potential and limitations of enzyme activity, providing a more realistic evaluation of their ability to degrade epoxy materials similar to real-world polymers.

4.3 Bacterial laccase ItL-03 induces partial surface modification of epoxy resins post pre-treatment targeting amine linkages

Epoxy model substrates were readily oxidized by bacterial laccases. However, they did not have the ability to break down the epoxy matrix to recover carbon fibers. The epoxy functional groups, particularly the C–N bonds, may not significantly impede biodegradation; rather, the steric hindrance from the densely packed, cross-linked structure of the cured polymer likely limits the access of enzymes to the certain regions within the molecule (Escayola et al., 2024; Pinter et al., 2012). In this context, pre-treatment is essential to improve enzyme accessibility and potentially enable resin breakdown. This is analogous to natural systems, such as those observed in beetles, where pre-treatment mechanisms, including mechanical, chemical, and enzymatic processes, are employed to break down complex substrates into smaller components, which can then be further degraded by bacterial laccases. In this study, the ability of laccase ItL-03 to further oxidize the epoxy extract from RTM6 was analyzed by ESI-MS and GC-MS, while its ability to modify the pre-treated powder was characterized by FTIR.

Direct injection ESI-MS revealed multiple peaks, particularly in the *m/z* ranges of 150-200 and 300-500 (Figure 25). Notably, an ion at *m/z* 483.3 showed a significant decrease in intensity following enzymatic treatment, suggesting it corresponds to a larger, polar intermediate or oligomer that serves as a primary enzymatic target. The 150-200 *m/z* range likely contains smaller fragments, some of which may overlap with those detected by GC-MS. GC-MS identified smaller

volatile products around *m/z* 50-180, which also appeared influenced by the enzyme (Figures 28-31). However, it remains unclear whether the enzyme truly oxidizes these compounds due to uncertainties regarding protonation/deprotonation states, which could be clarified using NMR. Additionally, peak E could correspond either to ABTS or oxidation products (Figure 32). Analyzing the epoxy extract incubated under identical conditions with ABTS but without the enzyme would help resolve this ambiguity. While the GC-MS results remain somewhat inconclusive and require further investigation, the complementary data from ESI-MS and GC-MS suggest that enzymatic activity can proceed through mid-sized polar intermediates (e.g., *m/z* ~400) clearly detected by ESI-MS, some of which may be further oxidized into volatile products detectable by GC-MS. Moreover, only a few soluble products from the propionic acid (PA)-H_2O_2 pre-treatment were further oxidized by laccase ItL-03 (Figures 25, 28), likely because the pre-treatment already fragmented them into small compounds containing chemical bonds that are either less reactive or not suitable substrates for the enzyme. Lowering the concentration of the PA-H_2O_2 pre-treatment could potentially preserve more reactive intermediate structures.

With pre-treated RTM6 powder, the enzyme only partially modified the surface, though the effect was slightly enhanced when using a mediator in combination. In fact, ItL-03 was able to target the modification of amine functionalities (e.g., C–N) in the pre-treated epoxy (Figure 35), whereas with non-treated epoxy, the enzyme primarily engaged in general oxidation, producing hydroxyl (–OH) and carbonyl (C=O) groups as oxidation products (Figure 34). The pre-treatment of the epoxy resin induces changes in its chemical structure, which influence how the laccase enzyme interacts with it. When the epoxy is not pre-treated, the enzyme mainly oxidizes accessible electron-rich regions (e.g., aromatic rings) and exposed aliphatic areas, rather than modifying specific functionalities like amines, which are likely buried, crosslinked, or sterically hindered. Using acid pre-treatment, DGEBA-based epoxy resins cured with amine hardeners were primarily cleaved at the C–O and C–N bonds (Ma et al., 2017). This indicates that pre-treatment can penetrate into the epoxy matrix and expose these functional groups, making them more accessible or reactive on the epoxy surface for enzymatic activity. A straightforward example of this is the composition of lignocellulosic material, where cellulose is embedded within a matrix of hemicellulose and lignin. Pre-treatment is a critical step in biofuel production to remove

hemicellulose and lignin, exposing cellulose to enzymatic cellulase, which breaks it down into glucose for fermentation into ethanol or biogas (Chandra et al., 2007; Meera et al., 2020).

Pre-treatment to facilitate enzyme access to the material for further modification is mimicked in nature by processes such as colonization by certain organisms and environmental factors, like seawater, which can accelerate oxidation and hydrolysis (Da Costa et al., 2018; Dang & Lovell Charles, 2015). Biofilm formation by microorganisms can reduce polymer's mechanical properties by creating oxidative microenvironments that accumulate moisture, promote hydrolysis of bonds and induce microcracking (Breister et al., 2020; Kychkin et al., 2025). Additionally, microorganisms can produce metabolites such as organic acids, which contribute to corrosion (Beale et al., 2013; Malviya et al., 2023), and secrete enzymes to further disrupt the polymer's integrity (Romaní et al., 2008; Teh et al., 2014). Similar observations in previous studies have shown that marine bacteria can decrease the corrosion resistance of epoxy-coated steel by forming biofilms after one month in seawater, which was subsequently confirmed by FTIR analysis indicating surface modification of the epoxy (Deng et al., 2019; Wang et al., 2016; S. Zhang et al., 2023). Considering this, *Pseudomonas putida* promoted an increase in hydroxyl (C–OH) groups, while *P. aeruginosa* reduced C–O–C and C–O groups, and *Bacillus flexus* broke down aromatic rings and epoxy groups. Furthermore, another research effort showed that a soil bacterial consortium comprising Bacterium Te68R PN12, *Microbacterium* sp. MK3, and *P. putida* MK4 survived in minimal media where epoxy served as the primary carbon source. This resulted in less observable C–N, CH_3, CH_2, and C–O groups, along with a 34% weight reduction of the polymer (Pardi-Comensoli et al., 2022). Published studies suggest that these bacteria and fungi capable of colonizing epoxy resins (Deng et al., 2019; Gu et al., 1997; Pardi-Comensoli et al., 2022; Wang et al., 2016; S. Zhang et al., 2023), possess oxidoreductases (EC1), such as laccases, peroxidases, monooxygenases, and alcohol dehydrogenases (Haq et al., 2024; Kumar & Chandra, 2020; Leynaud Kieffer Curran et al., 2022; Naveed et al., 2025; Padayachee et al., 2020), which are reported to have the potential to modify non-hydrolysable plastics like PE, PP, PS, and PVC (Chow et al., 2023; Mohanan et al., 2020; Zampolli et al., 2024). This could explain the similar FTIR results observed after laccase treatment of pre-treated epoxy, which mimic the effects of the enzyme following environmental influences.

4.4 Pre-treatment as a key to enhancing bio-based recycling efficiency of eCFRPs

So far, the degradation of recalcitrant plastics or non-hydrolysable polymers using sole enzymes has primarily resulted, in most studies, in surface modification rather than significant degradation throughout the material, including this one. Only the combination with a pre-treatment has shown promising results that facilitate the use of biocatalysts such as enzymes, making the integration of biological approach more practical and effective. Thus, pre-treatment is as well a critical aspect of this study for epoxy decomposition, which is essential to accelerate the initial oxidation—a bottleneck step in the process. Propionic acid and H_2O_2 were applied to initially disrupt the network density of the epoxy matrix, making it more accessible to subsequent enzymatic action. Additionally, applying such pre-treatment methods to depolymerize eCFRPs facilitates the recovery of clean CFs, which could potentially be reused in future applications. To verify the quality of the recovered CFs for reuse, thermogravimetric analysis (TGA) and tensile strength testing should be conducted.

Propionic acid is a carboxylic acid with the general formula R-COOH. When it reacts with H_2O_2, peracids or peroxyacids are produced, resulting in compounds of the form R-COOOH (Leveneur et al., 2009). These peroxy derivatives of organic carboxylic acids are generally strong oxidizers, highlighting the importance of H_2O_2 in the reaction process. They are more effective at decomposing epoxy compared to using acid alone. Das et al. (2018) proposed a reaction mechanism involving the use of peracids (acetic acid and H_2O_2) for the decomposition of the cross-linked epoxy. Initially, unstable peracids generates acyloxyl ($CH_3COO^{\bullet}$) and hydroxyl ($^{\bullet}OH$) radicals. The acyloxyl radicals can then oxidize C-OH group into carbonyl (C=O) groups, which subsequently lead to the breaking of C–N linkages, ultimately disrupting cross–linking. The preference of acid digestion targeting C–N bond cleavage over other bonds, such as C–C in epoxy, aligns with findings from the study of Ma et al. (2017). Meanwhile, the hydroxyl radicals primarily oxidize the hydroxyl groups to from carbonyls, but are less effective at breaking other bonds. Thus, the breakdown of amine-cured epoxy with PA-H_2O_2 involves the generation of acylperoxyl ($CH_3CH_2COO^{\bullet}$) and hydroxyl ($^{\bullet}OH$) radicals, as depicted in Figure 39.

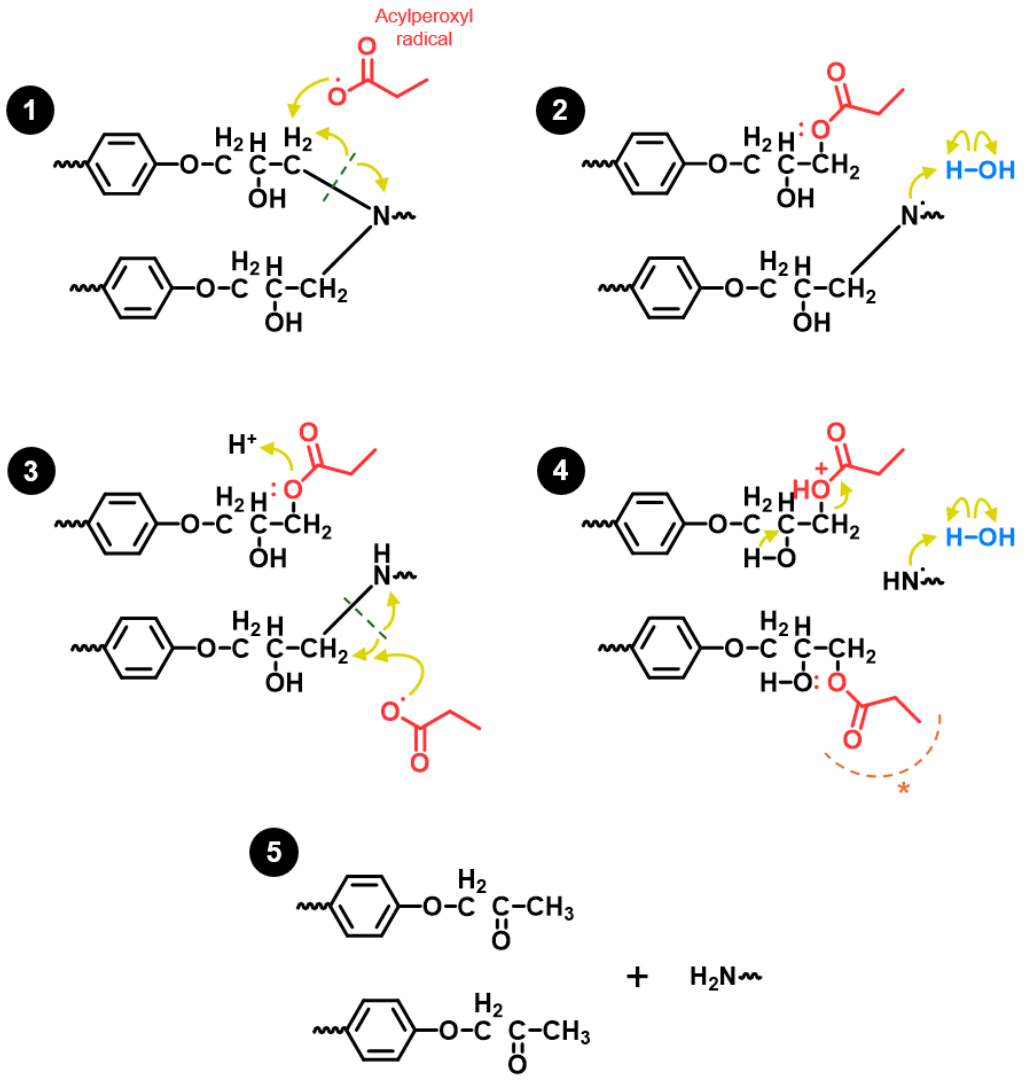

Figure 39. Reaction pathway for the breakdown of amine cross-linked epoxy resin initiated by acyloxy radicals generated from peracids. * refers to acylperoxyl radical attack, which follows the same mechanism as previously depicted (2–4). Figure modified from (Das et al., 2018).

Among the organic acids tested, propionic acid combined with H_2O_2 proved to be the most effective, resulting in 100% epoxy weight loss. This was followed by acetic acid with approximately 70%, formic acid at 15%, and other higher molecular weight organic acids showing less than 10% weight loss (Figure 20). The higher effectiveness of perpropionic acid (PPA) in epoxy decomposition may be attributed to its better balance between reactivity and stability compared to performic acid (PFA) and peracetic acid (PAA). Although shorter-chain acids such as formic and acetic acids are more polar and thus more reactive, they tend to be highly unstable

and decompose quickly (Luukkonen et al., 2015; Mattila & Aksela, 2000; Swern, 1949). In contrast, propionic acid remains stable longer in the reaction medium, and its slightly longer alkyl chain makes it more hydrophobic, which helps it diffuse into the epoxy matrix and enhances oxidative attack. Moreover, the organic radicals generated from PPA and PAA are reported to be more selective in attacking N-containing compounds more than those from PFA (Deng et al., 2024). Polycarboxylic acids (e.g., malic, tartaric, and citric acid) contain multiple carboxylic groups capable of undergoing multiple dissociation steps, as well as at least one hydroxyl group (Apelblat, 2014; Sochorova et al., 2018), whereas a monocarboxylic acid like lactic acid has a hydroxyl group in addition to a carboxylic group (Castillo Martinez et al., 2013). The presence of multiple reactive groups is hypothesized to cause competition among the carboxylic groups for reaction with H_2O_2, resulting in inefficient and uneven formation of peracids. Additionally, hydroxyl groups may react with peracids or generated radicals, which can deactivate the oxidative properties itself. Due to these complications, the formation of peracids by polycarboxylic acids has not been reported (Kiejza et al., 2021). Therefore, monocarboxylic acids like propionic acid are more effective and potent in generating radicals that can attack and break down epoxy efficiently.

In the standard protocol, a 3:1 mixture of sulfuric acid and hydrogen peroxide (SA–H_2O_2) is commonly known as piranha solution and is often used to retrieve clean carbon fibers by aggressively oxidizing organic residues (e.V., 2019). However, in this study, the SA–H_2O_2 mixture used to evaluate epoxy weight loss had a sulfuric acid to H_2O_2 ratio of 19:1. This significantly lower concentration of H_2O_2 results in a much milder oxidizing environment compared to traditional piranha mixtures. Therefore, this diluted oxidative acid system is more appropriately referred to as peroxymonosulfate (PMS) in the context of this study. PPA and PAA treatments were shown to target different functional groups within epoxy materials compared to the PMS system (Figure 24). Specifically, epoxy samples treated with PPA and PAA exhibited increased signals corresponding to C=C aromatic bands, hydroxyl (OH), and carbonyl (C=O) groups, while PMS was more effective at converting C–N stretches in aromatic amines into C–N bonds characteristic of primary amines. This is likely due to their differing acid strengths (Munegumi, 2013), which influence reaction mechanisms and selectivity of oxidation pathways (Cook et al., 2024; Zima et al., 2022). PMS, characterized by a strongly acidic and highly oxidative

environment, generates reactive species such as sulfate and hydroxyl radicals (Kiejza et al., 2021), which may promote extensive protonation of the relatively stable C–N bonds in epoxy, thereby increasing their susceptibility to further oxidative cleavage. The lower presence of C=C groups after PMS treatment also suggests that aromatic rings are more effectively modified or broken down under these conditions. Stronger acids, such as hydrofluoric acid, have been reported to be more effective than weaker acids like acetic acid in breaking down aromatic structures found in coal (Xu et al., 2021). PPA and PAA, as weak acids, generate milder oxidative conditions dominated by peracids or hydroxyl radicals (Kiejza et al., 2021). They predominantly attack electron-rich site, exhibiting a faster reaction rate toward aromatic compounds bearing phenolic groups compared to those containing nitrogen functionalities (Kim & Huang, 2021). This selectivity leads to most of products being oxygen-containing compounds, such as C=C, OH, and C=O functional groups. These findings suggest that while PMS's strong acid–oxidant combination preferentially targets and modifies amine groups, weak organic acids promote a broader oxidation of the epoxy matrix, which can ultimately result in similar decomposition outcomes.

PFA and PAA have been extensively studied for environmental applications such as wastewater treatment, whereas literature on PPA is relatively limited (Yujie Chen et al., 2023; Luukkonen & and Pehkonen, 2017). Instead, propionic acid is primarily used in the food industry, for example, as a food preservative, as well as in specialized applications involving pesticides and pharmaceuticals (Rachmawati & Triwibowo, 2024; Samel et al., 2018). It can be biologically produced through microbial fermentation by well-known propionic acid producers, such as *Propionibacterium freudenreichii* and *P. acidipropionici* (Gonzalez-Garcia et al., 2017; Ranaei et al., 2020). However, biosynthesis of propionic acid is not yet economically attractive, with ongoing challenges such as cell growth inhibition at high concentrations and the production of other organic acids, which increase extraction costs (Ammar & Philippidis, 2021). While fermentative production offers a sustainable approach, improvements, such as developing metabolically engineered mutants, employing immobilization techniques, and utilizing alternative renewable substrates, are needed to enhance both yield and productivity. For industrial-scale production, propionic acid is synthesized via chemical routes under mild conditions through the hydroformylation of ethylene, followed by oxidation of propionaldehyde with O_2, achieving yields of over 90% (Teles, 2024). Any leftover propionic acid from applications can be recovered through

methods such as microchannel distillation or reactive extraction for reuse (Keshav et al., 2009; Lu et al., 2023; Singh et al., 2021). Similarly, another carboxylic acid, acetic acid, can be recovered with over 90% volume by simple distillation, after its use in the pre-treatment of CFRPs (Das et al., 2018).

Other studies have also demonstrated that a combination of pre-treatment with enzymes can more effectively depolymerize non-hydrolysable polymers, which are poorly affected by any known enzymes. Branson et al. (2023) demonstrated that pretreating polyether polyurethane foams through chemical glycolysis, specifically transurethanization at 200 °C using an excess of diethylene glycol (DEG) with 1% (w/w) tin (II)-2-ethylhexanoate as a catalyst, yielded low-molecular-weight (LMW) dicarbamates. These dicarbamates could be further hydrolyzed into aromatic diamines by the metagenome urethanase UMG-SP-2, found in soil contaminated with polyurethane waste, achieving a 65% conversion in 24 h (Branson et al., 2023). Another study reported that applying a pre-treatment with *m*-chloroperoxybenzoic acid (*m*CPBA) and ultrasonication to form LMW PE improved accessibility for an enzyme cascade that included catalase-peroxidase, alcohol dehydrogenase, Baeyer-Villiger monooxygenase, and lipase. This chemo-enzymatic depolymerization resulted in approximately 27% polymer conversion and the release of medium-chain products, such as aliphatic carboxylic acids (Oiffer et al., 2024). Therefore, to improve chemo-enzymatic treatment for epoxy decomposition, alternative chemical pre-treatments should be further explored, with continued emphasis on environmental sustainability. Additionally, implementing enzymatic cascades involving multiple enzymes capable of targeting abundant epoxy functional groups (e.g., amine and ether bonds) could significantly enhance the efficiency of the two-step oxidative process. Promising candidates include cytochrome P450 (CYP) monooxygenases, fungal laccases, and other oxidases involved in lignin degradation, which could act synergistically to broaden substrate specificity and improve overall performance.

The two-step oxidation process, combining chemical and enzymatic treatments, is key to enhancing the bio-based recycling efficiency of eCFRPs. Chemical pre-treatment facilitates the breakdown of the resin matrix, enabling clean recovery of carbon fibers and converting the epoxy into intermediates that are more accessible to enzymatic oxidation. The high selectivity of enzymes provides additional advantages for downstream applications. Overall, chemo-enzymatic treatment

represents a promising and environmentally friendly strategy for addressing highly recalcitrant polymers such as epoxy.

5 CONCLUSION AND FUTURE PERSPECTIVES

Epoxy-based CFRPs are widely used in high-tech sectors such as aerospace, automotive, and wind energy, where lightweight properties and durability are critical. Although these materials are typically used in long-life applications, their end-of-life management remains important due to the high economic and environmental costs associated with carbon fiber production. Efficient recycling of CFRPs, therefore, focuses on conserving valuable resources and promoting circular material use in advanced industries, ideally through methods that are also environmentally sustainable. However, recycling the recalcitrant epoxy matrices within CFRPs often relies on energy-intensive or chemically harsh methods that raise environmental concerns. Biological recycling, particularly through enzymatic or microbial degradation of epoxy resins, presents a more sustainable alternative. Yet, this area remains poorly understood and significantly underexplored, with current biocatalytic approaches showing limited effectiveness. Advancing this area is crucial for enabling more sustainable waste management for epoxy-based composites.

This study investigated the use of laccases, enzymes known for their ability to degrade lignin, a complex natural polymer with a chemical structure similar to that of epoxy resins. Preliminary tests with these bacterial enzymes on eCFRPs showed no significant degradation. To advance this line of research, chemo-enzymatic approach under milder conditions than the standard method was developed, aiming to enhance the potential for environmentally friendly epoxy recycling. Combining organic peracid treatment (PA-H_2O_2) with enzymatic activity (bacterial laccase ItL-03) has shown promise in enhancing the decomposition of epoxy polymers compared to using enzymes alone. The pre-treatment facilitated the recovery of carbon fibers in a clean state, demonstrating potential for reuse in industrial applications. Further studies are required to investigate the mechanical properties of the recovered fibers to confirm their suitability for such applications. However, the enzyme primarily induced surface modification of the pre-treated epoxy rather than achieving significant degradation throughout the material. Although the pre-treatment enhances enzyme accessibility, the subsequent enzymatic activity on the pre-treated epoxy may still fall short of industrial requirements. Nevertheless, enzymatic treatment can help standardize or simplify the composition of byproducts after pre-treatment, which is valuable for downstream applications such as recovery and potential upcycling. While direct recycling to

regenerate epoxy may be challenging, producing higher-value compounds from resulting products could offer a promising alternative. Therefore, further development is required to improve enzyme efficiency and to optimize enzyme-mediated processes that facilitate downstream applications.

First and foremost, since bacterial laccases exhibit low redox potentials, it is crucial to expand enzyme screening to include a broader range of mediators with higher redox potentials. This is essential for optimizing laccase-mediator systems for the oxidation of amine-cured epoxy, especially given the challenges of oxidizing this complex polymer, thereby enhancing enzyme efficiency. Although bacterial laccases offer advantages such as easier and faster production and genetic manipulability, they may not be ideally suited for epoxy breakdown. More promising enzymes should be investigated, including fungal laccases with higher redox potentials, as well as other oxidative enzymes like cytochrome P450 monooxygenases, peroxidases, and UPOs, which are more effective in targeting tertiary amines. Despite their potential, expressing these enzymes remains challenging. Moreover, broadening enzyme screening to encompass various types of epoxy functional groups would deepen our understanding of enzymatic mechanisms and facilitate the development of more effective degradation strategies. Employing larger model substrates could better represent the structural complexity of actual polymers. In addition, optimizing the extent of pre-treatment is important to ensure sufficient enzyme access while adhering to greener practices. Other alternative pre-treatments, such as UV irradiation, which are inspired by natural processes and thus have a lower environmental impact, should also be examined.

Importantly, effective recycling of epoxy resins requires a multifaceted approach that integrates mechanical, chemical, and enzymatic methods. Increasing the surface area of epoxy materials relative to their volume can improve enzyme access when combined with mechanical treatments, while chemical methods can help accelerate depolymerization reactions. Both strategies aim to facilitate more efficient biological recycling. There is a growing trend towards developing biodegradable epoxy composites with ester bonds, which may enhance microbial degradation susceptibility. Nonetheless, ester bonds also increase the risk of hydrolysis under high humidity and water exposure (Kajdas, 2004), which could compromise the material's performance in applications such as aircraft, where resistance to weather conditions is critical.

In summary, although significant challenges remain in the biodegradation of epoxy resins, this study advances our understanding of the enzymes involved in epoxy degradation and provides

insights into their reaction mechanisms, an area that has been rarely explored. While enzyme alone may not yet be sufficient to fully break down epoxy, chemo-enzymatic oxidation offers a promising strategy for epoxy waste management and enabling potential downstream applications. Continued research is essential to develop these approaches into practical, scalable recycling solutions.

6 REFERENCES

Abramson, J., Adler, J., Dunger, J., Evans, R., Green, T., Pritzel, A., Ronneberger, O., Willmore, L., Ballard, A. J., Bambrick, J., Bodenstein, S. W., Evans, D. A., Hung, C.-C., O'Neill, M., Reiman, D., Tunyasuvunakool, K., Wu, Z., Žemgulytė, A., Arvaniti, E.,…Jumper, J. M. (2024). Accurate structure prediction of biomolecular interactions with AlphaFold 3. *Nature*, *630*(8016), 493–500. https://doi.org/10.1038/s41586-024-07487-w

Addou, F., Duguet, T., Bosso, P., Zhang, A., Amin-Chalhoub, E., Fanelli, F., & Vahlas, C. (2016). Metallization of carbon fiber reinforced polymers: Chemical kinetics, adhesion, and properties. *Surface and Coatings Technology*, *308*, 62–69. https://doi.org/https://doi.org/10.1016/j.surfcoat.2016.06.098

Agarwal, C., & Pandey, A. K. (2023). Remediation and recycling of inorganic acids and their green alternatives for sustainable industrial chemical processes [10.1039/D3VA00112A]. *Environmental Science: Advances*, *2*(10), 1306–1339. https://doi.org/10.1039/D3VA00112A

Airbus. (2025). Airbus Global Market Forecast 2025-2044.

Akter, M., Inoue, C., Komori, H., Matsuda, N., Sakurai, T., Kataoka, K., Higuchi, Y., & Shibata, N. (2016). Biochemical, spectroscopic and X-ray structural analysis of deuterated multicopper oxidase CueO prepared from a new expression construct for neutron crystallography. *Acta Crystallographica Section F*, *72*(10), 788–794. https://doi.org/doi:10.1107/S2053230X1601400X

Ammar, E. M., & Philippidis, G. P. (2021). Fermentative production of propionic acid: prospects and limitations of microorganisms and substrates. *Applied Microbiology and Biotechnology*, *105*(16), 6199–6213. https://doi.org/10.1007/s00253-021-11499-1

Apelblat, A. (2014). *Citric acid*. Springer.

Arakane, Y., Muthukrishnan, S., Beeman, R. W., Kanost, M. R., & Kramer, K. J. (2005). Laccase 2 is the phenoloxidase gene required for beetle cuticle tanning. *Proceedings of the National Academy of Sciences*, *102*(32), 11337–11342.

Armougom, F., Moretti, S., Poirot, O., Audic, S., Dumas, P., Schaeli, B., Keduas, V., & Notredame, C. (2006). Expresso: automatic incorporation of structural information in multiple sequence alignments using 3D-Coffee. *Nucleic Acids Res*, *34*(Web Server issue), W604–608. https://doi.org/10.1093/nar/gkl092

Arnal, G., Anglade, J., Gavalda, S., Tournier, V., Chabot, N., Bornscheuer, U. T., Weber, G., & Marty, A. (2023). Assessment of Four Engineered PET Degrading Enzymes Considering Large-Scale Industrial Applications. *ACS Catalysis*, *13*(20), 13156–13166. https://doi.org/10.1021/acscatal.3c02922

Asokan, P., Osmani, M., & Price, A. D. F. (2009). Assessing the recycling potential of glass fibre reinforced plastic waste in concrete and cement composites. *Journal of Cleaner Production*, *17*(9), 821–829. https://doi.org/https://doi.org/10.1016/j.jclepro.2008.12.004

Aučynaitė, A., Rutkienė, R., Tauraitė, D., Meškys, R., & Urbonavičius, J. (2018). Discovery of Bacterial Deaminases That Convert 5-Fluoroisocytosine Into 5-Fluorouracil [Original

Research]. *Frontiers in Microbiology*, *Volume 9 - 2018*. https://doi.org/10.3389/fmicb.2018.02375

Avison, M. B., von Heldreich, C. J., Higgins, C. S., Bennett, P. M., & Walsh, T. R. (2000). A TEM-2beta-lactamase encoded on an active Tn1-like transposon in the genome of a clinical isolate of Stenotrophomonas maltophilia. *J Antimicrob Chemother*, *46*(6), 879–884. https://doi.org/10.1093/jac/46.6.879

Azimi, M., Nafissi-Varcheh, N., Mogharabi, M., Faramarzi, M., & Aboofazeli, R. (2016). Study of laccase activity and stability in the presence of ionic and non-ionic surfactants and the bioconversion of indole in laccase-TX-100 system. *Journal of Molecular Catalysis B: Enzymatic*, *126*. https://doi.org/10.1016/j.molcatb.2016.02.001

Aziz, T., Haq, F., Farid, A., Cheng, L., Chuah, L. F., Bokhari, A., Mubashir, M., Tang, D. Y. Y., & Show, P. L. (2024). The epoxy resin system: function and role of curing agents. *Carbon Letters*, *34*(1), 477–494. https://doi.org/10.1007/s42823-023-00547-7

Bach, C. E., Warnock, D. D., Van Horn, D. J., Weintraub, M. N., Sinsabaugh, R. L., Allison, S. D., & German, D. P. (2013). Measuring phenol oxidase and peroxidase activities with pyrogallol, l-DOPA, and ABTS: Effect of assay conditions and soil type. *Soil Biology and Biochemistry*, *67*, 183–191. https://doi.org/https://doi.org/10.1016/j.soilbio.2013.08.022

Bailey, W. F., Bobbitt, J. M., & Wiberg, K. B. (2007). Mechanism of the Oxidation of Alcohols by Oxoammonium Cations. *The Journal of Organic Chemistry*, *72*(12), 4504–4509. https://doi.org/10.1021/jo0704614

Baltierra-Trejo, E., Márquez-Benavides, L., & Sánchez-Yáñez, J. M. (2015). Inconsistencies and ambiguities in calculating enzyme activity: The case of laccase. *Journal of Microbiological Methods*, *119*, 126–131. https://doi.org/https://doi.org/10.1016/j.mimet.2015.10.007

Barreca, A. M., B., S., M., F., C., G., & and Gentili, P. (2004). Catalytic Efficiency of some Mediators in Laccase-Catalyzed Alcohol Oxidation. *Biocatalysis and Biotransformation*, *22*(2), 105–112. https://doi.org/10.1080/10242420410001692750

Bassanini, I., Grosso, S., Tognoli, C., Fronza, G., & Riva, S. (2023). Studies on the Oxidation of Aromatic Amines Catalyzed by Trametes versicolor Laccase. *International Journal of Molecular Sciences*, *24*(4), 3524.

Batista, L. A. P. d. S., Morgado, G. F. d. M., Rodrigues Brazil, T., dos Anjos, E. G. R., Guimarães, A., Rezende, M. C., & Passador, F. R. (2024). Comparative Analysis of Thermal Recycling Approaches for Carbon Fiber Recovery from CFRP Waste. *ACS Sustainable Resource Management*, *1*(9), 2108–2118. https://doi.org/10.1021/acssusresmgt.4c00201

Battistuzzi, G., Bellei, M., Bortolotti, C. A., & Sola, M. (2010). Redox properties of heme peroxidases. *Archives of Biochemistry and Biophysics*, *500*(1), 21–36. https://doi.org/https://doi.org/10.1016/j.abb.2010.03.002

Beale, D. J., Morrison, P. D., Key, C., & Palombo, E. A. (2013). Metabolic profiling of biofilm bacteria known to cause microbial influenced corrosion. *Water Science and Technology*, *69*(1), 1–8. https://doi.org/10.2166/wst.2013.425

Berglund, G. I., Carlsson, G. H., Smith, A. T., Szöke, H., Henriksen, A., & Hajdu, J. (2002). The catalytic pathway of horseradish peroxidase at high resolution. *Nature*, *417*(6887), 463–468. https://doi.org/10.1038/417463a

Bertani, G. (1951). Studies on lysogenesis I: the mode of phage liberation by lysogenic Escherichia coli. *Journal of bacteriology*, *62*(3), 293–300.

Birkemoe, T., Jacobsen, R. M., Sverdrup-Thygeson, A., & Biedermann, P. H. W. (2018). Insect-Fungus Interactions in Dead Wood Systems. In M. D. Ulyshen (Ed.), *Saproxylic Insects: Diversity, Ecology and Conservation* (pp. 377–427). Springer International Publishing. https://doi.org/10.1007/978-3-319-75937-1_12

Blattner, F. R., Plunkett, G., 3rd, Bloch, C. A., Perna, N. T., Burland, V., Riley, M., Collado-Vides, J., Glasner, J. D., Rode, C. K., Mayhew, G. F., Gregor, J., Davis, N. W., Kirkpatrick, H. A., Goeden, M. A., Rose, D. J., Mau, B., & Shao, Y. (1997). The complete genome sequence of Escherichia coli K-12. *Science*, *277*(5331), 1453–1462. https://doi.org/10.1126/science.277.5331.1453

Bombardier. (2017). *Projected number of passenger aircraft to be removed from service between 2017 and 2036, by region*. https://www.statista.com/statistics/750562/passenger-and-freighter-aircraft-removed-from-service/

Boone, C. K., Keefover-Ring, K., Mapes, A. C., Adams, A. S., Bohlmann, J., & Raffa, K. F. (2013). Bacteria associated with a tree-killing insect reduce concentrations of plant defense compounds. *J Chem Ecol*, *39*(7), 1003–1006. https://doi.org/10.1007/s10886-013-0313-0

Boratyn, G. M., Schäffer, A. A., Agarwala, R., Altschul, S. F., Lipman, D. J., & Madden, T. L. (2012). Domain enhanced lookup time accelerated BLAST. *Biol Direct*, *7*, 12. https://doi.org/10.1186/1745-6150-7-12

Borges, P. T., Brissos, V., Hernandez, G., Masgrau, L., Lucas, M. F., Monza, E., Frazão, C., Cordeiro, T. N., & Martins, L. O. (2020). Methionine-Rich Loop of Multicopper Oxidase McoA Follows Open-to-Close Transitions with a Role in Enzyme Catalysis. *ACS Catalysis*, *10*(13), 7162–7176. https://doi.org/10.1021/acscatal.0c01623

Branson, Y., Söltl, S., Buchmann, C., Wei, R., Schaffert, L., Badenhorst, C. P. S., Reisky, L., Jäger, G., & Bornscheuer, U. T. (2023). Urethanases for the Enzymatic Hydrolysis of Low Molecular Weight Carbamates and the Recycling of Polyurethanes. *Angewandte Chemie International Edition*, *62*(9), e202216220. https://doi.org/https://doi.org/10.1002/anie.202216220

Breister, A., Imam, M., Zhou, Z., Ahsan, A., Noveron, J., Anantharaman, K., & Prabhakar, P. (2020). Soil microbiomes mediate degradation of vinyl ester-based polymer composites. *Communications Materials*, *1*. https://doi.org/10.1038/s43246-020-00102-1

Brijwani, K., Rigdon, A., & Vadlani, P. V. (2010). Fungal laccases: production, function, and applications in food processing. *Enzyme Res*, *2010*, 149748. https://doi.org/10.4061/2010/149748

Buchholz, P. C. F., Feuerriegel, G., Zhang, H., Perez-Garcia, P., Nover, L. L., Chow, J., Streit, W. R., & Pleiss, J. (2022). Plastics degradation by hydrolytic enzymes: The plastics-active enzymes database-PAZy. *Proteins*, *90*(7), 1443–1456. https://doi.org/10.1002/prot.26325

Budelmann, D., Schmidt, C., & Meiners, D. (2022). Tack of epoxy resin films for aerospace-grade prepregs: Influence of resin formulation, B-staging and toughening. *Polymer Testing*, *114*, 107709. https://doi.org/https://doi.org/10.1016/j.polymertesting.2022.107709

Bugg, T. D. H., Ahmad, M., Hardiman, E. M., & Singh, R. (2011). The emerging role for bacteria in lignin degradation and bio-product formation. *Current Opinion in Biotechnology*, *22*(3), 394–400. https://doi.org/https://doi.org/10.1016/j.copbio.2010.10.009

Cappitelli, F., Principi, P., Pedrazzani, R., Toniolo, L., & Sorlini, C. (2007). Bacterial and fungal deterioration of the Milan Cathedral marble treated with protective synthetic resins. *Science of The Total Environment*, *385*(1), 172–181. https://doi.org/https://doi.org/10.1016/j.scitotenv.2007.06.022

Capricho, J. C., Fox, B., & Hameed, N. (2020). Multifunctionality in Epoxy Resins. *Polymer Reviews*, *60*(1), 1–41. https://doi.org/10.1080/15583724.2019.1650063

Castillo Martinez, F. A., Balciunas, E. M., Salgado, J. M., Domínguez González, J. M., Converti, A., & Oliveira, R. P. d. S. (2013). Lactic acid properties, applications and production: A review. *Trends in Food Science & Technology*, *30*(1), 70–83. https://doi.org/https://doi.org/10.1016/j.tifs.2012.11.007

Chandra, R. P., Bura, R., Mabee, W. E., Berlin, A., Pan, X., & Saddler, J. N. (2007). Substrate Pretreatment: The Key to Effective Enzymatic Hydrolysis of Lignocellulosics? In L. Olsson (Ed.), *Biofuels* (pp. 67–93). Springer Berlin Heidelberg. https://doi.org/10.1007/10_2007_064

Chen, Y., Yang, Y., Liu, X., Shi, X., Wang, C., Zhong, H., & Jin, F. (2023). Sustainable production of formic acid and acetic acid from biomass. *Molecular Catalysis*, *545*, 113199. https://doi.org/https://doi.org/10.1016/j.mcat.2023.113199

Chen, Y., Zhang, J., Li, Z., Zhang, H., Chen, J., Yang, W., Yu, T., Liu, W., & Li, Y. (2023). Manufacturing Technology of Lightweight Fiber-Reinforced Composite Structures in Aerospace: Current Situation and toward Intellectualization. *Aerospace*, *10*(3), 206.

Cheng, H., Huang, H., Zhang, J., & Jing, D. (2017). Degradation of carbon fiber-reinforced polymer using supercritical fluids. *Fibers and Polymers*, *18*, 795–805. https://doi.org/10.1007/s12221-017-1151-4

Chow, J., Perez-Garcia, P., Dierkes, R., & Streit, W. R. (2023). Microbial enzymes will offer limited solutions to the global plastic pollution crisis. *Microbial Biotechnology*, *16*(2), 195–217. https://doi.org/https://doi.org/10.1111/1751-7915.14135

Chris, B., & Nithesh Chandrasekharan, C. B. (2020). Fitting enzyme kinetics data with Solver. *protocols.io*.

Christiansen, E., & Bakke, A. (1988). The spruce bark beetle of Eurasia. In *Dynamics of forest insect populations: patterns, causes, implications* (pp. 479–503). Springer.

Christopher, L. P., Yao, B., & Ji, Y. (2014). Lignin Biodegradation with Laccase-Mediator Systems [Review]. *Frontiers in Energy Research*, *Volume 2 - 2014*. https://doi.org/10.3389/fenrg.2014.00012

Christov, L., & Driessel, B. (2003). Waste Water Bioremediation in the Pulp and Paper Industry. *Indian Journal of Biotechnology*, *2*.

Contaldo, U., Savant-Aira, D., Vergnes, A., Becam, J., Biaso, F., Ilbert, M., Aussel, L., Ezraty, B., Lojou, E., & Mazurenko, I. (2024). Methionine-rich domains emerge as facilitators of copper recruitment in detoxification systems. *Proceedings of the National Academy of Sciences*, *121*(42), e2402862121. https://doi.org/10.1073/pnas.2402862121

Cook, E. N., Flaxman, L. A., Reid, A. G., Dickie, D. A., & Machan, C. W. (2024). Acid Strength Effects on Dimerization during Metal-Free Catalytic Dioxygen Reduction. *Journal of the American Chemical Society*, *146*(36), 24892–24900. https://doi.org/10.1021/jacs.4c05708

d'Ambrières, W. (2019). Plastics recycling worldwide: current overview and desirable changes. *Field Actions Science Reports. The journal of field actions*(Special Issue 19), 12–21.

Da Costa, J. P., Nunes, A. R., Santos, P. S. M., Girão, A. V., Duarte, A. C., & Rocha-Santos, T. (2018). Degradation of polyethylene microplastics in seawater: Insights into the environmental degradation of polymers. *Journal of Environmental Science and Health, Part A*, *53*(9), 866–875. https://doi.org/10.1080/10934529.2018.1455381

Dang, H., & Lovell Charles, R. (2015). Microbial Surface Colonization and Biofilm Development in Marine Environments. *Microbiology and Molecular Biology Reviews*, *80*(1), 91–138. https://doi.org/10.1128/mmbr.00037-15

Dang, W., Kubouchi, M., Yamamoto, S., Sembokuya, H., & Tsuda, K. (2002). An approach to chemical recycling of epoxy resin cured with amine using nitric acid. *Polymer*, *43*(10), 2953–2958. https://doi.org/https://doi.org/10.1016/S0032-3861(02)00100-3

Das, M., Chacko, R., & Varughese, S. (2018). An Efficient Method of Recycling of CFRP Waste Using Peracetic Acid. *ACS Sustainable Chemistry & Engineering*, *6*(2), 1564–1571. https://doi.org/10.1021/acssuschemeng.7b01456

Deng, S., Wu, J., Li, Y., Wang, G., Chai, K., Yu, A., & Liu, F. (2019). Effect of Bacillus flexus on the Degradation of Epoxy Resin Varnish Coating in Seawater. *International Journal of Electrochemical Science*, *14*(1), 315–328. https://doi.org/https://doi.org/10.20964/2019.01.64

Deng, S., Yang, Z., Yu, X., Li, M., & Cao, H. (2024). The reactivity of organic radicals in the performic, peracetic, perpropionic acids-based advanced oxidation process: A case study of sulfamethoxazole. *Journal of Hazardous Materials*, *476*, 135033. https://doi.org/https://doi.org/10.1016/j.jhazmat.2024.135033

do Nascimento, C. W. A., Amarasiriwardena, D., & Xing, B. (2006). Comparison of natural organic acids and synthetic chelates at enhancing phytoextraction of metals from a multi-metal contaminated soil. *Environmental Pollution*, *140*(1), 114–123. https://doi.org/https://doi.org/10.1016/j.envpol.2005.06.017

Dokl, M., Copot, A., Krajnc, D., Fan, Y. V., Vujanović, A., Aviso, K. B., Tan, R. R., Kravanja, Z., & Čuček, L. (2024). Global projections of plastic use, end-of-life fate and potential changes in consumption, reduction, recycling and replacement with bioplastics to 2050. *Sustainable Production and Consumption*, *51*, 498–518. https://doi.org/https://doi.org/10.1016/j.spc.2024.09.025

Dolz, M., Mateljak, I., Méndez-Sánchez, D., Sánchez-Moreno, I., Gomez de Santos, P., Viña-Gonzalez, J., & Alcalde, M. (2022). Colorimetric High-Throughput Screening Assay to Engineer Fungal Peroxygenases for the Degradation of Thermoset Composite Epoxy Resins [Original Research]. *Frontiers in Catalysis*, *2*. https://doi.org/10.3389/fctls.2022.883263

Duan, Y., Wei, Y., Xing, M., Liu, J., Jiang, L., Lu, Q., Liu, X., Liu, Y., Ang, E. L., Liao, R.-Z., Yuchi, Z., Zhao, H., & Zhang, Y. (2022). Anaerobic Hydroxyproline Degradation Involving C–N

Cleavage by a Glycyl Radical Enzyme. *Journal of the American Chemical Society*, *144*(22), 9715–9722. https://doi.org/10.1021/jacs.2c01673

Dutta, D., Arya, S., & Kumar, S. (2021). Industrial wastewater treatment: Current trends, bottlenecks, and best practices. *Chemosphere*, *285*, 131245. https://doi.org/https://doi.org/10.1016/j.chemosphere.2021.131245

e.V., D. (2019). *Aerospace series - Carbon fibre laminates - Determination of the fibre, resin and void contents* B. V. GmbH.

Eliaz, N., Ron, E. Z., Gozin, M., Younger, S., Biran, D., & Tal, N. (2018). Microbial Degradation of Epoxy. *Materials*, *11*(11), 2123.

Escayola, S., Bahri-Laleh, N., & Poater, A. (2024). %VBur index and steric maps: from predictive catalysis to machine learning [10.1039/D3CS00725A]. *Chemical Society Reviews*, *53*(2), 853–882. https://doi.org/10.1039/D3CS00725A

Falade, A. O., Nwodo, U. U., Iweriebor, B. C., Green, E., Mabinya, L. V., & Okoh, A. I. (2017). Lignin peroxidase functionalities and prospective applications. *MicrobiologyOpen*, *6*(1). https://doi.org/10.1002/mbo3.394

Fang, D., Gao, G., Yang, Y., Wang, Y., Gao, L., & Zhi, J. (2020). Redox Mediator-Based Microbial Biosensors for Acute Water Toxicity Assessment: A Critical Review. *ChemElectroChem*, *7*(12), 2513–2526. https://doi.org/https://doi.org/10.1002/celc.202000367

Feraboli, P., Kawakami, H., Wade, B., Gasco, F., DeOto, L., & Masini, A. (2012). Recyclability and reutilization of carbon fiber fabric/epoxy composites. *Journal of Composite Materials*, *46*(12), 1459–1473. https://doi.org/10.1177/0021998311420604

Fernandes, A. T., Damas, J. M., Todorovic, S., Huber, R., Baratto, M. C., Pogni, R., Soares, C. M., & Martins, L. O. (2010). The multicopper oxidase from the archaeon Pyrobaculum aerophilum shows nitrous oxide reductase activity. *The FEBS Journal*, *277*(15), 3176–3189. https://doi.org/https://doi.org/10.1111/j.1742-4658.2010.07725.x

Flippen-Anderson, J. L. G., R. (1981). Diglyeldyl Ether of Bisphenol A (DGEBA). *Acta Cryst*, *B37*, 1433–1435.

Fujii, K., Uemura, M., Hayakawa, C., Funakawa, S., & Kosaki, T. (2013). Environmental control of lignin peroxidase, manganese peroxidase, and laccase activities in forest floor layers in humid Asia. *Soil Biology and Biochemistry*, *57*, 109–115. https://doi.org/https://doi.org/10.1016/j.soilbio.2012.07.007

Gall, R. J., & Greenspan, F. P. (1955). A modified peracid process for making epoxy compounds from unsaturated fatty acid esters. *Industrial & Engineering Chemistry*, *47*(1), 147–148.

Galletti, P., Funiciello, F., Soldati, R., & Giacomini, D. (2015). Selective Oxidation of Amines to Aldehydes or Imines using Laccase-Mediated Bio-Oxidation. *Advanced Synthesis & Catalysis*, *357*(8), 1840–1848. https://doi.org/https://doi.org/10.1002/adsc.201500165

Gandomkar, S., Fischereder, E.-M., Schrittwieser, J. H., Wallner, S., Habibi, Z., Macheroux, P., & Kroutil, W. (2015). Enantioselective Oxidative Aerobic Dealkylation of N-Ethyl Benzylisoquinolines by Employing the Berberine Bridge Enzyme. *Angewandte Chemie International Edition*, *54*(50), 15051–15054. https://doi.org/https://doi.org/10.1002/anie.201507970

Geib, S. M., Filley, T. R., Hatcher, P. G., Hoover, K., Carlson, J. E., Jimenez-Gasco, M. d. M., Nakagawa-Izumi, A., Sleighter, R. L., & Tien, M. (2008). Lignin degradation in wood-feeding insects. *Proceedings of the National Academy of Sciences*, *105*(35), 12932–12937.

Gondaliya, R., Sypeck, D., & Feng, Z. (2016). *Improving Damage Tolerance of Composite Sandwich Structure Subjected to Low Velocity Impact Loading: Experimental Analysis*.

Gong, X., Kang, H., Liu, Y., & Wu, S. (2015). Decomposition mechanisms and kinetics of amine/anhydride-cured DGEBA epoxy resin in near-critical water. *RSC advances*, *5*(50), 40269–40282.

Gonzalez-Garcia, R. A., McCubbin, T., Navone, L., Stowers, C., Nielsen, L. K., & Marcellin, E. (2017). Microbial Propionic Acid Production. *Fermentation*, *3*(2).

González, M., Cabanelas, J., & Baselga, J. (2012). Applications of FTIR on Epoxy Resins - Identification, Monitoring the Curing Process, Phase Separation and Water Uptake. In. https://doi.org/10.5772/36323

Gräff, M., Buchholz, P. C. F., Le Roes-Hill, M., & Pleiss, J. (2020). Multicopper oxidases: modular structure, sequence space, and evolutionary relationships. *Proteins: Structure, Function, and Bioinformatics*, *88*(10), 1329–1339. https://doi.org/https://doi.org/10.1002/prot.25952

Grass, G., & Rensing, C. (2001). CueO Is a Multi-copper Oxidase That Confers Copper Tolerance in Escherichia coli. *Biochemical and Biophysical Research Communications*, *286*(5), 902–908. https://doi.org/https://doi.org/10.1006/bbrc.2001.5474

Gu, J. D., Lu, C., Thorp, K., Crasto, A., & Mitchell, R. (1997). Fiber-reinforced polymeric composites are susceptible to microbial degradation. *Journal of Industrial Microbiology and Biotechnology*, *18*(6), 364–369. https://doi.org/10.1038/sj.jim.2900401

Guan, Z. B., Luo, Q., Wang, H. R., Chen, Y., & Liao, X. R. (2018). Bacterial laccases: promising biological green tools for industrial applications. *Cell Mol Life Sci*, *75*(19), 3569–3592. https://doi.org/10.1007/s00018-018-2883-z

Gunne, M., Höppner, A., Hagedoorn, P. L., & Urlacher, V. B. (2014). Structural and redox properties of the small laccase Ssl1 from Streptomyces sviceus. *Febs j*, *281*(18), 4307–4318. https://doi.org/10.1111/febs.12755

Gunne, M., & Urlacher, V. B. (2012). Characterization of the Alkaline Laccase Ssl1 from Streptomyces sviceus with Unusual Properties Discovered by Genome Mining. *PLOS ONE*, *7*(12), e52360. https://doi.org/10.1371/journal.pone.0052360

Hamerton, I., Howlin, B. J., & Jepson, P. (2002). Metals and coordination compounds as modifiers for epoxy resins. *Coordination Chemistry Reviews*, *224*(1), 67–85. https://doi.org/https://doi.org/10.1016/S0010-8545(01)00393-9

Han, Y., Wang, R., Wang, D., & Luan, Y. (2024). Enzymatic degradation of synthetic plastics by hydrolases/oxidoreductases. *International Biodeterioration & Biodegradation*, *189*, 105746. https://doi.org/https://doi.org/10.1016/j.ibiod.2024.105746

Haq, I. u., Saleem, A., Chaudhary, R., Alessa, A. H., Nawaz, A., & Du, C. (2024). Role of microbial laccases in valorization of lignocellulosic biomass to bioethanol [Review]. *Frontiers in Bioengineering and Biotechnology*, *12*. https://doi.org/10.3389/fbioe.2024.1441075

Harris, Z. L. (2019). Chapter 9 - Ceruloplasmin. In N. Kerkar & E. A. Roberts (Eds.), *Clinical and Translational Perspectives on WILSON DISEASE* (pp. 77–84). Academic Press. https://doi.org/https://doi.org/10.1016/B978-0-12-810532-0.00009-4

Hegde, S., Satish Shenoy, B., & Chethan, K. N. (2019). Review on carbon fiber reinforced polymer (CFRP) and their mechanical performance. *Materials Today: Proceedings*, *19*, 658–662. https://doi.org/https://doi.org/10.1016/j.matpr.2019.07.749

Henriksen, A., Schuller, D. J., Meno, K., Welinder, K. G., Smith, A. T., & Gajhede, M. (1998). Structural interactions between horseradish peroxidase C and the substrate benzhydroxamic acid determined by X-ray crystallography. *Biochemistry*, *37*(22), 8054–8060. https://doi.org/10.1021/bi980234j

Higuchi, T. (2004). Microbial degradation of lignin: Role of lignin peroxidase, manganese peroxidase, and laccase. *Proceedings of the Japan Academy, Series B*, *80*(5), 204–214.

Hilgers, R., Vincken, J.-P., Gruppen, H., & Kabel, M. A. (2018). Laccase/Mediator Systems: Their Reactivity toward Phenolic Lignin Structures. *ACS Sustainable Chemistry & Engineering*, *6*(2), 2037–2046. https://doi.org/10.1021/acssuschemeng.7b03451

Hofrichter, M., Kellner, H., Pecyna, M. J., & Ullrich, R. (2015). Fungal Unspecific Peroxygenases: Heme-Thiolate Proteins That Combine Peroxidase and Cytochrome P450 Properties. In E. G. Hrycay & S. M. Bandiera (Eds.), *Monooxygenase, Peroxidase and Peroxygenase Properties and Mechanisms of Cytochrome P450* (pp. 341–368). Springer International Publishing. https://doi.org/10.1007/978-3-319-16009-2_13

Hornung, C., Poehlein, A., Haack, F. S., Schmidt, M., Dierking, K., Pohlen, A., Schulenburg, H., Blokesch, M., Plener, L., Jung, K., Bonge, A., Krohn-Molt, I., Utpatel, C., Timmermann, G., Spieck, E., Pommerening-Röser, A., Bode, E., Bode, H. B., Daniel, R.,…Streit, W. R. (2013). The Janthinobacterium sp. HH01 Genome Encodes a Homologue of the V. cholerae CqsA and L. pneumophila LqsA Autoinducer Synthases. *PLOS ONE*, *8*(2), e55045. https://doi.org/10.1371/journal.pone.0055045

Huang, C. C., Meng, E. C., Morris, J. H., Pettersen, E. F., & Ferrin, T. E. (2014). Enhancing UCSF Chimera through web services. *Nucleic Acids Res*, *42*(Web Server issue), W478–484. https://doi.org/10.1093/nar/gku377

Huang, H., Yin, Y., Cheng, H., Zhao, Z., & Zhang, B. (2017). Degradation Mechanism of CF/EP Composites in Supercritical n-Butanol with Alkali Additives. *Journal of Polymers and the Environment*, *25*(2), 115–125. https://doi.org/10.1007/s10924-016-0776-5

Ikai, A. (1980). Thermostability and aliphatic index of globular proteins. *J Biochem*, *88*(6), 1895–1898.

Janusz, G., Pawlik, A., Świderska-Burek, U., Polak, J., Sulej, J., Jarosz-Wilkołazka, A., & Paszczyński, A. (2020). Laccase Properties, Physiological Functions, and Evolution. *International Journal of Molecular Sciences*, *21*(3).

Jha, H. (2019). Fungal Diversity and Enzymes Involved in Lignin Degradation. In R. Naraian (Ed.), *Mycodegradation of Lignocelluloses* (pp. 35–49). Springer International Publishing. https://doi.org/10.1007/978-3-030-23834-6_3

Jin, F.-L., Li, X., & Park, S.-J. (2015). Synthesis and application of epoxy resins: A review. *Journal of Industrial and Engineering Chemistry*, *29*, 1–11. https://doi.org/https://doi.org/10.1016/j.jiec.2015.03.026

Jin, X., Yu, X., Zhu, G., Zheng, Z., Feng, F., & Zhang, Z. (2016). Conditions Optimizing and Application of Laccase-mediator System (LMS) for the Laccase-catalyzed Pesticide Degradation. *Scientific Reports*, *6*(1), 35787. https://doi.org/10.1038/srep35787

Jolivalt, C., Raynal, A., Caminade, E., Kokel, B., Le Goffic, F., & Mougin, C. (1999). Transformation of N′,N′-dimethyl-N-(hydroxyphenyl)ureas by laccase from the white rot fungus Trametes versicolor. *Applied Microbiology and Biotechnology*, *51*(5), 676–681. https://doi.org/10.1007/s002530051451

Kadnikova, E. N., & Kostić, N. M. (2002). Oxidation of ABTS by hydrogen peroxide catalyzed by horseradish peroxidase encapsulated into sol–gel glass.: Effects of glass matrix on reactivity. *Journal of Molecular Catalysis B: Enzymatic*, *18*(1), 39–48. https://doi.org/https://doi.org/10.1016/S1381-1177(02)00057-7

Kajdas, C. (2004). Hydrolysis. In *Surface modification and mechanisms* (pp. 247–294). CRC Press.

Karshikoff, A., Nilsson, L., & Ladenstein, R. (2015). Rigidity versus flexibility: the dilemma of understanding protein thermal stability. *The FEBS Journal*, *282*(20), 3899–3917. https://doi.org/https://doi.org/10.1111/febs.13343

Keith, M. J., Román-Ramírez, L. A., Leeke, G., & Ingram, A. (2019). Recycling a carbon fibre reinforced polymer with a supercritical acetone/water solvent mixture: Comprehensive analysis of reaction kinetics. *Polymer Degradation and Stability*, *161*, 225–234. https://doi.org/https://doi.org/10.1016/j.polymdegradstab.2019.01.015

Kemmer, G., & Keller, S. (2010). Nonlinear least-squares data fitting in Excel spreadsheets. *Nature Protocols*, *5*(2), 267–281. https://doi.org/10.1038/nprot.2009.182

Keshav, A., Wasewar, K. L., & Chand, S. (2009). Recovery of propionic acid from an aqueous stream by reactive extraction: effect of diluents. *Desalination*, *244*(1), 12–23. https://doi.org/https://doi.org/10.1016/j.desal.2008.04.032

Khatami, S. H., Vakili, O., Movahedpour, A., Ghesmati, Z., Ghasemi, H., & Taheri-Anganeh, M. (2022). Laccase: Various types and applications. *Biotechnology and Applied Biochemistry*, *69*(6), 2658–2672. https://doi.org/https://doi.org/10.1002/bab.2313

Kiejza, D., Kotowska, U., Polińska, W., & Karpińska, J. (2021). Peracids - New oxidants in advanced oxidation processes: The use of peracetic acid, peroxymonosulfate, and persulfate salts in the removal of organic micropollutants of emerging concern − A review. *Science of The Total Environment*, *790*, 148195. https://doi.org/https://doi.org/10.1016/j.scitotenv.2021.148195

Kim, J.-H., Jung, Y.-H., Lambiase, F., Moon, Y.-H., & Ko, D.-C. (2022). Novel Approach toward the Forming Process of CFRP Reinforcement with a Hot Stamped Part by Prepreg Compression Molding. *Materials*, *15*(14), 4743.

Kim, J., & Huang, C.-H. (2021). Reactivity of Peracetic Acid with Organic Compounds: A Critical Review. *ACS ES&T Water*, *1*(1), 15–33. https://doi.org/10.1021/acsestwater.0c00029

Kim, K.-W., Lee, H.-M., An, J.-H., Chung, D.-C., An, K.-H., & Kim, B.-J. (2017). Recycling and characterization of carbon fibers from carbon fiber reinforced epoxy matrix composites by a novel super-heated-steam method. *Journal of Environmental Management*, *203*, 872–879. https://doi.org/https://doi.org/10.1016/j.jenvman.2017.05.015

Klose, L., Meyer-Heydecke, N., Wongwattanarat, S., Chow, J., Pérez García, P., Carré, C., Streit, W., Antranikian, G., Romero, A. M., & Liese, A. (2023). Towards Sustainable Recycling of

Epoxy-Based Polymers: Approaches and Challenges of Epoxy Biodegradation. *Polymers*, *15*(12).

Komori, H., & Higuchi, Y. (2010). Structure and molecular evolution of multicopper blue proteins. *Biomolecular Concepts*, *1*(1), 31–40. https://doi.org/doi:10.1515/bmc.2010.004

Komori, H., & Higuchi, Y. (2015). Structural insights into the O2 reduction mechanism of multicopper oxidase. *The Journal of Biochemistry*, *158*(4), 293–298. https://doi.org/10.1093/jb/mvv079

Komori, H., Miyazaki, K., & Higuchi, Y. (2009). X-ray structure of a two-domain type laccase: A missing link in the evolution of multi-copper proteins. *FEBS Letters*, *583*(7), 1189–1195. https://doi.org/https://doi.org/10.1016/j.febslet.2009.03.008

Komori, H., Sugiyama, R., Kataoka, K., Miyazaki, K., Higuchi, Y., & Sakurai, T. (2014). New insights into the catalytic active-site structure of multicopper oxidases. *Acta Crystallographica Section D*, *70*(3), 772–779. https://doi.org/doi:10.1107/S1399004713033051

Konermann, L., Ahadi, E., Rodriguez, A. D., & Vahidi, S. (2013). Unraveling the Mechanism of Electrospray Ionization. *Analytical Chemistry*, *85*(1), 2–9. https://doi.org/10.1021/ac302789c

Könst, P., Kara, S., Kochius, S., Holtmann, D., Arends, I. W. C. E., Ludwig, R., & Hollmann, F. (2013). Expanding the Scope of Laccase-Mediator Systems. *ChemCatChem*, *5*(10), 3027–3032. https://doi.org/https://doi.org/10.1002/cctc.201300205

Koschorreck, K., Richter, S. M., Ene, A. B., Roduner, E., Schmid, R. D., & Urlacher, V. B. (2008). Cloning and characterization of a new laccase from Bacillus licheniformis catalyzing dimerization of phenolic acids. *Applied Microbiology and Biotechnology*, *79*(2), 217–224. https://doi.org/10.1007/s00253-008-1417-2

Kumar, A., & Chandra, R. (2020). Ligninolytic enzymes and its mechanisms for degradation of lignocellulosic waste in environment. *Heliyon*, *6*(2), e03170. https://doi.org/https://doi.org/10.1016/j.heliyon.2020.e03170

Kunamneni, A., Ballesteros, A., Plou, F. J., & Alcalde, M. (2007). Fungal laccase—a versatile enzyme for biotechnological applications. *Communicating current research and educational topics and trends in applied microbiology*, *1*, 233–245.

Kychkin, A. K., Startsev, O. V., Lebedev, M. P., Kychkin, A. A., & Lukachevskaia, I. G. (2025). The Effect of Biocontamination on Mechanical Strength and Moisture Transfer Performance of Epoxy Basalt Fiber Reinforcement Bar Exposed to Arctic Conditions. *Polymers (Basel)*, *17*(4). https://doi.org/10.3390/polym17040460

Ladenstein, R., & Ren, B. (2006). Protein disulfides and protein disulfide oxidoreductases in hyperthermophiles. *The FEBS Journal*, *273*(18), 4170–4185.

Larrondo, L. F., Salas, L., Melo, F., Vicuña, R., & Cullen, D. (2003). A novel extracellular multicopper oxidase from Phanerochaete chrysosporium with ferroxidase activity. *Appl Environ Microbiol*, *69*(10), 6257–6263. https://doi.org/10.1128/aem.69.10.6257-6263.2003

Lawton, T. J., Sayavedra-Soto, L. A., Arp, D. J., & Rosenzweig, A. C. (2009). Crystal Structure of a Two-domain Multicopper Oxidase*. *Journal of Biological Chemistry*, *284*(15), 10174–10180. https://doi.org/https://doi.org/10.1074/jbc.M900179200

Leveneur, S., Murzin, D. Y., Salmi, T., Mikkola, J.-P., Kumar, N., Eränen, K., & Estel, L. (2009). Synthesis of peroxypropionic acid from propionic acid and hydrogen peroxide over

heterogeneous catalysts. *Chemical Engineering Journal*, *147*(2), 323–329. https://doi.org/https://doi.org/10.1016/j.cej.2008.11.045

Leynaud Kieffer Curran, L. M. C., Pham, L. T. M., Sale, K. L., & Simmons, B. A. (2022). Review of advances in the development of laccases for the valorization of lignin to enable the production of lignocellulosic biofuels and bioproducts. *Biotechnology Advances*, *54*, 107809. https://doi.org/https://doi.org/10.1016/j.biotechadv.2021.107809

Li, J., Xu, P.-L., Zhu, Y.-K., Ding, J.-P., Xue, L.-X., & Wang, Y.-Z. (2012). A promising strategy for chemical recycling of carbon fiber/thermoset composites: self-accelerating decomposition in a mild oxidative system. *Green Chemistry*, *14*(12), 3260–3263.

Li, X., Wei, Z., Zhang, M., Peng, X., Yu, G., Teng, M., & Gong, W. (2007). Crystal structures of E. coli laccase CueO at different copper concentrations. *Biochemical and Biophysical Research Communications*, *354*(1), 21–26. https://doi.org/https://doi.org/10.1016/j.bbrc.2006.12.116

Liu, H., Jin, Y., Zhang, R., Ning, Y., Yu, Y., Xu, P., Deng, L., & Wang, F. (2023). Recent advances and perspectives on production of value-added organic acids through metabolic engineering. *Biotechnology Advances*, *62*, 108076. https://doi.org/https://doi.org/10.1016/j.biotechadv.2022.108076

Liu, T., Shao, L., Zhao, B., Chang, Y.-C., & Zhang, J. (2022). Progress in Chemical Recycling of Carbon Fiber Reinforced Epoxy Composites. *Macromolecular Rapid Communications*, *43*(23), 2200538. https://doi.org/https://doi.org/10.1002/marc.202200538

Liu, W., Wang, Z., Chen, Z., Li, J., & Zhao, L. (2012). Synthesis and properties of two novel silicon-containing cycloaliphatic epoxy resins for electronic packaging application. *Polymers for Advanced Technologies*, *23*(3), 367–374. https://doi.org/https://doi.org/10.1002/pat.1882

Liu, Y., Liu, J., Jiang, Z., & Tang, T. (2012). Chemical recycling of carbon fibre reinforced epoxy resin composites in subcritical water: Synergistic effect of phenol and KOH on the decomposition efficiency. *Polymer Degradation and Stability*, *97*(3), 214–220. https://doi.org/https://doi.org/10.1016/j.polymdegradstab.2011.12.028

Liu, Z., Xie, T., Zhong, Q., & Wang, G. (2016). Crystal structure of CotA laccase complexed with 2, 2-azinobis-(3-ethylbenzothiazoline-6-sulfonate) at a novel binding site. *Structural Biology and Crystallization Communications*, *72*(4), 328–335.

Loi, M., Glazunova, O., Fedorova, T., Logrieco, A. F., & Mulè, G. (2021). Fungal Laccases: The Forefront of Enzymes for Sustainability. *J Fungi (Basel)*, *7*(12). https://doi.org/10.3390/jof7121048

Lu, S.-Y., Liu, C.-C., Huang, K.-H., Yu, C.-X., & Fu, L.-M. (2023). Microfluidic Distillation System for Separation of Propionic Acid in Foods. *Micromachines*, *14*(6).

Luukkonen, T., & and Pehkonen, S. O. (2017). Peracids in water treatment: A critical review. *Critical Reviews in Environmental Science and Technology*, *47*(1), 1–39. https://doi.org/10.1080/10643389.2016.1272343

Luukkonen, T., Heyninck, T., Rämö, J., & Lassi, U. (2015). Comparison of organic peracids in wastewater treatment: Disinfection, oxidation and corrosion. *Water Research*, *85*, 275–285. https://doi.org/https://doi.org/10.1016/j.watres.2015.08.037

Ma, J. H., Wang, X. B., Li, B., & Huang, L. N. (2009). Investigation on Recycling Technology of Carbon Fiber Reinforced Epoxy Resin Cured with Amine. *Advanced Materials Research*, *79-82*, 409–412. https://doi.org/10.4028/www.scientific.net/AMR.79-82.409

Ma, Y., Kim, D., & Nutt, S. R. (2017). Chemical treatment for dissolution of amine-cured epoxies at atmospheric pressure. *Polymer Degradation and Stability*, *146*, 240–249. https://doi.org/https://doi.org/10.1016/j.polymdegradstab.2017.10.014

Machczynski, M. C., Vijgenboom, E., Samyn, B., & Canters, G. W. (2004). Characterization of SLAC: A small laccase from Streptomyces coelicolor with unprecedented activity. *Protein Science*, *13*(9), 2388–2397. https://doi.org/https://doi.org/10.1110/ps.04759104

Majumdar, S., Lukk, T., Solbiati, J. O., Bauer, S., Nair, S. K., Cronan, J. E., & Gerlt, J. A. (2014). Roles of Small Laccases from Streptomyces in Lignin Degradation. *Biochemistry*, *53*(24), 4047–4058. https://doi.org/10.1021/bi500285t

Malviya, J., Alameri, A. A., Al-Janabi, S. S., Fawzi, O. F., Azzawi, A. L., Obaid, R. F., Alsudani, A. A., Alkhayyat, A. S., Gupta, J., Mustafa, Y. F., Karampoor, S., & Mirzaei, R. (2023). Metabolomic profiling of bacterial biofilm: trends, challenges, and an emerging antibiofilm target. *World Journal of Microbiology and Biotechnology*, *39*(8), 212. https://doi.org/10.1007/s11274-023-03651-y

Manis, F., Wölling, J., & Drechsler, K. (2015). Damage Behaviour of Fibre Reinforced Materials Induced by High Temperature Oxidation for Optimisation of Thermal Recycling Routes. *Materials Science Forum*, *825-826*, 1088–1095. https://doi.org/10.4028/www.scientific.net/MSF.825-826.1088

Marketsandmarkets. (2023). Epoxy Resin Market.

Markowitz, V. M., Chen, I. M., Palaniappan, K., Chu, K., Szeto, E., Grechkin, Y., Ratner, A., Jacob, B., Huang, J., Williams, P., Huntemann, M., Anderson, I., Mavromatis, K., Ivanova, N. N., & Kyrpides, N. C. (2012). IMG: the Integrated Microbial Genomes database and comparative analysis system. *Nucleic Acids Res*, *40*(Database issue), D115–122. https://doi.org/10.1093/nar/gkr1044

Martínez-Franco, E., Gomez Culebro, V. A., & Franco-Urquiza, E. A. (2024). Technologies for Mechanical Recycling of Carbon Fiber-Reinforced Polymers (CFRP) Composites: End Mill, High-Energy Ball Milling, and Ultrasonication. *Polymers*, *16*(16), 2350.

Martins, L. O., Soares, C. M., Pereira, M. M., Teixeira, M., Costa, T., Jones, G. H., & Henriques, A. O. (2002). Molecular and biochemical characterization of a highly stable bacterial laccase that occurs as a structural component of the Bacillus subtilis endospore coat. *Journal of Biological Chemistry*, *277*(21), 18849–18859.

Mattila, T., & Aksela, R. (2000). Method for the preparation of aqueous solutions containing performic acid as well as their use. In: Google Patents.

May, C. (2018). *Epoxy resins: chemistry and technology*. Routledge.

May, S. W., & Padgette, S. R. (1983). Oxidoreductase Enzymes in Biotechnology: Current Status and Future Potential. *Bio/Technology*, *1*(8), 677–686. https://doi.org/10.1038/nbt1083-677

Meera, Y., Nivedita, R., Singh, Y. H., & Anindita, H. (2020). Bioconversion of lignocellulose materials using different pre-treatment strategies. *Res J Chem Environ*, *24*, 12.

Mehra, R., & Kepp, K. P. (2019). Contribution of substrate reorganization energies of electron transfer to laccase activity. *Physical Chemistry Chemical Physics*, *21*(28), 15805–15814.

Mester, T., Ambert-Balay, K., Ciofi-Baffoni, S., Banci, L., Jones, A. D., & Tien, M. (2001). Oxidation of a Tetrameric Nonphenolic Lignin Model Compound by Lignin Peroxidase *. *Journal of Biological Chemistry*, *276*(25), 22985–22990. https://doi.org/10.1074/jbc.M010739200

Meure, S., Wu, D.-Y., & Furman, S. A. (2010). FTIR study of bonding between a thermoplastic healing agent and a mendable epoxy resin. *Vibrational Spectroscopy*, *52*(1), 10–15. https://doi.org/https://doi.org/10.1016/j.vibspec.2009.09.005

Milgrom, L. R. (2016). Why is catalase so fast? A preliminary network hypothesis for the rapid enzyme-catalysed decomposition of hydrogen peroxide. *Water*, *7*, 129–146.

Miyazaki, K. (2005). A hyperthermophilic laccase from Thermus thermophilus HB27. *Extremophiles*, *9*(6), 415–425. https://doi.org/10.1007/s00792-005-0458-z

Mohanan, N., Montazer, Z., Sharma, P. K., & Levin, D. B. (2020). Microbial and Enzymatic Degradation of Synthetic Plastics [Review]. *Frontiers in Microbiology*, *11*. https://doi.org/10.3389/fmicb.2020.580709

Mohanty, A. K., Vivekanandhan, S., Tripathi, N., Roy, P., Snowdon, M. R., Drzal, L. T., & Misra, M. (2023). Sustainable composites for lightweight and flame retardant parts for electric vehicles to boost climate benefits: A perspective. *Composites Part C: Open Access*, *12*, 100380. https://doi.org/https://doi.org/10.1016/j.jcomc.2023.100380

Molina-Guijarro, J. M., Pérez Torres, J., Muñoz Dorado, J., Guillén Carretero, F., Moya Lobo, R., Hernández Cutuli, M., & Arias Fernández, M. E. (2009). Detoxification of azo dyes by a novel pH-versatile, salt-resistant laccase from Streptomyces ipomoea.

Morales, M., Mate, M. J., Romero, A., Martínez, M. J., Martínez, Á. T., & Ruiz-Dueñas, F. J. (2012). Two Oxidation Sites for Low Redox Potential Substrates: A DIRECTED MUTAGENESIS, KINETIC, AND CRYSTALLOGRAPHIC STUDY ON PLEUROTUS ERYNGII VERSATILE PEROXIDASE *. *Journal of Biological Chemistry*, *287*(49), 41053–41067. https://doi.org/10.1074/jbc.M112.405548

More, S. S., P. S, R., K, P., M, S., Malini, S., & S. M, V. (2011). Isolation, Purification, and Characterization of Fungal Laccase from Pleurotus sp. *Enzyme Research*, *2011*(1), 248735. https://doi.org/https://doi.org/10.4061/2011/248735

Moretti, S., Armougom, F., Wallace, I. M., Higgins, D. G., Jongeneel, C. V., & Notredame, C. (2007). The M-Coffee web server: a meta-method for computing multiple sequence alignments by combining alternative alignment methods. *Nucleic Acids Res*, *35*(Web Server issue), W645–648. https://doi.org/10.1093/nar/gkm333

Mot, A. C., & Silaghi-Dumitrescu, R. (2012). Laccases: Complex architectures for one-electron oxidations. *Biochemistry (Moscow)*, *77*(12), 1395–1407. https://doi.org/10.1134/S0006297912120085

Munegumi, T. (2013). Where is the border line between strong acids and weak acids. *World J Chem Educ*, *1*(1), 12–16.

Najmi, A. A., Bischoff, R., & Permentier, H. P. (2022). N-Dealkylation of Amines. *Molecules*, *27*(10), 3293.

Nakamura, K., Kawabata, T., Yura, K., & Go, N. (2003). Novel types of two-domain multi-copper oxidases: possible missing links in the evolution. *FEBS Letters*, *553*(3), 239–244. https://doi.org/https://doi.org/10.1016/S0014-5793(03)01000-7

Navapour, L., Mogharrab, N., & Amininasab, M. (2014). How modification of accessible lysines to phenylalanine modulates the structural and functional properties of horseradish peroxidase: a simulation study. *PLOS ONE*, *9*(10), e109062. https://doi.org/10.1371/journal.pone.0109062

Naveed, M., Iqbal, F., Aziz, T., Saleem, A., Javed, T., Afzal, M., Waseem, M., Alharbi, M., & Albekairi, T. H. (2025). Exploration of alcohol dehydrogenase EutG from Bacillus tropicus as an eco-friendly approach for the degradation of polycyclic aromatic compounds. *Scientific Reports*, *15*(1), 3466. https://doi.org/10.1038/s41598-025-86624-5

Negi, H., Kapri, A., Zaidi, M. G. H., Satlewal, A., & Goel, R. (2009). Comparative in-vitro biodegradation studies of epoxy and its silicone blend by selected microbial consortia. *International Biodeterioration & Biodegradation*, *63*(5), 553–558. https://doi.org/https://doi.org/10.1016/j.ibiod.2009.03.001

Nguyen, C., Young, J. T., Slade, G. G., Oliveira, R. J., & McCully, M. E. (2019). A Dynamic Hydrophobic Core and Surface Salt Bridges Thermostabilize a Designed Three-Helix Bundle. *Biophysical Journal*, *116*(4), 621–632. https://doi.org/10.1016/j.bpj.2019.01.012

Nicell, J. A., & Wright, H. (1997). A model of peroxidase activity with inhibition by hydrogen peroxide. *Enzyme and Microbial Technology*, *21*(4), 302–310. https://doi.org/https://doi.org/10.1016/S0141-0229(97)00001-X

Nicolucci, C., Rossi, S., Menale, C., Godjevargova, T., Ivanov, Y., Bianco, M., Mita, L., Bencivenga, U., Mita, D. G., & Diano, N. (2011). Biodegradation of bisphenols with immobilized laccase or tyrosinase on polyacrylonitrile beads. *Biodegradation*, *22*(3), 673–683. https://doi.org/10.1007/s10532-010-9440-2

Nielsen, H., Teufel, F., Brunak, S., & von Heijne, G. (2024). SignalP: The Evolution of a Web Server. *Methods Mol Biol*, *2836*, 331–367. https://doi.org/10.1007/978-1-0716-4007-4_17

Nunna, S., Blanchard, P., Buckmaster, D., Davis, S., & Naebe, M. (2019). Development of a cost model for the production of carbon fibres. *Heliyon*, *5*(10). https://doi.org/10.1016/j.heliyon.2019.e02698

O'Reilly, E., & Turner, N. (2014). Enzymatic Cascades for the Regio- and Stereoselective Synthesis of Chiral Amines. *Perspectives in Science*, *6*. https://doi.org/10.1016/j.pisc.2014.12.009

Obleser, K., Kalaus, H., Seidl, B., Kozich, M., Stanetty, C., & Mihovilovic, M. D. (2022). An Organic Chemist's Guide to Mediated Laccase Oxidation. *ChemBioChem*, *23*(23), e202200411. https://doi.org/https://doi.org/10.1002/cbic.202200411

Oh, S., & Choi, D. (2019). Microbial Community Enhances Biodegradation of Bisphenol A Through Selection of Sphingomonadaceae. *Microbial Ecology*, *77*(3), 631–639. https://doi.org/10.1007/s00248-018-1263-4

Oiffer, T., Leipold, F., Süss, P., Breite, D., Griebel, J., Khurram, M., Branson, Y., de Vries, E., Schulze, A., Helm, C. A., Wei, R., & Bornscheuer, U. T. (2024). Chemo-Enzymatic Depolymerization of Functionalized Low-Molecular-Weight Polyethylene. *Angewandte Chemie International Edition*, *63*(50), e202415012. https://doi.org/https://doi.org/10.1002/anie.202415012

Okajima, I., Hiramatsu, M., Shimamura, Y., Awaya, T., & Sako, T. (2014). Chemical recycling of carbon fiber reinforced plastic using supercritical methanol. *The Journal of Supercritical Fluids*, *91*, 68–76. https://doi.org/https://doi.org/10.1016/j.supflu.2014.04.011

Oliveux, G., Dandy, L. O., & Leeke, G. A. (2015). Degradation of a model epoxy resin by solvolysis routes. *Polymer Degradation and Stability*, *118*, 96–103. https://doi.org/https://doi.org/10.1016/j.polymdegradstab.2015.04.016

Othman, R., Ismail, N. I., Ab, M., Pahmi, H., Hisyam, M., Hisyam Basri, M., Sharudin, H., & Hemdi, A. (2019). APPLICATION OF CARBON FIBER REINFORCED PLASTICS IN AUTOMOTIVE INDUSTRY: A REVIEW.

Ozaki, S.-i., Roach, M. P., Matsui, T., & Watanabe, Y. (2001). Investigations of the Roles of the Distal Heme Environment and the Proximal Heme Iron Ligand in Peroxide Activation by Heme Enzymes via Molecular Engineering of Myoglobin. *Accounts of Chemical Research*, *34*(10), 818–825. https://doi.org/10.1021/ar9502590

Padayachee, T., Nzuza, N., Chen, W., Nelson, D. R., & Syed, K. (2020). Impact of lifestyle on cytochrome P450 monooxygenase repertoire is clearly evident in the bacterial phylum Firmicutes. *Scientific Reports*, *10*(1), 13982. https://doi.org/10.1038/s41598-020-70686-8

Pal, M. K., & Lavanya, M. (2022). Microbial Influenced Corrosion: Understanding Bioadhesion and Biofilm Formation. *Journal of Bio- and Tribo-Corrosion*, *8*(3), 76. https://doi.org/10.1007/s40735-022-00677-x

Pandey, V. P., Awasthi, M., Singh, S., Tiwari, S., & Dwivedi, U. N. (2017). A comprehensive review on function and application of plant peroxidases. *Biochem Anal Biochem*, *6*(1), 308.

Pardi-Comensoli, L., Tonolla, M., Colpo, A., Palczewska, Z., Revikrishnan, S., Heeb, M., Brunner, I., & Barbezat, M. (2022). Microbial Depolymerization of Epoxy Resins: A Novel Approach to a Complex Challenge. *Applied Sciences*, *12*(1), 466.

Parsons, A. J., Gonciaruk, A., Zeng, X., Thomann, F. S., Schubel, P., Lorrillard, J., & Johnson, M. S. (2022). Controlling mass loss from RTM6 epoxy resin under simulated vacuum infusion conditions. *Polymer Testing*, *107*, 107473. https://doi.org/https://doi.org/10.1016/j.polymertesting.2022.107473

Patrick, H. R., Griffith, K., Liotta, C. L., Eckert, C. A., & Gläser, R. (2001). Near-Critical Water: A Benign Medium for Catalytic Reactions. *Industrial & Engineering Chemistry Research*, *40*(26), 6063–6067. https://doi.org/10.1021/ie010178+

Pérez-García, P. (2020). *Enzyme promiscuity at the origin of metallo-β-lactamases and within the α/β-hydrolase superfamily* Staats-und Universitätsbibliothek Hamburg Carl von Ossietzky].

Pham, H. Q., & Marks, M. J. (2005). Epoxy Resins. In *Ullmann's Encyclopedia of Industrial Chemistry*. https://doi.org/https://doi.org/10.1002/14356007.a09_547.pub2

Pinter, B., Fievez, T., Bickelhaupt, F. M., Geerlings, P., & De Proft, F. (2012). On the origin of the steric effect [10.1039/C2CP41090G]. *Physical Chemistry Chemical Physics*, *14*(28), 9846–9854. https://doi.org/10.1039/C2CP41090G

Piontek, K., Antorini, M., & Choinowski, T. (2002). Crystal Structure of a Laccase from the FungusTrametes versicolor at 1.90-Å Resolution Containing a Full Complement of

Coppers*. *Journal of Biological Chemistry*, *277*(40), 37663–37669. https://doi.org/https://doi.org/10.1074/jbc.M204571200

Plasticseurope. (2024). Plastics – the fast Facts 2024.

Pollegioni, L., Tonin, F., & Rosini, E. (2015). Lignin-degrading enzymes. *The FEBS Journal*, *282*(7), 1190–1213. https://doi.org/https://doi.org/10.1111/febs.13224

Pradhan, S., Pandey, P., Mohanty, S., & Nayak, S. (2015). An Insight on the Chemistry of Epoxy and Its Curing for Coating Applications: A Detailed Investigation and Future Perspectives. *Polymer-Plastics Technology and Engineering*, *55*. https://doi.org/10.1080/03602559.2015.1103269

Rachmawati, N., & Triwibowo, R. (2024). An overview of propionic acid as food additives in the global trades of traditional fermented products. *AIP Conference Proceedings*, *2957*(1). https://doi.org/10.1063/5.0184008

Rahban, M., Zolghadri, S., Salehi, N., Ahmad, F., Haertlé, T., Rezaei-Ghaleh, N., Sawyer, L., & Saboury, A. A. (2022). Thermal stability enhancement: Fundamental concepts of protein engineering strategies to manipulate the flexible structure. *International Journal of Biological Macromolecules*, *214*, 642–654. https://doi.org/https://doi.org/10.1016/j.ijbiomac.2022.06.154

Ralph, J., Lapierre, C., & Boerjan, W. (2019). Lignin structure and its engineering. *Current Opinion in Biotechnology*, *56*, 240–249. https://doi.org/https://doi.org/10.1016/j.copbio.2019.02.019

Ranaei, V., Pilevar, Z., Khaneghah, A. M., & Hosseini, H. (2020). Propionic Acid: Method of Production, Current State and Perspectives. *Food Technol Biotechnol*, *58*(2), 115–127. https://doi.org/10.17113/ftb.58.02.20.6356

Reiss, R., Ihssen, J., Richter, M., Eichhorn, E., Schilling, B., & Thöny-Meyer, L. (2013). Laccase versus Laccase-Like Multi-Copper Oxidase: A Comparative Study of Similar Enzymes with Diverse Substrate Spectra. *PLOS ONE*, *8*(6), e65633. https://doi.org/10.1371/journal.pone.0065633

Romaní, A. M., Fund, K., Artigas, J., Schwartz, T., Sabater, S., & Obst, U. (2008). Relevance of Polymeric Matrix Enzymes During Biofilm Formation. *Microbial Ecology*, *56*(3), 427–436. https://doi.org/10.1007/s00248-007-9361-8

Ruggaber Timothy, P., & Talley Jeffrey, W. (2006). Enhancing Bioremediation with Enzymatic Processes: A Review. *Practice Periodical of Hazardous, Toxic, and Radioactive Waste Management*, *10*(2), 73–85. https://doi.org/10.1061/(ASCE)1090-025X(2006)10:2(73)

Saba, N., Jawaid, M., Alothman, O. Y., Paridah, M., & Hassan, A. (2016). Recent advances in epoxy resin, natural fiber-reinforced epoxy composites and their applications. *Journal of Reinforced Plastics and Composites*, *35*(6), 447–470. https://doi.org/10.1177/0731684415618459

Sabellico, G., Baggetta, A., Sandrucci, E., Zanellato, G., Martinelli, A., Montanari, A., & Bianchi, M. M. (2025). Oxidative deterioration of polypropylene by redox mediators and yeast expressing a fungal recombinant laccase. *International Biodeterioration & Biodegradation*, *196*, 105947. https://doi.org/https://doi.org/10.1016/j.ibiod.2024.105947

Sakurai, T., & Kataoka, K. (2007). Basic and applied features of multicopper oxidases, CueO, bilirubin oxidase, and laccase. *The Chemical Record*, *7*(4), 220–229. https://doi.org/https://doi.org/10.1002/tcr.20125

Samel, U.-R., Kohler, W., Gamer, A. O., Keuser, U., Yang, S.-T., Jin, Y., Lin, M., Wang, Z., & Teles, J. H. (2018). Propionic Acid and Derivatives. In *Ullmann's Encyclopedia of Industrial Chemistry* (pp. 1–20). https://doi.org/https://doi.org/10.1002/14356007.a22_223.pub4

Samygina, V. R., Sokolov, A. V., Bourenkov, G., Schneider, T. R., Anashkin, V. A., Kozlov, S. O., Kolmakov, N. N., & Vasilyev, V. B. (2017). Rat ceruloplasmin: a new labile copper binding site and zinc/copper mosaic†. *Metallomics*, *9*(12), 1828–1838. https://doi.org/10.1039/c7mt00157f

Sanluis-Verdes, A., Colomer-Vidal, P., Rodriguez-Ventura, F., Bello-Villarino, M., Spinola-Amilibia, M., Ruiz-Lopez, E., Illanes-Vicioso, R., Castroviejo, P., Aiese Cigliano, R., Montoya, M., Falabella, P., Pesquera, C., Gonzalez-Legarreta, L., Arias-Palomo, E., Solà, M., Torroba, T., Arias, C. F., & Bertocchini, F. (2022). Wax worm saliva and the enzymes therein are the key to polyethylene degradation by Galleria mellonella. *Nature Communications*, *13*(1), 5568. https://doi.org/10.1038/s41467-022-33127-w

Sasal, F. N., Dogangun Akın, A., Kılıc, A., Erteği, G., Duygu, C., İşler, E., Newman, B., Koimtzoglou, C., Maroulas, P., & Bara, P. (2015). Manufacturing of Nano-treated Lower Panel Demonstrators for Aircraft Fuselage. Smart Intelligent Aircraft Structures (SARISTU) Proceedings of the Final Project Conference,

Scheelhaase, J., Müller, L., Ennen, D., & Grimme, W. (2022). Economic and Environmental Aspects of Aircraft Recycling. *Transportation Research Procedia*, *65*, 3–12. https://doi.org/10.1016/j.trpro.2022.11.002

Schorn, A. (2020). *How to bark up the right tree–Novel metagenomic laccase-like multicopper oxidases from the European spruce bark beetle Ips typographus* Staats-und Universitätsbibliothek Hamburg Carl von Ossietzky].

Schüppel, M. S. a. D. (2023). *Composites market report 2022-The global market for carbon fibers and carbon composites*.

Scully, E. D., Geib, S. M., Hoover, K., Tien, M., Tringe, S. G., Barry, K. W., Glavina del Rio, T., Chovatia, M., Herr, J. R., & Carlson, J. E. (2013). Metagenomic Profiling Reveals Lignocellulose Degrading System in a Microbial Community Associated with a Wood-Feeding Beetle. *PLOS ONE*, *8*(9), e73827. https://doi.org/10.1371/journal.pone.0073827

Shaffer, C. L., Morton, M. D., & Hanzlik, R. P. (2001). N-Dealkylation of an N-Cyclopropylamine by Horseradish Peroxidase. Fate of the Cyclopropyl Group. *Journal of the American Chemical Society*, *123*(35), 8502–8508. https://doi.org/10.1021/ja0111479

Sharma, P., Goel, R., & Capalash, N. (2007). Bacterial laccases. *World Journal of Microbiology and Biotechnology*, *23*(6), 823–832. https://doi.org/10.1007/s11274-006-9305-3

Shetty, K., Bojja, R., & Srihari, S. (2020). Effect of hygrothermal aging on the mechanical properties of IMA/M21E aircraft-grade CFRP composite. *Advanced Composites Letters*, *29*, 2633366X20926520. https://doi.org/10.1177/2633366x20926520

Shundo, A., Yamamoto, S., & Tanaka, K. (2022). Network Formation and Physical Properties of Epoxy Resins for Future Practical Applications. *JACS Au*, *2*(7), 1522–1542. https://doi.org/10.1021/jacsau.2c00120

Singh, S., Gosu, V., Upadhyaya, S., & Kumar, U. K. A. (2021). Process Intensification of Propionic Acid Separation – Effect of Channel Geometry on Microchannel Distillation. *Chemical Engineering and Processing - Process Intensification*, *169*, 108599. https://doi.org/https://doi.org/10.1016/j.cep.2021.108599

Six, D. L. (2013). The Bark Beetle Holobiont: Why Microbes Matter. *Journal of Chemical Ecology*, *39*(7), 989–1002. https://doi.org/10.1007/s10886-013-0318-8

Skálová, T., Dohnálek, J., Østergaard, L. H., Østergaard, P. R., Kolenko, P., Dušková, J., Štěpánková, A., & Hašek, J. (2009). The Structure of the Small Laccase from Streptomyces coelicolor Reveals a Link between Laccases and Nitrite Reductases. *Journal of Molecular Biology*, *385*(4), 1165–1178. https://doi.org/https://doi.org/10.1016/j.jmb.2008.11.024

Skelton, J., Jusino, M. A., Carlson, P. S., Smith, K., Banik, M. T., Lindner, D. L., Palmer, J. M., & Hulcr, J. (2019). Relationships among wood-boring beetles, fungi, and the decomposition of forest biomass. *Molecular Ecology*, *28*(22), 4971–4986. https://doi.org/https://doi.org/10.1111/mec.15263

Sochorova, L., Torokova, L., Baron, M., & Sochor, J. (2018). Electrochemical and others techniques for the determination of malic acid and tartaric acid in must and wine. *International Journal of Electrochemical Science*, *13*(9), 9145–9165. https://doi.org/https://doi.org/10.20964/2018.09.20

Somarathna, Y., Herath, M., Epaarachchi, J., & Islam, M. M. (2024). Formulation of Epoxy Prepregs, Synthesization Parameters, and Resin Impregnation Approaches—A Comprehensive Review. *Polymers*, *16*(23), 3326.

Sondhi, S., Sharma, P., George, N., Chauhan, P. S., Puri, N., & Gupta, N. (2015). An extracellular thermo-alkali-stable laccase from Bacillus tequilensis SN4, with a potential to biobleach softwood pulp. *3 Biotech*, *5*(2), 175–185. https://doi.org/10.1007/s13205-014-0207-z

Song, D., & Gupta, R. K. (2012). 6 - The use of thermosets in the building and construction industry. In Q. Guo (Ed.), *Thermosets* (pp. 165–188). Woodhead Publishing. https://doi.org/https://doi.org/10.1533/9780857097637.2.165

Soni, V. K., Singh, G., Vijayan, B. K., Chopra, A., Kapur, G. S., & Ramakumar, S. S. V. (2021). Thermochemical Recycling of Waste Plastics by Pyrolysis: A Review. *Energy & Fuels*, *35*(16), 12763–12808. https://doi.org/10.1021/acs.energyfuels.1c01292

Sozer, E. M., Simacek, P., & Advani, S. G. (2012). 9 - Resin transfer molding (RTM) in polymer matrix composites. In S. G. Advani & K.-T. Hsiao (Eds.), *Manufacturing Techniques for Polymer Matrix Composites (PMCs)* (pp. 245–309). Woodhead Publishing. https://doi.org/https://doi.org/10.1533/9780857096258.3.243

Ström, L., Owen, A. G., Godbold, D. L., & Jones, D. L. (2001). Organic acid behaviour in a calcareous soil: sorption reactions and biodegradation rates. *Soil Biology and Biochemistry*, *33*(15), 2125–2133. https://doi.org/https://doi.org/10.1016/S0038-0717(01)00146-8

Strong, P. J., & and Claus, H. (2011). Laccase: A Review of Its Past and Its Future in Bioremediation. *Critical Reviews in Environmental Science and Technology*, *41*(4), 373–434. https://doi.org/10.1080/10643380902945706

Studier, F. W. (2005). Protein production by auto-induction in high-density shaking cultures. *Protein Expression and Purification*, *41*(1), 207–234. https://doi.org/https://doi.org/10.1016/j.pep.2005.01.016

Subadra, S. P., & Griskevicius, P. (2021). Sustainability of polymer composites and its critical role in revolutionising wind power for green future. *Sustainable technologies for green economy.*, *1*(1), 1–7.

Sukanto, H., Raharjo, W. W., Ariawan, D., Triyono, J., & Kaavesina, M. (2021). Epoxy resins thermosetting for mechanical engineering. *Open Engineering*, *11*(1), 797–814. https://doi.org/doi:10.1515/eng-2021-0078

Sumathi, T., Viswanath, B., Sri Lakshmi, A., & SaiGopal, D. V. R. (2016). Production of Laccase by Cochliobolus sp. Isolated from Plastic Dumped Soils and Their Ability to Degrade Low Molecular Weight PVC. *Biochemistry Research International*, *2016*(1), 9519527. https://doi.org/https://doi.org/10.1155/2016/9519527

Swern, D. (1949). Organic Peracids. *Chemical Reviews*, *45*(1), 1–68.

Tambe, S. P., Jagtap, S. D., Chaurasiya, A. K., & Joshi, K. K. (2016). Evaluation of microbial corrosion of epoxy coating by using sulphate reducing bacteria. *Progress in Organic Coatings*, *94*, 49–55. https://doi.org/https://doi.org/10.1016/j.porgcoat.2016.01.009

Tamura, K., Stecher, G., & Kumar, S. (2021). MEGA11: Molecular Evolutionary Genetics Analysis Version 11. *Molecular Biology and Evolution*, *38*(7), 3022–3027. https://doi.org/10.1093/molbev/msab120

Taniguchi-Takizawa, T., Shimizu, M., Kume, T., & Yamazaki, H. (2015). Benzydamine N-oxygenation as an index for flavin-containing monooxygenase activity and benzydamine N-demethylation by cytochrome P450 enzymes in liver microsomes from rats, dogs, monkeys, and humans. *Drug Metabolism and Pharmacokinetics*, *30*(1), 64–69. https://doi.org/https://doi.org/10.1016/j.dmpk.2014.09.006

Tator, K. B. (2015). Epoxy Resins and Curatives. In K. B. Tator (Ed.), *Protective Organic Coatings* (Vol. 5B, pp. 0). ASM International. https://doi.org/10.31399/asm.hb.v05b.a0006077

Teh, K. H., Flint, S., Palmer, J., Andrewes, P., Bremer, P., & Lindsay, D. (2014). Biofilm − An unrecognised source of spoilage enzymes in dairy products? *International Dairy Journal*, *34*(1), 32–40. https://doi.org/https://doi.org/10.1016/j.idairyj.2013.07.002

Teles, J. H. (2024). Sustainable Production of Propionic acid and Derivatives on Industrial Scale. *ChemSusChem*, *17*(9), e202301666. https://doi.org/https://doi.org/10.1002/cssc.202301666

Temporiti, M. E. E., Nicola, L., Nielsen, E., & Tosi, S. (2022). Fungal Enzymes Involved in Plastics Biodegradation. *Microorganisms*, *10*(6), 1180.

Thamizh Selvan, R., Vishakh Raja, P., Mangal, P., Mohan, N., & Bhowmik, S. (2021). Recycling technology of epoxy glass fiber and epoxy carbon fiber composites used in aerospace vehicles. *Journal of Composite Materials*, *55*(23), 3281–3292. https://doi.org/10.1177/00219983211011532

Thomas, S., Sinturel, C., & Thomas, R. (2014). *Micro and nanostructured epoxy/rubber blends*. John Wiley & Sons.

Trinick, M. J. (1980). Relationships Amongst the Fast-growing Rhizobia of Lablab purpureus, Leucaena leucocephala, Mimosa spp., Acacia farnesiana and Sesbania grandiflora and their Affinities with Other Rhizobial Groups. *Journal of Applied Bacteriology*, *49*(1), 39–53. https://doi.org/https://doi.org/10.1111/j.1365-2672.1980.tb01042.x

Tsizin, S., Bokka, R., Keshet, U., Alon, T., Fialkov, A., Tal, N., & Amirav, A. (2017). Comparison of electrospray LC–MS, LC–MS with Cold EI and GC–MS with Cold EI for sample identification. *International Journal of Mass Spectrometry*, *422*. https://doi.org/10.1016/j.ijms.2017.09.006

Vázquez-Loureiro, P., Lestido-Cardama, A., Sendón, R., López-Hernández, J., Paseiro-Losada, P., & Rodríguez-Bernaldo de Quirós, A. (2021). Identification of Volatile and Semi-Volatile Compounds in Polymeric Coatings Used in Metal Cans by GC-MS and SPME. *Materials*, *14*(13), 3704.

Veitch, N. C. (2004). Horseradish peroxidase: a modern view of a classic enzyme. *Phytochemistry*, *65*(3), 249–259. https://doi.org/https://doi.org/10.1016/j.phytochem.2003.10.022

Vlasits, J., Jakopitsch, C., Bernroitner, M., Zamocky, M., Furtmüller, P. G., & Obinger, C. (2010). Mechanisms of catalase activity of heme peroxidases. *Archives of Biochemistry and Biophysics*, *500*(1), 74–81. https://doi.org/https://doi.org/10.1016/j.abb.2010.04.018

Voisin, T., Erriguible, A., Ballenghien, D., Mateos, D., Kunegel, A., Cansell, F., & Aymonier, C. (2017). Solubility of inorganic salts in sub- and supercritical hydrothermal environment: Application to SCWO processes. *The Journal of Supercritical Fluids*, *120*, 18–31. https://doi.org/https://doi.org/10.1016/j.supflu.2016.09.020

Walter, H., Hölck, O., Dobrinski, H., Stuermann, J., Braun, T., Bauer, J., Wittler, O., & Lang, K. D. (2013, 28–31 May 2013). Moisture induced swelling in epoxy moulding compounds. 2013 IEEE 63rd Electronic Components and Technology Conference,

Wang, G., Chai, K., Wu, J., & Liu, F. (2016). Effect of Pseudomonas putida on the degradation of epoxy resin varnish coating in seawater. *International Biodeterioration & Biodegradation*, *115*, 156–163. https://doi.org/https://doi.org/10.1016/j.ibiod.2016.08.017

Wang, Y., Cui, X., Ge, H., Yang, Y., Wang, Y., Zhang, C., Li, J., Deng, T., Qin, Z., & Hou, X. (2015). Chemical Recycling of Carbon Fiber Reinforced Epoxy Resin Composites via Selective Cleavage of the Carbon–Nitrogen Bond. *ACS Sustainable Chemistry & Engineering*, *3*(12), 3332–3337. https://doi.org/10.1021/acssuschemeng.5b00949

Waterhouse, A., Bertoni, M., Bienert, S., Studer, G., Tauriello, G., Gumienny, R., Heer, F. T., de Beer, T. A. P., Rempfer, C., Bordoli, L., Lepore, R., & Schwede, T. (2018). SWISS-MODEL: homology modelling of protein structures and complexes. *Nucleic Acids Res*, *46*(W1), W296–w303. https://doi.org/10.1093/nar/gky427

Wong, K.-S., Cheung, M.-K., Au, C.-H., & Kwan, H.-S. (2013). A Novel Lentinula edodes Laccase and Its Comparative Enzymology Suggest Guaiacol-Based Laccase Engineering for Bioremediation. *PLOS ONE*, *8*(6), e66426. https://doi.org/10.1371/journal.pone.0066426

Wu, Z., Liu, C., Zhang, Z., Zheng, R., & Zheng, Y. (2020). Amidase as a versatile tool in amide-bond cleavage: From molecular features to biotechnological applications. *Biotechnol Adv*, *43*, 107574. https://doi.org/10.1016/j.biotechadv.2020.107574

Xiong, J., An, T., Li, G., & Peng, P. a. (2017). Accelerated biodegradation of BPA in water-sediment microcosms with Bacillus sp. GZB and the associated bacterial community structure. *Chemosphere*, *184*, 120–126. https://doi.org/https://doi.org/10.1016/j.chemosphere.2017.05.163

Xu, F. (1997). Effects of redox potential and hydroxide inhibition on the pH activity profile of fungal laccases. *Journal of Biological Chemistry*, *272*(2), 924–928.

Xu, F., Kulys, J. J., Duke, K., Li, K., Krikstopaitis, K., Deussen, H. J., Abbate, E., Galinyte, V., & Schneider, P. (2000). Redox chemistry in laccase-catalyzed oxidation of N-hydroxy compounds. *Appl Environ Microbiol*, *66*(5), 2052–2056. https://doi.org/10.1128/aem.66.5.2052-2056.2000

Xu, Q., Liu, R., & Ramakrishna, S. (2021). Comparative experimental study on the effects of organic and inorganic acids on coal dissolution. *Journal of Molecular Liquids*, *339*, 116730. https://doi.org/https://doi.org/10.1016/j.molliq.2021.116730

Yadav, D., & Kudanga, T. (2023). *Bacterial Laccases: Engineering, Immobilization, Heterologous Production, and Industrial Applications*. Academic Press.

Yan, H., Lu, C., Jing, D., & Hou, X. (2013). Chemical degradation of TGDDM/DDS epoxy resin in supercritical 1-propanol: Promotion effect of hydrogenation on thermolysis. *Polymer Degradation and Stability*, *98*(12), 2571–2582. https://doi.org/https://doi.org/10.1016/j.polymdegradstab.2013.09.026

Yang, Y., Boom, R., Irion, B., van Heerden, D.-J., Kuiper, P., & de Wit, H. (2012). Recycling of composite materials. *Chemical Engineering and Processing: Process Intensification*, *51*, 53–68. https://doi.org/https://doi.org/10.1016/j.cep.2011.09.007

Yang, Y., Wang, Z., & Xie, S. (2014). Aerobic biodegradation of bisphenol A in river sediment and associated bacterial community change. *Science of The Total Environment*, *470-471*, 1184–1188. https://doi.org/https://doi.org/10.1016/j.scitotenv.2013.10.102

Yariv, B., Yariv, E., Kessel, A., Masrati, G., Chorin, A. B., Martz, E., Mayrose, I., Pupko, T., & Ben-Tal, N. (2023). Using evolutionary data to make sense of macromolecules with a "face-lifted" ConSurf. *Protein Sci*, *32*(3), e4582. https://doi.org/10.1002/pro.4582

Yoshida, S., Hiraga, K., Takehana, T., Taniguchi, I., Yamaji, H., Maeda, Y., Toyohara, K., Miyamoto, K., Kimura, Y., & Oda, K. (2016). A bacterium that degrades and assimilates poly(ethylene terephthalate). *Science*, *351*(6278), 1196–1199. https://doi.org/doi:10.1126/science.aad6359

Zámocký, M., Gasselhuber, B., Furtmüller, P. G., & Obinger, C. (2014). Turning points in the evolution of peroxidase–catalase superfamily: molecular phylogeny of hybrid heme peroxidases. *Cellular and Molecular Life Sciences*, *71*(23), 4681–4696. https://doi.org/10.1007/s00018-014-1643-y

Zampolli, J., Collina, E., Lasagni, M., & Di Gennaro, P. (2024). Insights into polyethylene biodegradative fingerprint of Pseudomonas citronellolis E5 and Rhodococcus erythropolis D4 by phenotypic and genome-based comparative analyses [Original Research]. *Frontiers in Bioengineering and Biotechnology*, *12*. https://doi.org/10.3389/fbioe.2024.1472309

Zampolli, J., Mangiagalli, M., Vezzini, D., Lasagni, M., Ami, D., Natalello, A., Arrigoni, F., Bertini, L., Lotti, M., & Di Gennaro, P. (2023). Oxidative degradation of polyethylene by two novel laccase-like multicopper oxidases from Rhodococcus opacus R7. *Environmental Technology & Innovation*, *32*, 103273. https://doi.org/https://doi.org/10.1016/j.eti.2023.103273

Zhang, A., Hou, Y., Wang, Q., & Wang, Y. (2022). Characteristics and polyethylene biodegradation function of a novel cold-adapted bacterial laccase from Antarctic sea ice psychrophile Psychrobacter sp. NJ228. *Journal of Hazardous Materials*, *439*, 129656. https://doi.org/https://doi.org/10.1016/j.jhazmat.2022.129656

Zhang, J., Abidin, M. Z., Saravanan, T., & Poelarends, G. J. (2020). Recent Applications of Carbon-Nitrogen Lyases in Asymmetric Synthesis of Noncanonical Amino Acids and Heterocyclic Compounds. *ChemBioChem*, *21*(19), 2733–2742. https://doi.org/10.1002/cbic.202000214

Zhang, J., Chevali, V. S., Wang, H., & Wang, C.-H. (2020). Current status of carbon fibre and carbon fibre composites recycling. *Composites Part B: Engineering*, *193*, 108053. https://doi.org/https://doi.org/10.1016/j.compositesb.2020.108053

Zhang, J., Lin, G., Vaidya, U., & Wang, H. (2023). Past, present and future prospective of global carbon fibre composite developments and applications. *Composites Part B: Engineering*, *250*, 110463. https://doi.org/https://doi.org/10.1016/j.compositesb.2022.110463

Zhang, S., Dong, Z., Shi, J., Yang, C., Fang, Y., Chen, G., Chen, H., & Tian, C. (2022). Enzymatic hydrolysis of corn stover lignin by laccase, lignin peroxidase, and manganese peroxidase. *Bioresource Technology*, *361*, 127699. https://doi.org/https://doi.org/10.1016/j.biortech.2022.127699

Zhang, S., Yang, A., He, P., Wang, Y., Liu, Y., Li, G., Ren, J., & Han, R. (2024). How does prepolymerization affect the curing and properties of the thermosetting resins–benzoxazine resin as an example. *Progress in Organic Coatings*, *189*, 108291. https://doi.org/https://doi.org/10.1016/j.porgcoat.2024.108291

Zhang, S., Zheng, H., Chang, W., Lou, Y., & Qian, H. (2023). Microbiological Deterioration of Epoxy Coating on Carbon Steel by Pseudomonas aeruginosa. *Coatings*, *13*(3).

Zhang, W., Wang, W., Wang, J., Shen, G., Yuan, Y., Yan, L., Tang, H., & Wang, W. (2021). Isolation and Characterization of a Novel Laccase for Lignin Degradation, LacZ1. *Applied and Environmental Microbiology*, *87*(23), e01355–01321. https://doi.org/10.1128/AEM.01355-21

Zhang, Y., Plesner, T. J., Ouyang, Y., Zheng, Y.-C., Bouhier, E., Berentzen, E. I., Zhang, M., Zhou, P., Zimmermann, W., Andersen, G. R., Eser, B. E., & Guo, Z. (2023). Computer-aided discovery of a novel thermophilic laccase for low-density polyethylene degradation. *Journal of Hazardous Materials*, *458*, 131986. https://doi.org/https://doi.org/10.1016/j.jhazmat.2023.131986

Zheng, F., An, Q., Meng, G., Wu, X.-J., Dai, Y.-C., Si, J., & Cui, B.-K. (2017). A novel laccase from white rot fungus Trametes orientalis: Purification, characterization, and application. *International Journal of Biological Macromolecules*, *102*, 758–770. https://doi.org/https://doi.org/10.1016/j.ijbiomac.2017.04.089

Zhu, B., Wang, D., & Wei, N. (2022). Enzyme discovery and engineering for sustainable plastic recycling. *Trends in Biotechnology*, *40*(1), 22–37. https://doi.org/10.1016/j.tibtech.2021.02.008

Zhu, Y., Ksibe, A. Z., Schäfer, H., Blindauer, C. A., Bugg, T. D. H., & Chen, Y. (2016). O2-independent demethylation of trimethylamine N-oxide by Tdm of Methylocella silvestris. *The FEBS Journal*, *283*(21), 3979–3993. https://doi.org/https://doi.org/10.1111/febs.13902

Zima, A. M., Lyakin, O. Y., Bryliakova, A. A., Babushkin, D. E., Bryliakov, K. P., & Talsi, E. P. (2022). Effect of Brønsted Acid on the Reactivity and Selectivity of the Oxoiron(V) Intermediates in C-H and C=C Oxidation Reactions. *Catalysts*, *12*(9), 949.

Zotti, A., Elmahdy, A., Zuppolini, S., Borriello, A., Verleysen, P., & Zarrelli, M. (2020). Aromatic Hyperbranched Polyester/RTM6 Epoxy Resin for EXTREME Dynamic Loading Aeronautical Applications. *Nanomaterials*, *10*(2).

7 ACKNOWLEDGEMENTS

This mission was very challenging, but it was made possible thanks to the invaluable support of many individuals behind this study.

My deepest gratitude goes to Prof. Dr. Wolfgang R. Streit for providing me with the opportunity to begin my PhD journey in his research group, for always welcoming discussions and ideas, and for encouraging me when things did not go as planned. I also would like to thank Prof. Dr. Andrea Liese and the other members of the examination committee for taking the time to evaluate my work.

Very special thanks to Dr. Pablo Pérez-García, who has mentored me since my Master's thesis. Muchas gracias! I truly appreciate his endless support from day one and his well-rounded expertise in scientific matters, which has greatly contributed to bringing this research to completion. This also goes to all my colleagues and friends in the Microbiology and Biotechnology Department, who created a very positive atmosphere in the lab and helped me avoid mental breakdowns from time to time. I would also like to sincerely thank Inka, Petra, and Angela for their assistance with German bureaucratic processes and lab-related matters. Vielen Dank für ihre Unterstützung und Geduld mit meinem Deutsch!

My work would not have been possible without the support and expertise of these individuals. I especially thank my project partners, Dr. Ana Malvis Romero and Leon Klose, for their valuable input and collaboration. Additionally, I thank Phillip Schlottau for laser cutting on epoxy, Elke Wölken for SEM analysis, Gaby Graack and Erik Mordhorst for mass spectrometry, and Siraphat Weerathaworn for FTIR measurements.

Finally, I am deeply grateful to my friends from all over the world who endured with me through the highs and lows of this journey. To the most important people in my life—my parents and Tida—who always provide endless support and love:

"ขอบคุณแม่กับป๊าสำหรับความรักความทุ่มเททั้งชีวิตเพื่อให้ลูกคนนี้ได้มีชีวิตที่ดี วันนี้นุ้ยเรียนจบป. เอกแล้วนะ". Thanks also to the Feuerriegel family and Golo for always listening to my research struggles, cheering me on throughout this PhD journey, encouraging me to speak German, and making Germany feel like home. Without these incredible people, I would not be where I am today.

8 APPENDIX

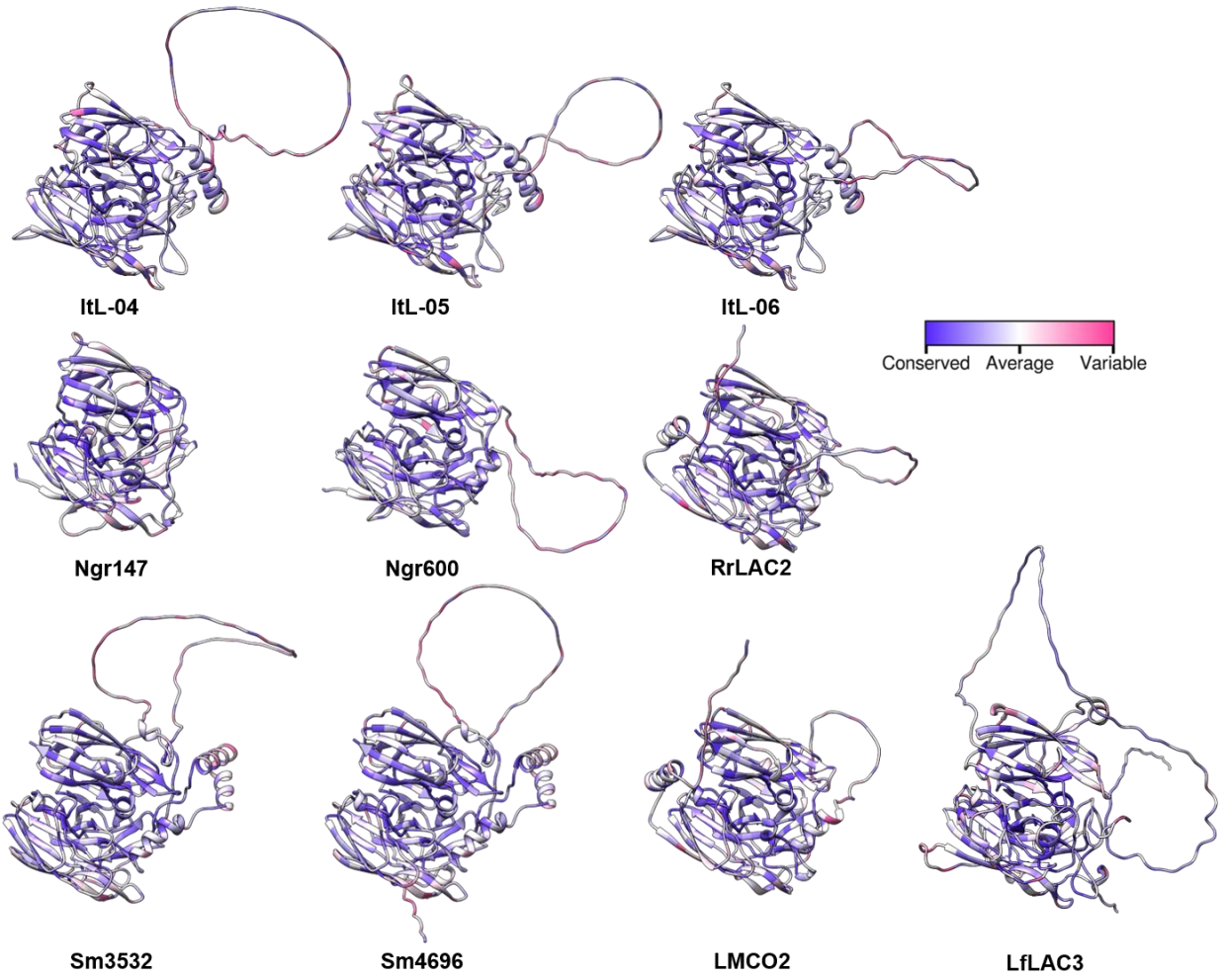

Figure S1. Evolutionary conservation profile of putative and characterized laccases. The conservation of amino acid positions is depicted, with B-factors predicted by Consurf (Yariv et al., 2023) indicating variable and conserved regions, as illustrated by the colour scheme in the legend. Most regions are highly conserved, whereas the loops, believed to be methionine-rich regions and not well modelled, exhibit high variability.

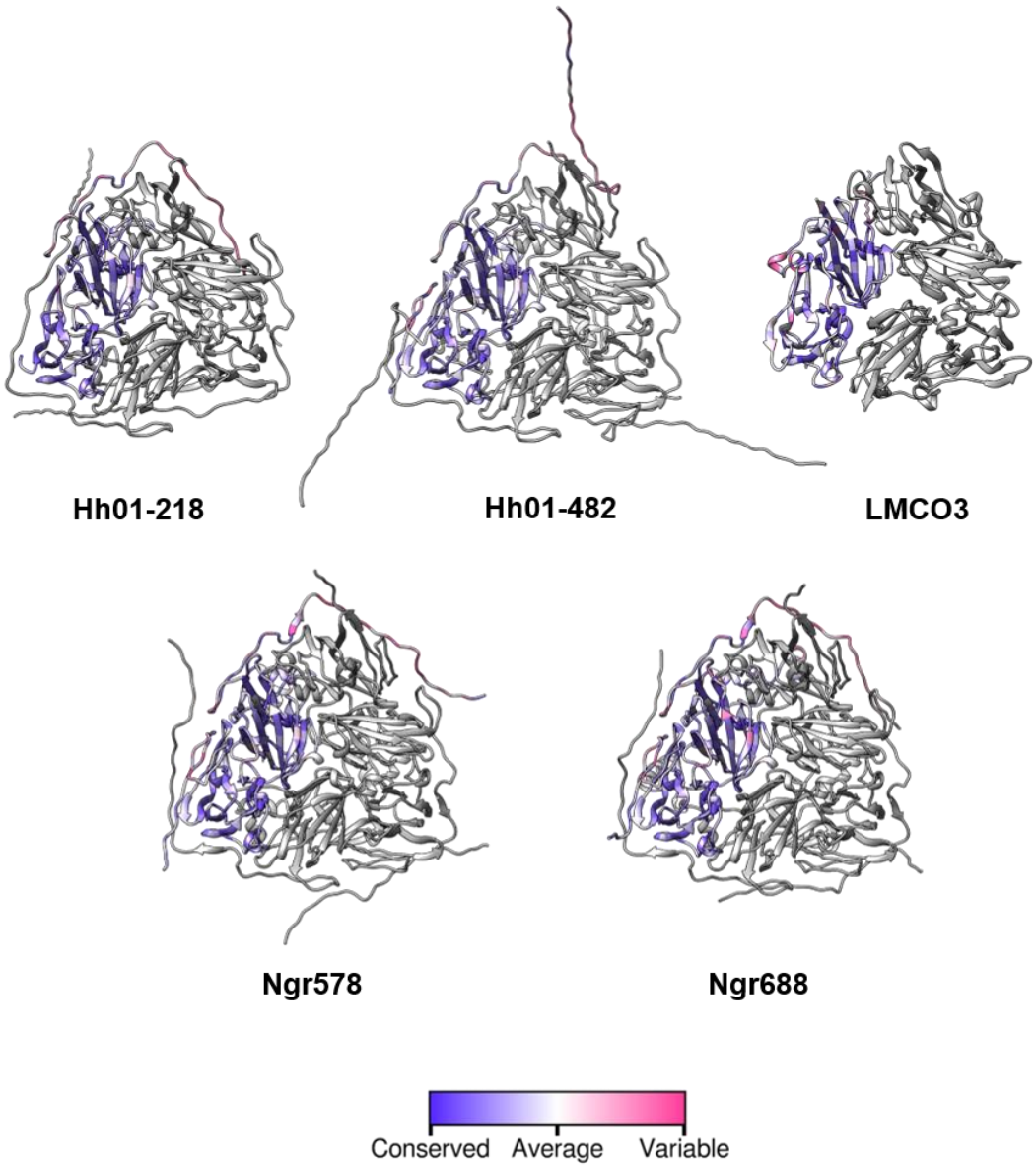

Figure S2. Evolutionary conservation profile of potential two-domain multicopper oxidases (2dMCOs). The models comprise three distinct domains that form a homotrimeric quaternary protein structure; however, the evolutionary conservation was calculated based solely on a single chain. The conservation of amino acid positions is illustrated, with B-factors predicted by Consurf (Yariv et al., 2023) indicating variable and conserved regions, as depicted by the colour scheme in the legend. Most regions are highly conserved, particularly the inner regions where the copper binding sites (CBS) are situated.

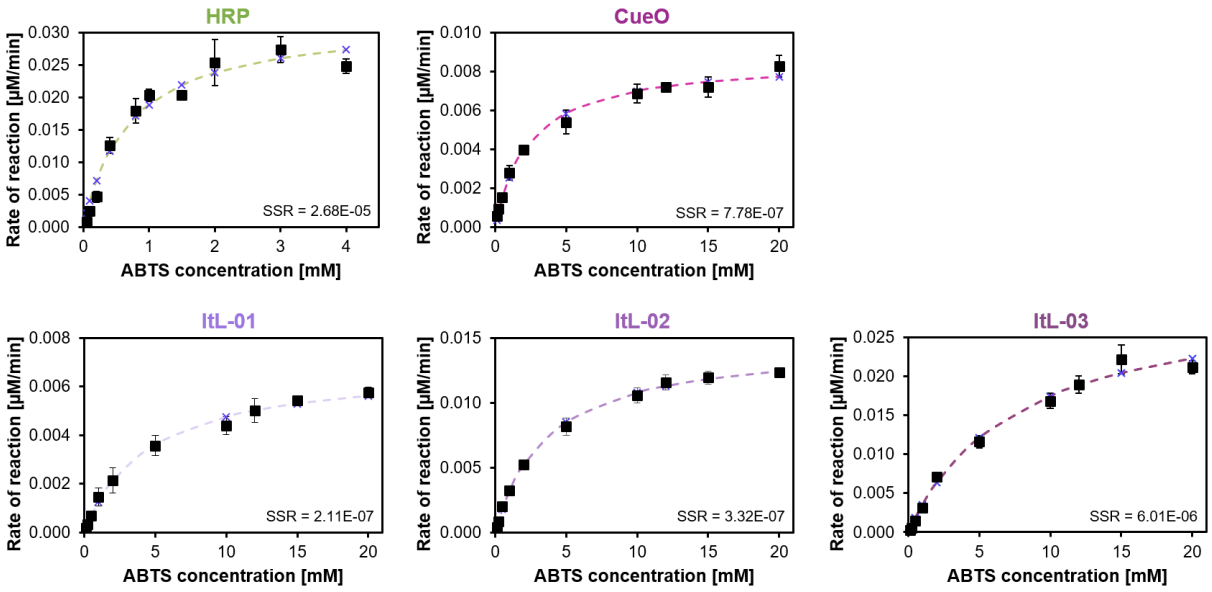

Figure S3. Kinetic constants of oxidoreductases for ABTS oxidation. Kinetic parameters were estimated by fitting the initial rates to the Michaelis-Menten equation using Solver, with the corresponding sum of squared residuals (SSR). Error bars indicate the standard deviation (n = 3). The kinetic parameters obtained after fitting the data to the equation are presented in Table 19.

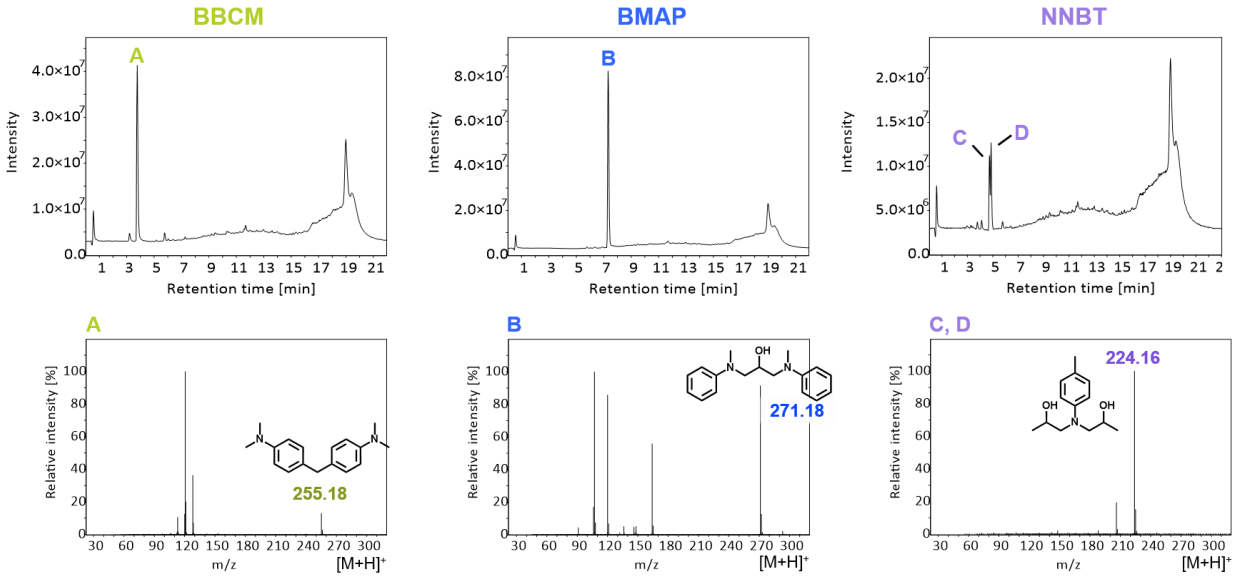

Figure S4. LC-MS analysis identifying epoxy model compounds in positive mode, based on their retention times, with specific signals (A-D) corresponding to their exact masses: BBCM (A): 3.8 min, *m/z* 254, BMAP (B): 7.3 min, *m/z* 270, NNBT (C, D): 4.7 and 4.8 min, *m/z* 223.

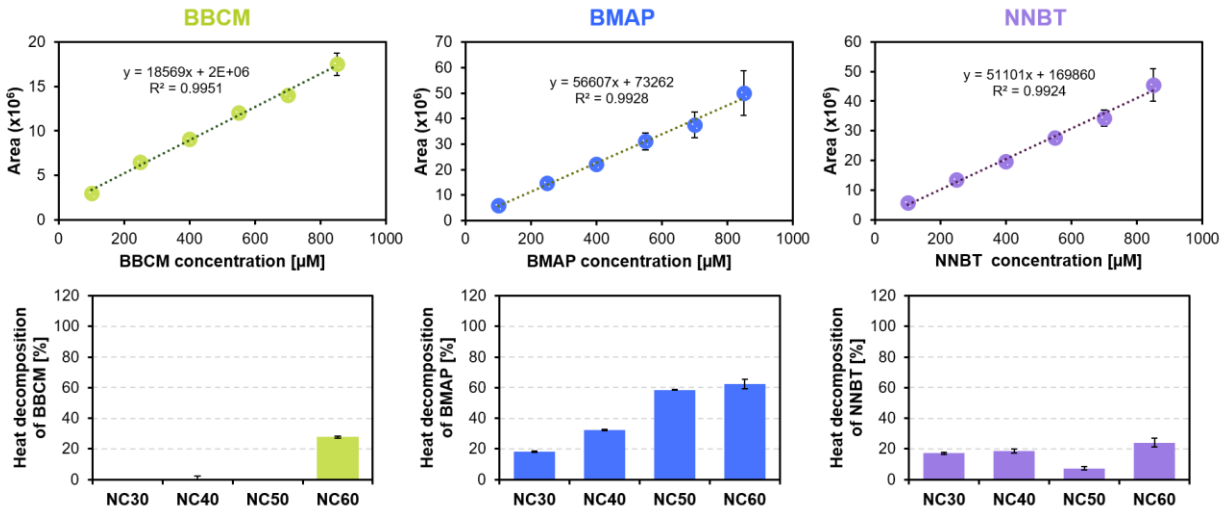

Figure S5. Standard calibration for concentration determination and temperature control. (top) Calibration curve for determining the concentrations of epoxy model substrates using LC-MS. (bottom) Evaluation of the effect of temperature (30-60 °C) on the decomposition of epoxy models after 2 hours, serving as a negative control in the absence of enzymes. Error bars indicate the standard deviation (n = 3).

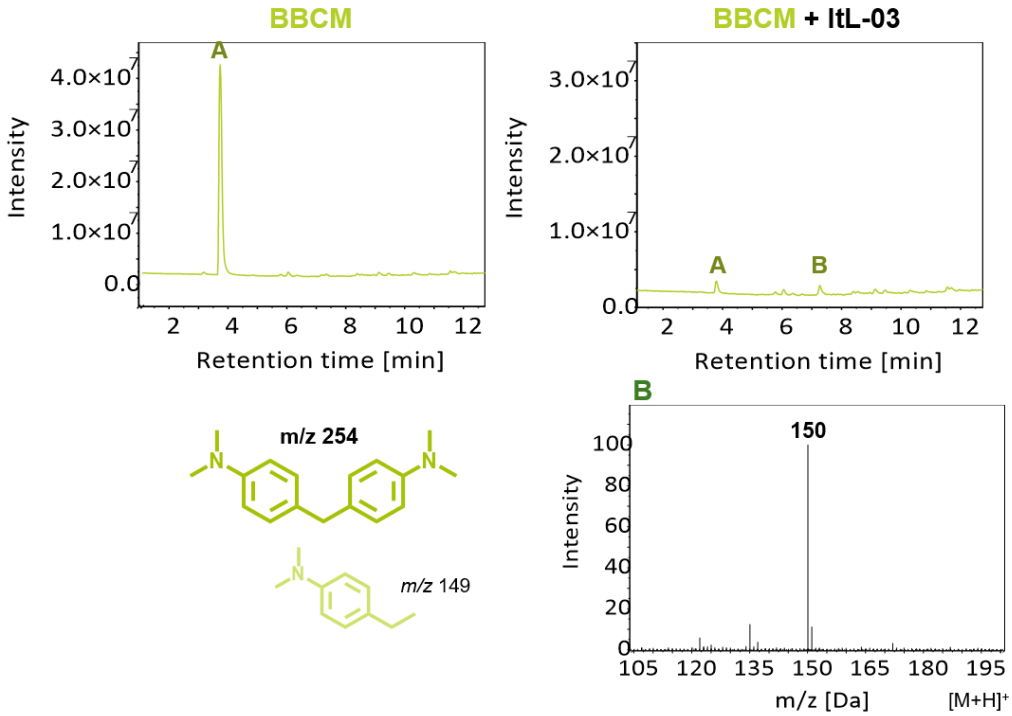

Figure S6. LC-MS chromatogram of the reaction involving laccase ItL-03 and BBCM. (A) The mass of BBCM is observed at 3.7 minutes. (B) The mass spectrum of the converted product reveals a peak that appears at 7.2 minutes.

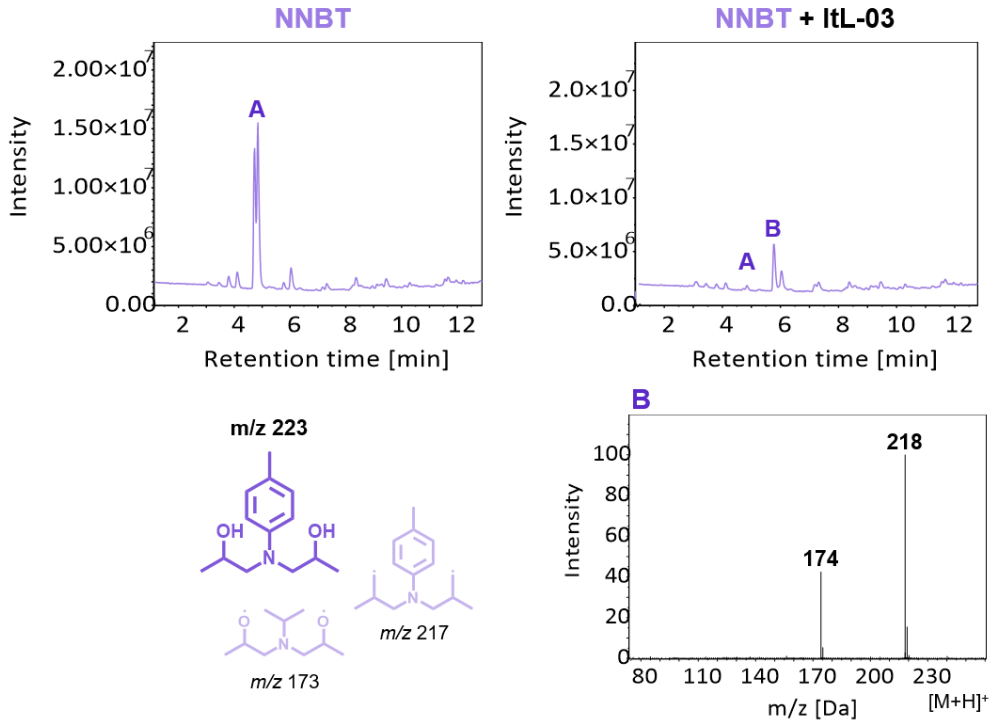

Figure S7. LC-MS chromatogram of the reaction involving laccase ItL-03 and NNBT. (A) The mass of NNBT is observed at 4.8 minutes. (B) The mass spectrum of the converted product reveals a peak that appears at 5.7 minutes.

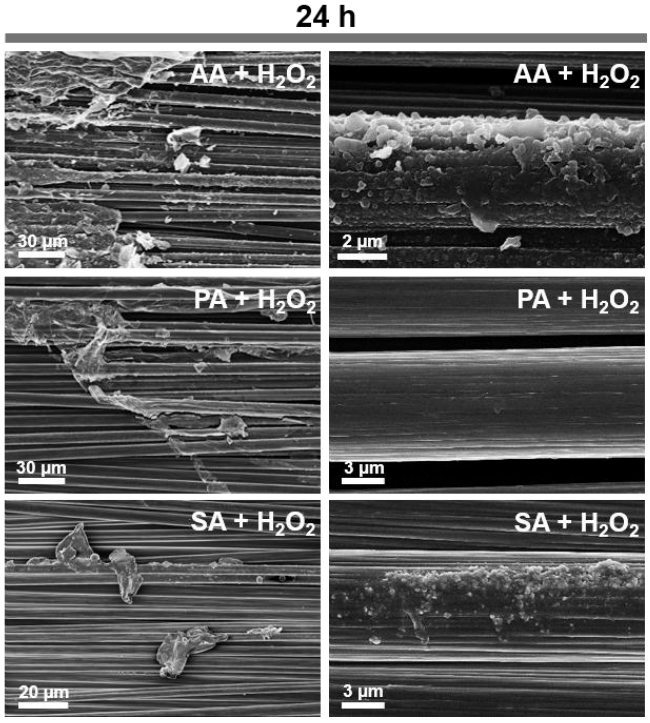

Figure S8. SEM images of eCFRPs after 24-hour treatment with 5 M acidic-peroxide solution (A-H_2O_2). The acids tested included acetic acid (AA), propionic acid (PA), and sulfuric acid (SA). Some areas of the composites still exhibited epoxy residues after a 24-hour treatment.

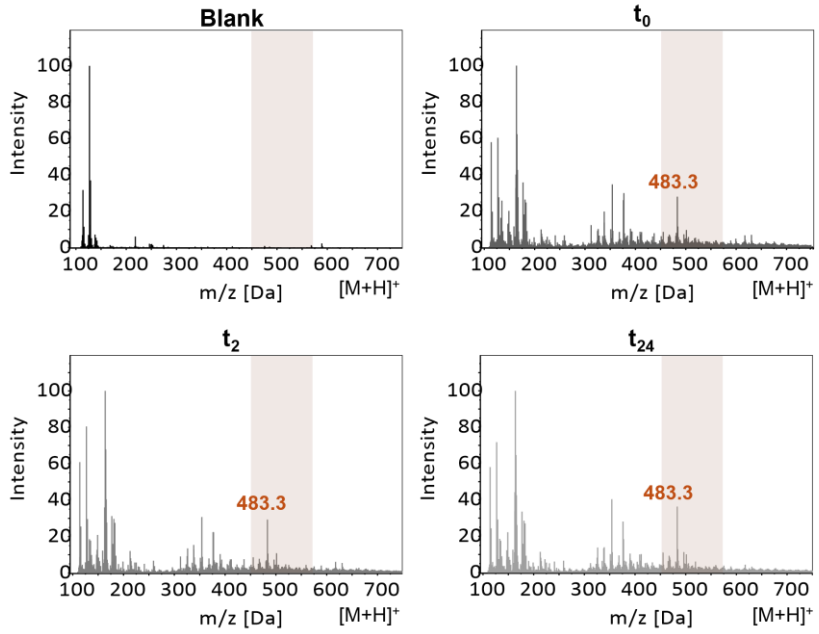

Figure S9. Blank sample compared to negative controls for ESI-MS analysis. The ESI-MS spectrum was obtained via direct injection in positive mode. The blank sample refers to a sample containing dichloromethane (DCM) used to assess the background signal. Samples t_0, t_2, and t_{24} representing controls without the enzyme at the beginning, between, and end of the incubation period, respectively. The ion at *m/z* 483.3 was absent in the blank sample, while present in the controls.

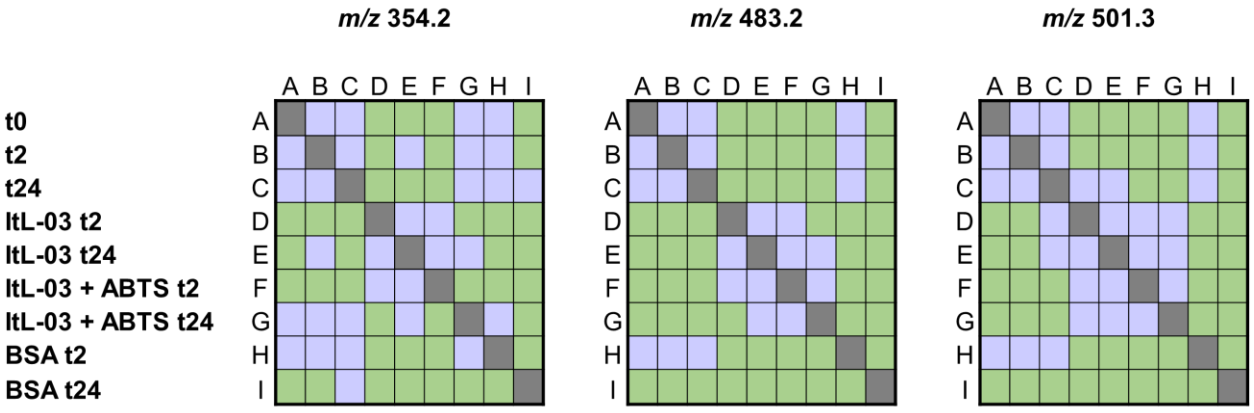

Figure S10. Significant differences between sample pairs for each *m/z* peak from Figure 26 were determined by one-way ANOVA followed by Tukey's HSD post-hoc test ($p < 0.05$). Green indicates statistically significant differences, and red indicates non-significant differences. No sample pairs were significant for peaks 113.94 and 126.96. Groups A–I correspond to the following samples: t0, t2, t24, ItL-03 t2, ItL-03 t24, ItL-03 + ABTS t2, ItL-03 + ABTS t24, BSA t2, and BSA t24, respectively.

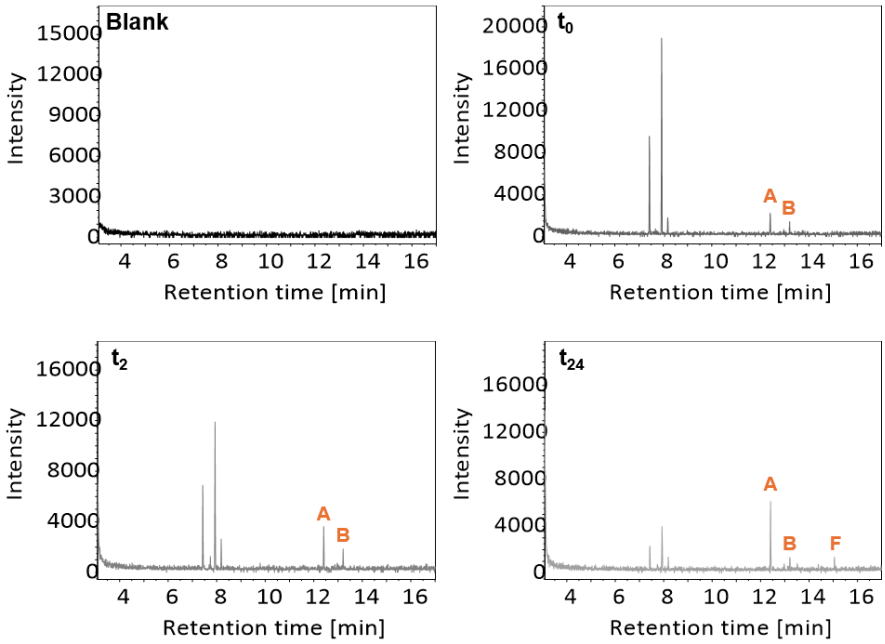

Figure S11. Blank sample compared to negative controls for GC-MS analysis. The blank sample refers to a sample containing dichloromethane (DCM) used to assess the background signal. Samples t_0, t_2, and t_{24} representing controls without the enzyme at the beginning, between, and end of the incubation period, respectively. The peaks of interest are labelled A, B, and F. These peaks were absent in the blank sample.

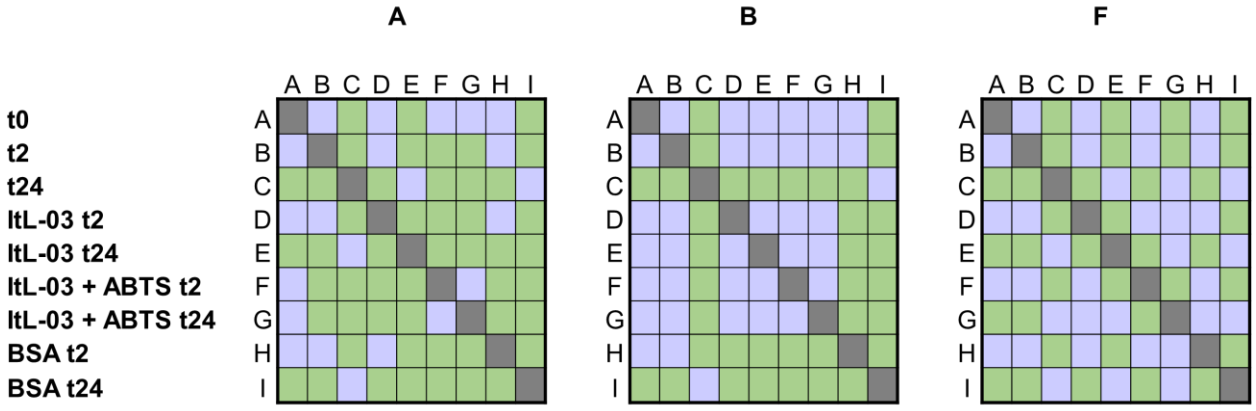

Figure S12. Significant differences between sample pairs for peaks A, B, and F from Figure 29 were determined by one-way ANOVA followed by Tukey's HSD post-hoc test ($p < 0.05$). Green indicates statistically significant differences, and red indicates non-significant differences. Groups A–I correspond to the following samples: t0, t2, t24, ItL-03 t2, ItL-03 t24, ItL-03 + ABTS t2, ItL-03 + ABTS t24, BSA t2, and BSA t24, respectively.

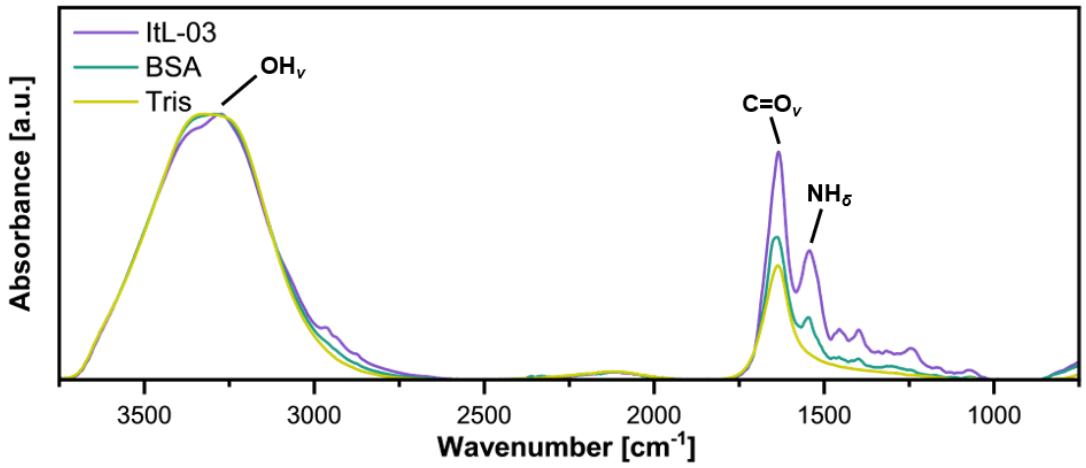

Figure S13. FTIR analysis of enzyme controls. Laccase ItL-03, BSA, and tris buffer that was used for the enzyme stock solution. The corresponding functional groups are indicated. ν — stretching; δ — deformation.

CueO

Nucleotide sequence (1476 nt):

ATGGCAGAACGCCCAACGTTACCGATCCCTGATTTGCTCACGACCGATGCCCGTAATCGCATTCAGTTAACTA
TTGGCGCAGGCCAGTCCACCTTTGGCGGGAAAACTGCAACTACCTGGGGCTATAACGGCAATCTGCTGGGGCC
GGCGGTGAAATTACAGCGCGGCAAAGCGGTAACGGTTGATATCTACAACCAACTGACGGAAGAGACAACGTTG
CACTGGCACGGGCTGGAAGTACCGGGTGAAGTCGACGGCGGCCCGCAGGGAATTATTCCGCCAGGTGGCAAGC
GCTCGGTGACGTTGAACGTTGATCAACCTGCCGCTACCTGCTGGTTCCATCCGCATCAGCACGGCAAAACCGG
GCGACAGGTGGCGATGGGGCTGGCTGGGCTGGTGGTGATTGAAGATGACGAGATCCTGAAATTAATGCTGCCA
AAACAGTGGGGTATCGATGATGTTCCGGTGATCGTTCAGGATAAGAAATTTAGCGCCGACGGGCAGATTGATT
ATCAACTGGATGTGATGACCGCCGCCGTGGGCTGGTTTGGCGATACGTTGCTGACCAACGGTGCAATCTACCC
GCAACACGCTGCCCCGCGTGGTTGGCTGCGCCTGCGTTTGCTCAATGGCTGTAATGCCCGTTCGCTCAATTTC
GCCACCAGCGACAATCGCCCGCTGTATGTGATTGCCAGCGACGGTGGTCTGCTACCTGAACCAGTGAAGGTGA
GCGAACTGCCGGTGCTGATGGGCGAGCGTTTTGAAGTGCTGGTGGAGGTTAACGATAACAAACCCTTTGACCT
GGTGACGCTGCCGGTCAGCCAGATGGGGATGGCGATTGCGCCGTTTGATAAGCCTCATCCGGTAATGCGGATT
CAGCCGATTGCTATTAGTGCCTCCGGTGCTTTGCCAGACACATTAAGTAGCCTGCCTGCGTTACCTTCGCTGG
AAGGGCTGACGGTACGCAAGCTGCAACTCTCTATGGACCCGATGCTCGATATGATGGGGATGCAGATGCTAAT
GGAGAAATATGGCGATCAGGCGATGGCCGGGATGGATCACAGCCAGATGATGGGCCATATGGGGCACGGCAAT
ATGAATCATATGAACCACGGCGGGAAGTTCGATTTCCACCATGCCAACAAAATCAACGGTCAGGCGTTTGATA
TGAACAAGCCGATGTTTGCGGCGGCGAAAGGGCAATACGAACGTTGGGTTATCTCTGGCGTGGGCGACATGAT
GCTGCATCCGTTCCATATCCACGGCACGCAGTTCCGTATCTTGTCAGAAAATGGCAAACCGCCAGCGGCTCAT
CGCGCGGGCTGGAAAGATACCGTTAAGGTAGAAGGTAATGTCAGCGAAGTGCTGGTGAAGTTTAATCACGATG
CACCGAAAGAACATGCTTATATGGCGCACTGCCATCTGCTGGAGCATGAAGATACGGGGATGATGTTAGGGTT
TACGGTAGAGCTCTAG

Amino acid sequence (491 aa):

MAERPTLPIPDLLTTDARNRIQLTIGAGQSTFGGKTATTWGYNGNLLGPAVKLQRGKAVTVDIYNQLTEETTL
HWHGLEVPGEVDGGPQGIIPPGGKRSVTLNVDQPAATCWF**HPH**QHGKTGRQVAMGLAGLVVIEDDEILKLMLP
KQWGIDDVPVIVQDKKFSADGQIDYQLDVMTAAVGWFGDTLLTNGAIYPQHAAPRGWLRLRLLNGCNARSLNF
ATSDNRPLYVIASDGGLLPEPVKVSELPVLMGERFEVLVEVNDNKPFDLVTLPVSQMGMAIAPFDKPHPVMRI
QPIAISASGALPDTLSSLPALPSLEGLTVRKLQLSMDPMLDMMGMQMLMEKYGDQAMAGMDHSQMMGHMGHGN
MNHMNHGGKFDFHHANKINGQAFDMNKPMFAAAKGQYERWVISGVGDMML**H**PF**H**I**H**GTQFRILSENGKPPAAH
RAGWKDTVKVEGNVSEVLVKFNHDAPKEHAYMA**HCH**LLE**H**EDTG**M**MLGFTVEL

ItL-01

Nucleotide sequence (1638 nt):

*optimized for *E. coli* expression (see original sequence in Schorn (2020))

GCTAGCATGCAACGTCGCGATTTCATCAAGCTGAGCGCAGCGATGGGTGCGGCCTCGGCCCTGCCTCTGTGGT
CACGTAGCCTTATGGCAGAACAAGTGCGTCTGGAGCTGCCCGTACCGGCGTTACTGACGGCAGATCCGCGTGG
CATCATTAACATTGCCGTGCAGCAAGGCCAAACCCAGTGGATGGGCAAATCCGTGACTACGTGGGGATACAAC
GGTAATCTCTTAGGCCCGGCAATTCAGCTGGATCGCGGCAAACCGGTGACGTTGAATTTGCACAATACCCTGC
CGGAAGCGACAACCATTCATTGGCATGGCTTAGCGTTACCGGGCGAAGTAGATGGTGGTCCACAAGCTGTGAT
CGCCCCAGGAGCTTTTCGTCGGGTAAGTTTTACGCCGGATCAGCCTGGTGCTACATGCTGGTTTCATCCGCAT
CAGCATGGTCGCACTGGTTACCAGGTTGCGCAAGGTCTGGCGGGACTGGTGATCTTAAAAGATGACGCAGGCG

AGAAACTGCTGCTTCCGAAAATCTGGGGAGTTGACGATATTCCCGTCATTCTGCAGGATAAACGCCTGTCCAC
CGATGGCAGCAAAATCGATTATGCGCTGGACATGATGTCAGCCACTGTCGGTTGGTTTGGCAACACCATGTTG
ACCAACGGCGTCATTTATCCACTCCAAGCTGTTCCACGTGGGTGGTTACGCCTCCGCTTGCTTAATGGGTGCA
ATGCTCGTAGCCTGAATCTCACCACATCGGATCAGCGCCCGCTGTATGTGATTGGTAGCGATGGTGGGTTGCT
GGCTGAGCCGGTAAAGCTGACCGAACTGTCCATGATGCCAGGGGAACGCTTTGAAGTTCTCGTTGACACCCAC
GATGGCAAAACCTTCGACCTTCAGACGCTGCCTGTTCGCCAAGCCGGAATGACGCTTGCCCCGTTTGATCAGC
CATTACCGCTGCTGACCATCCAGCCTTTGCAGATTCTGGCCTCCGGCAGTCTGCCGGACAAACTGGTGGACAT
GCCAGCGTTACCGGCTCACGACGGTGTCAAAGAACGTTGGCTTCAGTTGATGATGGACACGGAACTGGATGAC
CGCGGTATGCAGGCCCTGATGGAGAAGTATGGCCGTAGTGCGCTGGCGGGTAGTCGCCATGATGCGCACAACA
CAGATGGCGATATGTCGTCTGCAGTCGGTAAAGGCATGGACCACGATGCAATGGCCGGTATGGCCAATGGCTC
TATGCCGGGGATGGCCCACAATCTGCCCGCGCAGAAACCGTACGATTTCCATCACGGAAACAAGATCAACGGC
GTTGCGTTCGACATGAACACTCCGAGCTTTGACGTCAAACAAGGCGCACTGGAGAAATGGACTATTTCTGGCG
AAGGGGATGGGATGTTGCATCCTTTCCACATTCATGGTGCGCAGTTTCGCATTCTGAGCGAAAACGGTAAACC
CGCAGCTGCGCATCGGTCAGGGTGGAAGGACATGGTGCGTGTGGAAGGCTGGCGCTCGGAAGTGCTGGTTCGC
TTCAACCATCTTGCCACGAAAGATCAGGCGTATATGGCACATTGTCATCTCCTGGAACACGAGGATACCGGTA
TGATGCTCGGCTTTACCGTATCTGCGGAGCTC

Amino acid sequence (542 aa):

MQRRDFIKLSAAMGAASALPLWSRSLMAEQVRLELPVPALLTADPRGIINIAVQQGQTQWMGKSVTTWGYNGN
LLGPAIQLDRGKPVTLNLHNTLPEATTI**H**W**H**GLALPGEVDGGPQAVIAPGAFRRVSFTPDQPGATCWF**H**P**H**QH
GRTGYQVAQGLAGLVILKDDAGEKLLLPKIWGVDDIPVILQDKRLSTDGSKIDYALDMMSATVGWFGNTMLTN
GVIYPLQAVPRGWLRLRLLNGCNARSLNLTTSDQRPLYVIGSDGGLLAEPVKLTELSMMPGERFEVLVDTHDG
KTFDLQTLPVRQAGMTLAPFDQPLPLLTIQPLQILASGSLPDKLVDMPALPAHDGVKERWLQLMMDTELDDRG
MQALMEKYGRSALAGSRHDAHNTDGDMSSAVGKGMDHDAMAGMANGSMPGMAHNLPAQKPYDFHHGNKINGVA
FDMNTPSFDVKQGALEKWTISGEGDGML**H**PF**H**I**H**GAQFRILSENGKPAAAHRSGWKDMVRVEGWRSEVLVRFN
HLATKDQAYMA**HCH**LLE**H**EDTG**M**MLGFTVSA

ItL-02

Nucleotide sequence (1575 nt):

ATGCATCGTCGTGATTTTCTGAAATATTCTGCTGCTTTTGGCGCATTCAGCGCGCTGCCGCTCTGGAGCCGTA
CGGCATTGGCTGCGGAACGCCCTATTTTGCCTGTCCCTGAATTACTTGCACCCGATGCCAGAAACAGCATCCG
TCTTACGGCCCAGGCCGGGAAAACCGTCTTCGGCGGCAAAACTGCGACAACCTGGGGCTATAACGGCAACTTG
TTAGGGCCAGCGCTGCGCCTGACCCAGGGTGAAAGCGTTACCGTAGATATTCATAATAGCCTGGCTGAAGAAA
CAACGGTGCACTGGCATGGTCTGGAAGTGCCGGGCGACGTCGACGGCGGCCCGCAGGGTGTGATTGCCGCCGG
GGGCAAGCGCACCGTCAAATTCACGCCTCAGCAGCGTGCCGCAACCTGCTGGTTCCATCCCCATCAGCACGGT
AAAACCGGACATCAGGTGGCAATGGGGCTCGCGGGGCTGGTGCTGATCGAAGACAGCGAAAGCCGCAGGCTGA
TGCTGCCGAAGCAGTGGGGCATCGACGATATCCCGCTCATCATTCAGGACAAGCGTTTTGGCGCCGACGGCGA
GATTGATTACAAGCTGGACGTGATGAGCGCCGCCGTTGGCTGGTTTGGCGACACGCTGCTGTGCAACGGTGTT
AATTACCCGCAGCATTCCAATCCTCGCGGCTGGCTGCGTTTACGCCTGCTTAACGGCTGTAACGCCCGTTCAT
TGAATATTGCGGCAAGCGACAATCGCCCTCTGTATGTTATCGCCAGCGACGGCGGCCTGCTGGCCGAACCGGT
GAAAGTCACGGAGCTGCCGCTGGTGATGGGTGAGCGCTTTGAAGTGCTGGTGGACACCAGCGACGGTAAGCCG
TTTGATATCGTGACCCTGCCGGTGAAGCAAATGGGTATGACCGTTGCGCCGTTCGACCAGCCGCAGCCCATCG
CGCGTATTCAGCCGGTGCGTATTGCTGCTTCTGGCGAGCTGCCGGATAAGCTGGTGGAGGTTCCCGCTCTGCC
AGCGCTCGAGGGCGTGACCGAACGCTGGTTACAGCTGATGATGGACCCCATGCTCGACATGATGGGCATGCAG
GCGCTGATGGAGAAATACGGCGAGAAAGCGATGGCGGGCATGAGCATGGCCGGCCACGGTAGTATGGGCGGCA
TGAAGCAGGGCGGTATGGATCACGGCAAGATGAATCATGGTCAGATGGGCCAGGGTTTCGACTTCCACAATGC

CAACAAGATCAACGGCAAGGCCTTTGATATGGCCACCCCGGCGTTCGCCGCGCAGAAGGGTAAATACGAGAAA
TGGACCATTTCCGGGGAAGGGGACATGATGCTGCATCCGTTCCACATCCACGGCACGCAGTTCCGCATTCTGA
GCGAGAACGGTCAGCCGGTTGCTGCCCATCGTCAGGGCTGGAAAGATACGGTTCGTGTGGAAGGGGCGCGGAG
CGAGGTGTTAGTACGCTTCGATCACGAAGCCTCGAAAGAACATGCCTATATGGCCCACTGTCATCTGCTGGAG
CATGAAGACACCGGCATGATGCTTGGCTTCACCGTGGCATAA

Amino acid sequence (524 aa):

MHRRDFLKYSAAFGAFSALPLWSRTALAAERPILPVPELLAPDARNSIRLTAQAGKTVFGGKTATTWGYNGNL
LGPALRLTQGESVTVDIHNSLAEETTV**HWH**GLEVPGDVDGGPQGVIAAGGKRTVKFTPQQRAATCWF**HPH**QHG
KTGHQVAMGLAGLVLIEDSESRRLMLPKQWGIDDIPLIIQDKRFGADGEIDYKLDVMSAAVGWFGDTLLCNGV
NYPQHSNPRGWLRLRLLNGCNARSLNIAASDNRPLYVIASDGGLLAEPVKVTELPLVMGERFEVLVDTSDGKP
FDIVTLPVKQMGMTVAPFDQPQPIARIQPVRIAASGELPDKLVEVPALPALEGVTERWLQLMMDPMLDMMGMQ
ALMEKYGEKAMAGMSMAGHGSMGGMKQGGMDHGKMNHGQMGQGFDFHNANKINGKAFDMATPAFAAQKGKYEK
WTISGEGDMML**H**PF**H**I**H**GTQFRILSENGQPVAAHRQGWKDTVRVEGARSEVLVRFDHEASKEHAYMA**HCH**LLE
HEDTG**M**MLGFTVA

ItL-03

Nucleotide sequence (1605 nt):

ATGAACCGTCGTGATTTCGTAAAATGGACAACCCTGATGGGGGCCGCCAGTACGCTGCCCGGCTGGAGCCGCT
TCGCGCTCGCCGCAGATCGCCCTGCATTACCCATTCCTGCGCTGCTGGAACCGGATATCCGTAACGCCATTAT
GCTGACGTTGCAGCGCGGTCAGAGCCAGTTTCTGCCGGGTGTAAACACCGAAACCTGGGGCGTTAACGGTAAT
CTTCTCGGCCCGGCGCTGCGTATCCGTCGCGGCAAACAGGTCGATGTCACCGTCAATAACCGTCTGGATGTTG
CCAGCACCGTTCACTGGCACGGGCTGGAAATCCCCGGTGACGTCGATGGCGGTCCTCAGGCACTGATCGCTCC
AGGTCAGAAAAGAAAAGTCAGTTTCACACTCGATCAGCCAGCGTCGACCTGCTGGTTCCATCCGCATCCGCAT
CAGACCAGCGGTTATCAGGTGGCGATGGGGCTGGCCGGTATGGTGCTGATTGAAGATGAAGCCAGCGACTTGT
TGCAGATCCCTAAACGTTGGGGCGTGGATGATATTCCGGTCATTTTGCAGGATAAACGCCTGAACGACGCCGG
ACAGATTGATTATCAGATGGACGTGATGACCGCGGCTGTCGGCTGGTTCGGGCAACATATGCTGACCAACGGC
GCGGTGTATCCGCAGCACGGTATTTCCCGCGGCTGGGTGCGTTTTCGTCTGCTCAATGGCTGTAATGCACGCT
CGCTGCACATCGCCACCAGTGACCAGCGGCCGATGTACGTCATCGCCAGCGACGGCGGTTTCCTGCCTGAACC
GGTGAAAGTCAGCGATTTATCCTTGCTGATGGGCGAGCGTTTTGAAGTGCTGATTGATTGCAGCGACGGCAAA
GCCTTTGATCTGGTTACGCTGCCGGTGAAACAGATGGGTATGACGCTGGCACCTTTCGACAAACCGTTGCCGG
TGCTGCGTATTCAGCCGACGCTGACGCAAAGCGGCAGTTCTCTGCCGGACACGCTGGTCCCGCTGCCGGCGCT
GGTGTCCGTCGATAATCTGCCAACCCGCTGGCTGCAACTGATGATGGATCCGCAACTGGATCAGCAGGGCATG
GCGGCGCTGATGAAACGCTATGGTCACAAGGCAATGGCCGGCATGAGCATGGATCATGGCGGCGGCGATATGG
CGGCAATGCCGGGCATGTCGGGTTCAGAACATGAGGGTCACGGCAGCATGGCGGGTATGGATATGAGCAAATC
GTCCGCCGGTTACGACTTCATGCAGGGCAACAAAATTAACGGCAAAGCCTATGACATGAATGTACCCGCTTTC
GATGTGAAACAAGGCCAGTACGAAAAATGGACCATTTCCGGCGAAGGCGACATGATGCTGCATCCTTTCCATA
TCCACGGCACGCAGTTCCGTATTCTTTCTGAAAATGGTCAGCCTGTGCCGCCGCACCGGCAGGGCTGGAAAGA
TATCGTGCGCGTTGAGGGTGCCCGCAGTGAAGTTCTGGTGCGCTTCAACCATCTGGCCAATAAACAACATGCT
TATATGGCGCACTGTCATCTGCTGGAACATGAAGATACCGGCATGATGCTTGGATTTACGGTATCGGCGTAA

Amino acid sequence (534 aa):

MNRRDFVKWTTLMGAASTLPGWSRFALAADRPALPIPALLEPDIRNAIMLTLQRGQSQFLPGVNTETWGVNGN
LLGPALRIRRGKQVDVTVNNRLDVASTV**HWH**GLEIPGDVDGGPQALIAPGQKRKVSFTLDQPASTCWF**HPH**PH
QTSGYQVAMGLAGMVLIEDEASDLLQIPKRWGVDDIPVILQDKRLNDAGQIDYQMDVMTAAVGWFGQHMLTNG

AVYPQHGISRGWVRFRLLNGCNARSLHIATSDQRPMYVIASDGGFLPEPVKVSDLSLLMGERFEVLIDCSDGK
AFDLVTLPVKQMGMTLAPFDKPLPVLRIQPTLTQSGSSLPDTLVPLPALVSVDNLPTRWLQLMMDPQLDQQGM
AALMKRYGHKAMAGMSMDHGGGDMAAMPGMSGSEHEGHGSMAGMDMSKSSAGYDFMQGNKINGKAYDMNVPAF
DVKQGQYEKWTISGEGDMML**H**PF**H**I**H**GTQFRILSENGQPVPPHRQGWKDIVRVEGARSEVLVRFNHLANKQHA
YMA**HCH**LLE**H**EDTG**M**MLGFTVSA